skb.se

SKB TR-25-05

ISSN 1404-0344
ID 1969342
June 2025

Post-closure safety evaluation of a carbon steel KBS-3 canister insert

Allan Hedin, Anna Alvestav, Peter Eriksson, Lena Zetterström Evins,
Johannes Johansson, Christina Lilja, Ulf Ronneteg, Jan Sarnet, Kastriot Spahiu
Svensk Kärnbränslehantering AB

Daniel Mångård, Erik Öbrink
Kiwa Technical Consulting AB

This report is published on www.skb.se

Abstract

Purpose

The current (May 2025) reference design of the KBS-3 canister for spent nuclear fuel consists of a corrosion resistant copper shell and a cast iron insert providing mechanical strength. There are two versions of the insert, one housing 12 BWR fuel elements and one housing 4 PWR elements.

In an effort to optimise the canister design, SKB is studying alternative BWR and PWR carbon steel inserts. An important purpose in this so-called Rebus project is to develop an insert that can be more reliably produced on an industrial scale than the cast iron insert, while fulfilling the same design requirements as the latter concerning e.g. mechanical loads in the repository.

The Rebus insert consists of an outer tube as the main load bearing component, BWR and PWR variants of an internal framework, a base and a lid, see Figure 1. The steel grades for the Rebus components are P355N (tube), S355J2+N (framework) and P355GH+N (lid and base). The outer dimensions of the Rebus inserts are the same as those of the cast iron inserts. The corrosion resistant copper shell is also the same.

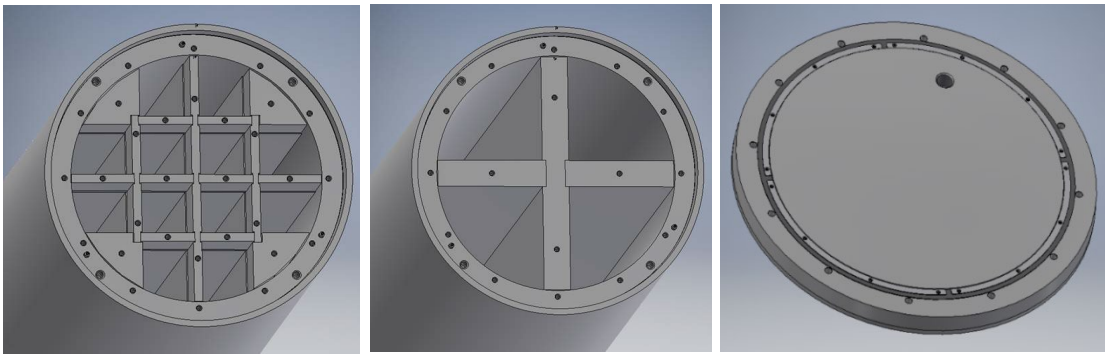

Figure 1. *The Rebus BWR (left) and PWR (middle) inserts. The rightmost figure shows the base/lid.*

The present report documents an evaluation of the post-closure performance a KBS-3 canister with the carbon steel inserts in a final repository. The purposes of the report are

i) to evaluate issues related to post-closure safety for the Rebus canisters to the level achieved for canisters with a cast iron insert and

ii) to assess the ability of the Rebus canisters to fulfil stipulated design requirements in a KBS-3 repository.

The prospects of producing canister inserts according to the specifications of the design on an industrial scale such that the design requirements are achieved is beyond the scope of the present report, but is assessed elsewhere in the documentation emerging from the Rebus project.

Conducted analyses

The post-closure safety relevant issues for the Rebus insert are expected to be the same as those identified for a cast iron insert, and to ascertain that this is the case, international data bases of features, events and processes of relevance for post-closure safety of geological repositories were searched for entries of relevance for carbon steel. This did not yield any new issues compared to those already identified in similar searches for the cast iron insert and that are hence incorporated in the assessment of post-closure safety for that insert. Based on this evaluation, the following subject areas were analysed for the Rebus insert:

- Radiation intensities in and around a Rebus canister and radiation damage in the canister materials;
- the thermal development inside a Rebus canister and possible effects of thermal expansion;
- the hydrological development in a sealed Rebus canister due to remaining water after drying of the fuel;

- radiolysis in the gas phase in a sealed canister and the associated generation of species detrimental for the canister materials;
- potentially detrimental phenomena in the canister materials like stress corrosion cracking (SCC), hydrogen embrittlement, static and dynamic strain ageing, and several forms of radiation induced embrittlement;
- resilience to mechanical loads in the repository for a complete set of load cases derived from the design requirements for the canister;
- criticality of a failed, water-filled canister in the final repository, for both intact and altered insert geometry, and
- some minor additional issues.

The subject areas were addressed by literature studies, experimental work and/or modelling efforts, resulting in a range of dedicated specialist reports.

Conclusions

The overall conclusions of the analyses of the different subject areas are in summary as follows.

Radiation intensity

The neutron and gamma radiation intensity in and around a Rebus canister is similar to that of the canister with a cast iron insert. This is expected since the two are to be loaded with the same fuel and since the dimensions and the radiation attenuation properties of the insert materials are similar. The rate of radiation induced damage (the rate of creation of pairs of vacancies and interstitial atoms) in the metal materials is also similar. The peak dose rate outside a Rebus canister is well below the requirement of <1 Gy/h, and somewhat lower than that of a canister with a cast iron insert.

Thermal evolution

The fuel temperature in a Rebus insert would be somewhat higher than that in the cast iron insert, primarily due to the gaps between the Rebus insert outer tube and inner framework. The peak fuel temperatures are, however, far lower than any temperature of concern for post-closure safety. The framework of the Rebus insert is expected to experience peak temperature in the repository (around 130 °C and 125 °C for 1700 W BWR and PWR canisters, respectively) that are somewhat higher than those of the cast iron insert, and the temperature will have decreased to much lower values when the highest mechanical loads are expected. The Rebus tubes are expected to experience repository temperatures (peak around 100 °C) that are very similar to those of the outer surface of the cast iron insert. The temperature development of the copper shell and the system parts external to the canister are identical for the Rebus and cast iron inserts since these temperatures are determined by the residual power of the fuel and the thermal properties of the system external to the canister. A requirement on a maximum residual power of 1700 W per canister together with a site-specific layout is used to ensure that detrimental temperatures do not occur in the repository.

Hydrological evolution

The hydrological evolution inside a sealed Rebus canister is largely determined by the temperature development, the amount of residual water in the sealed insert and the progress of aqueous corrosion of the insert material, in particular its dependence on relative humidity (RH). The development is generally quite similar to that of the canister with a cast iron insert, with some differences caused by differences in geometry and thermal development. Few, if any, of the around 6000 sealed canister inserts are expected to contain amounts of residual water even close to the allowed maximum of 600 g. For the majority of canisters containing no leaking fuel pins, the amount of water is expected to be negligible from the point-of-view of post-closure safety. For some tens of canisters up to 240 g of water is pessimistically assessed to remain. If the corrosion is assumed to proceed independent of RH, then all water is expected to be consumed within a few years after closure, whereas if there is an RH limit below which corrosion does not occur, a small amount of water vapour, but no liquid water, could remain in the insert for a very long time. The limited amount of water assessed to be present in the majority of canisters is an important finding for subsequent evaluations of radiolysis and hydrogen embrittlement.

Radiolysis

Radiolysis could lead to the formation of agents active in stress corrosion cracking (SCC) of the canister materials. The extent of radiolysis reactions in the gas phase of the insert interior are, in addition to the radiation intensity, largely determined by the amounts of argon, residual water and air in the sealed insert. With a requirement of > 97 % argon and with the limited amounts of residual water expected in the canister insert, limited amounts of SCC active agents are generated according to the radiolysis calculations performed. These are used in the assessment of SCC.

Stress corrosion cracking, SCC

Stress corrosion cracking of the Rebus insert materials and/or of the copper shell requires a simultaneous occurrence of tensile stresses and a chemical environment conducive to SCC. The SCC promoting factors related to the chemical environment in a sealed canister concern the occurrence of oxidising conditions and the radiation induced SCC active agents ammonium (NH_4^+), nitrate (NO_3^-) and nitrite (NO_2^-). Comparing the times of occurrence of tensile stresses (as an effect of saturation of the clay buffer surrounding the canister) and the persistence of the SCC active agents and of oxidising species, it is concluded that the likelihood of SCC in the Rebus insert is negligible. The same is concluded for the copper shell regarding SCC from the interior atmosphere.

Hydrogen embrittlement

Hydrogen embrittlement is not expected to affect the Rebus materials with their as-manufactured properties because of the low initial hydrogen content. Hydrogen gas generated due to anaerobic steel corrosion by residual water is the only identified significant additional hydrogen source in a sealed canister insert. It has been demonstrated that this hydrogen would have only a limited impact on the mechanical properties (the fracture toughness) of the Rebus materials if the maximum allowed 600 g of residual water in the canister is pessimistically assumed. Hydrogen embrittlement is therefore not expected to deteriorate the Rebus insert materials in a sealed canister. This was further corroborated by demonstrating that the pessimistically assessed limited reduction in fracture toughness causes a reduction of acceptable defect sizes that is of no concern.

Static and dynamic strain ageing

Static and dynamic strain ageing could lead to deteriorated mechanical properties over time. The phenomena have been investigated experimentally with the conclusion that both are expected to have a negligible impact on post-closure safety, in agreement with earlier findings for the canister with a cast iron insert.

Radiation-induced embrittlement

The direct effects of damage caused by the radiation doses are assessed as negligible, even when annealing effects that greatly reduce the damage are neglected. Radiation-induced embrittlement could be caused by radiation-enhanced i) precipitation of Cu clusters, ii) precipitation of more complex intermetallic phases or iii) phosphorous segregation to grain boundaries.

Updated calculations of Cu cluster formation, with a dislocation density measured for the Rebus material and with repository-relevant temperatures and damage rates, confirm earlier findings that a Cu content of at most 0.05 at.% is sufficient to avoid detrimental Cu cluster formation in the Rebus material. Results of calculations with higher Cu concentrations indicate that a relaxation to the standard requirement of 0.35 at.% Cu for the quality of the P355N steel grade intended for use in the canister inserts would not yield an unacceptable extent of Cu clustering. This indication would be strengthened if verified experimentally.

Precipitation of more complex intermetallic phases consisting of in particular Ni, Mn and Si has been observed in irradiated reactor steels. Based on available literature data, it is concluded for the Rebus steel that irradiation induced precipitation of such intermetallic phases will give negligible, if any, degradation of the insert under repository conditions. The conclusion is primarily based on the fact that total radiation doses many orders of magnitude higher than those in a final repository are required for such effects to be observed.

Radiation enhanced phosphorus segregation to grain boundaries may embrittle steel, as has been observed in studies of reactor steels that resemble the steel suggested as the Rebus insert material. However, effects have only been seen in conditions where dose rates and total doses are several orders of magnitude higher than in the repository environment, and at temperatures exceeding what is expected for the canister insert in the repository. It is therefore concluded that irradiation induced phosphorus segregation will give negligible, if any, degradation of the insert.

Resilience to mechanical loads

The assessment of the Rebus canisters' resilience to mechanical loads in a repository environment lead in summary to the following key conclusions.

- Analyses of loads from asymmetric swelling due to uneven water saturation of the bentonite buffer and deposition hole geometry, during temperate climate conditions expected to last for tens of thousands of years, show a sufficient margin against global plastic collapse for load cases stipulated in the design requirements.
- Deterministic and probabilistic analyses show that the Rebus canisters will withstand a 50 MPa isostatic load, as stipulated in the design requirements. The modelling is verified by isostatic pressure tests.
- The Rebus canisters are also demonstrated to withstand a 5 cm shear load occurring at a rate of up to 1 m/s and for the buffer properties as stipulated in the design requirements. The canisters are also demonstrated to withstand possible sequences of shear and isostatic loads.
- Defect tolerance analyses for the load cases yield, together with measured fracture toughness data for the Rebus materials, acceptable defect sizes that are expected to be rare and readily avoidable with available detection methods. The derived acceptable defect sizes include allowance for a pessimistically assessed extent of hydrogen embrittlement.
- Creep in insert materials is assessed to be negligible. Creep in the copper shell has not been explicitly modelled. Rather, it has been demonstrated that stresses and strains in the copper shell with a Rebus insert for the shear and isostatic load cases will be similar to those with a cast iron insert. Since copper creep is assessed not to jeopardise the post-closure integrity of canisters with cast iron inserts, the same conclusion is drawn for the Rebus canisters.

Criticality

In order to rule out criticality in the final repository it needs to be demonstrated that the neutron multiplication factor (k_{eff}) does not exceed 0.95 for normal conditions, which is assumed to be a water-filled canister with intact geometry and 0.98 for unlikely scenarios, which are assumed to be a water-filled canister where the canister integrity is lost and corrosion processes have changed the material properties and the geometrical configuration.

The criticality assessment demonstrates that the vast majority of the fuel currently in Clab can be deposited safely with regards to criticality in canisters with Rebus inserts. It is necessary to utilize fuel properties that reduces reactivity to show compliance with criteria and burnup credit has been used to this end.

Criticality safety in the final repository in canisters with the Rebus insert is upheld for fuel that meet the following:

- For PWR fuel, burnup credit is necessary from initial enrichments of 2.3 % U-235. At 5 % it is necessary that the fuel has a burnup of at least 25 MWd/kgU.
- For BWR fuel, burnup credit is necessary from initial enrichments of 3.2 % U-235. At 5 % it is necessary that the fuel has a burnup of at least 38 MWd/kgU.

A minor part of the fuel assemblies does not comply with the requirement on burnup and those assemblies need to be handled in a case specific manner, for example by loading these assemblies in canisters together with less-reactive fuel and showing subcriticality with case-specific calculations. It is also assessed that criticality safety in the final repository will not be adversely affected by leaving a position empty in a canister with a Rebus insert.

The Rebus PWR canisters have a somewhat larger margin to the criticality requirements than the canisters with cast iron inserts. The opposite is true for the BWR canisters, where burn-up credit is not required to demonstrate non-criticality in the final repository for the cast iron design.

Fulfilment of report purposes

The first purpose of the report, i.e. to evaluate issues related to post-closure safety for the Rebus canisters to a level comparable to that for canisters with a cast iron insert, is assessed as having been achieved based on the results presented in the report and summarised above. For many of the issues addressed, e.g. the thermal and hydrological evolution, radiolysis, SCC, and embrittlement due to radiation induced copper clusters, the work has resulted in an advanced level of knowledge also for the cast iron design.

Regarding the second purpose, based on the conclusions summarised above, with details provided in the report, the canister design requirements and applicable requirements on the handling of the spent nuclear fuel, are assessed to be fulfilled for a Rebus canister with the design analysed in the report. The focus has been on insert-related aspects of the requirements, whereas aspects related to the copper shell have been treated only if they are affected by the choice of design for the insert.

Further work

As with many aspects of post-closure safety for the KBS-3 repository concept, continued research could further strengthen the conclusions and be used as a basis for further optimisations. Some issues that could be considered for further research have been identified. Many of these are also relevant for the cast iron insert.

Sammanfattning

Syfte

SKB:s nuvarande (maj 2025) referensutformning av KBS-3-kapseln för använt kärnbränsle utgörs av ett korrosionsbeständigt kopparhölje och en segjärnsinsats som ger mekanisk hållfasthet. Det finns två versioner av insatsen, en för 12 BWR-element och en för 4 PWR-element.

För att optimera kapseldesignen studerar SKB alternativa BWR- och PWR-insatser av kolstål. Ett viktigt syfte med detta så kallade Rebusprojekt är att utveckla en insats som kan tillverkas mer tillförlitligt i industriell skala än segjärnsinsatsen, samtidigt som den uppfyller samma konstruktionsförutsättningar som den senare.

Rebusinsatsen består av ett yttre rör som utgör den huvudsakliga lastbärande komponenten, BWR- och PWR-varianter av ett inre fackverk, en botten och ett lock, se Figur 1. Stålsorterna för Rebus-komponenterna är P355N (rör), S355J2+N (fackverk) och P355GH+N (lock och botten). Yttermåtten på Rebusinsatserna är desamma som för segjärnsinsatserna. Det korrosionsbeständiga kopparhöljet är också detsamma.

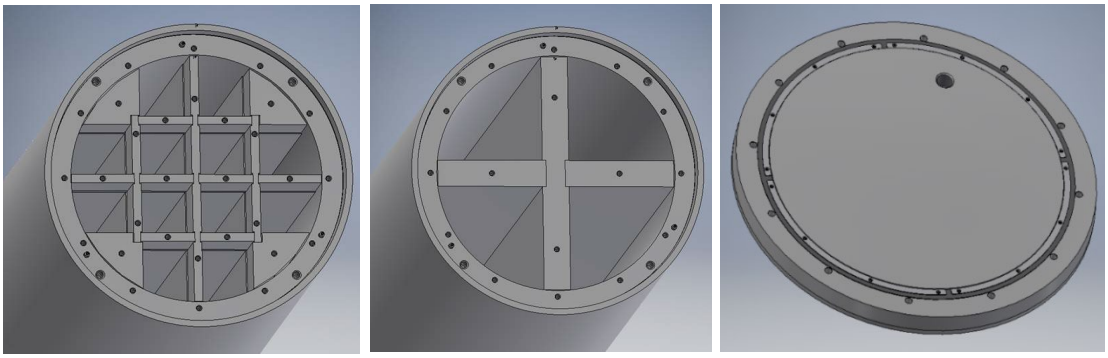

Figur 1. *Rebusinsatserna för BWR- (vänster) och PWR-bränsle (mitten). Till höger lock/botten.*

Föreliggande rapport dokumenterar en utvärdering av funktionen hos en KBS-3-kapsel med Rebusinsatser i ett slutförvar. Syftet med rapporten är

i) att utvärdera frågor relaterade till säkerheten efter förslutning för Rebus-kapslarna till den nivå som uppnåtts för kapslar med segjärnsinsatser och

ii) att bedöma Rebuskapslarnas förmåga att uppfylla gällande konstruktionsförutsättningar i ett KBS-3-förvar.

Möjligheterna att tillverka kapselinsatser enligt designens specifikationer i industriell skala så att konstruktionsförutsättningarna uppnås faller utom ramen för föreliggande rapport. Detta bedöms på annat håll i den dokumentation som arbetas fram inom Rebusprojektet.

Genomförda analyser

Frågorna av betydelse för säkerhet efter förslutning för Rebusinsatsen förväntas vara desamma som de som identifierats för en segjärnsinsats, och för att säkerställa att så är fallet har internationella databaser med egenskaper, händelser och processer av relevans för säkerhet hos geologiska förvar genomsökts efter poster av relevans för kolstål. Detta gav inte några nya frågor jämfört med de som redan identifierats i liknande sökningar för segjärnsinsatsen och som därför är inkluderade i bedömningen av säkerheten efter förslutning för den insatsen. Baserat på denna utvärdering analyserades följande ämnesområden för Rebusinsatsen:

- Strålintensitet i och kring en Rebuskapsel samt strålskador i kapselmaterialen;
- den termiska utvecklingen inuti en Rebuskapsel och möjliga effekter av termisk expansion;
- den hydrauliska utvecklingen i en försluten Rebuskapsel, till följd av kvarvarande vatten efter torkning av bränslet;

- radiolys i gasfas i en försluten kapsel och bildning av species som är skadliga för kapselmaterialen;
- potentiellt skadliga fenomen i kapselmaterialen som spänningskorrosion (SCC), väteförsprödning, statisk och dynamisk deformationsåldring samt flera former av strålningsinducerad försprödning;
- tålighet mot mekaniska laster i förvaret för en fullständig uppsättning lastfall härledda ur kapselns konstruktionsförutsättningar;
- kriticitet hos en skadad, vattenfylld kapsel i slutförvaret, för både intakt och förändrad geometri, samt
- några mindre ytterligare frågor.

Slutsatser

Strålintensitet

Nivåerna av neutron- och gammastrålning i och omkring en Rebuskapsel liknar dem för kapseln med en segjärnsinsats. Detta är förväntat eftersom kapslarna ska laddas med samma bränsle och eftersom dimensionerna och de stråldämpande egenskaperna hos insatsmaterialen är likartade. De momentana nivåerna av bildning av strålningsinducerade skador (generering av par av vakanser och interstitiella atomer) i metallmaterialen är också likartade. Den maximala dosraten utanför en Rebus-kapsel ligger långt under kravet på < 1 Gy/h, och är något lägre än den för en kapsel med segjärnsinsats.

Termisk utveckling

Bränsletemperaturen i en Rebus-insats blir något högre än den i segjärnsinsatsen, främst på grund av spalterna mellan Rebusinsatsens yttre rör och inre fackverk. De högsta bränsletemperaturerna är dock långt under de som skulle kunna orsaka problem för säkerheten efter förslutning. Fackverket hos Rebusinsatsen förväntas nå maximala temperaturer i slutförvaret (cirka 130 °C och 125 °C för 1700 W BWR- respektive PWR-kapslar) som är något högre än de i segjärnsinsatsen. Temperaturen kommer att ha sjunkit till betydligt lägre värden när de högsta mekaniska belastningarna förväntas. Rebusrören förväntas nå förvarstemperaturer (maximalt cirka 100 °C) som är snarlika dem på segjärnsinsatsen yttre delar. Temperaturutvecklingen för kopparhöljet och systemdelarna utanför kapseln är identiska för Rebus- och segjärnsinsatserna eftersom dessa temperaturer bestäms av bränslets resteffekt och de termiska egenskaperna hos systemet utanför kapseln. Ett krav på en maximal resteffekt på 1700 W per kapsel tillsammans med en platsspecifik layout säkerställer att skadliga temperaturer inte uppstår i förvaret.

Hydrologisk utveckling

Den hydrologiska utvecklingen inuti en försluten Rebuskapsel bestäms väsentligen av temperaturutvecklingen, mängden kvarvarande vatten i den förslutna insatsen och den korrosion av insatsmaterialen som vattnet orsakar, särskilt dess beroende av relativ fuktighet (RH). Utvecklingen är lik den för kapseln med segjärnsinsats, med mindre skillnader orsakade av skillnader i geometri och inre termisk utveckling. Få, om någon, av de cirka 6000 förslutna kapselinsatserna förväntas innehålla mängder kvarvarande vatten i närheten av det maximalt tillåtna 600 g. För majoriteten av kapslarna som inte innehåller några läckande bränslestavar förväntas vattenmängden vara försumbar vad gäller säkerhet efter förslutning. För ett tiotal kapslar bedöms pessimistiskt upp till 240 g vatten finnas kvar. Om korrosionen antas pågå oberoende av RH, förväntas allt vatten vara förbrukat inom några år efter förslutning, medan om det finns en RH-gräns under vilken korrosionen avstannar kan en liten mängd vattenånga, men inget vatten i vätskeform, finnas kvar i insatsen under mycket lång tid. Den begränsade mängden vatten som bedöms finnas i majoriteten av kapslarna är en viktigt grund för efterföljande utvärderingar av radiolys och väteförsprödning.

Radiolys

Radiolys kan leda till bildning av ämnen som kan orsaka spänningskorrosion (eng. stress corrosion cracking, SCC) i kapselmaterialen. Omfattningen av radiolysen i insatsens inre gasfas bestäms, förutom av strålningsintensiteten, till stor del av mängderna argon, och kvarvarande vatten och luft i den förslutna insatsen. Med ett krav på > 97 % argon och med de begränsade mängder kvarvarande vatten som förväntas i kapselinsatsen, bildas begränsade mängder ämnen av relevans för SCC enligt de radiolysberäkningar som gjorts.

Spänningskorrosion, SCC

Spänningskorrosion av Rebusinsatsmaterialen och/eller kopparhöljet kräver en samtidig förekomst av dragspänningar och en kemisk miljö som gynnar SCC. De SCC-relaterade faktorerna kopplade till den kemiska miljön i en försluten kapsel gäller förekomsten av oxiderande förhållanden och de strålningsinducerade ämnena ammonium (NH_4^+), nitrat (NO_3^-) och nitrit (NO_2^-). Genom att jämföra tidsintervallet för förekomsten av dragspänningar i insatsen (som en effekt av ojämn bevätning och därmed svällning av lerbufferten som omger kapseln) med intervallen för förekomster av kemiska förhållanden som gynnar SCC, bedöms sannolikheten för SCC i Rebusinsatsen som försumbar. Samma bedömning görs för kopparhöljet vad gäller SCC orsakad av den inre miljön.

Väteförsprödning

Väteförsprödning förväntas inte påverka Rebusmaterialen i leveranstillståndet på grund av den låga initiala vätehalten. Vätgas som genereras på grund av anaerob stålkorrosion orakad av kvarvarande vatten är den enda identifierade signifikanta ytterligare källan till väte i en försluten kapselinsats. Denna mängd väte har visats endast kunna ha en begränsad inverkan på de mekaniska egenskaperna (brottsegheten) hos Rebusmaterialen, också för den maximalt tillåtna mängden (600 g) kvarvarande vatten i kapseln. Väteförsprödning förväntas därför inte försämra materialegenskaperna hos Rebusinsatsen i en försluten kapsel. Detta bekräftades ytterligare genom att i de efterföljande mekaniska analyserna visa att den pessimistiskt bedömda begränsade minskningen av brottseghet inte orsakar någon minskning av acceptabla defektstorlekar av betydelse.

Statisk och dynamisk deformationsåldring

Statisk och dynamisk deformationsåldring kan med tiden leda till försämrade mekaniska egenskaper. Fenomenen har undersökts experimentellt med slutsatsen att båda förväntas ha en försumbar inverkan på säkerheten efter förslutning, i likhet med tidigare resultat för en kapsel med segjärnsinsats.

Strålinducerad försprödning

Den direkta defektbildningen orsakad av stråldoserna bedöms som försumbara, även när rekombinationseffekter, som kraftigt minskar de beräknade defektnivåerna pessimistiskt försummas. Utöver defektbildning kan strålinducerad försprödning orsakas av *i*) utfällning av kopparkluster, *ii*) utfällning av mer komplexa intermetalliska faser eller *iii*) fosforsegregering till korngränser.

Uppdaterade beräkningar av bildning av kopparkluster, med en experimentellt bestämd dislokationstäthet för Rebusmaterialet och med förvarsrelevanta temperaturer och strålnivåer, bekräftar tidigare resultat att en kopparhalt om högst 0,05 atomprocent är tillräckligt för att undvika skadlig bildning av kopparkluster i Rebus-materialet. Resultat av beräkningar med högre kopparhalter tyder på att en relaxering till standardkravet på 0,35 atomprocent koppar som gäller för stålkvaliteten P355N inte heller skulle ge någon oacceptabel grad av bildning av kopparkluster. Denna indikation skulle förstärkas om den verifierades experimentellt.

Utfällning av mer komplexa intermetalliska faser bestående av framför allt nickel, mangan och kisel har observerats i bestrålade reaktorstål. Baserat på tillgängliga litteraturdata bedöms strålinducerad utfällning av sådana intermetalliska faser endast ge försumbar, om någon, försprödning av insatsen under förvarsförhållanden. Slutsatsen baseras i första hand på att totala stråldoser många storleksordningar högre än de i ett slutförvar har krävts för att sådana effekter ska kunna observeras.

Strålinducerad fosforsegregering till korngränser kan förspröda stål, vilket observerats i studier av reaktorstål som liknar stålet som avses användas som Rebusmaterial. Effekter har dock bara setts under förhållanden där doshastigheter och totaldoser är flera storleksordningar högre än i förvarsmiljön och vid temperaturer som överstiger vad som förväntas för kapselinsatsen i förvaret. Därför bedöms strålinducerad fosforsegregering bara ge försumbar, om någon, försämring av insatsens mekaniska egenskaper.

Tålighet mot mekaniska laster

Bedömningen av Rebuskapslarnas tålighet mot mekaniska laster i förvarsmiljön har sammanfattningsvis givit följande slutsatser.

- Analyser av laster orsakade av asymmetrisk svällning av bentonitbufferten kring kapslarna på grund av ojämn bevätning och ojämn form hos deponeringshålen visar tillräcklig marginal mot global plastisk kollaps för relevanta lastfall.
- Deterministiska och probabilistiska analyser visar att Rebuskapslarna kommer att klara en isostatisk belastning på 50 MPa i enlighet med konstruktionsförutsättningarna. Resultaten stöds av genomförda trycktester.
- Rebuskapslarna har också visat sig motstå en skjuvbelastning på 5 cm med en hastighet på upp till 1 m/s och för buffertegenskaperna enligt konstruktionsförutsättningarna. Kapslarna har också visat sig motstå olika sekvenser av skjuv- och isostatiska laster.
- Skadetålighetsanalyser ger, tillsammans med uppmätta brottseghetsdata för Rebusmaterialen, acceptabla defektstorlekar som förväntas vara sällsynta och lätta att upptäcka med tillgängliga detektionsmetoder. I härledningen av acceptabla defektstorlekar har hänsyn också tagits till en pessimistiskt bedömd omfattning av väteförsprödning.
- Krypning hos insatsmaterialen bedöms vara försumbar. Krypning i kopparhöljet har inte explicit modellerats. Det har i stället visats att spänningar och töjningar i kopparhöljet med en Rebusinsats kommer att likna dem med en segjärnsinsats, för skjuvlast och isostatisk last. Eftersom kopparkrypning bedömts inte äventyra integriteten hos kapslar med segjärnsinsats dras samma slutsats för Rebuskapslarna.

Kriticitet

För att utesluta kriticitet i slutförvaret behöver det visas att neutronmultiplikationsfaktorn (k_{eff}) inte överstiger 0,95 för normala förhållanden, vilket antas vara en vattenfylld kapsel med intakt geometri och 0,98 för osannolika scenarier, som antas vara en vattenfylld kapsel där kapseln har förlorat sin geometriska integritet och där korrosion har ändrat materialegenskaper och den geometriska konfigurationen.

Kriticitetsanalysen visar att den stora majoriteten av bränsle som för närvarande finns i Clab kan deponeras säkert med avseende på kriticitet i kapslar med Rebusinsatser. Det är nödvändigt att tillgodoräkna bränsleegenskaper som minskar reaktiviteten för att visa överensstämmelse med kriterier och utbränningskreditering har använts för detta.

Kriticitetssäkerhet i slutförvaret för kapslar med Rebusinsats upprätthålls för bränsle som uppfyller följande:

- För PWR-bränsle krävs utbränningskreditering från initiala anrikningar av 2,3 % U-235. Vid 5 % behöver bränslet ha en utbränning om minst 25 MWd/kgU.
- För BWR-bränsle krävs utbränningskreditering från initiala anrikningar av 3,2 % U-235. Vid 5 % behöver bränslet ha en utbränning om minst 38 MWd/kgU.

En mindre del av bränsleelementen uppfyller inte kravet på utbränning och dessa behöver hanteras fallspecifikt, till exempel genom att deponera dem i kapslar tillsammans med mindre reaktivt bränsle och påvisa underkriticitet med kapselspecifika beräkningar. Det bedöms också att kriticitetssäkerheten i slutförvaret inte påverkas negativt av att lämna en bränsleposition tom i en kapsel med Rebusinsats.

PWR-kapslarna i Rebusutformningen har något större marginal till kriticitetskraven än kapslarna med segjärnsinsats. Det motsatta gäller för BWR-kapslarna, där utbränningskreditering inte krävs för att visa underkriticitet i slutförvaret för segjärnsutformningen.

Uppfyllelse av rapportens syften

Det första syftet med rapporten, det vill säga att utvärdera frågor relaterade till säkerhet efter förslutning för Rebuskapslarna till en nivå som är jämförbar med den för kapslar med segjärnsinsats, bedöms ha uppnåtts utifrån resultaten som presenteras i rapporten och som sammanfattas ovan. För många av frågorna, t ex den termiska och hydrologiska utvecklingen, radiolys, SCC och försprödning på grund av strålinducerad bildning av kopparkluster, har arbetet resulterat i ökad kunskap även för segjärnsinsatsen.

Vad gäller det andra syftet bedöms, baserat på de slutsatser som sammanfattats ovan, med detaljer som ges i rapporten, konstruktionsförutsättningarna för kapseln och gällande krav på hanteringen av det använda kärnbränslet kunna uppfyllas av en Rebuskapsel med den utformning som analyserats i rapporten. Fokus har legat på insatsrelaterade aspekter av kraven, medan aspekter relaterade till kopparhöljet endast behandlats om de påverkas av valet av insatsdesign.

Fortsatt arbete

Som för många aspekter av säkerhet efter förslutning för KBS-3-konceptet, kan fortsatt forskning ytterligare stärka slutsatserna och användas som underlag för fortsatta optimeringar. Några kandidatfrågor för vidare forskning har identifierats. Dessa är ofta relevanta också för segjärnsinsatsen.

Content

1 Introduction

1.1 Context and purpose

The current (May 2025) reference design of the KBS-3 canister for spent nuclear fuel consists of a corrosion resistant copper shell and a cast iron insert providing mechanical strength, see e.g. Jonsson et al. (2018). There are two versions of the cast iron insert, one housing 12 BWR fuel elements and one housing 4 PWR elements.

In an effort to optimise the canister design, SKB is evaluating an alternative canister insert in the so-called Rebus project. An important purpose of this effort is to develop a canister insert that can be more reliably produced on an industrial scale than the canister with a cast iron insert, while fulfilling the same design requirements as the latter concerning e.g. mechanical loads in the repository. Originally, three alternative insert concepts, denoted Rebus Concept 1, 2 and 3, respectively, were considered. Currently (May 2025), the development work, however, concerns only Concept 1, following a preliminary evaluation of the prospects of the three concepts. In this concept, the insert is manufactured of low-alloyed carbon steel and in Section 2.2 details are given for the Concept 1 design. In the present report, expressions like “the Rebus concept”, “the Rebus design”, “the Rebus insert”, etc refer to Rebus Concept 1. The term “Rebus canister” is used for a KBS-3 canister with a Rebus insert and with the same copper shell as that with the cast iron insert.

A key area in the evaluation of the alternative concept is obviously its post-closure performance in a final repository. This report presents an evaluation of this performance for a KBS-3 canister with a Rebus insert. A general ambition with the evaluation has been to treat post-closure safety issues for the Rebus insert to the same depth that has been done for the canister with a cast iron insert, as summarised in SKB (2022a) and Jonsson et al. (2018). The studies and results presented in this report would form an important basis if a Rebus version of SKB (2022a) were to be produced and for a post-closure safety assessment for a KBS-3 repository with Rebus canisters. The latter is essentially achieved by evaluating whether the canister is assessed to fulfil its stipulated design requirements in a repository environment. As elaborated in Chapter 3, the relevant issues are largely the same for the Rebus and the cast iron inserts, whereas their treatment may differ. In some cases, the treatment of an issue for the Rebus insert has led to a deeper understanding also for the cast iron insert and this is noted where relevant. The purposes of the report are thus

i) to evaluate issues related to post-closure safety for the Rebus canisters to the level achieved for canisters with a cast iron insert and

ii) to assess the ability of the Rebus canisters to fulfil stipulated design requirements in a KBS-3 repository.

Generally, pessimistic approaches have been adopted when evaluating the design requirements. Furthermore, based on the design requirements, design specifications to be applied in the production (of in this case canister inserts) are defined for engineered components of the KBS-3 concept. A strict and formal definition of design specifications for the Rebus inserts has not been done at this stage of the development. The specifications of the geometry of the design with its tolerances in Section 2.2.1, and the materials specifications based on standard materials in Section 0 would, however, be a basis for such formal design specifications. These are also the data used to analyse compliance with the design requirements in the present report.

The outer dimensions of the Rebus insert are the same as those of the cast iron insert, and the design of the copper shell that it would be emplaced in is also the same as that for the cast iron insert. Therefore, the performance of the copper shell is generally expected to be the same for the Rebus insert. The performance of the shell is, therefore, not considered in this report, other than for a few aspects where the interaction with the insert or the fuel may affect the performance of the shell in a way that differs from that of the cast iron insert.

An assessment of the prospects of producing canister inserts according to design specifications on an industrial scale such that the design requirements are achieved is beyond the scope of the present report.

1.2 Structure of the report

The design requirements of a KBS-3 canister, applicable for both a canister with a cast iron insert and a Rebus canister, are given in Chapter 2. The chapter also contains a detailed account of the design of the Rebus inserts and other information of relevance for the status of a sealed canister.

Issues of relevance for the post-closure safety evaluations are identified in Chapter 3, based on those of relevance for the canister with a cast iron insert and an effort to identify additional issues related to the materials used in the Rebus insert.

Radiation in and around Rebus canisters is discussed in Chapter 4.

The thermal and hydrological evolution in a sealed canister is discussed in Chapter 5.

The evolution of gases and liquids in the sealed canisters as a consequence of corrosion and radiolysis is discussed in Chapter 6.

Embrittlement and aging phenomena of the insert material are discussed in Chapter 7.

The ability of the canister to withstand mechanical loads in the repository is analysed in Chapter 8.

Post-closure criticality in a failed canister is treated in Chapter 9.

Some additional issues are treated in Chapter 10 and conclusions are provided in Chapter 11.

2 The Rebus design and other bases for the evaluation

2.1 Technical design requirements relating to post-closure safety

2.1.1 General

To guide the design and production of the repository, technical design requirements on characteristics that can be inspected and verified in the production are defined for each repository component. They are based on assessments of repository post-closure safety and available technology and constraints imposed by the operation procedures in the encapsulation facility. For the canister, most of the requirements are sufficiently general to apply to a wide range of canister designs and are relevant for the insert design considered in this report. They thus provide important guidance for the evaluation of post-closure safety of alternative canister designs.

The characteristics of the fuel also need to be considered in the canister design. There are no technical design requirements for the fuel, since the fuel is not produced as a repository component. Rather, there are a set of requirements on the handling of the fuel in SKB's facilities, and on the handling related to its final disposal in the repository. These relate to e.g. residual power in the loaded canister, dose rate on the outer canister surface and criticality. There are also acceptance criteria for fuels entering SKB's facilities, but these are not of interest in the present report.

In the following, the technical design requirements of the canister and the handling requirements on the fuel are given. In both cases the presentation is limited to the requirements of relevance to the present report, i.e. those related to post-closure safety, whereas demands regarding e.g. operational safety are not included.

2.1.2 Canister technical design requirements

Technical design requirements for the canister are stated in Posiva SKB (2017).[1] The following design requirements relating to post-closure safety are given.

- The copper shell shall remain leak tight and the canister maintain its ability to resist loads for an isostatic pressure of 50 MPa.
- The copper shell shall remain tight and the canister maintain its ability to resist loads for
  - 5 cm rock displacements at all angles and a rate of 1 m/s,
  - exerted on the canister by a buffer with an unconfined compressive strength at failure lower than 4 MPa at a deformation rate of 0.8 %/min.
- The copper shell shall remain tight and the canister maintain its ability to resist loads for bending of the canister resulting from asymmetric loads according to Figure 2-1.
- The copper shell shall remain tight and the canister maintain its ability to resist loads for shearing of the canister resulting from asymmetric loads according to Figure 2-2.
- The radiation attenuation over the canister components shall, given the encapsulated spent fuel assemblies and their radiation emission rate, yield a dose rate at the canister surface < 1 Gy/h.
- The canister material properties shall lie within the range for the validity of the criticality analyses.[2]

[1] The requirements for some parts of the KBS-3 concept have since been updated. The canister requirements stated here are, however, unaltered.

[2] This requirement refers to criticality analyses carried out for the canister with a cast iron insert. More generally applicable requirements are stated in Section 2.1.3.

- The thermal conductivity over the canister components and internal gaps shall, given the encapsulated spent fuel assemblies and their decay power, yield a temperature on the canister surface < 100 °C.
- To limit gamma radiation caused hardness and brittleness in cast iron the Cu-content shall be < 0.05 %.[3]
- No organic materials in insert components.
- The copper material shall be highly pure copper. To avoid grain boundary corrosion the oxygen content shall be ≤ 5 wt-ppm.
- At deposition the copper thickness shall be ≥ 40 mm.[4]

Requirements on allowed water content and on gas composition in a sealed canister are given in Section 2.1.3.

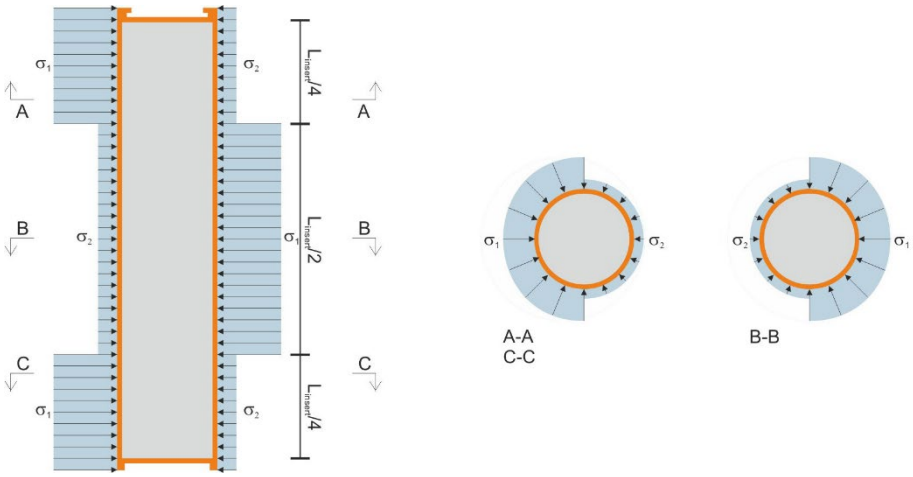

Figure 2-1. *Bending of the canister, σ_1 is the maximum swelling pressure and σ_2 the minimum swelling pressure of the buffer, i.e. 10 and 3 MPa respectively. To σ_1 and σ_2 the hydrostatic pressure at repository depth, 5 MPa, is added.*

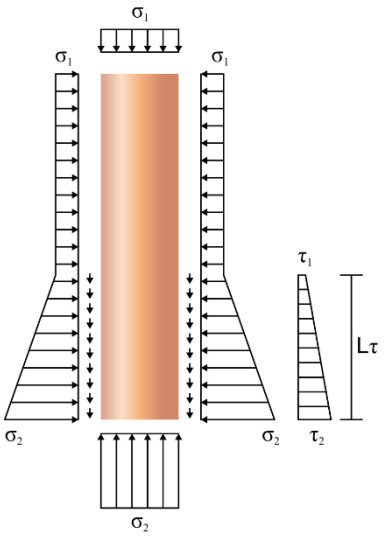

Figure 2-2. *Shearing of the copper canister induced by a buffer swelling pressure between 3 MPa (σ_1) and 10 MPa (σ_2). The hydrostatic pressure at repository depth, 5 MPa, shall be added to σ_1 and σ_2. The parameters τ_1 and τ_2 are the resulting shear stresses that act along the length L_τ of the surface of the canister.*

[3] It is currently being considered if this requirement can be relaxed. For the Rebus insert, the requirement applies to the carbon steel.

[4] After the publication of Posiva SKB (2017) it has been specified that local reductions to a thickness of 35 mm is acceptable for 10 % of the copper shell surface area.

2.1.3 Requirements on the handling of the spent nuclear fuel

The handling of the fuel in SKB's facilities, and the requirements on the handling related to its final disposal in the repository, is presented in SKB (2021)[5]. The most important handling requirements and criteria related to post-closure safety are the following.

- The fuel assemblies to be encapsulated in any single canister shall be selected with respect to burnup and age so that the total decay power in the canister will not result in temperatures exceeding the maximum allowed in the buffer. The total decay power in each canister must not exceed 1700 W.
- The fuel assemblies to be encapsulated shall be selected with respect to enrichment, burnable absorbers (BA), burnup, geometrical configuration and materials in the canister so that criticality will not occur during the handling and storage of canisters even if the canister is filled with water. The effective multiplication factor (k_{eff}) must not exceed 0.95 including uncertainties.
- The increase in reactivity in a failed canister where the cast iron has corroded to form magnetite and siderite and, together with groundwater, has filled the voids in the insert shall be calculated.[6] No further measures to decrease the reactivity are required if $k_{eff} < 0.98$, taking into account uncertainties in calculations, groundwater composition and the properties of the oxidised insert.
- Before the fuel assemblies are placed in the canister they shall be dried so that it can be justified that the allowed amount of water stated as a technical design requirement for the canister is not exceeded. The amount of water left in any one canister shall be less than 600 g.
- Before the canister is finally sealed, the atmosphere in the insert shall be changed so that acceptable chemical conditions can be ensured. The atmosphere in a canister insert shall consist of at least 97 % argon.
- It shall be verified that the radiation dose rate on the canister surface will not exceed the level used as a premise in the assessment of the post-closure safety. The radiation dose rate at the surface of the canister must not exceed 1 Gy/h.

It is, furthermore, noted that in the analyses of post-closure safety of the cast iron insert, credit is taken for the fact that the insert material reacts with residual water and oxygen in the insert voids, thus e.g. reducing the extent to which these constituents contribute to oxidation of potentially damaged fuel rods.

2.2 The Rebus design

In the following sub-sections the design in terms of geometry and material properties of the Rebus insert is presented. The data are taken from Ronneteg (2025) whereas some of the analyses accounted for in the present report are based on an earlier design version (Ronneteg 2022) available at the time those analyses were carried out. The differences between the two design versions is deemed irrelevant for the analyses in question.

[5] **SKB, 2021.** Hantering av använt kärnbränsle inom KBS-3-systemet. SKBdoc 1380283 ver 2.0, Svensk Kärnbränslehantering AB. (Internal document, in Swedish.)

[6] It is noted that this requirement implicitly assumes that the insert is made of cast iron. A more general formulation could preferably be considered. The relevant corrosion products for the Rebus materials are evaluated in a reference to the present report, see further Chapter 9.

2.2.1 Geometry

The Rebus insert consists of a main load bearing component in the form of a cylindrical outer steel tube and an inner steel plate framework within which the fuel is emplaced, see Figure 2-3. The main components are, with numbering according to the Figure:

1. Outer tube, P355N steel
2. Internal framework (steel plates), S355J2+N steel
3. Internal framework (corner beams), S355J2+N steel
4. Steel base/lid, P355GH+N steel
5. Gasket

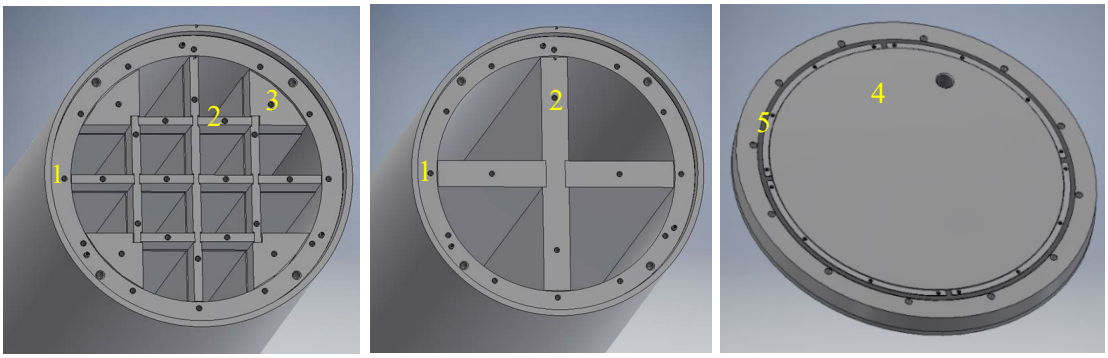

Figure 2-3. *Main components of the Rebus BWR (left) and PWR (middle) inserts.*

The corner beams of the BWR insert improve criticality safety by reducing the void volume. Cross sections of the BWR and the PWR versions of the Rebus insert are shown in Figure 2-4 and key geometry data are given in Table 2-1. The steel base and steel lid are bolted to the steel tube with twelve M16 screws. Tightness is achieved by gaskets (see Section 2.2.3) between the components.

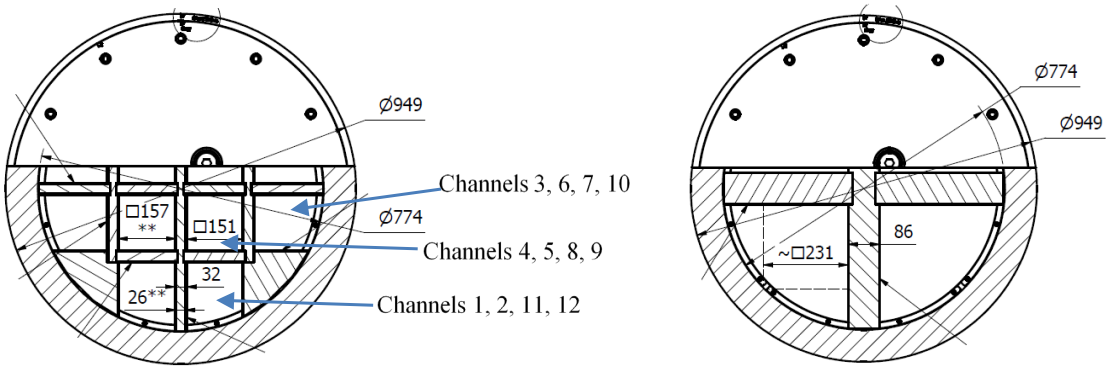

Figure 2-4. *Cross sections of the BWR (left) and PWR (right) versions of the Rebus insert.*

Table 2-1. Key geometry data (nominal values) for the BWR and the PWR versions of the Rebus insert. See Ronneteg (2025) for references to detailed drawings. All values in metres.

	BWR	PWR
Tube length	4.573	
Tube outer diameter	0.949	
Tube inner diameter	0.774	
Framework plate lengths	4.458	
Framework plate thicknesses	0.032	0.086
Side length of fuel compartments in framework	0.151	0.231
Steel lid and base diameter	0.910	
Steel lid and base thickness	0.056	

In locations where the inner framework terminates against the steel tube, i.e. at the ends of the carbon steel plates, a gap exists between the framework and the tube. The gap is 1.5–2 mm for the BWR insert and 1.5–4 mm for the PWR insert. A detailed consideration of the geometry of the interface yields average gap sizes of about 1.65 mm and 2.7 mm for the BWR and PWR inserts, respectively. This has a bearing on the thermal evolution of the canister, see Chapter 5.

The interior areas and void volumes of the Rebus inserts are specified in Table 2-2 and Table 2-3, respectively.

Table 2-2. Interior carbon steel areas (nominal values) in BWR and PWR Rebus inserts (Ronneteg 2025).

Design	Internal framework	Steel tube (Internal part inside seal)	Lid (inside seal)	Base (inside seal)	Total area
BWR	45.20 m^2	10.85 m^2	0.47 m^2	0.47 m^2	56.99 m^2
PWR	15.91 m^2	10.85 m^2	0.47 m^2	0.47 m^2	27.70 m^2

Table 2-3. Void volumes in BWR and PWR Rebus inserts (Ronneteg 2025). Fuel volumes from SKB (2022b, Section 4.1.10). All values in m^3.

Design	Channels 1, 2, 11, 12	Channels 3, 6, 7, 10	Channels 4, 5, 8, 9	Total void volume unloaded	Fuel volume	Total void volume, loaded
BWR	4×0.118	4×0.124	4×0.102	1.376	12×0.033	0.971

Design	Channels 1, 2, 3, 4	Total void volume, unloaded	Fuel volume	Total void volume, loaded
PWR	4×0.386	1.544	4×0.074	1.248

2.2.2 Steel materials

The manufacturing requirements regarding chemical composition of the outer steel tube, the framework and the lid and base materials are given in Table 2-4, Table 2-5 and Table 2-6, respectively. The steel grades for these components are P355N (tube), S355J2+N (framework) and P355GH+N (lid and base).

At a certain stage of the development, the alternative standard steel grade P460 was considered for the outer steel tube, with the conclusion that it did not offer any obvious advantage over P355N, while it could be more demanding to demonstrate the long-term properties such as creep, and reliable manufacturing since P460 is a considerably less common material than P355. This material is, therefore, not considered in the present report. The propensity for criticality for a Rebus insert with a P460 outer tube is, however, evaluated in the supporting document to Chapter 9 since large parts of that report were produced while P460 was being considered.

Table 2-4. Manufacturing requirements on chemical composition of the steel tubes, see Ronneteg (2022) for detailed reference. The two columns refer to alternative, but similar standard qualities of the material P355N.

Parameter/Element (% by mass) [a]	Specification for 1.0562	Specification for 1.0565
Carbon (C)	≤ 0.20	≤ 0.20
Silicon (Si)	≤ 0.50	≤ 0.50
Manganese (Mn)	0.90 to 1.70	0.90 to 1.70
Phosphorus (P)	≤ 0.025	≤ 0.025
Sulphur (S)	≤ 0.020	≤ 0.010
Chromium (Cr)	≤ 0.30 [c]	≤ 0.30 [c]
Molybdenum (Mo)	≤ 0.08 [c]	≤ 0.08 [c]
Nickel (Ni)	≤ 0.50	≤ 0.50
Aluminium (Altot) [b]	0.020 to 0.040 (≥ 0.020)	0.020 to 0.040 (≥ 0.020)
Copper (Cu)	≤ 0.05 [c d]	≤ 0.05 [c d]
Nitrogen (N)	≤ 0.020	≤ 0.020
Niobium (Nb)	≤ 0.05	≤ 0.05
Titanium (Ti)	≤ 0.040	≤ 0.040
Vanadium (V)	≤ 0.10	≤ 0.10
Nb+Ti+V	≤ 0.12	≤ 0.12

a) Elements not included in this table shall not be intentionally added to the steel without the agreement of the purchaser, except for elements which may be added for finishing the cast. All appropriate measures shall be taken to prevent the addition of undesirable elements from scrap or other materials used in the steel making process.
b) Al/N ≥ 2, if nitrogen is fixed by niobium, titanium or vanadium the requirements for Al_{tot} and Al/N do not apply.
c) The sum of the percentage by mass of the three elements chromium, copper and molybdenum shall not exceed 0.45 %. (The stricter-than-standard requirement on Cu content renders this standard requirement superfluous.)
d) Option 2: In order to facilitate subsequent forming operation, an agreed maximum copper content lower than indicated and an agreed specified maximum tin content shall apply.

Table 2-5. Manufacturing requirements on chemical composition of the carbon steel framework material S355J2+N, see Ronneteg (2022) for detailed reference.

Parameter/Element	% by mass
Carbon (C)	≤ 0.17
Manganese (Mn)	≤ 1.40
Phosphorus (P)	≤ 0.035
Sulfur (S)	≤ 0.035
Copper (Cu)	≤ 0.55 [a]

a) Contrary to the case for the steel tube and the steel lid, there is no stricter-than-standard requirement on Cu content for the framework material since it is not a primary load bearing component. This means that embrittlement e.g. due to radiation induced Cu cluster formation (Section 7.5.3) is less of a concern for the framework.

Table 2-6. Manufacturing requirements on chemical composition of the carbon steel lid and base material P355GH+N, see Ronneteg (2022) for detailed reference.

Parameter/Element [a]	% by mass
Carbon (C)	0.10 to 0.22
Silicon (Si)	≤ 0.60
Manganese (Mn)	1.10 to 1.70
Phosphorus (P)	≤ 0.025
Sulfur (S)	≤ 0.010
Aluminium (Al) total	≥ 0.020
Nitrogen (N)	≤ 0.012 [b]
Chromium (Cr)	≤ 0.30
Copper (Cu)	≤ 0.05 [c]
Molybdenum (Mo)	≤ 0.08
Niobium (Nb)	≤ 0.040
Nickel (Ni)	≤ 0.30
Titanium (Ti) max	0.03
Vanadium (V)	≤ 0.02
Others Cr+Cu+Mo+Ni	≤ 0.70

a) Elements not included in this table shall not be intentionally added to the steel without the agreement of the purchaser, except for elements which may be added for finishing the cast. All appropriate measures shall be taken to prevent the addition of undesirable elements from scrap or other materials used in the steel making process.
b) A ratio Al/N ≥ 2 shall apply.
c) Additional requirement as supplement to the standard.

2.2.3 Gasket

A graphite based gasket is used to seal the insert when closing it. The required function of the gasket is to seal the insert in the time interval between the completion of the gas exchange in the insert (see below) and the completion of the welding of the lid to the copper cylinder. This operation will be carried out in close connection to the sealing of the insert and the requirement on longevity of the function of the gasket is therefore set to 72 h.[7] The composition of the gasket is described in Bergendal (2024). In addition to graphite, the sealing contains two 50 µm thick plies of stainless steel of grade 316L for structural integrity. To provide a good contact between the graphite and stainless-steel laminates, the gaskets are impregnated with a phenolic resin. This is an organic material, and its use is thus in principle a violation of the requirement that no organic materials are allowed in the canister.

Bergendal (2024) evaluates the function of the gasket in the canister environment and the potential impact of the materials on post-closure safety. It is also concluded *i*) that the gasket materials are expected to have negligible impact on post-closure and *ii*) that the gasket material could realistically be expected to retain its sealing properties for several hundred years or longer in the insert environment (Bergendal 2024).

2.3 Gases and liquids in the canister interior

The fuel will be dried prior to being placed in the canister. The current reference method[8] entails vacuum drying of the fuel assemblies before emplacement in the canister insert and without external heating. All assemblies to be emplaced in a particular canister are dried together in a purpose-designed transfer canister. The maximum allowed amount of water in a sealed canister is currently 600 g, according to the design requirements in Section 2.1.

[7] A change of this requirement to 30 days rather than 72 h is under consideration, to facilitate operation logistics. This graphite gasket is expected to meet this stricter requirement.
[8] **SKB 2024.** Clink - Teknikbeslut - metod för torkning av bränsle. SKBdoc 2026518 ver 2.0. Svensk Kärnbränslehantering AB. (Internal document, in Swedish.)

Few, if any, of the approximately 6000 canisters to be deposited in the final repository are, however, expected to contain amounts even close to 600 g. A compilation in Hedin (2025) of available data and analyses of relevance for water content in a sealed canister concludes that the remaining amount of water after drying in a canister containing no leaking fuel pins will be negligible.

The total number of leaking fuel pins in the Swedish programme are currently of the order of 1000, where the overwhelming majority of such pins are deposited in purpose-designed quivers that are subsequently emplaced in a canister. The quivers are expected to remain tight for more than 1000 years in an intact KBS-3 canister. For the few (estimated to be fewer than 20) canisters where up to 5 known leaking fuel pins are allowed to be emplaced without quivers, the water content is expected to be up to 40 g in most, and up to 240 g in a single canister with 5 known leaking pins and an additional assumed unknown leaking pin.

In addition to water, the initial gas composition in the interior of a sealed canister is of relevance for the evaluation of post-closure safety. After drying, the canister insert and the smaller void between the insert and the copper shell will be filled with argon. The design requirement states that the gas in the interior of the insert should consists of at least 97 percent argon (Section 2.1.3) whereas the production system aims at achieving at least 99 percent argon and thus at most one percent air. The void between the insert and the shell will be filled with argon prior to welding of the copper lid, in order to reduce oxide formation in the welds. A preliminary requirement[9] on the composition of the gas in the void states that the oxygen content should be at most 100 at.ppm, which is negligible in the context of post-closure safety.

2.4 Fuel types and residual power

The fuel types and the procedures for selecting fuel assemblies for a canister are the same for the Rebus canisters as for the canisters with cast iron inserts. A key requirement is that the residual power of the fuel in a loaded canister may not exceed 1700 W.

[9] SKBdoc 1670112 ver 1.0. Svensk Kärnbränslehantering AB. (Internal document, in Swedish.)

3 Identification of issues related to post-closure safety

3.1 Introduction

A main function of the canister insert is to withstand mechanical loads in the repository environment, making this an evident issue to analyse in an evaluation of post-closure safety for any alternative insert design. Another central function is that of contributing to avoiding criticality, both during operation and post-closure. There are, however, a range of additional radiation-related, thermal, chemical and mechanical issues that need to be addressed in a complete evaluation of post-closure safety. This list of issues for the Rebus inserts can be expected to be similar to that for the canister with a cast iron insert since *i*) the insert material is similar (iron alloys), *ii*) the fuel is the same, and *iii*) other aspects of the internal environment in a sealed canister (initial gas composition and water content) are similar. The list of processes should hence be similar, whereas the outcome of the analysis of an issue could differ due to different geometries and material compositions affecting e.g. the mechanical properties and the propensity for criticality.

A list of processes relevant to post-closure safety for the canister with a cast iron insert has been identified based on decades of research and safety assessments. This list is presented in Section 3.2, and reference is given to Sections in the present report where an issue is addressed.

Furthermore, an effort was made to identify additional issues that could be of relevance due to the replacement of cast iron by carbon steel, see Appendix A. Briefly, the result of this effort was that a number of issues of relevance for the present work were found, but that all these have already been identified by the procedures described in the following. In this effort, also issues previously screened out for the cast iron insert were re-visited and evaluated for the Rebus insert.

Finally, it is noted that there are issues related to deviations of the initial state of the repository from that intended. Most aspects of such issues concern other parts than the canister insert and are thus not an issue for the Rebus project. In order to identify and evaluate initial state deviations of the insert, a so called failure modes and effects analysis, FMEA, will be carried out for the Rebus insert. That analysis is, however, not included in the scope of the present report and will be reported in the final, overall reporting of the Rebus project. Should anything of concern for post-closure emerge from the FMEA, that will also be evaluated in the final reporting.

3.2 Processes identified as relevant to post-closure safety for the canister with a cast iron insert

Table 3-1 lists the processes relevant to post-closure safety for the canister with a cast iron insert. The list is taken from SKB (2022b).

The list is the result of decades of research and safety assessments of the KBS-3 repository. One aspect of that work entails the screening of lists of internationally compiled features, events and processes (FEPs) of relevance for post-closure safety in general. A number of canister related issues have then been screened out as being negligible or irrelevant for the canister. The list in Table 3-1 is thus consolidated such that it only contains issues that cannot be readily assessed as irrelevant to post-closure safety. It is also noted that some issues are embedded in other processes in the table, since this is how the issues were structured in the post-closure safety assessment from which the list is taken. Such embedded processes include hydrogen embrittlement and ageing effects of the insert material. This has not precluded a thorough treatment of these issues in the present report, see Chapter 7.

Table 3-1 also provides a mapping of the processes to Sections in this report where the issue is addressed; alternatively it is noted that the treatment of the issue is identical to that for the canister with a cast iron insert.

Table 3-1. Processes relevant to post-closure safety for the canister with a cast iron insert and their treatment for the Rebus canister.

Fuel processes	
Radioactive decay	No difference relative to a canister with a cast iron insert.
Radiation attenuation/heat generation	Chapters 4 and 5.
Induced fission (criticality)	Chapter 9.
Heat transport	Chapter 5.
Water and gas transport in the canister, boiling/condensation	Chapter 6 and Section 10.4.
Mechanical cladding failure	No difference relative to a canister with a cast iron insert.
Structural evolution of the fuel matrix	No difference relative to a canister with a cast iron insert.
Advection and diffusion	Chapter 9.
Residual gas radiolysis/acid formation	Chapter 6.
Water radiolysis	Chapter 6.
Metal corrosion	Chapter 9, as concerns impact on criticality in failed canister.
Fuel dissolution	Impact of hydrogen production in Section 10.2. Otherwise no difference relative to a canister with a cast iron insert.
Dissolution of the gap inventory	No difference relative to a canister with a cast iron insert.
Speciation of radionuclides, colloid formation	No difference relative to a canister with a cast iron insert.
Helium production	Section 10.3.
Chemical alteration of the fuel matrix	No difference relative to a canister with a cast iron insert.
Radionuclide transport	No difference relative to a canister with a cast iron insert.
Canister processes	
Radiation attenuation/heat generation	Chapters 4 and 5.
Heat transport	Chapter 5.
Deformation of canister insert (including creep)	Chapter 8.
Deformation of copper shell from external pressure (including creep)	Chapter 8.
Thermal expansion	Section 5.2.2.
Deformation from internal corrosion products	Section 10.4.
Radiation effects	Section 7.5.
Hydrogen embrittlement of copper	No difference relative to a canister with a cast iron insert.
Corrosion of canister insert	Chapter 9.
Galvanic corrosion	Section 10.4.
Stress corrosion cracking of canister insert	Section 7.2.
Corrosion of copper canister	Corrosion of inner surface of intact canister in Chapter 4. Radiation induced corrosion in Section 10.5. Otherwise no difference relative to a canister with a cast iron insert.
Stress corrosion cracking of the copper canister	No difference relative to a canister with a cast iron insert; new analyses in Section 7.2 relevant also for the latter.
Earth currents – stray current corrosion	No difference relative to a canister with a cast iron insert.
Deposition of salts on the canister surface	No difference relative to a canister with a cast iron insert.

4 Radiation intensity in and around a Rebus canister

4.1 Introduction

The intensity of β, γ and neutron radiation in and around the canister is of relevance for several aspects of post-closure safety. Radiation:

- drives the extent of radiolysis of water and gases in a sealed canister, as discussed in Section 6;
- causes (limited) damage to the canister materials, as further discussed in Section 7.5.2;
- may enhance some embrittlement phenomena like precipitation of impurity clusters and segregation of impurity elements to grain boundaries as evaluated in Sections 7.5.3, 7.5.4 and 7.5.5;
- is crucial for the propensity for criticality, as evaluated in Section 9; and
- determines the extent of copper oxidant production through radiolysis outside the canister and hence gives a minor contribution to corrosion damage of the copper shell, as discussed in Section 10.5.

The radiation intensity outside the canister is also of relevance during encapsulation, transport and operation in the final repository as it puts requirements on protective measures required to achieve a safe working environment.

The radiation intensity is determined by the decay rate of the radionuclides in the fuel and the attenuation of radiation in the canister materials. Comprehensive analyses of radiation intensity exist for the canister with a cast iron insert (Karlsson 2009) and evaluations of radiation related post-closure safety issues, such as radiation damage in the canister materials (Guinan 2001), have shown that these are acceptable for post-closure safety. The fuel is the same for the Rebus canisters as for a canister with a cast iron insert. The copper shell is also the same, and the carbon steel in the Rebus insert has similar radiation attenuation properties as the nodular cast iron in the cast iron insert, since the attenuation is essentially determined by the density of iron that is similar for the two materials.

For the Rebus insert, the presence of the carbon steel tube implies that the radiation intensity in the copper shell and outside the canister vary less with the cylinder azimuth angle than for the cast iron insert. The peak intensity is expected to be somewhat lower and the lowest intensity somewhat higher compared to the values for a canister with a cast iron insert, see Section 7.5. Also, since there is less metal mass in the interior of the Rebus insert, the location in the carbon steel exposed to the highest intensity in the Rebus framework could receive a somewhat higher intensity than the corresponding location in the cast iron insert, see Section 7.5.

The abovementioned differences between the two canisters are not expected to affect the evaluations of radiation effects significantly, but a detailed radiation calculation for the Rebus insert is, nevertheless, required to obtain a well-substantiated basis for the safety evaluation of this insert and to reach a similar level of assessment as for the cast iron insert. In addition, evaluations of neutron radiation intensities dedicated for criticality analyses are discussed in Section 9.

4.2 Basis and methods for dose rate calculations

In order to calculate relevant dose rates to gas, materials and humans for the inserts designs discussed within the Rebus project, a model had been set up based on the chosen canister design, fuel characteristics and surrounding material. The computational method is described by Loberg (2023) and involves the code MCNP (Monte Carlo N-particle) for calculation of particle transport and the SNF code for source term determination. The calculations are performed for quarter canister models.

4.2.1 Canister design

During the initial stages of the Rebus project, different canister designs were developed and evaluated. The dose rate calculations needed to be performed at an early stage, as they were required as input data for other calculations. The canister design used in the dose rate calculations is described by Ronneteg (2022). The design chosen here was later updated and a few details regarding the design were changed: At the time of dose rate calculations, the design included a steel beam to reach the amount of steel required based on criticality analyses. In the later design this steel beam was not required. These details were deemed to be minor with regard to aspects affecting dose rates, and thus the dose rate calculations are also valid for the final selected design (Ronneteg 2025).

Calculations are performed for both BWR and PWR type canisters, see Figure 4-1. Individual fuel pins are included in the model, as is axial distribution of the source, resulting in weaker source terms in the top and bottom of the modelled fuel.

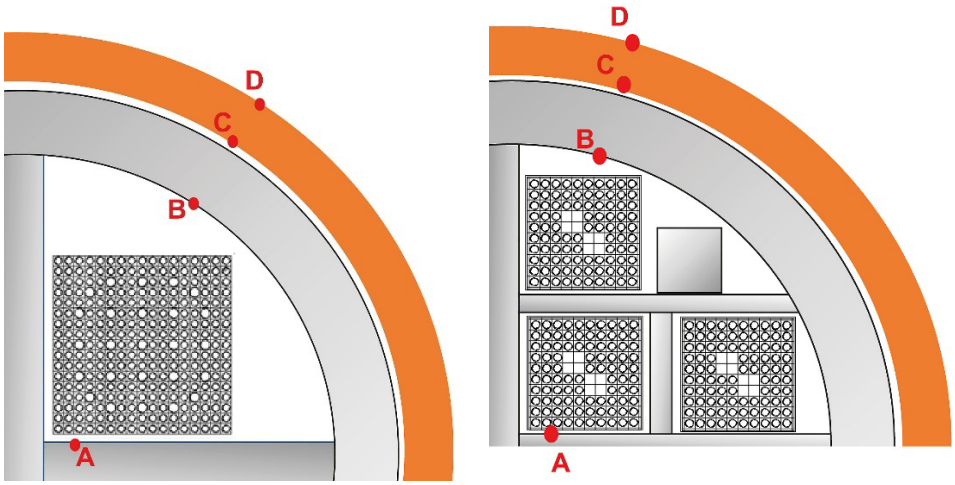

Figure 4-1. *The points in the metal materials for which gamma and neutron doses are determined by Loberg (2023). Left: PWR, Right: BWR. Orange: copper, Grey: steel insert.*

4.2.2 Fuel

For post-closure performance, the following fuels have been considered in the MCNP modelling (Loberg 2023):

High burnup
PWR, 55 MWd/kgU, 20 years decay time at encapsulation
BWR 50 MWd/kgU, 20 years decay time at encapsulation

Low burnup
PWR 30 MWd/kgU, 55 years decay time at encapsulation
BWR 30 MWd/kgU, 60 years decay time at encapsulation

The lower burnup fuels are only used for calculations of the dose to the gas inside the sealed canister.

4.3 Results from dose rate calculations

The results provided by Loberg (2023) relevant to the current report are dose rates to: 1) gas inside the sealed canister, 2) canister materials and 3) gamma and neutron spectra for the BWR and PWR cases.

4.3.1 Dose to gas

The dose rates to gas inside a sealed canister are required for the calculation of gas radiolysis described in Chapter 6. The majority of cases are concerned with the higher burnup fuels for which the average dose rates are modelled in Loberg (2023) to be166 Gy/h (BWR) and 246 Gy/h (PWR). For lower burnup fuels the average dose rates at the time of encapsulation are 39 Gy/h (BWR) and 57 Gy/h (PWR).

4.3.2 Doses to materials

The materials relevant here are mainly the steel components in the canister insert. In addition, dose rates to copper are given by Loberg (2023). Gamma dose rates are given for four different points, identified as the locations of highest dose rate on the steel framework, the steel ring and the inner and outer surfaces of the copper shell. Neutron dose rates, orders of magnitude lower than gamma dose rates, are neglected by Loberg (2023) but are given, based on the Loberg (2023) MCNP model, by Andgren (2023). Gamma and neutron doses as a function of time are given in Figure 4-2 and Figure 4-3, respectively. Note that the bentonite outside the canister acts as a neutron reflector and the dose rate is therefore highest at position D for both the BWR and the PWR canister.

The data for point D, on the copper surface, verify that the radiation dose rate on the canister surface will not exceed 1 Gy/h. For BWR, the gamma dose rate on the copper surface is 0.127 Gy/h at the time of encapsulation, and for PWR the value is 0.0939 Gy/h (Loberg 2023).

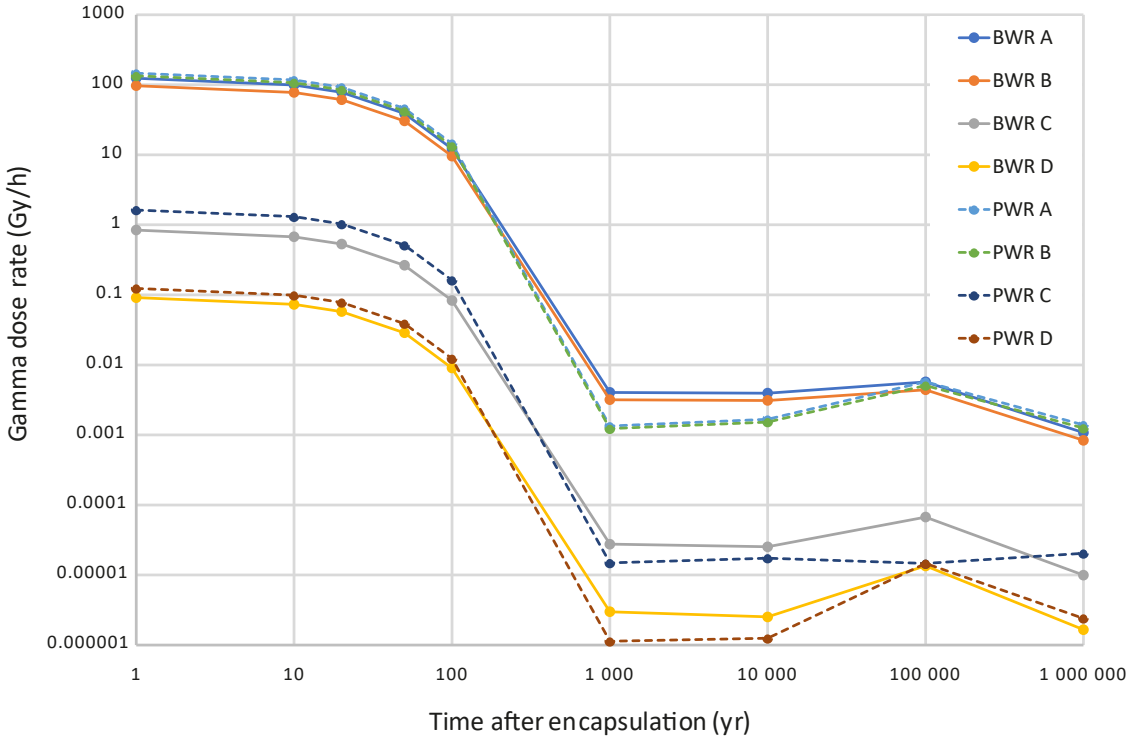

Figure 4-2. *Gamma dose rates as a function of time after encapsulation. Data from Tables 3-3 (PWR) and 3-4 (BWR) in Loberg (2023). Locations A, B, C, and D are defined in Figure 4-1.*

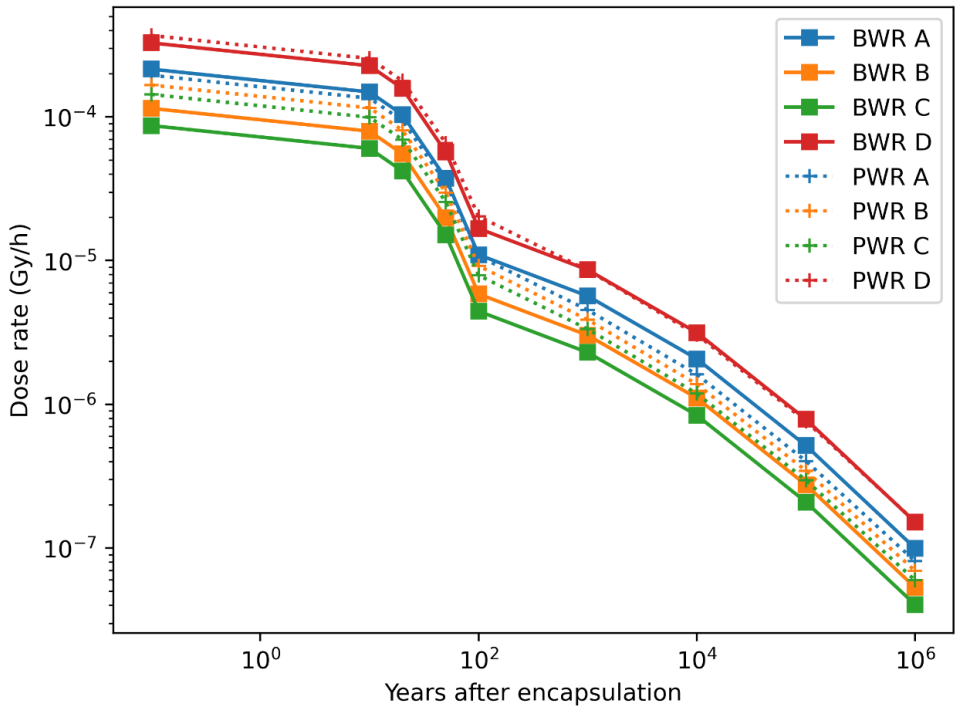

Figure 4-3. *Neutron dose rates as a function of time after encapsulation. Figure 3-2 in Andgren (2023). Locations A, B, C, and D are defined in Figure 4-1.*

4.3.3 Neutron and gamma spectra

For further calculations relating to radiation damage (Section 4.4), the particle flux for different particle energies and decay times are needed, and these are provided by Loberg (2023) for the four points A, B, C, and D. Results for PWR point A are shown in Figure 4-4 and Figure 4-5 for gamma and neutron flux, respectively. The figures show binned fluxes, i.e. summed fluxes in a number of specified energy intervals, bins.

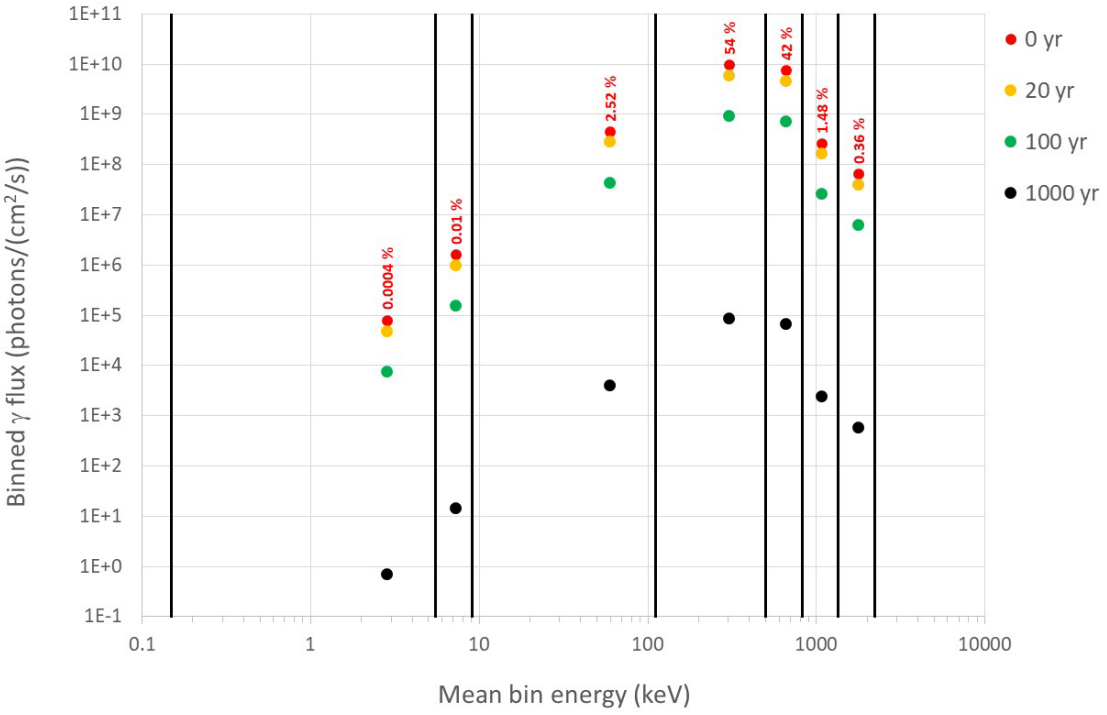

Figure 4-4. *Binned gamma flux over time for PWR position A. The red percent numbers show the fraction of the total flux in each bin at 0 years. The black vertical lines show bin boundaries.*

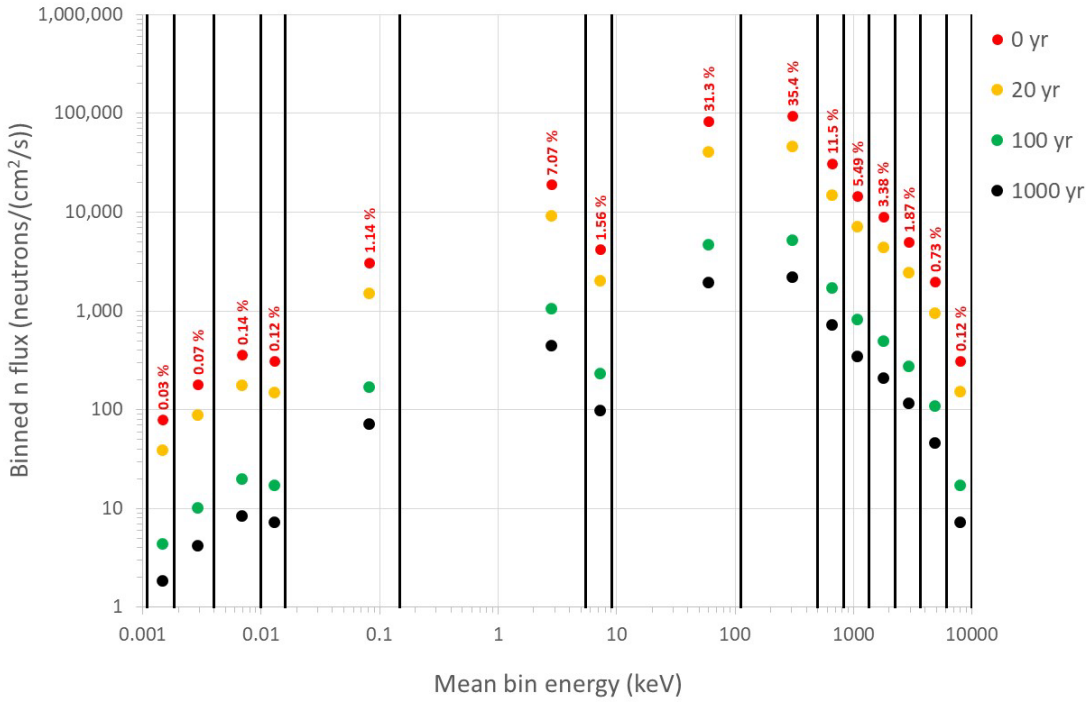

Figure 4-5. *Binned neutron flux over time for PWR position A. The red percent numbers show the fraction of the total flux in each bin at 0 years. The black vertical lines show bin boundaries.*

4.4 Damage rates

The flux of gamma and neutron radiation in the material reported above are used in Andgren (2023) to estimate the rate of displacements per atom (dpa), which can be used to quantify radiation damage in the canister's steel material. The dpa rate describes the rate at which the gamma and neutron radiation creates point defects in the form of Frenkel pairs, i.e. pairs of vacancies and interstitial atoms. The dpa result also forms a crucial input to calculations of e.g. the formation of clusters of Cu atoms emanating from Cu impurities in the steel. Andgren (2023) report dpa rates for gamma and neutrons according to Figure 4-6 for inner (A) and outer (B) canister insert positions of both BWR and PWR spent fuel.

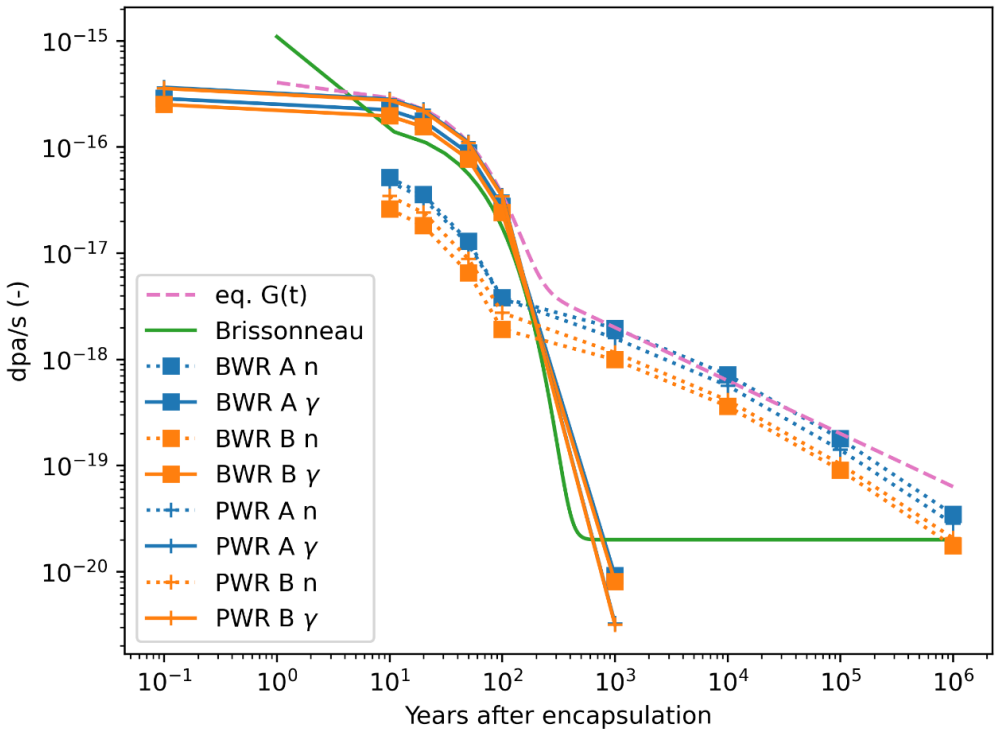

Figure 4-6. *Dpa rates for spent nuclear fuel. The curve "eq. G(t)" shows Eq (1), and the curve "Brissonneau" shows a corresponding curve from earlier work by Brissonneau et al. (2004). Figure slightly modified after Andgren (2023).*

Andgren (2023) also gives an analytical expression for the calculated results (the curve "eq. G(t)" in Figure 4-6):

$$G(t) = b' \exp(y't) + gt^{-0.5} \quad (1)$$

with $b' = 3.52\times10^{-16}$ dpa/s, $y' = -7.886\times10^{-10}$/s and $g = 3.548\times10^{-13}$ dpa/s$^{0.5}$. Here t (s) is the time after encapsulation of the fuel. The last term in Eq (1) is valid for times beyond 300 years and describes the contributions of neutrons to the dpa rate. As seen in Figure 4-6, this expression slightly overestimates R at the most exposed locations in the material. Integration of Eq (1) to 10^6 years gives a total dpa of 3.7×10^{-6}. It is noted that radiation-induced vacancy concentration as a function of time will, due to recombination effects and the presence of vacancy sinks, in general be much lower than the total dpa obtained by integrating Eq (1).

4.5 Conclusion

Gamma and neutron dose rates and the related damage rates have been determined for the two Rebus inserts. The results are similar to the corresponding results for a canister with a cast iron insert and are used in the evaluations of radiolysis in the gas phase of the insert void in Chapter 6 and of effects of radiation on material properties in Section 7.5.

5 Thermal and hydrological evolution in a sealed canister

5.1 Introduction

The evolution of the thermal and hydrological conditions in a sealed canister is of importance for several phenomena of relevance for the post-closure performance of the canister insert. The temperature affects virtually all such phenomena and the potential formation of detrimental species through radiolysis is strongly dependent on the hydrological conditions in the insert. In the following, the thermal evolution is discussed in Section 5.2, and the hydrological conditions are discussed in Section 5.3.

5.2 Thermal evolution

The temperature of the canister interior needs to be assessed as it affects e.g. the evolution of gases and liquids in the early stages after deposition and material properties in general. The thermal evolution in the Rebus inserts is expected to be similar to that in the cast iron insert, since i) the fuel types and thereby the heat load will be the same, and since ii) much of the Rebus insert is solid metal materials with a high heat conductivity, and iii) the conditions exterior to the canister are the same. There are, however, differences in particular as concerns the gaps and voids between the Rebus inner carbon steel framework and the outer steel tube; such gaps and voids are not present in the cast iron insert.

There are no design requirements on the temperature of the insert or the fuel for post-closure conditions. However, during interim storage and encapsulation, it is required that the fuel cladding temperature does not exceed 400 °C for normal operation, to ensure the integrity of the cladding.[10] For post-closure conditions, this could also formally be seen as a cladding temperature that should not be exceeded, even though the consequences of the much lower temperatures expected for the fuel for post-closure conditions need to be assessed. In a post-closure safety assessment it should, moreover, be verified that the mechanical analyses of the insert are valid for the temperature ranges obtained in the thermal analysis of the canister. The main mechanical loads occur as asymmetric and isostatic loads in early stages of the repository development, isostatic loads during glacial conditions and as shear loads in the event of a large, predominantly post-glacial earthquake in the vicinity of the repository. For the latter two, it is noted that the peak canister temperature will occur long before such loads are expected in the repository. The validity of the mechanical analyses for the expected temperature range in the repository is discussed in Section 8.3.5.

The internal temperature of the canister and the fuel is also relevant for the analyses of radiolysis effects in the sealed canister, see Chapter 6. Another temperature-related aspect in a sealed canister is the rate of release of water remaining in fuel pins with damaged cladding. As suggested by the reports discussed in Hedin (2025), this process is highly temperature dependent and it is of interest to estimate the range of fuel rod temperatures in the canister.

It is also noted that the temperature evolution of the copper shell and the system parts exterior to the canister is independent of that of the canister interior. The exterior evolution is determined by the residual power of the fuel, the external geometry of the canister, the canister spacing in the repository and the thermal properties of the repository system exterior to the canister. Since all these factors are the same for canisters with Rebus and with cast iron inserts, the external temperature evolution will also be the same.

In this Chapter, the steady-state internal temperature distribution in Rebus BWR and PWR canisters for a set copper shell temperature of 100 °C and a fixed residual power of 1700 W is analysed numerically in Section 5.2.1. The temporal evolution of the interior temperature distribution is then obtained by applying to the numerical canister model a set of copper shell temperatures and residual power values from an analytical model used in earlier assessments of the repository thermal evolution. Thermal expansion effects caused by the temperature developments are discussed in Section 5.2.2 and conclusions are provided in Section 5.2.3. The procedure is described in more detail in Appendix B.

[10] **Annell A, 2020.** Konstruktionsstyrande krav Clink utifrån Kärnsäkerhetsperspektiv. SKBdoc 1866397 ver 4.0, Svensk Kärnbränslehantering AB. (Internal document, in Swedish.)

5.2.1 Thermal development of the Rebus canister and fuel

Steady-state temperature distribution for a postulated copper shell temperature of 100 °C and a fixed residual power of 1700 W

As a first and bounding case, a situation is considered where the copper shell is postulated to have a steady temperature of 100 °C, the maximum temperature allowed in the bentonite in contact with the copper surface in the final repository. The residual power is fixed at 1700 W, the maximum allowed in a canister. Such cases were analysed for the cast iron BWR and PWR canister inserts for a range of fuel types in a numerical study by Ikonen (2020). Results of 2D modelling in Ikonen (2020) are used as benchmark cases for the canisters with cast iron inserts below.

A numerical 2D model is used to obtain results for the Rebus canister. The numerical model, described in Appendix B, is similar to the 2D model used by Ikonen (2020). In both models convection is neglected, and all residual power in the fuel is assumed to be released as heat energy in the fuel rods, whereas in reality, a minor part of this energy will exit the fuel rods as gamma radiation that will mostly be deposited in the metal parts of the canister (Renström 2020). The same pessimistically simplifying assumptions are made by Ikonen (2020). Furthermore, Ikonen (2020) demonstrated that the use of this type of 2D models yields pessimistic, i.e. slightly higher, peak temperatures compared to a 3D model.

Data on thermal properties of the materials are taken from Ikonen (2020). The residual power is assumed to be 1700 W, the maximum allowed in a canister. In accordance with Ikonen (2020), the power is multiplied by a factor of 1.16 (BWR) and 1.06 (PWR) to account for the fact that the power is unevenly distributed in the vertical direction, such that the peak power occurs at mid-height. The size of the gaps between the framework and the outer tube in the Rebus inserts are set to 1.65 and 2.7 mm for the Rebus BWR and PWR inserts, respectively, in accordance with the data given in Section 2.2.1.

Results for the BWR and PWR inserts are presented in Table 5-1, showing also benchmark results for BWR and PWR canisters with cast iron inserts that are compared to those in Ikonen (2020). As seen in the table, the models give similar results in locations where they are compared. Generally, the Rebus BWR and PWR inserts have central temperatures that exceed those of the cast iron inserts by 20–25 °C. This is essentially caused by the temperature differences over the gaps between the insert framework and the outer tube. As a consequence, the temperatures of the fuels are up to 20 °C higher in the Rebus canisters.

Table 5-1. Calculated temperatures in Rebus BWR and PWR canisters and in canisters with cast iron inserts. All temperatures in °C. Values given with unrealistically high precision to facilitate comparison between models. Red: 2D numerical model (Appendix B); Green: 2D numerical model (Ikonen 2020).

	Cast iron BWR	Cast iron PWR	Rebus BWR	Rebus PWR
Copper shell (set temperature)	100	100	100	100
Insert/tube outer surface	111.8 111.2	110.1 110.2	- -	- -
Insert/framework centre point	116.1 115.0	113.0 112.7	140.1 -	134.5 -
Inner fuel pins	138.8 135.0	166.8 165.4	158.6 -	175.1 -

Thermal development in a repository environment

To obtain the thermal development inside the Rebus canisters in a repository environment, an analytical model (Hedin 2004) used in earlier assessments of the repository thermal evolution is utilised. This model simulates the thermal development in the buffer and the host rock. Heat contributions from all other canisters in the repository are included. A set of pairs of values of copper shell temperature and fuel residual power obtained from the analytical model when applied to the host rock conditions at the Forsmark site are applied to the numerical model described above, see further Appendix B. (The analytical model is capable of approximately accounting for the canister interior development for the cast iron BWR insert, but not the more complex internal structures of the Rebus inserts.)

Figure 5-1 shows the thermal development of a BWR canisters with a Rebus and a cast iron insert, located centrally in the repository, where the heat contributions from other canisters is highest. Figure 5-2 shows the corresponding data for PWR canisters.

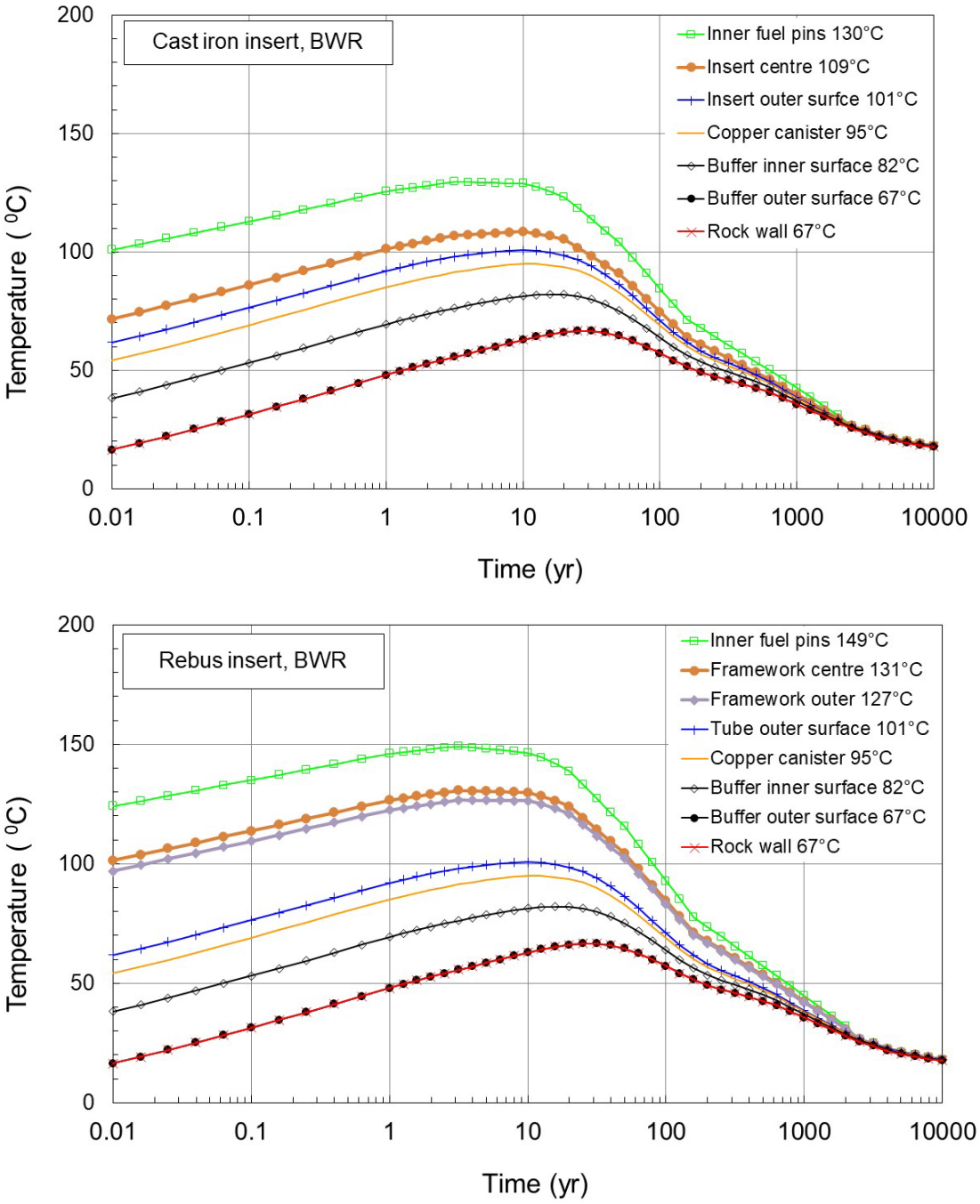

Figure 5-1. *Thermal development of a BWR canister with a cast iron insert (upper) and a Rebus insert (lower) in the repository environment. Peak temperatures for each component are shown in the legend. Site data from Forsmark. Note that the curves representing the tube and the insert outer surface in the two graphs are virtually identical, as are all pairs of curves representing points outside the inserts.*

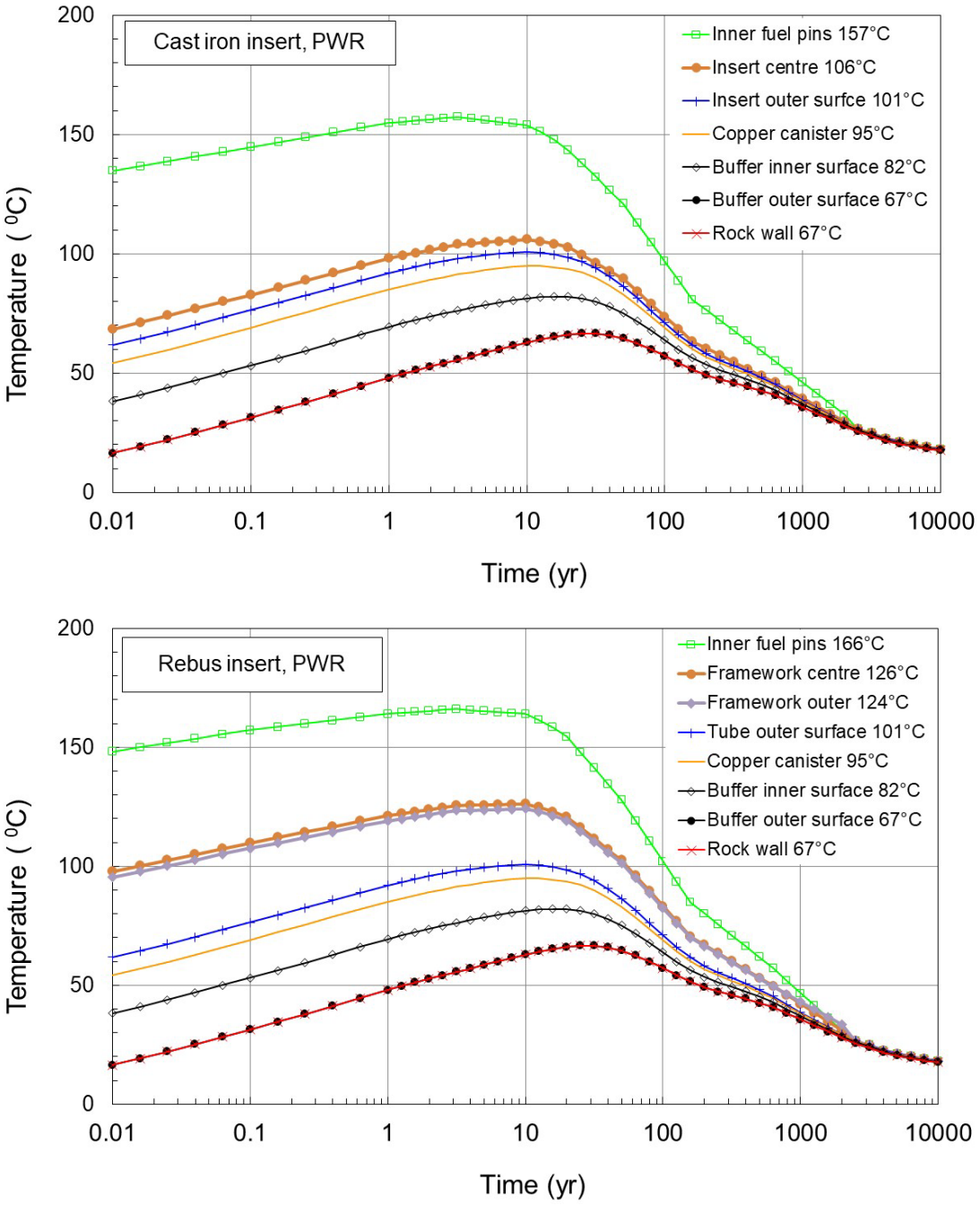

Figure 5-2. *Thermal development of a PWR canister with a cast iron insert (upper) and a Rebus insert (lower) in the repository environment. Peak temperatures for each component are shown in the legend. Site data from Forsmark. Note that the curves representing the tube and the insert outer surface in the two graphs are virtually identical, as are all pairs of curves representing points outside the inserts.*

Host rock thermal data are representative of the Forsmark site in which SKB is planning to build a final repository for spent nuclear fuel. The layout of canister positions is made such that the peak temperature in the buffer is lower than 100 °C with a margin. In about 10 000 years the whole system has attained a temperature that is slightly above the 11 °C background temperature of the host rock.

The peak temperatures are lower than the steady state temperatures reported in the above sub section primarily since it takes about 10 years to reach the peaks, in which time the residual power has decreased and, to a lesser extent, since the factors introduced to capture the highest temperatures in the vertical direction for the canister interior are not included in the modelling of the repository development.

The inner parts of the fuel in a Rebus framework are calculated to reach peak temperatures of about 149 °C (BWR) and 166 °C (PWR) in the final repository. That is some 20 °C (BWR) and 10 °C (PWR) higher than for the cast iron insert, due to the higher temperature of the framework. The somewhat higher temperatures are assessed as being of no concern for the mechanical integrity of the fuel cladding in the sealed canister, based on results in Alvarez Holston (2021).

It may also be of interest to consider a lower limit on the temperature of the fuel pins, since this is of relevance for the rate of release of water from a damaged fuel pin, which in turn is of importance for the assessment of radiolysis-related processes in a sealed canister, see Chapter 6. Here, it is noted that *i*) the outer fuel pins in any assembly will have temperatures that are marginally higher than that of the insert material irrespective of insert concept; shown for the canister with a cast iron insert in the more detailed modelling in Ikonen (2020), and *ii*) some insert temperatures may be considerably lower than those reported above since in reality not all canisters will be filled with fuel assemblies with a total residual power of 1700 W, the maximum allowed in the final repository, and since canisters in a peripheral location in the repository will be less heated by surrounding canisters. In the calculations in Section 5.3, the peak temperature of the framework is used as a lower limit of the fuel temperature.

5.2.2 Thermal expansion

Thermal expansion of carbon steel framework

As seen in Table 5-1, the temperature in a Rebus framework may exceed that of the steel tube by up to 25 °C, both for the postulated steady state conditions considered in Section 5.2.1 and for the development in a real repository (Figure 5-2).

The thermal expansion coefficient of carbon steel is can be taken to be the same as that of cast iron given in SKB (2022a, Section 3.4.4) as 1.17×10^{-5} m/(m °C). A plate across the diameter of the steel tube (0.789 m) increasing in temperature 25 °C more than the tube thus expands $1.17\times10^{-5}\times0.789\times25$ m $\approx 2\times10^{-4}$ m more than the inner diameter of the tube. If the gap between the plate and the steel tube is initially 1.7 mm, the width would thus be reduced by about 10 % due to thermal expansion. It is noted that a reduction of the gap width yields a more efficient heat transfer to the tube and thus a reduction in plate temperature and consequently in plate thermal expansion. This negative feedback further implies that this type of minor thermal expansion of the framework is not expected to jeopardise the function of the framework. It is, furthermore, noted that in reality not all gaps in the model are expected to exist, due to deviations from ideal alignment of the inner framework. This effect has not been analysed but should result in somewhat lower framework temperatures.

Thermal expansion of insert relative to the copper shell

The clay buffer surrounding the canister in the repository is expected to become water saturated at a time that may vary from around 10 years to several thousand years, depending on the hydraulic conditions at the position of the canister (SKB 2022c, Section 10.3.8). At saturation, the buffer develops a swelling pressure that will exert a force on the canister. This may close the radial gap between the insert and the copper shell due to creep or plastic deformation. The size of the gap when the swelling pressure is developed will depend on the canister temperature, as the copper shell and the insert undergo thermal expansion when the canister temperature changes. The expansion coefficient of copper is larger than that of the insert material. As seen in Figure 5-2, the canisters reach their maximum temperature in the repository after about 10 years, and hence the gap size is also largest at this time. If the gap is closed by the swelling pressure at a high temperature, the subsequent cooling to ambient temperature will cause a tensile strain in the copper shell since the copper will shrink more than the insert when the temperature is decreasing.

The extent of this effect has been estimated for the canister with a cast iron insert, and found to yield a strain of about 0.05 % in the copper shell, which was deemed to be negligible in comparison to the creep ductility of copper (SKB 2022a, Section 3.4.4). Jonsson et al. (2018) arrives at a strain of about 0.026 % assessed for a temperature difference of 50 °C, whereas SKB (2022a) considers a difference of 90 °C which appears more realistic considering e.g. the results in Section 5.2.1.

Since the initial gap size in the Rebus design is the same as that of the design with a cast iron insert, and since the materials have similar thermal expansion coefficients, the effect is also deemed to be negligible for the Rebus canister.

A more complete numerical treatment of the phenomenon could yield a more definite assessment, for both the design with a cast iron insert and the Rebus canister.

5.2.3 Conclusions

The following is concluded regarding the thermal evolution of the Rebus canisters.

- The Rebus outer steel tube is expected to reach a peak temperature very similar to that of the outer parts of the cast iron insert, for both BWR and PWR inserts.
- The Rebus insert framework is expected to reach peak temperatures that are around 20 °C higher than the inner parts of the cast iron insert in the final repository, for both BWR and PWR inserts. This is due to the gaps between the steel tube and the insert plates. These peak temperatures are upheld for some tens of years in the final repository.
- The minor thermal expansion of the Rebus framework is not expected to jeopardise the function of the framework.
- The thermal contraction of the copper shell relative to that of the insert as the canister temperature decreases is assessed as yielding negligible strains in the copper shell. A more complete numerical treatment of the phenomenon could yield a more definite assessment, for both the design with a cast iron insert and the Rebus canister.
- The somewhat higher temperatures of the inner fuel pins for the Rebus insert compared to the cast iron are assessed as being of no concern for the mechanical integrity of the fuel cladding in the sealed canister. (The requirement of a maximum cladding temperature of 400 °C, applicable during interim storage and encapsulation, is fulfilled with a wide margin in all post-closure situations.)

5.3 Hydrological evolution

5.3.1 Introduction

In the following, the hydrological conditions in a sealed canister are discussed, addressing primarily the time period during which gamma radiation is sufficiently intense to affect these conditions, i.e. up to around 300 years after sealing of the canister. These conditions are of key importance for e.g. the development of the chemical conditions in the insert void, including radiolysis in the gas phase. A more detailed evaluation of radiation-related processes is made in Chapter 6. The focus in the present Section is rather on factors important for the outcome of such processes; such factors are identified in, e.g., Henshaw and Spahiu (2021).

A summary account of processes of relevance for the hydrological evolution is given in Hedin (2025), based on a number of underlying sources. It is concluded that the hydrological conditions in the canister interior are determined primarily by the initial water content, the release rate of water from leaking fuel pins and the consumption of water in corrosion processes, while radiolytic processes are of minor importance. Therefore, the hydrological development can be modelled without consideration of radiolytic processes, or with a simplified representation.

A coupled model of the internal evolution has been set up. It addresses (Hedin 2025):

- the temperature development according to Section 5.2.1,
- water release from leaking fuel pins,
- evaporation/condensation,
- oxic and anoxic corrosion of the iron/steel surfaces by water,
- water consumption by radiation with a simplified expression, and
- the pressure development as determined by all the above processes.

Key uncertainties identified for the hydrological evolution concern:

- the initial amount of water,
- the release rate of water from a leaking fuel pin as determined by the gas permeability in the pin, and
- the dependence of steel and iron anoxic corrosion rates on relative humidity (RH).

Two base cases and a number of cases to address uncertainties are modelled in Hedin (2025). Base case 1 is a bounding case with 600 g of water initially present in a canister with a cast iron insert. Base case 2 is more realistic and concerns a situation with:

- two leaking fuel pins, with different temperature developments based on their different positions in the insert and each pessimistically assumed to contain 40 g of water initially,
- no oxic or anoxic corrosion below RH = 20 %, and a linear increase to full corrosion rates at RH = 60 %, and
- a best estimate value of the gas permeability in the leaking fuel pins.

As a representative example, results of the more realistic base case 2 are presented below. Base case 1 and most other cases exhibit similar trends as base case 2.

5.3.2 Results of Base Case 2

Figure 5-3 shows the development for the initial three years after encapsulation for Base case 2. The temperature is constant in the first year, during which the sealed canister is assumed to be transferred from the encapsulation facility to the deposition hole in the final repository. There is no free water initially, but the temperature of the hotter leaking fuel pin is sufficient for water to be released at the prevailing pressure. After about 0.4 years the RH reaches 20 % and oxic corrosion commences and continues until around 0.5 years when all oxygen is consumed. The rate is determined by the rate at which water is supplied from the leaking hot fuel pin, and the RH never exceeds 20 %. After one year the temperature increases since the canister is now in the final repository. As a consequence water is also released from the cooler leaking pin. The increasing temperature leads to a decrease in RH below 20 % and the corrosion ceases. The water in the hotter pin is released at an almost constant rate and all water is released during the first ca. 0.5 years. The water in the cooler pin is released at a similar rate starting after one year and continuing for about 0.6 years. These releases are the cause of the two increases of the green “nH2OVapor” curve in Figure 5-3. The first increase is interrupted when RH reaches 20 % and further releases from the hotter pin are consumed by corrosion, whereas the second increase fully reflects the release from the cooler pin, since RH never reaches 20 % during that release.

Figure 5-4 shows the development for the initial 30 years after encapsulation for Base case 2. The development at the end of the initial three year period continues; the RH is below 20 % meaning that no corrosion occurs. A small amount of water is consumed by radiation related reactions.

Figure 5-5 shows the development for the initial 300 years after encapsulation for Base case 2. After about 75 years the temperature has decreased to such a level that RH reaches 20 % and corrosion recommences, the rate being determined by the condensation rate controlled by the decreasing temperature.

Figure 5-6 shows the development for the initial 3000 years after encapsulation for Base case 2. The development during the initial 300 years continues, and not even in the 3000 year time frame is all of the water consumed. The development beyond the point where the RH is held at 20 % through a balance between corrosion and increasing RH due to the slow temperature decrease is very similar to that of other several cases modelled. Once this phase is reached, the development is determined by the temperature; the amount of water in vapour phase will be proportional to the void volume at a given temperature, but independent of the corrosion rate.

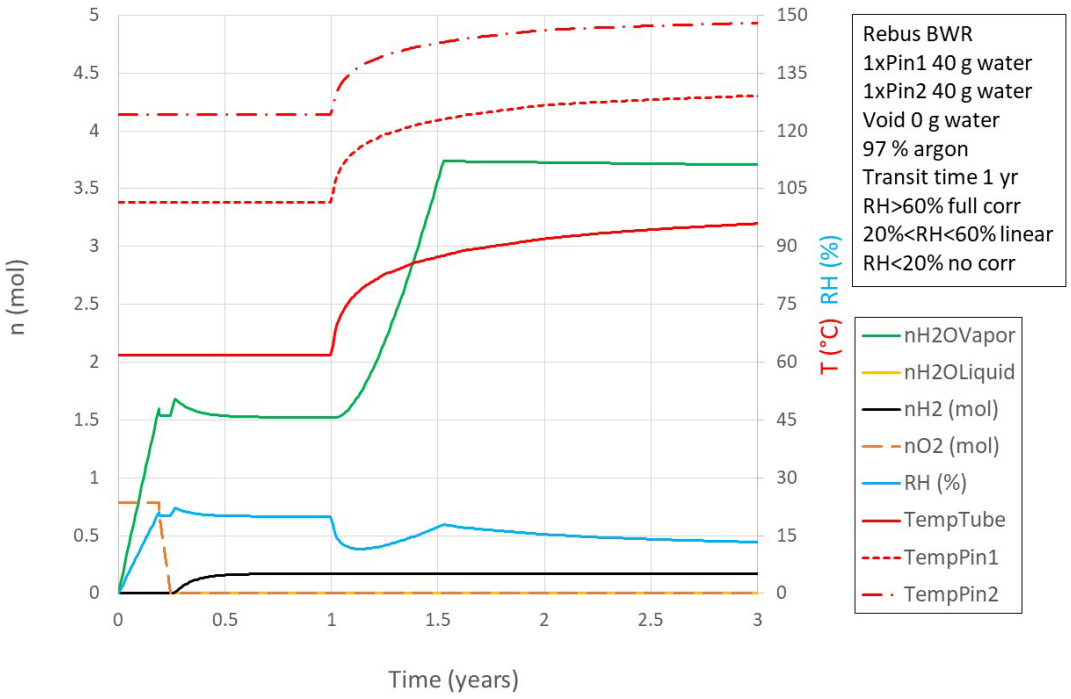

Figure 5-3. *Base case 2, initial 3 years. Left axis: Amounts (mol) of water in liquid and vapour phase, of O_2 and of generated hydrogen gas. Right axis: RH (%) and temperatures (°C) of the insert and of a hot and a cool fuel pin.*

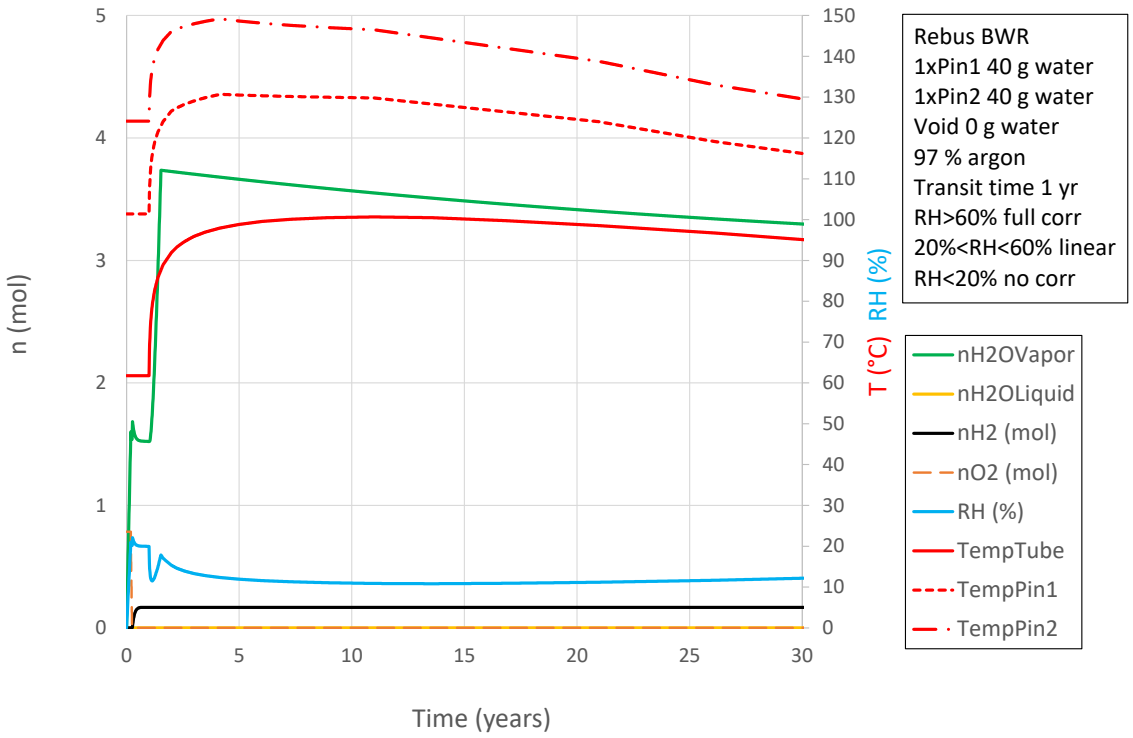

Figure 5-4. *Base case 2, initial 30 years. Left axis: Amounts (mol) of water in liquid and vapour phase and of generated hydrogen gas. Right axis: RH (%) and temperatures (°C) of the insert and of a hot and a cool fuel pin.*

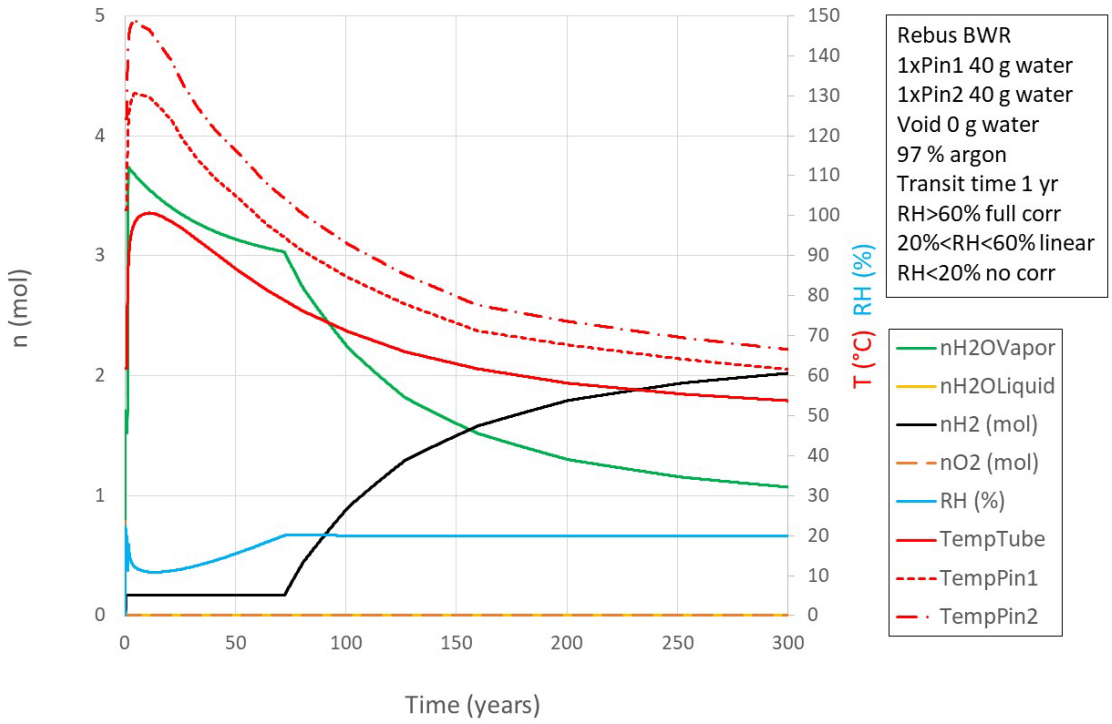

Figure 5-5. *Base case 2, for the period 0–300 years. Left axis: Amounts (mol) of water in liquid and vapour phase and of generated hydrogen gas. Right axis: RH (%) and temperatures (°C) of the insert and of a hot and a cool fuel pin.*

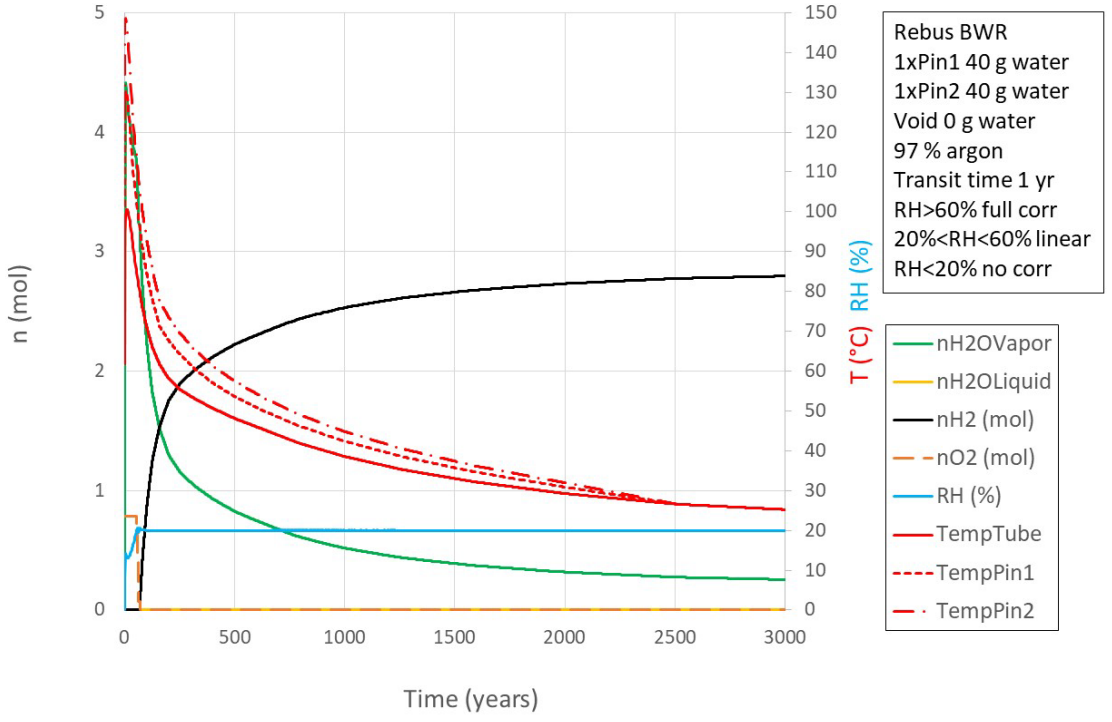

Figure 5-6. *Base case 2, for the period 0–3000 years. Left axis: Amounts (mol) of water in liquid and vapour phase and of generated hydrogen gas. Right axis: RH (%) and temperatures (°C) of the insert and of a hot and a cool fuel pin.*

5.3.3 Conclusions

The following conclusions are drawn from the Base case 2 results in Section 5.3.2 and the further cases analysed in Hedin (2025):

- Most cases modelled exhibit general trends in line with the above Base case 2.
- Uncertainties regarding gas permeability in a leaking fuel pin affects the rate at which water is released, but not the general trends of the development.
- The largest impact on the development is caused by uncertainties in the dependence of corrosion rates on RH. With the assumptions made in Hedin (2025), based on available information in the literature, water could be completely consumed within one or a few years. Alternatively, no corrosion could occur for decades if the threshold RH for corrosion is > 20 %, until the cooling of the system causes a sufficient increase in RH for corrosion to occur, and then at a slow rate.
- Irrespective of the corrosion rate, the amount of hydrogen that could be released through corrosion in the long term and hence contribute to hydrogen absorption by the insert materials (see further Section 7.3) is determined by the initial amount of water.

Additional data on relevant corrosion rates are given in a recent reference (Sarrasin et al. 2024). A first review suggests that these are encompassed by the cases studied in Hedin (2025) and by the uncertainties discussed in the third bullet point above.

In addition, it is noted that the differences between the cast iron and the carbon steel inserts are limited. Such differences are caused by the limited differences in geometry (Table 2-2 and Table 2-3) and temperature (Section 5.2.1), whereas all other aspects like water content, corrosion rates etc are common to both types of inserts.

It is also noted that most of the canisters are expected to contain no leaking fuel pins, see Section 2.3.

6 Radiolysis calculations of air, argon and water mixtures in a Rebus canister

6.1 Introduction

Gases and liquids in a sealed canister may affect both the inner surface of the copper shell, the insert and the fuel. Initially, the gas mixture in the canister will consist of approximately 97 percent argon and 3 percent air, according to the design premises, whereas the production system is aiming at an argon content of 99 percent, see Section 2.3. The maximum amount of water allowed in a sealed canister is 600 grams, and the vast majority of canisters are expected to contain considerably less water (Section 2.3). No other liquids are expected to be present in any appreciable amount initially.

The composition of gases and liquids will evolve over time due to interactions with the canister materials, homogeneous and heterogeneous chemical reactions and radiation-related effects. The evolution will depend on temperature and radiation intensity.

6.2 Evolution for a canister with a cast iron insert

6.2.1 Modelling by Henshaw and Spahiu (2021)

The evolution of gas compositions in a canister with a cast iron insert has been modelled in detail by Henshaw and Spahiu (2021).

The simulation model yields the gas phase concentrations of potential aggressive species such as HNO_3, NH_3 and H_2O_2 produced from the radiolysis chemistry of Ar-air-water gas mixtures. Neither radiolysis of liquid water nor partitioning of radiolytic species between liquid and gas are considered in the model. The issue of concentrations in the liquid water phase is further discussed in section 7.2.2. Inside the canister, corrosion of the cast iron surfaces is expected to occur, consuming O_2, H_2O and generating H_2, and the model also simulates these processes and their effect on the radiolysis chemistry. The model was validated against laboratory radiation studies on Ar-air-water type mixtures and then applied to the KBS-3 canister.

Fifteen cases with different combinations of initial water content (6.7, 244 and 600 g), initial Ar/air volume ratio (9/1 and 99/1), aerobic iron corrosion rate (0, 0.2 and 0.4 mm/yr) and anaerobic iron corrosion rate (0 and 0.003 mm/yr) were modelled for the cast iron insert in Henshaw and Spahiu (2021). Generally, the evolution is characterised by an initial oxic corrosion phase that lasts a few hours until all oxygen is consumed, followed by an anoxic corrosion phase that lasts until all water is consumed, which takes of the order of one year. After the anoxic corrosion phase the gas phase evolves further governed by the decreasing radiation intensity and temperature of the system. (For cases where no corrosion is assumed, there is of course only the development of the latter phase.) During all these phases potential aggressive species are formed in a complex scheme of reactions where different reactions dominate in the different phases.

The main conclusions were (here slightly reformulated):

- In the absence of iron corrosion, the amounts of nitric acid formed inside the canister may be significant.;
- The amount of nitric acid formed is smaller for a smaller initial air content;
- The presence of aerobic steel corrosion followed by anaerobic corrosion reduces the amount of nitric acid formed by many orders of magnitude;
- Anaerobic corrosion in the canister may lead to reducing conditions and the formation of ammonia. The water initially present in the system is consumed by the corrosion process and when ammonia reaches its peak concentration there is no water in the system. At high water content (600 g) and high air (10 %) there is a period when water and ammonia are present simultaneously.

Both nitric acid and ammonia is of concern for stress corrosion cracking, in both the insert and copper shell, see further Section 7.2.

6.2.2 Assessment of impact of post-closure safety for a canister with a cast iron insert

The results of the recent modelling of the cast iron insert interior by Henshaw and Spahiu (2021) are incorporated in the assessment of post-closure safety provided in SKB (2022c). Consequences for post-closure safety are taken from Spahiu (2021) who concludes the following:

"*…600 g water is acceptable for the canister even in the presence of 10 % air, with the reservation that this involves a ~ 150-day period during the first 1.6 years with the coexistence of water and ammonia. Ammonia could potentially alter the corrosion behaviour of canister materials. There is no such reservation for 600 g water, if air can be kept below 1 %. In conclusion, 600 g water is acceptable for the canister, with no reservation if air is below 1 %.*" … "*No literature data could be found on any long-term effects of small amounts of dry ammonia (< 22 mg/l) present in the canister atmosphere for the fuel or the canister materials.*"

Spahiu (2021) also concluded that the oxidants produced by 600 g residual water "*would oxidize a negligible part of fuel with breached cladding*".

6.3 Evolution for Rebus canisters

Since the work by Henshaw and Spahiu (2021) for a canister with a cast iron insert, the model has been adapted for the Rebus insert (Henshaw and Evins, 2023). For the Rebus canister, modelling has been performed separately for BWR and PWR canisters while previous models used values assumed representative of both canister types. The void volume and steel area available for corrosion are important parameters for these calculations and these differ between the cast iron inserts and the Rebus inserts. The different geometries may influence the amount of corrosive species formed (Henshaw and Spahiu, 2021). It could also influence the time period when water and ammonia and other nitrogen-containing species can exist simultaneously. The gas volume directly correlates to the initial amounts of N_2 and O_2, and also gas phase concentrations of species originating from the initial amount of water, e.g. of H_2 in the post-corrosion phase. As in Henshaw and Spahiu (2021), the modelling in Henshaw and Evins (2023) only concerns radiolysis of the gas phase. It is additionally noted that galvanic corrosion between different parts of the Rebus insert due to the different grades of steel used for the tube, the lid/base and the framework is assessed to be negligible. A main reason for this is the very limited differences in corrosion potential between the materials; such differences are judged to be of the order of mV or less.

6.3.1 Initial canister conditions

The following data have been used in the Rebus modelling:

- Initial gas temperature: 85 °C for BWR and 110 °C for PWR. A few PWR cases uses a lower temperature of 70 °C to investigate effects of initial liquid water. The initial temperature used by Henshaw and Spahiu (2021), for the cast iron insert, was 70 °C.
- Initial dose rate to the gas phase: For Rebus the dose rate to gas is based on calculations from Loberg (2023), giving representative values of 166 (BWR) and 238 (PWR) Gy/h. A couple of calculations use a low dose rate of 39 and 57 Gy/h, respectively. Henshaw and Spahiu (2021) used a dose rate of 310 Gy/h.
- Initial gas composition: For the Rebus base case an Ar content of 90 % was used. Other calculation cases assume 95 %, 98 % and 99 %. The rest is air in all cases.
- Initial water content of the canister: For the Rebus base case 600 g water is assumed. Other calculation cases assume 30 g and 0 g initially in the void. For the latter cases 600 g and 30 g water are then assumed to be released slowly to the void from failed fuel rods.

- Gas volume and available area for corrosion: The void volume in the BWR and PWR Rebus inserts are around 1.2 m^3 for BWR and 1.4 m^3 for PWR compared to around 1 m^3 for the cast iron inserts. Excluding the volume between the insert and the copper shell, the values are 1.0 and 1.2 m^3 (Table 2-3). The corroding carbon steel area in the BWR and PWR Rebus inserts are around 69 m^2 for BWR and 43 m^2 for PWR compared to around 35 m^2 for the cast iron design. Excluding the outside area of the steel tube (between steel and copper) the values are 54 and 28 m^2, according to the design version given by Ronneteg (2022). These deviate slightly from values given in Table 2-2 but the changes are deemed insignificant for the calculations performed here. The area-to-volume ratio is hence somewhat higher for the Rebus BWR insert compared to that of the cast iron design, while the opposite is true for PWR.

6.3.2 Summary and discussion of results

In total 31 cases were modelled: 15 BWR cases and 16 PWR cases. The resulting data are available internally at SKB[11].The cases explore effects of varying the initial values of dose rate, temperature, water content, gas composition, area and volume, and various assumptions regarding the rate and threshold RH for corrosion. The results express the evolution of the gas composition inside the intact canister for 500 years. Oxidative and corrosive species are formed and consumed via radiolysis and Fe corrosion, and the results allow identification of both the maximum amount of various species formed, and the time periods when liquid water and corrosive species co-exist. Of particular interest for effects on canister materials are compounds containing nitrogen, specifically nitrate, nitric acid and ammonia (see Section 7.2). Here, an overview of the results provided by Henshaw and Evins (2023) is presented and discussed. The main focus of the study is the production of aggressive nitrogen compounds, and to what extent these co-exist with oxygen, hydrogen peroxide and water. For more-detailed discussion relating to the effect on stress corrosion cracking, see Section 7.2.

Base case results

The base cases involve an initial amount of 600 g water and 90 % Ar. It should be noted here that the requirement is a minimum of 97 % Ar, while the canister production target is 99 % Ar, see Section 2.3. The effects of varying the amount of air are discussed below. It should also be noted that 600 g water is the maximum allowed according to the current technical design requirement; the effect of lower, more realistic water content is discussed below.

Results for BWR base case 2a (case nomenclature from Henshaw and Evins (2023)) are shown in Figure 6-1. In agreement with results in Henshaw and Spahiu (2021), Fe corrosion quickly consumes oxygen, and anoxic Fe corrosion produces hydrogen gas. As a result, once oxygen and hydrogen peroxide are consumed, nitrogen will be found mainly in the form of ammonia rather than as nitric acid or other oxygen-containing nitrogen compounds. Thus, ammonia does not co-exist with either oxygen or hydrogen peroxide. Before this time, which for base case 2a (BWR, Figure 6-1) and 13a (PWR) happens before 10 days, there is HNO_3 and HNO_2 in the gas phase together with some oxygen and hydrogen peroxide. The oxygen is, however, consumed in a few hours, at which point hydrogen peroxide starts to form; the maximum amount of hydrogen peroxide formed is ca 5.8×10^{-4} mol.

The Rebus canister base case results show that ammonia and water coexist for in total 300 days (BWR); for that time water is in the gas phase. There is no liquid water, such as a droplet or a pool of water (i.e. 100 % RH), in which aggressive species could be dissolved when ammonia starts to form. However, there is a possibility that a thin liquid water film could be formed on the insert surfaces at high relative humidity. Exactly at what relative humidity this happens is uncertain, but one can assume that when the relative humidity is above 60 %, corrosion can occur with a similar mechanism and at equal rates as in the presence of liquid water (see Section 5.3), noting that also these rates are uncertain. For the BWR base case (Figure 6-1), the relative humidity is above 60 % for ca 2000 hours (ca. 80 days), and during this time, ammonia is above 0.001 mol for 60 days, with the data and assumptions made in the modelling. This value is used somewhat arbitrarily by Henshaw and Evins (2023) as a limit below which an amount of ammonia inside the canister is considered as “small”. Further, it is rather the concentration (of nitrogen-containing species) in any liquid phase, than the amount in the gas phase, that is of importance for stress corrosion cracking

[11] BWR Cases, SKBdoc 2002171 ver 1.0, PWR Cases SKBdoc 2002172. (Internal documents.)

(see further Section 7.2.2). This is not included or evaluated in the modelling in Henshaw and Evins (2023), and thus the amount in the gas the phase is used as a proxy. The higher temperature in the PWR base case means that water is never in liquid form in the canister and thus there is no overlap between ammonia and liquid water in that case. Due to this, the effect of lower temperature was explored for PWR (see discussion below). For both the BWR and PWR base cases, most of the 33 mol hydrogen initially present in 600 g of water has formed H_2 gas in the void after around one year, Table 6-1.

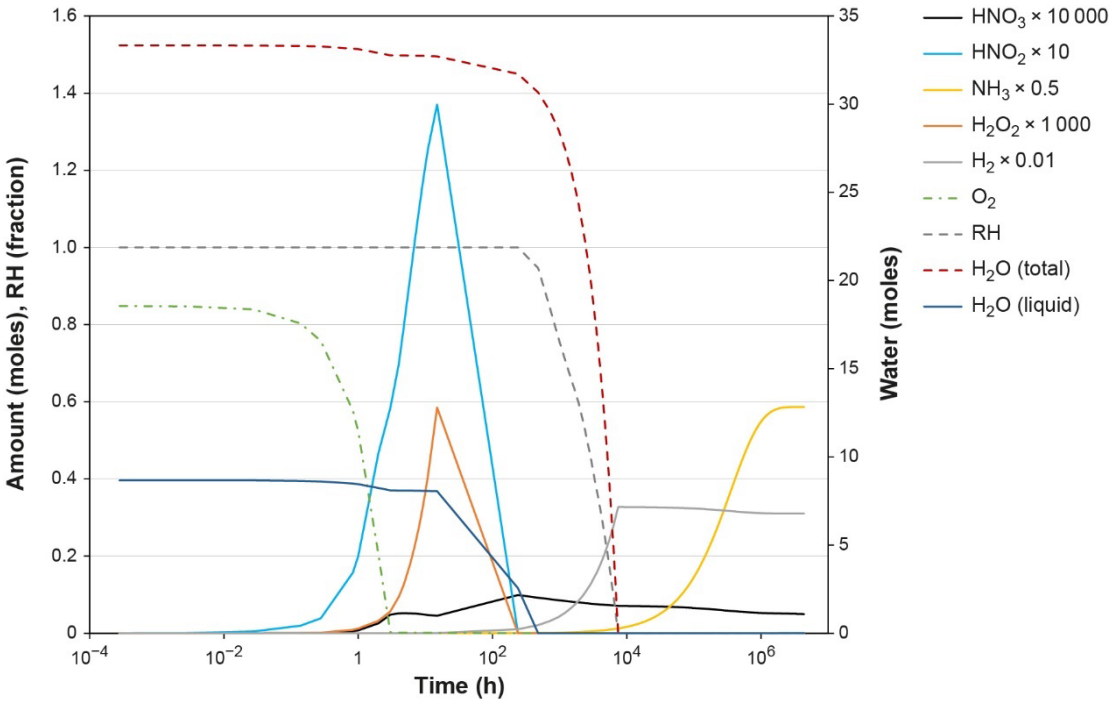

Figure 6-1*. BWR base case (case 2a): Calculated major species amounts for Case 2a, 600 g water, 10 % air, and corrosion allowed even at low relative humidity. From Henshaw and Evins (2023).*

In the following, the different cases varying air content, water content, temperature, and assumptions regarding Fe corrosion are presented and compared with the base cases.

Air content

The nitrogen-containing species that may be detrimental to the canister materials result from radiolysis reactions involving the nitrogen in the entrained air. Limiting the amount of air is beneficial for the environment inside the canister, which is why there is a requirement of a minimum 97 % Ar. The base cases involving 10 % air are an illustration of the consequences of an outdated design requirement that was in force when the modelling work started. Results from BWR cases 3, 4, 5 and PWR cases 14, 15, 16 are given in Table 6-1. It is clear that with less air, there is less nitrogen-containing species produced. The 600 g water is fully consumed in somewhat less than one year for BWR and in around 1.3 years for PWR cases, for the assumptions on corrosion rates made in Henshaw and Evins (2023). For BWR and 1 % air, there is no ammonia in high RH conditions. The amount of ammonia that has formed by the time water is fully consumed is only 0.26 mmol. For PWR and 1 % air, the amount of ammonia formed is 6.6 mmol when water is fully consumed. Since the temperature in the PWR insert is higher, the RH is never above 60 %.

Table 6-1. Base cases compared with cases for BWR and PWR with lower amount of air. RH = Relative humidity.

Case	Fuel type	Water (g)	Air (%)	Time to consume water (y)	Max HNO_3 (mol)	Max HNO_2 (mol)	NH_3 at zero H_2O (mol)	Steady state NH_3 (mol)	Steady state H_2 (mol)
2a (ref.)	BWR	600	10	0.9	9.9×10^{-6}	6.0×10^{-6}	0.026	1.17	31
3	BWR	600	5	0.9	4.4×10^{-6}	3.1×10^{-6}	0.012	0.59	33
4	BWR	600	2	0.9	2.0×10^{-6}	1.6×10^{-6}	0.0051	0.23	33
5	BWR	600	1	0.9	1.2×10^{-6}	1.0×10^{-6}	0.00026	0.17	33
13a (ref.)	PWR	600	10	1.3	1.8×10^{-5}	6.9×10^{-4}	0.064	1.9	30
14	PWR	600	5	1.3	6.4×10^{-6}	4.9×10^{-6}	0.033	0.94	32
15	PWR	600	2	1.3	2.5×10^{-6}	2.2×10^{-6}	0.013	0.38	33
16	PWR	600	1	1.3	1.4×10^{-6}	2.2×10^{-6}	0.0066	0.19	33

Water content

The amount of water available for radiolysis inside the canister clearly affects the outcome of these calculations, since it limits the amount of hydrogen and oxygen available for the formation of the corrosive species. The base case with 600 g water is a pessimistic upper bound whereas most canisters are expected to contain negligible amounts of water, Section 2.3. Water is mainly expected to be introduced into the canisters in fuel rods with failed fuel cladding, that may be difficult to dry. Therefore, an example of a more realistic amount of water could be 30 g (representing e.g. 6 failed fuel rods with 5 g water in each), the effect of which is explored in cases 6 (BWR) and 17 (PWR). Since water is likely to be released into the canister void from failed fuel rods, it is also possible that there is no water in the void initially but that water will slowly be added to the gas, with an assumed rate of 1.8 g/day, as the water escapes the failed rods. Results of cases 11 (BWR) and 22 (PWR) where 30 g of water is slowly added are also given in Table 6-2.

Table 6-2. Case 6, 7, 11 (BWR) and 17, 18, 22 (PWR) with 30 g water, either initially available or slowly introduced (cases 11 and 22).

Case	Fuel type	Water (g)	Air (%)	Time to consume water (y)	Max HNO_3 (mol)	Max HNO_2 (mol)	NH_3 at zero H_2O (mol)	Steady state NH_3 (mol)	Steady state H_2 (mol)
2a	BWR	600	10	0.88	9.9×10^{-6}	6.0×10^{-6}	0.026	1.2	31
6	BWR	30	10	0.05	1.2×10^{-5}*	4.0×10^{-6}	1.9×10^{-3}	0.73	8×10^{-7}
7	BWR	30	5	0.05	3.9×10^{-6}	2.3×10^{-6}	4.3×10^{-4}	0.79	0.2
11	BWR	30 (0 g initially)	5	0.05	5.2×10^{-6}	2.4×10^{-6}	8.8×10^{-4}	0.74	0.5
13a	PWR	600	10	1.31	1.8×10^{-5}	6.9×10^{-4}	0.064	1.9	30
17	PWR	30	10	0.05	2.4×10^{-5}	2.4×10^{-6}	1.4×10^{-3}	0.7	9×10^{-7}
18	PWR	30	5	0.08	6.3×10^{-6}	3.2×10^{-6}	2.5×10^{-3}	0.9	5×10^{-6}
22	PWR	30 (0 g initially)	5	0.08	7.8×10^{-6}	2.9×10^{-6}	2.3×10^{-3}	1.1	8×10^{-7}

* Less water but 10 % air means less H_2 and slightly more oxidising conditions and HNO_3.

Reducing the amount of water to a more realistic amount causes much less hydrogen to be produced, and the relative humidity will never reach 60 % and water is fully consumed within a month – assuming Fe corrosion is active at this low RH (further discussed below). Ammonia and liquid water will not coexist for BWR; for PWR, there are, with the assumptions made in the modelling, 10 days overlap but the amount of ammonia during this time is at most 2.5×10^{-3} mol. The maximum amount of nitric and nitrous acid is not very different with low water amounts. An interesting consequence of lowering the amount of air at low water content is that slightly more ammonia is formed. The reason is that aerobic corrosion will bind some hydrogen in FeOOH, which will then not be available for ammonia formation; hence a lower air content may increase the amount of ammonia formed. At 10 % air, and low amount of water, aerobic corrosion will be more extensive and thus less hydrogen is available to form ammonia during the anaerobic phase compared with the case with 5 % air. At 1–2 % air, the hydrogen lost via aerobic corrosion is not important; for these cases the amount of ammonia is lower for any water amount since the nitrogen amount is limiting. As seen in Table 6-2, the effects of slowly releasing water into the void instead of having immediately accessible, are small.

Temperature

In the PWR base case the initial temperature is above 100 °C and water is never in liquid form. Therefore, two cases with an initial temperature of 70 °C were explored. One of the additional cases combined a lower temperature with a lower surface area to volume ratio (SA/V). The results show that assuming a lower temperature yields quite similar amounts of ammonia and hydrogen at steady state. Lowering the temperature will however increase the time when water is present in the system. There is therefore also an increased time when water and ammonia co-exist. Water is however fully consumed after ca 1.4 years. Lowering the SA/V effectively means a longer period with corrosion and thus extending the time when water is present in the canister to ca. 2.1 years. It should be pointed out that the calculations were performed simply to test the effect of temperature and thus the fraction of the 600 g of water occurring in the liquid phase, but the initial dose rate was not lower. Realistically, a low initial temperature is connected to a lower dose rate (since these entities are correlated through the residual power of the fuel) which will yield less ammonia.

Fe corrosion and relative humidity

The evolution of the chemical environment inside the sealed canister depends to a large extent on Fe corrosion. One main uncertainty in this context is the RH required for active corrosion. Therefore, a few cases explore the effects of lower corrosion rates and also a case when no corrosion occurs at low RH, i.e. below 60 %. For one case (13c) the corrosion rate is assumed to be one order of magnitude lower for all situations, while one case (2c) assumed one order of magnitude lower corrosion rate at RH < 60 %. For other cases (10a, 11a, 13f) corrosion rates are assumed to be zero at RH < 60 %. A dependence of corrosion rates on RH is also used to describe possible evolution of the hydrological conditions inside the canister (Section 5.3). The effects of reducing the corrosion rate due to low relative humidity has very similar effects for the BWR and PWR cases (Table 6-3).

Table 6-3. Cases with low or zero corrosion rates at low relative humidity (2c, 10a,11a, 13f), and low corrosion rates at all times (13c). * = low SA/V.

Case	Fuel type	Water (g)	Air (%)	Time to consume water (y)	Max HNO_3 (mol)	Max HNO_2 (mol)	NH_3 at zero H_2O (mol)	Steady State NH_3 (mol)	Steady State H_2 (mol)
2a	BWR	600	10	0.88	9.9×10^{-6}	6.0×10^{-6}	0.026	1.2	31
2c*	BWR	600	10	8.8	8.3×10^{-6}	5.0×10^{-6}	0.17	0.88	32
10a	BWR	600 (0 g initially)	5	> 500 y	9.8×10^{-3}	3.8×10^{-3}	N/A	0.32	1
11a	BWR	30 (0 g initially)	5	> 500 y	1.5×10^{-2}	1.2×10^{-3}	N/A	0.16	0.58
13a	PWR	600	10	1.3	1.8×10^{-5}	6.9×10^{-4}	0.064	1.9	20
13c*	PWR	600	10	21	2.2×10^{-4}	1.8×10^{-5}	0.63	1.5	31
13f	PWR	600	10	> 500 y	0.26	0.08	N/A	0.94	26

In general, a low corrosion rate does not affect the steady state amounts of NH_3 and H_2 very much; it mainly affects the time period with water in the system. In Case 11a, 30 g water is slowly released from failed fuel rods, but the corrosion rate is very close to zero due to the low relative humidity. This means that water remains in the system for the full 500 years that was the limit for this analysis. Since there is 5 % air in this case, radiolysis produces some nitric acid and hydrogen peroxide; as time goes on these species are consumed in favour of ammonia and hydrogen. Ammonia and water overlap after ca 70 years (Figure 6-2), but RH is never above 60 % (never even above 13 %), and the amount of ammonia is much less than in the base case.

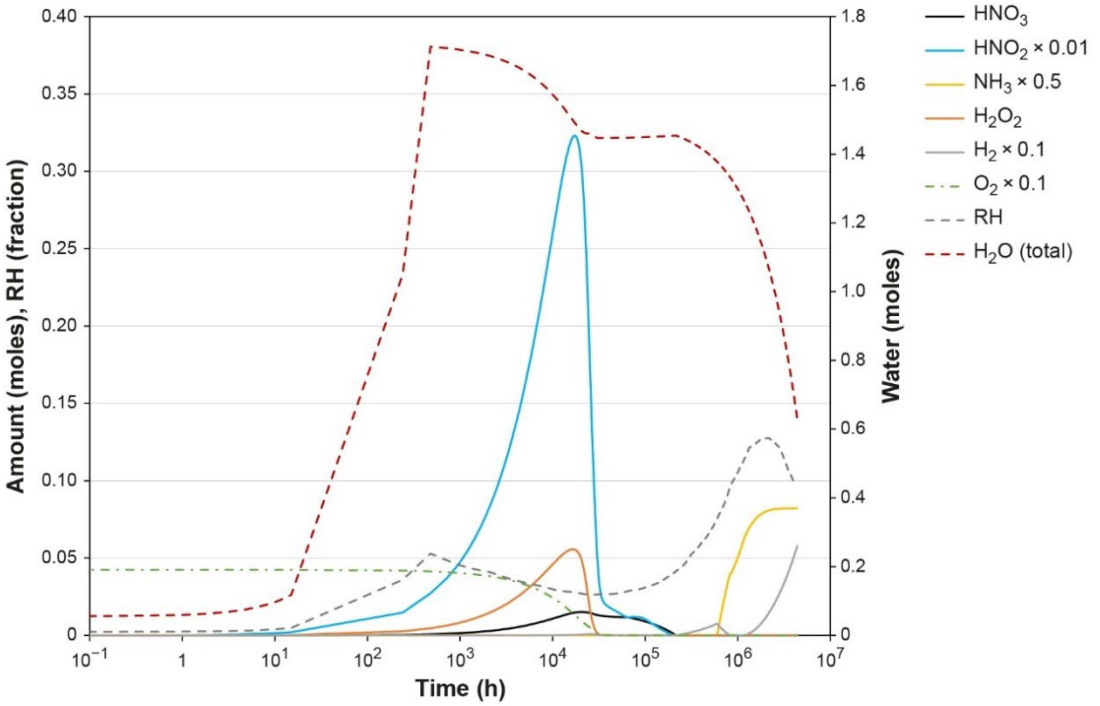

Figure 6-2. *Case 11a. 30 g water slowly released into the gas, and 10^{-5} times normal corrosion rate. From Henshaw and Evins (2023).*

With regards to production of nitric and nitrous acid and a prolonged period of co-existence of oxidizing species and water, the most extreme case is 13f, where no corrosion is assumed once RH is below 60 %. The temperature decreases over time, increasing the RH, but it stays at 60 % (in an oscillating manner switching the corrosion on and off, influenced by the slow water release, temperature and radiolysis, and the corrosion process itself) and the water consumption is very slow (Figure 6-3).

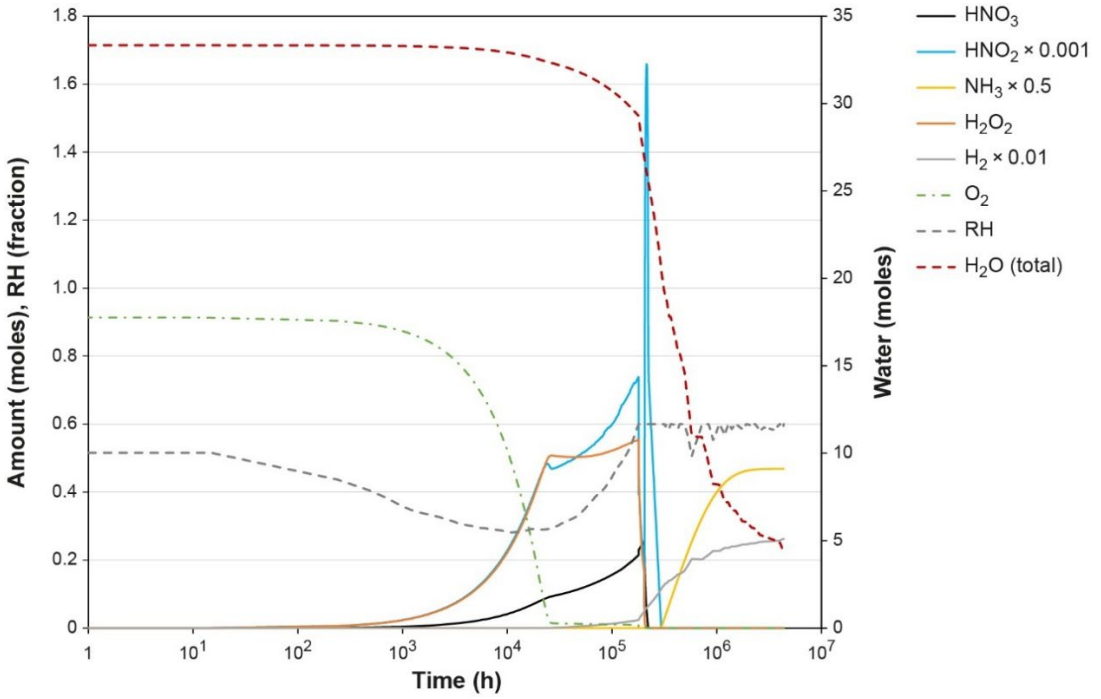

Figure 6-3. *Case 13f, assuming zero corrosion when RH drops below 60 %. RH increases as temperature decreases, and corrosion starts, consuming oxygen, of which after 23.9 years, there is less than 0.001 mol.*

Overall, the results show that if corrosion at low RH is non-existent or very slow, it significantly impacts the evolution of the chemical environment in a sealed canister, so that water remains as vapour for more than 500 years. Low amounts of water and therefore low RH is expected as an initial situation in canisters with a few failed fuel rods. If a higher amount of water is pessimistically assumed, the relative humidity will be higher. However, as illustrated by case 13f (Table 6-3, Figure 6-3) zero corrosion at RH below 60 % will allow some extended time period where nitric and nitrous acid will be formed and coexist with water and oxidizing species. This is, in general, similar to what has been modelled previously (Henshaw 1994) without Fe corrosion, albeit the current model allows a better insight into the complicated evolution of the system.

For a more detailed discussion on the hydrological evolution in a sealed canister, see Section 5.3.

6.4 Conclusions

A dedicated radiolysis model study of the Rebus canister was performed in order to properly substantiate the basis for assessing the effects of radiolysis on the post-closure performance, and to further explore uncertainties affecting the radiolysis analysis. With regards to comparing the cast iron and the Rebus inserts, the main differences of relevance to these calculations stems from the geometry of the insert. The analyses for the cast iron insert assumed a surface area to volume ratio (SA/V) of 35 m^{-1}. The Rebus PWR SA/V is less (23 to 30 m^{-1}), while the BWR is higher (53–55 m^{-1}). A lower surface area effectively means that corrosion takes a longer time and thus that water exists longer in the canister.

Conclusions from Henshaw and Evins (2023) are:

- After a short initial period with aerobic corrosion, anaerobic corrosion and radiolysis will primarily produce NH_3 and H_2.
- The aerobic corrosion will remove oxygen from the gas phase and by the time ammonia builds up, there is neither oxygen nor hydrogen peroxide remaining.
- The amounts of ammonia formed are influenced by the dose rate, area and volume of the insert, and initial amounts of air and water.

- Generally, changes in temperature do not significantly impact the amounts of corrosive species formed. It may affect corrosion rates mainly via relative humidity and the presence of liquid water.
- At high water content, a higher air content leads to higher amounts of NH_3, but at low water content the amount of NH_3 may decrease with increasing air content.
- Significant liquid water only exists in the canister for some cases, and in these, liquid water is lost after ca. 20 days. The amount of NH_3 at this point is very low (between 10^{-4} and 10^{-3} mol).
- The assumed corrosion rates at low RH controls the length of time H_2O is present in the system and therefore impacts the length of time aggressive species and H_2O exist simultaneously in the canister.
- Low or zero corrosion rates at low RH cause oxygen to remain longer, which means significant amounts of nitric acid and hydrogen peroxide form. Once oxygen is consumed, HNO_3 and H_2O_2 are decomposed by radiolysis.

Generally, the effects of radiolysis in a sealed Rebus canister are not significantly different than results reported for the canister with a cast iron insert. As long as the air content is kept low, the content of corrosive species such as nitric acid and ammonia will be low, even for the maximum allowed water content. As the canister gas will consist of at least 97 % Ar, cases with higher air content are relevant only as illustrations of the impact of hypothetically altered design requirements. The uncertainties concerning how RH influences the corrosion rates are problematic when estimating the length of time that water remains in the canister and thus coexists with the corrosive species. These uncertainties seem to have more influence on the final result than the possible slow introduction of water into the gas phase, and applies to both the cast iron and the Rebus inserts.

In the analyses by Henshaw and Evins (2023), most uncertainties are explored either through the formulation of dedicated calculation cases, or through pessimistic assumptions. This yields a relatively wide range of outcomes. These are all acceptable in terms of impact on the function of the Rebus canister, illustrated e.g. by the assessment of SCC in Section 7.2. In future assessments it may, however, be desirable to reduce the uncertainties, and this can be done by considering e.g. the following:

- Reduce the uncertainties regarding the impact of relative humidity on corrosion rates.
- Steel and copper corrosion involving the aggressive species formed such as ammonium and nitric acid can be included in the calculations. In the present model such corrosion reactions are pessimistically not included, meaning that all formed ammonium and nitric acid is available for SCC.
- The chemical evolution of the liquid water phase could be analysed. It would be preferable to know the concentration over time of the various aggressive nitrogen-containing compounds in order to assess its possible influence on the corrosion mechanism, e.g. SCC in copper.

7 SCC, embrittlement and ageing phenomena

7.1 Introduction

The properties of the insert materials and thus also their susceptibility to degradation mechanisms can potentially alter in the long term. Processes identified as requiring attention as potential causes of such effects are hydrogen embrittlement, static and dynamic strain ageing, effects of radiation and stress corrosion cracking (SCC). These processes and their potential effects are discussed in this Chapter. The results need to be considered in the analyses of mechanical loads in the repository in Chapter 8.

7.2 Stress corrosion cracking

7.2.1 Iron-based materials in general

Stress corrosion cracking (SCC) of metals requires a combination of tensile stresses, a specific chemical environment and a susceptible material. In this corrosion process, unfavourable combinations of these conditions can lead to the initiation and propagation of local cracks through the matrix over a period of time, while the surface is mostly not attacked by general corrosion.

There are several environments known to cause SCC in carbon steel, including solutions with chloride, nitrate, ammonia, phosphate, carbonate, sulfide and high pH (Ciaraldi 1992, King 2010). Of these, nitrate and ammonia are conceivable inside an intact canister. Nitric acid can form from the radiolysis of residual quantities of nitrogen in moist air (Jones 1959), and as described in Section 6.2 and 6.3 updated analyses show that ammonia can also be formed (Henshaw and Spahiu 2021, Henshaw and Evins 2023).

7.2.2 Carbon steel in the Rebus insert

Carbon steels are susceptible to SCC in various environments. The propensity for SCC is also influenced by the precise elemental composition and microstructure of the material and by other mechanical properties (Ciaraldi 1992). The precise combination of material, stress condition and environment must therefore be analysed.

The material

The material for the outer tube, P355N, is a ferritic carbon steel, and could, in general, be susceptible to stress corrosion cracking (see e.g. various reviews, e.g. Ciaraldi 1992, King 2010). The other parts in the insert also consist of carbon steel (see Section 0), and the differences between the materials with regard to susceptibility for stress corrosion cracking would be small.

The stress state

A prerequisite for SCC is the presence of tensile stresses. Residual stresses in a manufactured component can be tensile as well as compressive, depending on e.g. the cooling process (temperature, phase transformations) and later machining. Residual stresses have been measured for samples from three trial manufactured steel tubes (Lundin and Holmberg 2024, 2025). The measurements were performed with X-ray diffraction, on both the inner and outer surfaces of the tubes. For the tube ST7, the surface measurements show medium to high compressive stresses (250 to 500 MPa), while the measurements for the tubes ST13 and ST17 show tensile, and higher, stresses (up to slightly over 700 MPa). The stresses vary over the surfaces, but not in any consistent way between the tubes. The authors suggest these residual stresses (both tensile and compressive) originate from the machining (turning) process. Depth profiles were also measured, and showed that the residual stress state below the surface relatively rapidly approaches zero, at depths of around 50 µm, which means that any crack propagation further into the material would be retarded. Residual stresses in the framework plates have not been measured, but stresses from machining can in general be considered superficial and, by analogy to the case for the outer tube, assumed not to cause SCC.

Regarding stresses from external loads, asymmetric loads from the swelling buffer need to be considered, see Section 2.1.2. In Section 8.3.2 the possible load cases are described, and for the period up to 100 years, the only external load is from the swelling of the buffer (the internal load

from gas pressure is negligible in comparison). The saturation time differs depending on the inflow of groundwater to the deposition hole and, for deposition holes with no intersecting water-bearing fractures, on the permeability of the rock. The resulting time scales are discussed in Section 10.3.8 of SKB (2022c). Only a few percent of the deposition holes will be saturated faster than 100 years for the comparatively dry conditions at the Forsmark site intended for the final repository, while it will take considerably longer for the majority of the deposition holes; saturation times are generally on the order of 1000 years. The modelling in Jonsson et al. (2018) used saturation periods of 0–10 years for "wet holes" and 10–100 years for "dry holes". The sum of the swelling pressure and the hydrostatic pressure at 500 m depth will be a maximum of 15 MPa, but could be asymmetric due to uneven swelling or imperfections in the deposition hole geometry.

For the cast iron insert (Jonsson et al. 2018) the maximum stress in the insert from asymmetric loads is calculated to be 79 MPa (tensile), which is considered rather small and in the elastic region. For the Rebus insert, calculations of asymmetric loads are reported in Section 8.4 and show tensile stresses at 225° in the steel tube (Figure 8-2) and copper shell (Figure 8-3) for both load case 1a and 2a. The stresses are up to 200 MPa, and going all through the steel tube thickness at 225°. These stresses are higher than the ones calculated for the cast iron insert, which would make the Rebus insert more susceptible to SCC. The stresses in the framework have not been evaluated in detail.

In the PSAR assessment for the copper shell it is concluded that tensile stresses cannot be totally excluded (SKB 2022a).

For the further analysis, it is concluded that tensile stresses may develop as the buffer becomes water saturated. The swelling pressure will take time to develop, at the earliest in the range of 20 years, and with only a few percent of the deposition holes having developed significant swelling pressures in 100 years at the intended Forsmark site (SKB 2022c). The extent of asymmetry of the loads on the canister during and after swelling of the buffer is determined by deviations from the ideal geometry of the deposition hole and initial buffer inhomogeneities. It is also determined by the way in which water is supplied to the hole. This supply is generally a combination of inflow from water bearing fractures intersecting the deposition hole and water supplied from the deposition tunnel backfill above the hole and the rock mass surrounding it. At a dry site like Forsmark, the relatively few holes intersected by fractures with a significant water flow may generally be expected to exhibit more asymmetric loads than the majority of holes that are expected to require hundreds to thousands of years to fully saturate.

The environment

Usually, the occurrence of the "aggressive anions" that are needed is the starting point for the discussion of SCC, but equally important is the presence of oxidising species as well as water. Liquid water could condense if the RH exceeds the dew point, but also below this RH a thin surface film could be formed on the corroding surface, and thus be sufficient for corrosion reactions to occur (see e.g. Hedin (2025) for a further discussion and references). The oxidising environment is required for driving a cathode reaction, which together with the anodic reaction (metal oxidation), forms the corrosion reaction.

In the many reviews available, a number of environments are described as possible causes of SCC, but most of them can readily be shown not to be applicable for the sealed insert of the canister for spent nuclear fuel in a repository. The only compounds present initially in non-negligible amounts within the deposited canister are argon, air (nitrogen and oxygen gas) and water, and only the elements Ar, H, O and N need to be considered. The possible environments that can be formed from these elements and where SCC has been noted to occur in carbon steel, are listed in Table 7-1. Thus all SCC caused by chlorides, phosphates, sulfur (hydrogen sulfide, sulfates) or carbon components (carbon dioxide, carbon oxide, cyanides) can be ruled out. It can be concluded from the table that the only environments that need to be considered for the insert are nitrate and ammonia solutions. For the copper shell, environments causing SCC and including only the elements Ar, H, O and N, are nitrite and ammonia solutions (SKB 2022a).

The environment in the insert is evaluated in Hedin (2025) and summarised in Chapter 5 in the current report, with regards to the evolution of the composition of gases, caused by corrosion reactions whereas radiation effects are essentially left out of that analysis. The influence of the radiation is analysed in Henshaw and Evins (2023) and summarised in Chapter 6, where several

parameters are varied in a number of calculations cases, especially the amount of water (30 or 600 g), and the residual air (1, 2, 5 or 10 %, corresponding to 99, 98, 95 or 90 % argon). As described in Section 2.3, few, if any, canisters are expected to contain even close to 600 g water. Further, the design requirement of the atmosphere in the insert is given as > 97 % argon. Many of the calculation cases are thus pessimistic in relation to the expected conditions in a canister.

Table 7-1. Environments that have been noted to cause stress corrosion cracking in carbon steel, for the elements H, O and N, together with the main arguments on whether further assessment is needed.

Environment	
nitrate	Nitrate solutions are known to induce stress corrosion cracking in carbon steel (Ciaraldi 1992), generally at high concentrations, but also at lower concentrations in boiling solutions. Welded steel and high-strength steel seem to be more susceptible. Several factors can enhance or mitigate the SCC (temperature, potential, other ions etc), but are not easily evaluated in sufficient detail to be used as an argument for exclusion of nitrate as an SCC agent. For this study nitrate is therefore considered in the assessment.
ammonia	Anhydrous ammonia has been reported to cause stress corrosion cracking in transportation containers (Dawson 1956), but generally connected to cold-formed material, and not in stress-relieved material. Dawson (1956) also noted "anhydrous ammonia" used in the agricultural services (where the containers were used) could contain both air and water. As at least some studies show SCC in ammonia, this is considered in the assessment.
caustic (hydroxide)	Cracking in concentrated sodium hydroxide solutions has been noted, but iron corrosion will not cause the pH to increase to levels as in concentrated hydroxide solutions. Further no sodium is present in the Rebus insert, and the only possible cation could be NH_4^+. Such caustic environments are not considered possible in the Rebus insert.
high-temperature water	Cracking in water at temperatures of 200–320 °C has been observed (Ciaraldi 1992) and even down to 150 °C in laboratory experiments (Seifert and Ritter, 2005). The maximum temperature in the outer tube of the insert is around 100 °C (see Section 5.2.1), making SCC of the tube part of the insert due to exposure to high-temperature water unlikely. This SCC mechanism is not considered further in the assessment.
hydrogen gas	Cracking (by an SCC mechanism) of steel vessels by high-pressure hydrogen gas has been observed, but mostly in higher-strength steel (Ciaraldi 1992). As the partial pressure of hydrogen within the insert would not exceed of the order of 1 bar, this SCC mechanism is disregarded. (The maximum amount of water, 600 g, would give a maximum amount of hydrogen of 33 mol, which at 100 °C would give a pressure of around 1 bar, see Section 7.3.3.)

The consumption time for water for all the calculation cases are originally compiled in Table 4-1 in Henshaw and Evins (2023), and a subset is repeated in Table 6-1 to Table 6-3 in the current report. In Table 7-2 the consumption time for the oxidising species oxygen, hydrogen peroxide, nitric acid and nitrous acid has been added for the calculation cases where the water consumption time is longer than 2.5 years. The consumption times are determined with a cut-off of 0.001 mol (approximately, as interpolations are sometimes needed within the time steps in the calculation), from the supporting material[12] to Henshaw and Evins (2023). This cut-off is circa 5 times larger than the limit for HNO_3 below which no SCC was noted in experiments with radiolysis of humid air (Blackwood et al. 1996), making it pessimistic.

The cases in Table 7-2 all have an iron corrosion rate that is low (all the time or for RH < 60 %), or set to zero for RH < 60 %. Note that these cases all have an air content exceeding the maximum allowed 3 % (corresponding to the required Ar content of 97 %) and that all cases but one have the maximum allowed amount of water, 600 g.

[12] BWR Cases, SKBdoc 2002171, PWR Cases, SKBdoc 2002172 ver 1.0. (Internal documents.)

Table 7-2. Consumption times for water, oxygen, hydrogen peroxide, nitric acid and nitrous acid for the calculation cases in Henshaw and Evins (2023) that have a water consumption time longer than 2.5 years (with a cut-off of 0.001 mol). SA/V = surface area/volume ratio.

Case	Fuel type	Water (g)	Air (%)	Other parameters changed	Time to consume H_2O	Time to consume O_2	Time to consume H_2O_2	Time to consume HNO_3	Time to consume HNO_2
2c	BWR	600	10	low SA/V; low corr. rate for RH < 60 %	8.8 y	8 h	< 15 h	- (< 8×10^{-6} mol)	- (< 5×10^{-6} mol)
10a	BWR	600, released at 1.8 g/d	5	no corrosion for RH < 60 %	> 500 y	0.9 y	1.1 y	1.0 y	1.6 y
11a	BWR	30, released at 1.8 g/d	5	no corrosion for RH < 60 %	> 500 y	6.3 y	3.5 y	23 y	2.5 y
13c	PWR	600	10	low SA/V, low corr. rate all the time	21.1 y	< 10 d	< 15 h	- (< 2×10^{-4} mol)	- (< 2×10^{-5} mol)
13f	PWR	600	10	no corrosion for RH < 60 %	> 500 y	23.9 y	24.9 y	25 y	33 y

The species and environments that are necessary for SCC to occur may be initially present or formed by the radiation, but are also "consumed", either by radiation or corrosion reactions. A crucial question is whether there is any possibility that all the environmental conditions are fulfilled at the same time. The time periods could be summarised as follows:

- An amount of 600 g water is generally consumed in one or a few years (already 10–20 days for 30 g water), but with low corrosion rates (at RH < 60 %) it remains for about 20 years. Only the cases assuming no corrosion at RH < 60 %, gives water persisting for longer times, more than 500 years (Table 6-3).
- Most calculation cases in Henshaw and Evins (2023) show that oxygen and hydrogen peroxide is consumed very fast, in a few days. The consumption time increases to 25 years if no corrosion is assumed for RH < 60 % and the water is available from the start (case 13f).
- The nitrogen oxides are decomposed by radiation once the oxygen is consumed, giving approximately the same time periods for the occurrence of nitric acid (HNO_3) and nitrous acid (HNO_2) as for oxygen and hydrogen peroxide. It is not evaluated in detail how nitric and nitrous acid would influence the redox potential, but the persistence of these species does not exceed 35 years. The time period for nitrate and nitrite to exist in solution (a water film) and available to act as SCC agents, is thus also in the range of a few tens of years.
- Ammonia, NH_3, starts to be produced by radiation when the conditions change from oxidising to reducing and H_2 is formed. This, in itself, indicates that the prerequisites for SCC are not fulfilled, even if ammonia and water exist at the same time for some cases, as discussed Chapter 6.
- The assumptions on iron corrosion and its possible dependence on relative humidity have the largest impact on the calculated time periods for the persistence of water, and of nitric and nitrous acid (as also discussed in Section 6.3.2 and 6.4). However, only the assumption of strictly no corrosion for RH < 60 % gives consumption times for nitric and nitrous acid in the range of the shortest possible buffer saturation times (around 20 years).

- In the text above, the various time periods during which the different environments may persist in the insert are discussed, and it is concluded that only cases with no corrosion below RH < 60 % gives water persisting longer than 2.5 years. Such an assumption would influence also the evaluation of SCC, as it is hard to envisage that a more complex corrosion process like SCC could take place if not even corrosion by water is feasible. To make the assumptions consistent within a certain evaluated case in the analysis, the possible cases with water persisting more than 500 years due to low corrosion need not be analysed for SCC.

Further arguments

It could in principle be possible to calculate the concentrations of SCC agents in a liquid water phase in equilibrium with the gas phase in the interior of the insert. Nitric acid (HNO_3) is highly soluble (2100 mol/(m^3 Pa)), and nitrous acid (HNO_2) much less (0.48 mol/(m^3 Pa)) (Henry' law constants, Sander (2023)), and as the gas phase amounts of HNO_3 is larger than for HNO_2 (at least for the more critical cases 10a, 11a and 13f), this would cause the solution to be dominated by HNO_3 and the pH to be very low. This would in turn render HNO_2 in its protonated form and the concentration of NO_2^- (nitrite) very low, and further lessen the probability of SCC in the copper. There are though several reactions between the nitrogen- and oxygen-containing species, and radiolysis would also affect the solution composition, and together with the uncertainty of the volume of a water phase, this makes estimations of the solution composition difficult. The difficulties in estimating the concentrations in the water phase were also discussed in the Canadian programme, referring primarily to the many combinations of the water droplet and headspace geometries (Morco et al. 2017).

For the canister design with a cast iron insert it was argued in the PSAR assessment (SKB 2022a) that nitric acid formed would cause general corrosion rather than SCC. This would give reduction of the graphite nodules by intruding hydrogen and dissolution of the ferritic matrix and pearlitic structure constituents, and will counteract the formation of sharp cracks with passivated crack walls, which is a prerequisite for stress corrosion cracking with a slip-dissolution mechanism. The effect of ammonia on the cast iron was not evaluated, but it was noted that in recent experiment with copper exposed to irradiated humid air, the formation of nitrate species was confirmed, but neither ammonium nor nitrite were observed (Björkbacka et al. 2017, Ibrahim et al. 2018). The arguments used for the Rebus insert are thus somewhat different compared to those used for the cast iron insert, but would be applicable for the latter as well (except of course for the measurements of residual stresses on the Rebus steel tubes). Altogether, the arguments in the various approaches do strengthen the conclusion that SCC of the insert is not possible.

7.2.3 The copper shell

The insert is sealed with a gasket (see Section 2.2.3) with the requirement to keep the volume in the insert separated from the gap between the insert and copper tube for at least 72 h (the purpose of the gasket is to be tight during encapsulation). As noted in Section 2.2.3 the gasket material could realistically be expected to retain its sealing properties for several hundred years or longer.

Ammonia is one of the agents that can cause SCC of copper (SKB 2022a), but also in this case both water and oxidising conditions are required. The conclusion that SCC of the insert due to the presence of ammonia is not possible thus is also valid for the copper shell.

For copper it is nitrite, NO_2^- (rather than nitrate, NO_3^-), that can cause SCC. The amounts formed are small (Henshaw and Evins 2023), but show approximately the same pattern of consumption, so that in the most pessimistic case nitrite could persist for about 35 years. Nitrate could be reduced to nitrite, and nitrite could in itself influence the corrosion by nitric acid (Turnbull et al. 2021), but the use of the consumption time argument would cover also these complications.

7.2.4 Conclusions

The likelihood of stress corrosion cracking (SCC) in the Rebus insert has been assessed, by considering the possibilities of simultaneous occurrence of the necessary conditions. SCC is dependent on three factors (the material, the environment and tensile stresses), none of which can be used solely to disregard the process for the Rebus insert. The carbon steels, and the copper in the outer shell, are all materials that could be sensitive to SCC.

Tensile stresses in the surfaces facing the insert void could occur as residual stresses or stresses induced by asymmetric saturation of the buffer. Tests on trial manufactured Rebus tubes showed the possibility of tensile stresses in the surface of the steel, however, the stress state approached zero already at a depth of around 50 µm. This means any crack propagation further into the material would be counteracted. The saturation period, and hence the period where asymmetric swelling may occur, varies depending on the rock hydraulic conditions, and full saturation is reached in 20 years for a few canisters, but is expected to take much longer time for the majority of the deposition holes.

The development of the environment in the insert is mainly dependent on the radiation, temperature, and the residual amounts of water and oxygen (from air) enclosed at closure. The SCC active agents ammonium (NH_4^+), nitrate (NO_3^-) and nitrite (NO_2^-) could form through radiolysis. The necessary oxidising conditions do not prevail longer than 35 years (at the most), during which HNO_3 and HNO_2 could persist. This would though build on inconsistent assumptions of no corrosion but still SCC. Ammonia is not formed until the oxidising species have been depleted.

Taking into account the timing of the prerequisites for stress corrosion cracking, i.e. that the environment will neither contain water nor experience oxidising conditions longer than hours or days, while tensile stresses, as an effect of saturation of the buffer will not occur until later (full saturation in 20 years for a few canisters), it is concluded that the likelihood of SCC in the Rebus insert is negligible. The same is concluded for the copper shell regarding SCC from the interior atmosphere, for which also the gasket must have lost its function.

7.3 Hydrogen embrittlement

7.3.1 Introduction

An evaluation of hydrogen embrittlement on a KBS-3 canister throughout its service life requires information on the initial hydrogen content in the materials and the relationship between hydrogen content and material properties. Additional sources of hydrogen after sealing of the canister also need to be considered and the potential impact these may have on the material properties. The former points are addressed in Section 7.3.2 based largely on Sarnet (2024a), and the latter is addressed in Section 7.3.3 based on Appendix C. Conclusions are provided in Section 7.3.5.

7.3.2 Hydrogen embrittlement for the as-delivered Rebus materials

In general hydrogen embrittles most metals and alloys if loads are present and causes tensile stresses in the material. There are different sources of hydrogen and mechanisms of hydrogen embrittlement, and the hydrogen can be weakly or strongly trapped in the metal. Typically, cracks and cleavages are evident in the steel if embrittled and exposed to over-load. Hydrogen can be present as precipitated solid phases or trapped as atomic hydrogen in material defects. Hydrogen atoms can also recombine to form molecular hydrogen gas in micropores and voids, predominantly between grains in the material. The embrittlement mechanism may include elastic deformation of the steel crystal by hydrogen atoms and through fast diffusion of hydrogen atoms to local deformations or cracks. Two factors that promote hydrogen embrittlement in steel are high strength and the presence of tensile stresses.

The materials in the Rebus design of the canister insert are S355 and P355 steel for the framework and the outer tube, respectively. These are mild steels with yield strengths of 300–350 N/mm^2. The microstructure is ferrite with pearlite. An increased pearlite fraction in the microstructure of the plain carbon steel in combination with hydrogen has been shown to reduce the strength and ductility (Ogawa 2021). On the other hand, the finer the pearlite lamellae, the more resistant the material is to hydrogen embrittlement (Yu et al 2019). Therefore, it is probable that steel with lamellae transformed to spheroidized pearlite is also more resistant to hydrogen embrittlement.

A strong effect of the hydrogen content on embrittlement has been demonstrated by artificially charging hydrogen into ferritic materials by immersion in hydrogen containing acids, by exposure to high external hydrogen gas pressures, or through electrochemical or cathodic methods. The failure mode can change to brittle at high contents in iron and steel (Sahiluoma et al. 2021, Wang et al. 2004), resulting in decreasing tensile ductility and a change from dimple fracture to cleavage fracture. The extent of embrittlement increases with strength of the steel. By extrapolating down

from high-strength steels, low-alloy steels would allow for approximately 3 weight-ppm of hydrogen without an embrittlement effect (Wang et al 2004). The hydrogen content of plain carbon steel from modern steelmaking is typically below 2 weight-ppm and therefore safely below any effect on the ductility or change of the ductile failure mode.

The plain carbon steel of the open-die forged tubes and the rolled plates for the canister insert is generally expected to have a low initial hydrogen content, to have an adequate microstructure, and to have low residual tensile stresses. This further counteracts hydrogen embrittlement. It has been found in analyses of the Rebus materials[13] that the material, if appropriately heat treated, is indeed ferritic with spheroidized pearlite which is the most favourable micro-structure for this type of steel as regards insensitivity to hydrogen embrittlement.

Sarnet (2024a) gives an account of hydrogen embrittlement of steel in general and on the Rebus low carbon steel materials in particular. Nodular cast iron used in cast iron insert is also covered. For the Rebus materials, data on the content of hydrogen and other elements are presented, an account of the microstructure of the material is provided and relationships between these factors and measured mechanical properties are analysed. Figure 7-1 shows the measured hydrogen content for 28 samples from three test manufactured Rebus tubes. The data, from tube ST2 and ST3, adhere well to a log-normal distribution separately or aggregated. The total mean value including the four analyses from ST1 is 0.45 wt.ppm. Figure 7-1 also shows a hitherto unexplained outlier, denoted TC14 in the figure, with a measured content of 5.2 wt.ppm. The tensile specimens on which the measurements were made were stored at room temperature for a year before the hydrogen analyses were performed. This means that hydrogen that is not strongly bound in the material may have been outgassed during storage of the tensile specimens.

Sarnet (2024a) also notes that, as part of the quality assurance of the insert materials, a requirement on allowed hydrogen content of the materials could be considered. Should such a requirement be established, it is expected to be passed with current manufacturing techniques according to Sarnet (2024a).

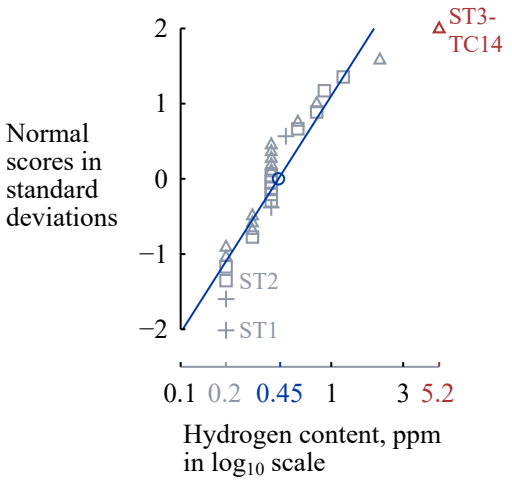

Figure 7-1. *Measured hydrogen content in three Rebus tubes (pencil grey symbols) and mean value (ink blue circle) compared to log-normal distributions. From Sarnet (2024a). Crosses: tube ST1, squares: ST2, triangles: ST3.*

Sarnet (2024a) concludes that hydrogen embrittlement is not expected to affect the Rebus materials with their as-manufactured properties. Sarnet (2024a) also notes that there is some degree of covariation of mechanical properties, yield strength, with microstructure properties like grain size, with contents of some elements like chromium and also to some extent with hydrogen content. An example is given in Figure 7-2. The few data points available are, however, not sufficient to draw definite conclusions regarding such covariations.

[13] SKBdoc 1952565 ver 1.0. Metallographic investigation of pipe samples [ST1]. TEK21-0113 ed 3

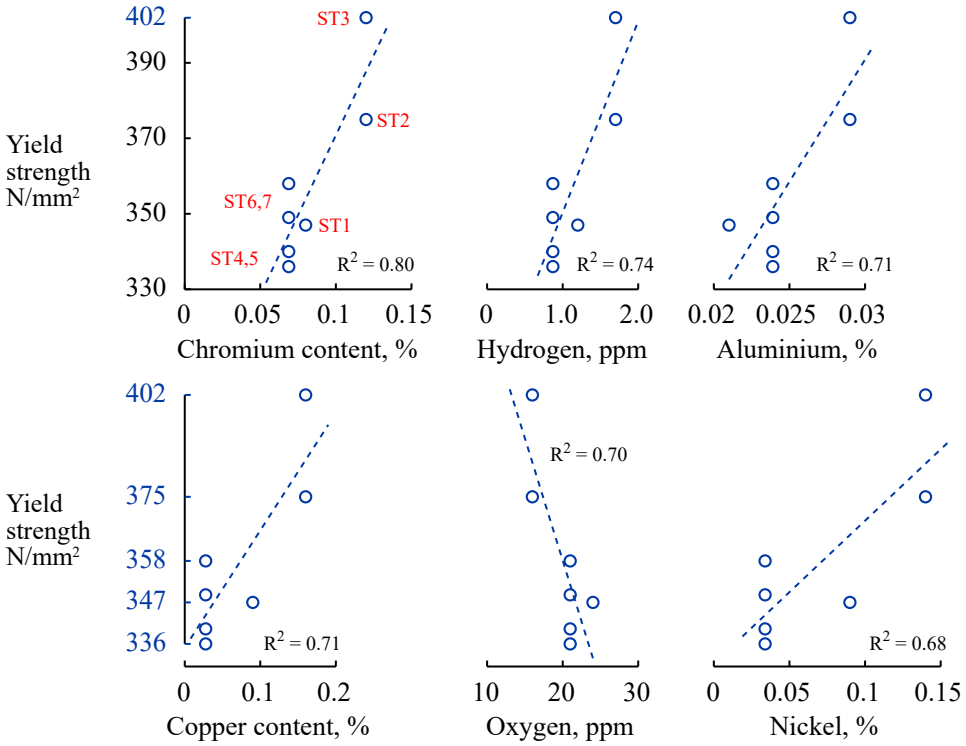

Figure 7-2. *Variation of the yield strength with some elements of the tubes ST1–ST7. The contents of the various elements were measured before casting, whereas the yield strengths were measured on specimens of the manufactured tubes (drawn by Sarnet (2024a) based on internal information[14]).*

7.3.3 Possible absorption of hydrogen in a sealed insert

Hydrogen absorption in a sealed Rebus canister insert is evaluated in Appendix C, building on studies in Turnbull (2009) and King (2009). Various sources of hydrogen are considered and the maximum diffusible hydrogen concentration (the sum of the lattice hydrogen and that located in reversible traps) is estimated. The potential consequences of this diffusible hydrogen on the mechanical properties of the insert are also considered. The following is a summary of Appendix C, with a somewhat extended discussion around Figure 7-3.

The source of hydrogen in a sealed canister that needs to be considered is that in residual water after drying of the fuel. As mentioned in Section 2.3 few, if any, of the approximately 6000 canisters to be deposited in the final repository are expected to contain amounts even close to the maximum allowed 600 g of water after sealing. If, nevertheless, all hydrogen in 600 g of water is made available for absorption through the formation of H_2 gas as the water corrodes the insert, then this corresponds to a hydrogen partial pressure of around 0.1 MPa in the void volume of the insert.

As regards detrimental effects on mechanical properties, it is primarily the concentration of hydrogen in the metal lattice that is of concern. This concentration varies as the square root of the external hydrogen pressure. A hydrogen partial pressure of 0.1 MPa corresponds to a lattice concentration of around 3.3×10^{-3} wt.ppm. Turnbull (2009) and King (2009) assessed ten times higher lattice concentrations and concluded that hydrogen damage in low carbon steel should be a limited problem also for such concentrations. The authors evaluated a range of damage mechanisms, several of which are not relevant for the Rebus design. Furthermore, the key mechanical entity to consider is the impact of hydrogen on the fracture toughness.

[14] SKBdoc 1947860 ver 1.0. Manufacturing report – ST1. Svensk Kärnbränslehantering AB. (Internal document.)
SKBdoc 1962861 ver 1.0. Tillverkningsdokumentation ST2. Svensk Kärnbränslehantering AB. (Internal document, in Swedish.)
SKBdoc 2003981 ver 1.0. KBP3021 - Manufacturing report steel tubes ST4-ST7. Svensk Kärnbränslehantering AB. (Internal document.)

Figure 7-3, based on the data compiled in Table 3.2.1.1 in San Marchi and Somerday (2012), shows the fracture toughness as a function of external H_2 pressure for the steel qualities X42 and A516. These materials resemble the steel qualities intended for the Rebus inserts, with A516 having the more similar chemical composition. To estimate the reduction in fracture toughness for a 0.1 MPa H_2 pressure, a trend line suggested in the investigation behind the X42 data (Gutierrez-Solana and Elices 1986) is also included. The trend line describes a reduction in fracture toughness in direct proportion to the lattice concentration of H, i.e. in direct proportion to the square root of the hydrogen pressure. The trend line indicates a reduction in fracture toughness of 6.0 % at 0.1 MPa. Also, as noted by Sarnet (2024a), severe shear loads in the repository are expected to occur on a time scale of typically one second, meaning that there will be a considerably shorter time for hydrogen to be active in any fracturing mechanism compared to the fracture toughness testing experiments yielding the results in Figure 7-3.

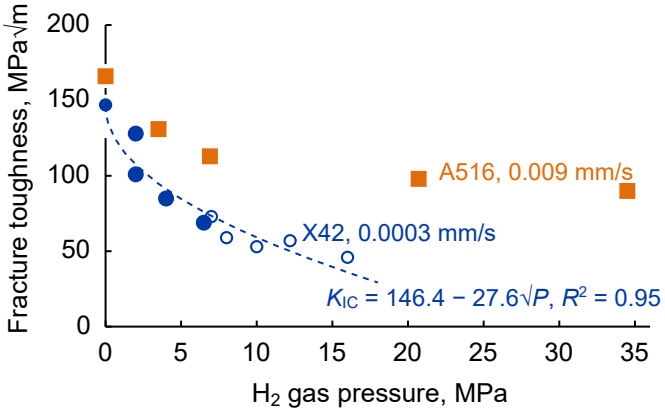

Figure 7-3. *Effect of hydrogen gas pressure on fracture toughness for two carbon steels tested at different strain rates. Data from San Marchi and Somerday (2012). Trend line from Gutierrez-Solana and Elices (1986).*

7.3.4 Hydrogen charging study

A limited effort (Sefer, 2025) was made to determine the effect of H charging on steel specimens sampled from the central part (mid-thickness, mid-height) of one of the Rebus cylinders. Specimens were exposed to a 1 bar pure H_2 atmosphere at 100 °C for 3 and 6 weeks. Hydrogen content was measured with thermal desorption mass spectrometry (TDMS) and melt extraction (ME) and mechanical properties were determined using slow strain rate testing (SSRT). The main conclusions of the study were:

- No significant change in the 0.5–1 wppm total hydrogen content of the steel specimens could be detected by TDMS or ME after up to 6 weeks exposure in the hydrogen atmosphere.
- The exposed specimens exhibited a small but detectable TDMS hydrogen peak that may be interpreted as absorption of weakly trapped/diffusible hydrogen. The hydrogen amount detected varied considerably between specimens and corresponded at most to a content of 0.05 wppm. It is, furthermore, unclear whether this hydrogen is located at or near the surface or if it is more evenly distributed in the specimens. It was not possible to establish if a final state of this uptake had been reached after 6 weeks.
- The measured hydrogen content of specimens after 6 weeks exposure and subsequent SSRT was higher than those of reference specimens and of specimens exposed for 6 weeks without SSRT. The reason for this is unclear as the SSRT does not involve any exposure to hydrogen. It was suggested that hydrogen may be redistributed between sections of the specimens subjected to different strain levels during SSRT.

- SSRT testing showed that 6 weeks exposure to a 1 bar hydrogen atmosphere at 100 °C in general has no significant effect on most of the relevant mechanical properties of the steel. However, an indicative drop of the upper yield strength (R_{eH}) was identified for the specimens exposed in hydrogen atmosphere as compared to the reference specimens. It was unclear what caused the reduction in R_{eH}. The reason could possibly be the 6 weeks holding time at 100 °C causing a tempering effect.

7.3.5 Conclusion

Based on the finding in Section 7.3.2 that hydrogen embrittlement is not expected to affect the Rebus materials with their as-manufactured properties, including a low initial hydrogen content, and the finding in Section 7.3.3 that hydrogen sources in the canister insert are expected to also have a limited impact on the mechanical properties of the materials if the maximum amount of residual water in the canister is pessimistically assumed, hydrogen embrittlement is not expected to deteriorate the Rebus insert materials in a sealed canister. The study by Sefer (2025) described in Section 7.3.4 does not alter this conclusion. The sensitivity to a 6 % reduction of fracture toughness is discussed in Section 8.10.3.

As mentioned both in Sarnet (2024a) and in Appendix C, to further understand the behaviour of hydrogen in the Rebus materials, it would be of interest to determine not only the total hydrogen content in the materials, but also the fraction of diffusible hydrogen, and how that fraction is bound in the materials. It could be of interest to carry out e.g. a J-integral test of the type made by Gutierrez-Solana and Elices (1986) for the Rebus material at repository relevant temperatures and internal H_2 pressures.

7.4 Ageing effects

Metals will work harden during plastic deformation resulting in increased strength. In addition to the work hardening, solutes such as nitrogen, carbon and, to a lesser extent, oxygen can strengthen the metal by a process called ageing. Softening processes could also occur but are assessed to be less important in the low strength ferritic iron. The ageing process is described in the literature as an elastic strain between the elements in solution in the metal matrix that may influence the deformation of the metal on an atomic level, with time and temperature, the accumulation of solutes to local deformations increases and locks or affects further deformation. This strain ageing effect is an additional and common hardening contribution for metals with solid solution elements. A consequence of the increased strength is a certain degree of reduced tensile ductility and fracture toughness of the strain-aged metal. Strain ageing may occur during deformation, *dynamic strain ageing*, or after deformation, *static strain ageing*.

The Rebus design of the canister insert consists of a seamless steel tube and a steel framework. The tube is made of a steel for pressure vessels, P355, and the framework is made of a structural steel S355, which are both ferritic carbon steels. These steels contain low amounts of carbide or nitride forming elements and the ferritic structure of the metals can dissolve carbon, nitrogen, oxygen, and hydrogen. Furthermore, the elements have a high mobility and the elastic strain energy between the ferrite and the solutes is high. Therefore, strain ageing effects cannot be categorically ruled out for these steels. Carbon and nitrogen can readily diffuse to the deformation site and add a minor hardening to the steel. Carbon might precipitate as cementite, but most probably nitrides do not precipitate and the hardening contribution of nitrogen might reverse and decrease over time, and the steel will recover part of the ductility. Furthermore, the low amount of dissolved nitrogen, oxygen, and hydrogen in modern steels should reduce the effect. In the following, static and dynamic strain ageing are discussed in more detail for the Rebus materials. The account is based on strain ageing and tensile testing experiments of specimens from Rebus tubes reported in Sarnet (2024b). Both the aforementioned ageing phenomena were examined in the experiments.

7.4.1 Influence of hot forming and heat treatment on strength

Hot forming and subsequent heat treatment secure appropriate strength and microstructure of the steels. When steels cool after forming or heat treatment, stresses and deformations (strains) can develop.

The P355 and S355 steels are low in carbon according to specification, and low in nitrogen due to modern steel manufacturing practices, and are heat treated (normalized) to refine the grain size. Therefore, hardening effects in connection with hot forming and heat treatment are expected to be low.

The effects of heat treatments and wall thicknesses on the yield points are analysed for the tubes ST1 and ST3 in Sarnet (2024b) and key results are shown by two graphs in Figure 7-4. The pencil grey numbers on the ordinate are the minimum and maximum values, and the ink blue numbers are the averages for each factor. The as-received state is indicated by black symbols, the stress-relieved state by red symbols and the annealed state by orange symbols, respectively. As seen, the strength increased slightly when the specimens had been stress-relieved or annealed, compared to the strength of the specimens in the as-received state (heat-treated condition). The recorded strength values of ST3 are generally higher than those of ST1, except for two mid wall specimens, one in the as-received state and another in the annealed state.

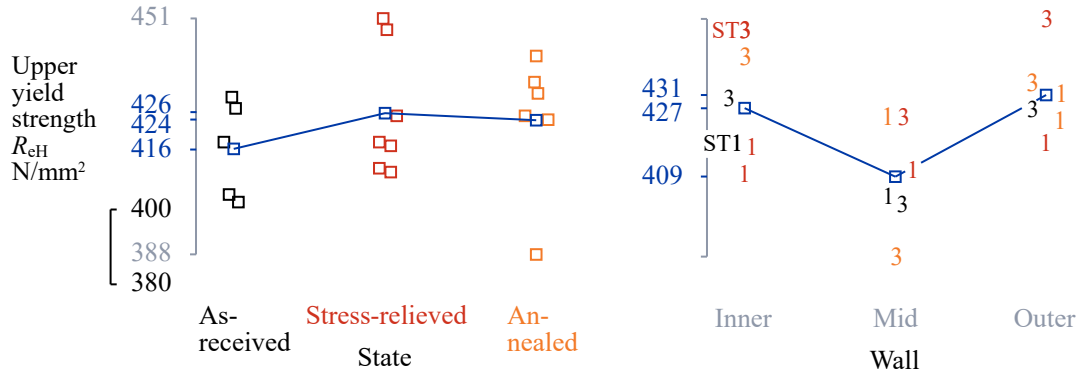

Figure 7-4. *Upper yield strength versus heat treatment state and radial position in wall influenced by hot forming inhomogeneities. From Sarnet (2024b).*

7.4.2 Dynamic strain ageing

At temperatures of about 100–200 °C, dynamic strain ageing of the steels intended for the Rebus insert is possible due to their content of nitrogen and carbon. There could be an intensified work hardening effect during deformation and an oscillating deformation behaviour. Together, these effects can result in a reduced ductility within this temperature range. Dynamic strain ageing can also reduce fracture toughness and low cycle fatigue life, but the number of defects in the steel parts is low and very few cycles of loads will affect the insert in load cases where dynamic strain ageing could be relevant in the final repository.

In the strain ageing and tensile testing experiments reported in Sarnet (2024b), dynamic strain ageing was analysed for specimens taken from Rebus tubes and for a set of temperatures and strain rates. In theory, an activation energy Q could be calculated for the occurrence of dynamic strain ageing from the slope of $\log_{10}$(strain rate) versus 100000/T[in Kelvin] which is given by Q/R, where R is the universal gas constant. From data in (Otterberg and Karlsson 1979), the activation energy for dynamic strain ageing was calculated to be 80 kJ/mol. The results show that dynamic strain ageing occurs for the tested temperature interval of 180–300 °C. Dynamic strain ageing can be identified as serrations in the stress-strain curve. It can be seen in Figure 7-5, that the maximum amplitude of the serrations and therefore of the dynamic strain ageing occurs at 250–275 °C at a strain rate of 0.002/s. At lower strain rates combined with such temperatures, there are in some cases no distinct yield points and quite limited serrations.

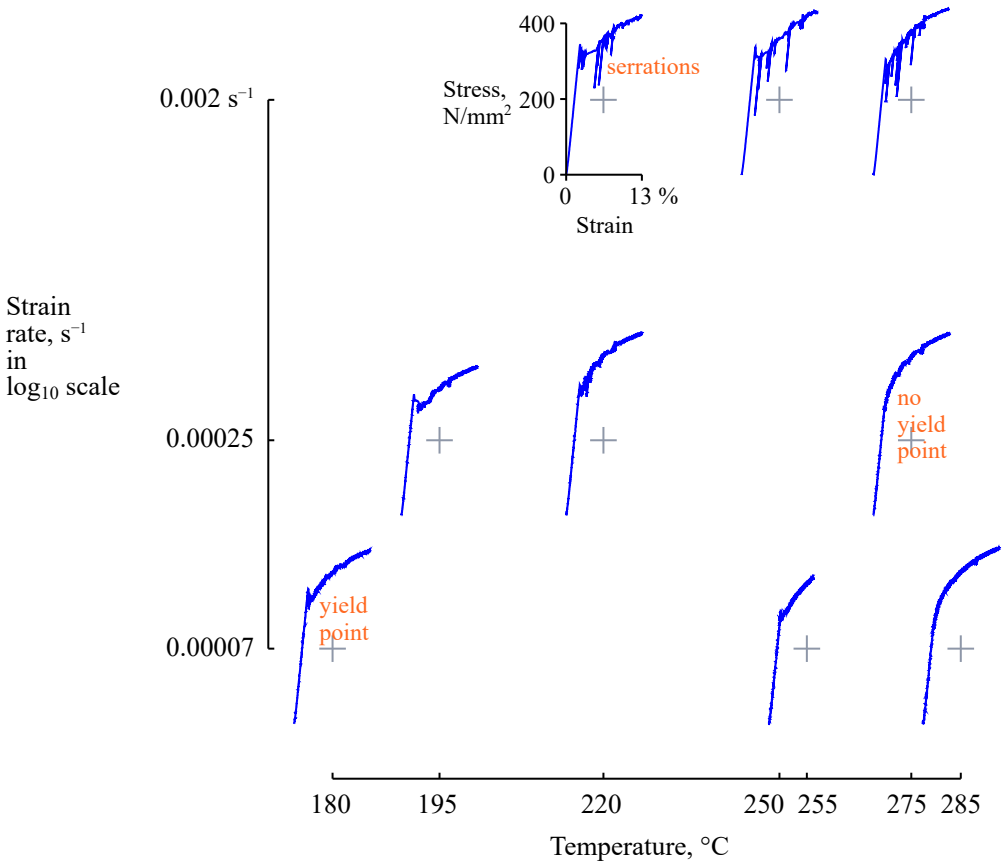

Figure 7-5. *Stress strain curves for dynamic strain ageing experiments, for nine combinations of strain-rate and temperature, denoted by a cross for each of curves. From Sarnet (2024b).*

The ductility measured as elongation at failure is, during dynamic strain ageing, lower than the average room temperature elongation 32 %, but remains relatively high at 24 %.

As mentioned in Section 5.2.1, the temperature of the canister insert will peak initially at below 115 °C, and it will in the long term eventually decrease to the background temperature of the host rock of about 11 °C. Room temperature can be expected after a few thousand years. In summary, it is concluded that dynamic strain ageing is not expected to occur for a P355 steel in a repository environment, given the lack of dynamic strain ageing of the P355-steel below 200 °C, according to the results in Sarnet (2024b).

It is additionally noted that dynamic strain ageing has been suggested for nodular cast iron at room temperature (Valmalle et al 2024). Other measurements in the temperature interval 20–125 °C do, however, not corroborate such room temperature dynamic effects for nodular cast iron (Sarnet 2022).

7.4.3 Static strain ageing

If steels are subjected to a high and permanent deformation, a static strain ageing may arise due to diffusion of elements to deformation sites, locking the deformation. A distinct yield point can appear and subsequent deformations could require higher stresses in addition to the work hardening of the steels. The increased strength of the steel can lead to a reduced ductility and fracture toughness. The permanent deformations of the seamless tube are, however, only marginally larger than the elastic deformations for the expected static loads in the repository environment, and for longer time spans an over-ageing and recovered properties may be expected.

In the strain ageing and tensile testing experiments reported in Sarnet (2024b), static strain ageing was analysed for specimens taken from Rebus tubes and for a set of ageing temperatures, ageing times and amount of strain the specimens were subjected to prior to ageing. From the results, it is clear that for ageing temperatures 20–155 °C, the pre-strain is the main influencing factor for strain ageing. Accounting for all data, irrespective of ageing time and temperature; for a pre-strain of 0.3 %, Figure 7-6 shows that the strain ageing is negligible, for 1 % pre-strain, the rise in lower tensile strength is 10 N/mm^2, and for 3 % pre-strain, the increase in lower tensile strength is 80 N/mm^2. Furthermore, as shown in Sarnet (2024b), there seems to be a lower critical pre-strain, below which static strain ageing does not occur. The ductility is almost unaffected, for a pre-strain of 3 %, the elongation is on average around 30 %. The elongation decreased to 26 % for a single specimen at most. Due to the moderate strain ageing reduction of the ductility, static strain ageing will not degrade the properties of the steel insert in the repository.

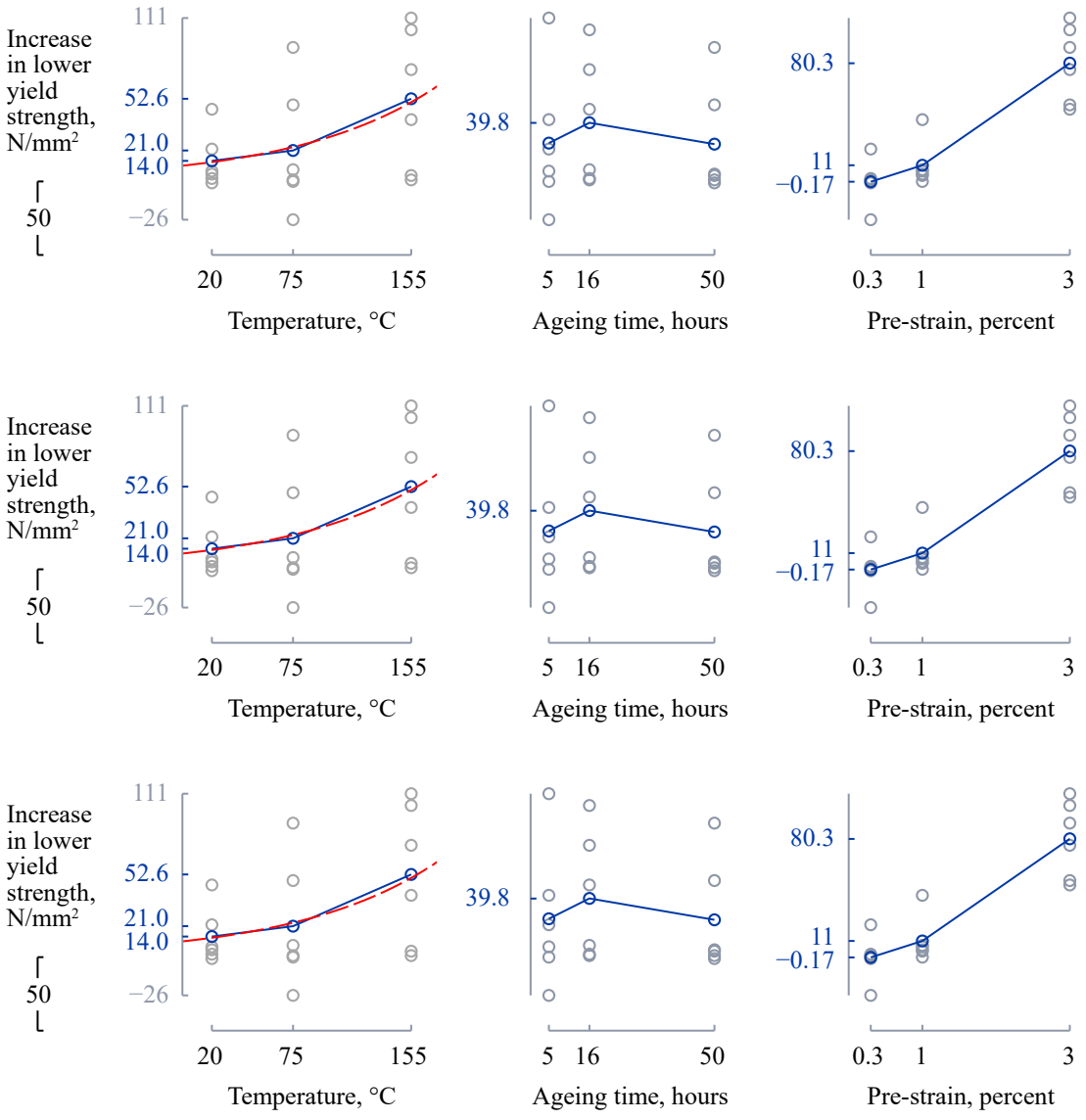

Figure 7-6. *Increase of lower yield stress versus the ageing temperature, ageing time, and pre-strain (Sarnet 2024b).*

7.4.4 Conclusions

The low carbon steels intended for the Rebus inserts are ferritic, like nodular cast iron. The ageing behaviour presented for the low carbon steels in (Sarnet 2024b) are comparable to those presented in the investigation on ageing of nodular cast iron (Sarnet 2022).

Tensile testing shows that the steel tubes have a ductility of 30 % elongation at failure. This is interpreted as a good resilience to strain ageing for the steel tubes.

Generally, the least favourable of the tested conditions for strain ageing of P355N steel is dynamic strain ageing at 200–300 °C for a strain rate of 0.002/s. The ductility decreases slightly, but retains an elongation of 24 % on average. Furthermore, during a 5 cm shear load the temperature will only increase about 1 °C by the energy released in the deformation of the material (SKB 2017) from a temperature in the interval 11–115 °C depending on the elapsed time after deposition of the canister. In mechanical analyses of the canister's resilience to shear loads in the repository, effects of dynamic strain ageing can, therefore, be neglected based on the findings in Sarnet (2024b).

The requirement on the ductility is a minimum of 3 % for the cast iron insert (Jonsson et al 2018), far below the standard values of 20 % (SS-EN 10216-3:2013). The carbon steel insert material is therefore assessed to be able to strain age without decreasing below that standard value. In mechanical analyses of the canister's resilience to shear loads in the repository, effects of static strain ageing can, therefore, be neglected based on the findings in Sarnet (2024b). After experiencing a shear load from a 5 cm rock displacement, the ductility measured as the elongation could change from around 34 % to 30 % due to static strain ageing, which can be considered negligible.

7.5 Effects of radiation

7.5.1 Introduction

The gamma and neutron radiation to which the canister materials will be exposed after fuel loading will potentially have some effects that require evaluation from the point-of-view of post-closure safety. These are all related to the fact that both gamma and neutron radiation will to some extent cause displacements of atoms in the iron lattice of the low-carbon steel insert, creating pairs of vacancies and interstitial atoms in the matrix. Such effects have been observed and extensively studied for steel materials in reactor pressure vessels (RPVs). The doses and dose rates RPV steels are exposed to are, however, at least three orders of magnitude higher than those of relevance for the Rebus insert materials in the final repository, at temperatures typically close to 300 °C, compared to a maximum of around 110 °C for the Rebus materials (Section 5.2.1).

The direct effects on material properties of such displacements is a first and obvious issue to evaluate, although earlier evaluations for the cast iron insert have shown that such effects are negligible (SKB 2019). Other effects are related to the increased mobility of impurities in the insert material caused by the displacements. Since impurities essentially move through substitutional diffusion in the lattice, the increased concentration of lattice vacancies leads to an increased mobility of impurities. This, in turn, leads to an increased propensity for precipitation of, in particular, Cu clusters, that may have an embrittling effect on the insert material. Precipitation of more complex intermetallic phases containing e.g. Ni, Si and Mn may also occur. Another embrittlement process that may be affected and possibly enhanced by irradiation is the segregation of phosphorus to grain boundaries, known to cause intergranular embrittlement in ferritic steels (Sandberg and Korzhavyi 2009).

In the following, each of the mentioned processes are discussed. The doses and dose rates of concern are those reported for the Rebus canister in Chapter 4. Based on those dose calculations, Andgren (2023) determined damage rates and accumulated radiation damage in the material.

7.5.2 Direct effects of radiation damage in the Rebus canister

The gamma and neutron induced radiation damage to the Rebus insert reported in Section 4.4 are similar to those calculated for the cast iron insert as reported by Guinan (2001) and Yang et al. (2019). The doses to the outer copper shell are also similar, meaning that the damage rates in the copper shell are also comparable for the two inserts. Guinan (2001) deemed the level of defects estimated in his work too small to cause any measurable effects on the mechanical properties of the materials, such as yield strength. The same conclusion is, therefore, drawn for the Rebus materials.

Importantly, all these doses are computed while disregarding effects of thermal annealing. When accounting for thermal annealing for the canister with a cast iron insert, it was estimated that the accumulated concentration of defects will never exceed 5×10^{-11} dpa in any of the canister materials (Padovani et al. 2019, SKB 2019), i.e. many orders of magnitude less than when disregarding annealing. This substantially strengthens the conclusion that direct impact of radiation damage is negligible for both canisters with Rebus and cast iron inserts.

7.5.3 Precipitation of copper clusters

Precipitation of copper nano-particles is known to cause embrittlement of reactor pressure vessel steels after exposure to high radiation doses. The process has therefore been studied for cast iron for reasonably repository-like conditions expected for the first 300 years post-closure (Brissonneau et al. 2004) using a rate model for cluster formation and a mechanical model developed by Russell and Brown (1972) to assess impact on the shear strength. Brissonneau et al. (2004) also present expressions for converting the increase in shear strength to increases in uniaxial shear stress and in ductile-to-brittle transition temperature. The conclusion of the study by Brissonneau et al. (2004) is that a copper content of < 0.05 weight-% is required to avoid harmful precipitation of copper particles, modelled by Brissonneau et al. (2004) to be of sizes up to around 2 nm. This has been adopted by SKB as a technical design requirement for the cast iron insert, i.e. the copper content must be < 0.05 %[15] in order to avoid embrittlement caused by clustering and precipitation (Posiva SKB, 2017). Brissonneau et al. (2004) also pointed out the need for further experiments on relevant materials at low dose rates and low temperatures. Such an experiment was reported by Yang et al. (2022). These authors used the experimental outcome and results of density functional theory (DFT) calculations to update the model parameters used by Brissonneau et al. (2004). Yang et al. (2022) concluded that the copper particle sizes will be smaller (around 0.5 nm for concentrations up to 0.12 weight-%) and argued, based on the results of Russell and Brown (1972), that such particle sizes will cause negligible mechanical effects in the material. Remaining uncertainties concern e.g. how the dislocation densities applied in the rate models compare with the actual dislocation density of the material, the impact of temperature under repository conditions and the fact that the neutron contribution to the long-term dpa rate is underestimated in Yang et al. (2022). Also, the considerable uncertainties in some of the input parameters relating to vacancy and cluster dynamics warrant further sensitivity analyses.

To address these issues, Hedin (2024) applied the same models as Brissonneau et al. (2004) and Yang et al. (2022), for temperatures according to Section 5.2.1, dpa rates according to Section 4.4, and for recently measured dislocation densities in test-manufactured Rebus tubes (Hagström 2024). The input data set used by Yang et al. formed the basis for the calculations, and sensitivities to the older data used by Brissonneau were explored.

Several benchmark cases show good agreement with earlier results. With the new data, it was confirmed that 0.05 at.% Cu is indeed a sufficient criterion to avoid detrimental Cu clustering in the Rebus materials. Figure 7-7 shows the extent of Cu clustering as a function of time for a Cu content of 0.08 at.%. According to the model by Russell and Brown (1972) used to evaluate the impact on mechanical properties of clustering, primarily an increase in shear strength, cluster sizes below a cut-off value of approximately 0.62 nm do not have any impacts. As seen in Figure 7-7, the cluster distributions also peak at much lower values than this after a one million year simulation period. The number densities of clusters around the cut-off value are negligible. Furthermore, calculation results with higher Cu concentrations also indicate that a relaxation of the requirement to the standard

[15] It needs to be clarified whether the requirement is given as a weight-% or an atom-%. (The difference between the two is, however, small in this context.)

requirement of 0.35 at.% Cu for the quality of the P355N steel grade intended for use in the canister inserts would not yield an unacceptable extent of Cu clustering. This indication would be strengthened if verified experimentally. It is also of interest to evaluate the sensitivity of a potential cluster-induced alteration of mechanical properties would affect the resilience of the Rebus inserts to expected loads in a final repository. This is to some extent addressed in Section 8.10.3.

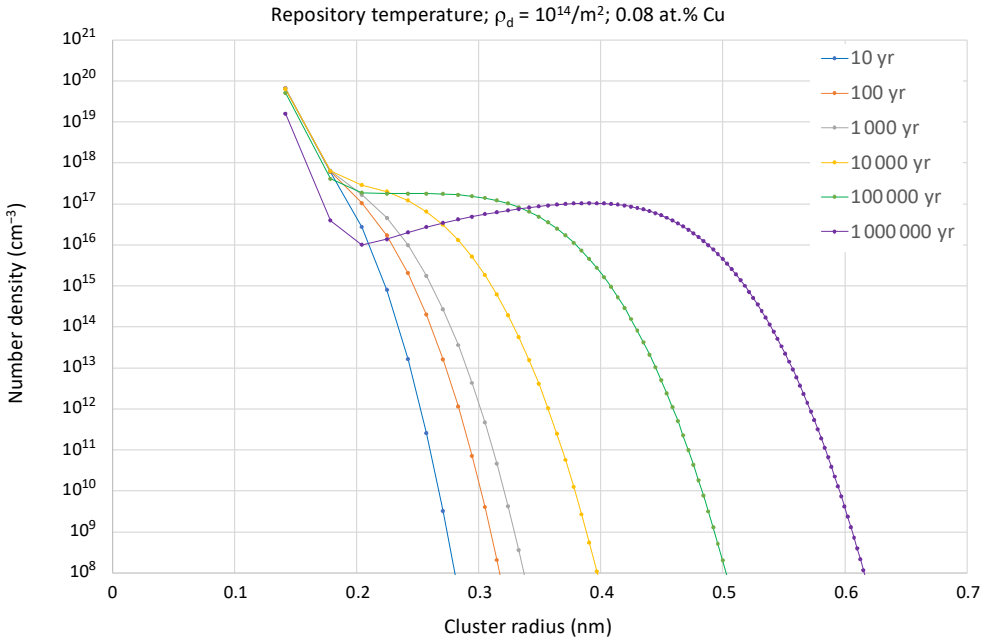

Figure 7-7. *Temporal evolution of Cu clustering under repository conditions for a Cu content of 0.08 at.%.*

7.5.4 Precipitation of other intermetallic phases

Precipitation of more complex intermetallic phases in reactor steels under irradiation has been observed experimentally (see e.g. the introduction in Korzhavyi et al. 2018). A number of alloying elements influence the microstructure. The most predominant elements are Cu, Ni, Mn, Si and C which may all form agglomerates as an effect of radiation (hardening effect), and P and S which are diffusing towards the grain boundaries (non-hardening effect). Computational studies of whether such phases (sometimes referred to as "late blooming phases", LBP, as they require extensive irradiation to grow to observable sizes) can occur in cast iron concluded that precipitation of such phases is thermodynamically possible for the "G-phase" (a phase rich in Ni, Mn and Si), metal phosphide phases of the stoichiometries M2P- and M3P (M equals Cr, Fe, or Ni), and a manganese sulfide phase MnS (Korzhavyi et al. 2018). The fact that these phases are thermodynamically stable does not necessarily mean that they will precipitate, as kinetic limitations may exist.

The elements identified as relevant for intermetallic phases and their levels according to requirements for cast iron (SKB 2010) and carbon steels (Section 0) are compared in Table 7-3. The allowed Mn content is higher in the specification of the carbon steel than in that of the cast iron. The content of Cr is typically one order of magnitude higher in the carbon steel, even though there is no formal requirement on Cr for the cast iron. The Ni and Si content (specification limits) is on the other hand lower in the carbon steel than in the cast iron.

Studies on low alloy steels irradiated at temperatures relevant to the operation of LWRs (light-water reactors) have shown a marked effect of Cu, and Ni, on the formation of agglomerates, but also the difficulties with synergistic effects, for example the interplay between the different elements, at different concentrations (Chaouadi et al. 2019). When it comes to the Ni/Mn/Si issue, investigations of reactor pressure vessel materials show a "cut-off limit" for the Ni content at approximately 1 % Ni, below which limited or no agglomerates appears even after significant irradiation in the laboratory (Chaouadi et al. 2019), as well as in pressure-water reactors (IAEA 2005, Roudén et al. 2023). At low Mn content, agglomerates are formed to a lesser extent, even with a Ni content above the 1%-level (IAEA, 2005), even though other mechanisms such as martensite formation may also play a role (Chaouadi et al. 2019). It must be noted that these effects have only been seen in

conditions where dose rates and total doses are several orders of magnitude higher than in the repository environment, and at temperatures exceeding what is expected for the canister insert in the repository. It is therefore concluded for the Rebus steel that irradiation induced precipitation of intermetallic phases consisting of Ni, Mn and Si will give negligible, if any, degradation of the insert.

Table 7-3. Key elements of the cast iron (requirements), and specifications for the carbon steels. Values in weight-%. The values for Fe are not requirements, but rather typical values calculated by subtraction of other main constituents.

Element	Cast iron, requirement	Carbon steel, tube	Carbon steel, framework	Carbon steel, lid and base
Fe	93	96	97	96
C	3.6	0.2	≤ 0.24	0.10 to 0.22
Ni	≤ 2.0	≤ 0.5	-	
Mn	0.05 to 1.0	0.9 to 1.7	≤ 1.70	1.10 to 1.70
Si	1.5 to 2.8	≤ 0.5	≤ 0.60	≤ 0.60
P	≤ 0.08	≤ 0.025	≤ 0.035	≤ 0.025
Cr	0.03 (typical, no req.)	≤ 0.3	-	≤ 0.30
S	≤ 0.02	≤ 0.02	≤ 0.035	≤ 0.010
Cu	≤ 0.05	≤ 0.05	≤ 0.05	≤ 0.05

7.5.5 Segregation of phosphorus to grain boundaries

Segregation of phosphorus to grain boundaries is known to cause intergranular embrittlement in ferritic steels (Sandberg and Korzhavyi 2009). This is a so-called non-hardening embrittlement mechanism where phosphorus causes a weakening of the grain-boundary cohesion, see e.g. Faulkner et al. (1996). The phosphorus content is lower in the Rebus insert material than in the cast iron insert. The specification for phosphorus in the steel tube is ≤ 0.025 %, which can be compared to the ≤ 0.08 % specified for the cast iron (see Table 7-3). In the tubes from the pilot production the content was even lower, and measured to be in the range 0.004 to 0.007 % (Johansson 2023). The achieved values for the cast iron are also lower than the specification, e.g. 0.024 (mean value, I53-I57) and 0.038 (mean value IP7-IP9), see Table 5-1 in SKB (2010).

Phosphorus is viewed as an impurity in modern steel making. In small quantities it can increase the strength but decreases the ductility and impact toughness. The phosphorus may be beneficial from a corrosion point of view, and for special applications, but most often it is preferable to keep the phosphorus content low.

Phosphorus can segregate to grain boundaries, enhanced either thermally or by radiation (Faulkner et al. 2005). In radiation-enhanced segregation excess point defects, Frenkel pairs, in regions remote from the grain boundaries and other interfaces are created by irradiation. A flux of radiation-induced point defect–impurity complexes is created, producing at steady-state a saturation of impurity atoms on a boundary. The driving forces are influenced by the presence of other impurities, especially carbon, which is competing with phosphorus for the sites at the grain boundaries. Further, larger grain size gives rise to an increase of segregated phosphorus, as shown in Faulkner et al. (2005).

For neutron irradiation there are studies of reactor material and typical reactor exposures for which segregation effects are seen. The effect on ferritic steels has been investigated thoroughly, with reported exposure times found in the literature up to some tens of years. Faulkner et al. (2005) find limited influence at temperatures at or below 100 °C for doses higher than 7×10^{-3} dpa. This is significantly higher than relevant dose levels in the repository. The sum of gamma and neutron induced displacements for the Rebus materials in the repository is calculated to be around 3.7×10^{-6} dpa, see Section 4.4.

Detailed comparisons of the phosphorus and carbon content, as well as grain sizes, between the steel (and cast iron) canister materials and the investigations of the steels compiled in e.g. Faulkner et al. (2005) would be possible, but will most probably be of limited value, as the irradiation levels and temperature are too high in the reactor materials tested.

The earlier SKB analysis for the cast iron insert, as given in Section 2.7 in Sandberg and Korzhavyi (2009), consisted of a pessimistically simplified estimate of the extent of phosphorus segregation to grain boundaries. It was concluded that such an estimate was not sufficient to disregard the effect over a time period of 300 years. The simplified treatment has been somewhat modified and, using updated input data, results suggest that the effect is negligibly small in a 300 year perspective, but not necessarily in a 10^6 year perspective, see Appendix D. The treatment is, however, still a pessimistic approach to the more complex diffusion mechanisms involved in phosphorus segregation, meaning that it cannot be seen as a realistic estimate of the extent of radiation-induced phosphorus segregation to grain boundaries.

To summarise, enhanced phosphorus segregation to grain boundaries has been observed in studies of reactor steels that resemble the steel suggested as the Rebus insert material. However, effects have only been seen in conditions where dose rates and total doses are several orders of magnitude higher than in the repository environment, and at temperatures exceeding what is expected for the canister insert in the repository. Since the observed effects are limited even for total doses three orders of magnitude higher than those in the repository, it is concluded that irradiation induced phosphorus segregation will give negligible, if any, degradation of the insert.

Even if the type of nodular cast iron intended for the cast iron insert design and the carbon steel type suggested for the Rebus insert differ in composition and microstructure, the resemblance is judged to be sufficient for the conclusions to be valid for both insert materials.

7.5.6 Conclusions

Conclusions from the assessments of the effects of radiation on the Rebus materials in the preceding Sections can be summarised as follows.

- The direct effects of damage caused by the radiation doses is assessed as negligible even when annealing effects, that greatly reduce the damage, are neglected.
- Updated calculations of Cu cluster formation, with a dislocation density measured for Rebus material and with repository-relevant temperatures and damage rates, confirm earlier findings that a Cu content of at most 0.05 at.% is sufficient to avoid detrimental Cu cluster formation in the Rebus material. Results of a calculation with higher Cu concentrations also indicate that a relaxation of the standard requirement of 0.35 at.% Cu for the quality of the P355N steel grade intended for use in the canister inserts would not yield an unacceptable extent of Cu clustering. This indication would be strengthened if verified experimentally. It is also of interest to evaluate how a potential cluster-induced increase in shear strength would affect the resilience of the Rebus inserts to expected loads in a final repository.
- Precipitation of more complex intermetallic phases consisting of in particular Ni, Mn and Si has been observed in irradiated reactor steels. Based on available literature data, it is concluded for the Rebus steel that irradiation induced precipitation of such intermetallic phases will give negligible, if any, degradation of the insert under repository conditions. The conclusion is primarily based on the fact that total radiation doses many orders of magnitude higher than those in a final repository are required for such effects to be observed.
- Radiation enhanced phosphorus segregation to grain boundaries may embrittle steel, as has been observed in studies of reactor steels that resemble the steel suggested as the Rebus insert material. However, effects have only been seen in conditions where dose rates and total doses are several orders of magnitude higher than in the repository environment, and at temperatures exceeding what is expected for the canister insert in the repository. It is therefore concluded that irradiation induced phosphorus segregation will give negligible, if any, degradation of the insert.

8 Resilience to mechanical loads in the repository

8.1 Introduction

One of the main functions of the canister insert is to withstand the mechanical loads that can be anticipated in the long term in the repository. Mechanical design analysis of the canister insert is therefore essential for the overall safety evaluation of the Rebus inserts.

As mentioned in Section 2.1, the technical design requirements on the canister regarding mechanical loads are currently as follows:

- The copper shell shall remain leak tight and the canister maintain its ability to resist loads for an isostatic pressure of 50 MPa.
- The copper shell shall remain tight and the canister maintain its ability to resist loads for
  - 5 cm rock displacements at all angles and a rate of 1 m/s,
  - exerted on the canister by a buffer with an unconfined compressive strength at failure lower than 4 MPa at a deformation rate of 0.8 %/min.
- The copper shell shall remain tight and the canister maintain its ability to resist loads for bending of the canister resulting from asymmetric loads according to Figure 2-1.
- The copper shell shall remain tight and the canister maintain its ability to resist loads for shearing of the canister resulting from asymmetric loads according to Figure 2-2.

The ability of the alternative insert to fulfil the technical requirements above has been assessed by mechanical analyses summarised and discussed in the following sections.

It is, furthermore, noted that isostatic pressures, arising from buffer swelling, groundwater hydrostatic pressure and glacial loads, affect all canisters in a final repository, whereas a shear load caused by the design basis rock shear of 5 cm is expected to affect only a very small fraction of the around 6000 canisters in the million-year time perspective of the safety assessment. The likelihood of the asymmetric loads is currently not possible to assess for the intended Forsmark site for the repository, but it is noted that the asymmetric load cases considered in the following include pessimistically formulated bounding cases.

8.2 General discussion about failure modes and damage mechanisms

The Rebus design of the canister insert consists of an outer tube, base, lid and an internal framework of plates, all of which are made of ferritic steel. Commonly considered failure modes for this type of material and structure are excessive plastic deformation, instability/buckling, local failure and fracture.

Degradation mechanisms are processes that over time, individually or when combined, weaken the structural integrity of the component, leading to decreased margin against the different failure modes.

Stress corrosion cracking, embrittlement and ageing phenomena are covered in Chapter 7. In addition, a supplementary systematic review of potential cracking damage and degradation mechanisms has been performed by Storesund and Feigin (2025). Conceivable cracking damage mechanisms were evaluated as well as other degradation mechanisms, which may increase the sensitivity to cracking damage mechanisms due to the environment in the canister insert. Creep was assessed to be negligible (< 0.2 %) for the canister insert at repository conditions (see further Section 8.9.1) and cracking damage mechanisms controlled by cyclic loads (e.g. fatigue, corrosion fatigue and strain induced corrosion cracking) could be ruled out simply because of the lack of repeated cyclic loads. In summary, Storesund and Feigin (2025) found no cracking damage or degradation mechanism, in addition to those already being considered, that require further attention for the Rebus inserts.

8.3 Introduction to analysis of load cases

8.3.1 Purpose and scope

Jonsson et al. (2018) summarise mechanical design analyses of the canister with a copper shell and a nodular cast iron insert. The report gives a systematic description of the canister, load cases, material properties, acceptance criteria, as well as analyses and results which are reported in detail in underlying references.

Deviations between the canister design with a cast iron insert and the Rebus design are such that new design verification analyses are required and a feasibility study with focus on the Rebus insert design was made.

The feasibility study (Mångård et al. 2023) reviewed and evaluated all load cases in Jonsson et al. (2018) with the aim of identifying the analysis work required to accomplish a basis for the mechanical design assessment for the Rebus insert.

The scope of analyses of load cases for the Rebus design follows the recommendations in the feasibility study and involves global plastic collapse analyses for a nominal alternative insert design as well as defect tolerance analyses of crack-like defects.

8.3.2 Load cases

Design requirements for the canister are systematically reviewed and reported in the design basis (Ljustell et al. 2024a) and complementary design basis (Ljustell et al. 2024b) for mechanical equipment. The design requirements follow the principles in ASME Sections III and XI. However, loads acting on the canister are associated with uncertainty and scatter other than those for the characterising parameters of loads in e.g. ASME Section III and European Norms. As a consequence, the safety factors for occasional loads and faulted-load conditions used in the current work may not strictly adhere to those from the standards. The design requirements apply to both the BWR and PWR versions unless otherwise stated. The design basis and complementary design basis have been developed in a general way and apply to the KBS-3 canister design with a cast iron insert as well as with a Rebus insert.

Prerequisites for the structural verification of the Rebus design, i.e. the analyses aimed at demonstrating that the design fulfils the mechanical design requirements, are reviewed and reported in Ljustell (2024a, b) with consideration of the recommendations in the feasibility study (Mångård et al. 2023). Five main load combinations fall into four different stages of the repository development as described by Table 2-1 in Jonsson et al. (2018), see Table 8-1. Some changes in the requirements and prerequisites for the deposition hole geometry and buffer dry density properties have later been established in Laitinen (2025) and Åkesson (2024).

Table 8-1. Five main load combinations, derived from the postulated repository evolution, fall into four different categories. Loads that may act simultaneously are combined. Coloured boxes correspond to the possible periods for the load case in question.

Repository evolution phase		Water saturation	Temperate	Glacial	Subsequent permafrost and glacial periods
Years after closure of the repository		0 – 10 000 years	10 000 – 50 000 years	50 000 – 60 000 years	60 000 – 1 000 000 years
Canister temperature T (°C)		T < 125/100 (Fe/Cu)	20 < T < 125/100 (Fe/Cu)	0 < T < 20	0 < T < 20
Load case and description	**Changes in load description relative to Jonsson et al. (2018)**				
1a (L02) Normal Load Condition Asymmetric pressure loads during water saturation	Hydrostatic pressure and axial swelling pressure now included. Pressure levels adjusted in Åkesson (2024).				
2a (L03) Normal Load Condition Asymmetric pressure loads after complete water saturation	Hydrostatic pressure and axial swelling pressure now included. Pressure levels adjusted in Åkesson (2024).				
3a (L04) Normal Load Condition Swelling and ground water pressure	No change				
4a (L05) Occasional Load Condition Glacial isostatic pressure	No change				
4b (L06) Occasional Load Condition Glacial isostatic pressure and asymmetric pressure loads after complete water saturation	Not analysed in the design analysis report for the canister with a cast iron insert (Jonsson et al., 2018).				
5a (L07) Faulted Load Condition Shear load due to rock displacement	No change				
5b (L08) Faulted Load Condition Shear load due to rock displacement combined with asymmetric pressure loads after complete water saturation	Hydrostatic pressure and axial swelling pressure now included. Pressure levels adjusted in Åkesson (2024).				

Based on the load cases and results presented in Jonsson et al. (2018) and the additional considerations in Laitinen (2025) and Åkesson (2024), the following load cases have been identified (Mångård et al. 2023) as requiring analysis in order to demonstrate that a canister with a Rebus insert fulfils the technical design requirements listed in Section 8.1 (load case names defined in the discussion of a wider set of cases in Mångård et al. (2023)):

- Load case 1a (L02)* considers the possible effect of asymmetric buffer swelling due to imperfections in the deposition hole geometry and uneven water saturation before full saturation. Since this event appears during the water saturation phase, it is assumed that groundwater hydrostatic pressure does not apply.
- Load case 2a (L03)* considers the situation at full water saturation. Although the uneven water saturation effects are expected to be evened out at full water saturation, asymmetric buffer swelling pressure may remain as a result of imperfections in the deposition hole geometry and inhomogeneities in the initial buffer density. These deviations are covered in Laitinen (2025) and Åkesson (2023). A groundwater hydrostatic pressure of 5 MPa acts in the repository at full water saturation. However, this load contribution is excluded from the current Rebus analyses of load case 2a as it is included in load case 3 that is enveloped by load case 4a below.

*Ljustell (2024) uses both the above nomenclature and the additional nomenclature L01-L08 for the load cases needing consideration, where L01 is the unloaded canister and L02-L08 are related to Cases 1a, 2a, 3, 4a, 4b, 5a and 5b according to the bullet list above.

- Load case 4a (L05)* considers the combined effect of a 10 MPa isostatic buffer swelling pressure at full water saturation, an additional 5 MPa groundwater hydrostatic pressure and a 35 MPa glacial isostatic pressure from a pessimistically chosen ice sheet thickness. The total isostatic pressure is thus 50 MPa. Load case 4 corresponds to load case 3 (L04)* with glacial isostatic pressure.
- Load case 4b (L06)* considers the same groundwater (5 MPa) and glacial (35 MPa) isostatic pressures as case 4a, but with asymmetric swelling pressure of the buffer.
- Load case 5a (L07)* considers a shear load due to rock displacement with symmetric swelling pressure assuming a nominal deposition hole geometry and density distribution.
- Load case 5b (L08)* considers a shear load due to rock displacement with asymmetric swelling pressure considering deviations covered in Laitinen (2025) and Åkesson (2024).

Shearing load due to rock displacement may in principle take place any time after sealing of the repository. This event is, however, most probable when a glacial ice sheet melts and least probable before full water saturation. This means that the load state at the onset of shearing displacement may be different depending on when the rock shearing is activated. Therefore, two different load sequences have been considered, each applying three consecutive load states as shown in Table 8-2. Load state 1 is identical for both load sequences.

For the isostatic load case 4a (L05) and the rock shear load case 5a (L07), both the PWR and the BWR inserts were analysed. The results showed that the PWR insert generally has lower margins against the failure criteria than the BWR insert, see Sections 8.5 and 8.7, respectively. The other load cases were therefore analysed only for the PWR canister.

Table 8-2. For the shear load, two different load sequences have been considered, each applying three consecutive load states.

	State 1	State 2	State 3
Sequence A	Swelling pressure and groundwater hydrostatic pressure	Rock shearing load	Glacial isostatic pressure
Sequence B		Glacial isostatic pressure	Rock shearing load

8.3.3 Acceptance criteria

Global plastic collapse

Criteria for global plastic collapse were established for the asymmetric swelling, isostatic- and the rock shear load cases, based on the ASME code and considerations regarding acceptance criteria in Jonsson et al. (2018).

For the asymmetric swelling and isostatic load cases, the twice elastic slope approach as described in the ASME code (ASME III Appendix II-1430-1), and illustrated in Figure 8-1, was established.

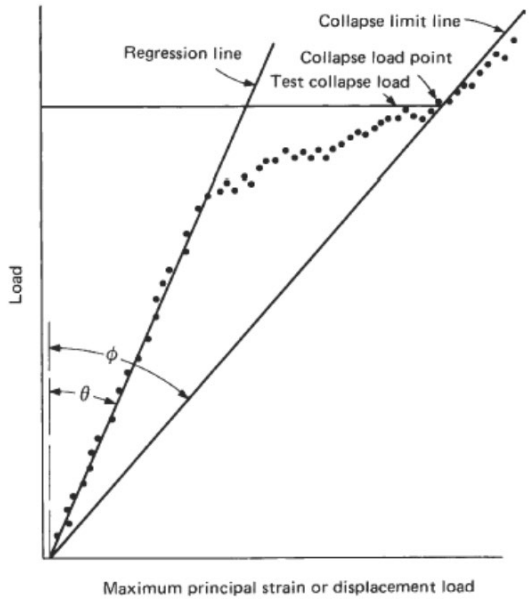

Figure 8-1. *Definition of plastic collapse load point according to the ASME code. The regression line is determined by the initial linear region, and the collapse limit line has by definition half the slope of the regression line. The collapse load point is determined by the load intercept of the collapse limit line and the dotted load-displacement curve.*

For the shear load cases, this criterion is not suitable since the elastic regimes required for application of it do not occur in this load case. Instead, a strain-based criterion, by analogy to what was used for the shear load cases in the mechanical design analyses of the cast iron insert (Jonsson et al. 2018) was derived and applied. The criterion states a limiting value of 5 % elongation for the displacement-controlled 5 cm rock shear load.

In the current work, the margin against global plastic collapse for the displacement-controlled shear loading has been assessed using a limiting value of at least 5 % absolute principal structural strains for P355N. This value is only to be used to support a sufficient margin against global plastic collapse, and should not be used as a material requirement. The rationale behind this limiting value is given in the corresponding reports Feigin et al. (2024a, b, c).

Defect tolerance

In the defect tolerance analysis, with the postulated defects, the critical defect size is given using the failure criterion $J = J_{mat}$, and the acceptable defect size is given using the criterion $J = J_{mat}/SF_J$. In these equations, the crack driving force J is the applied J-value, as given by FE modelling (see below), and J_{mat} is the fracture toughness. SF_J is the safety factor used when calculating the acceptable defect size.

Safety factors were selected in agreement with the SSM procedure for defect tolerance analyses (Dillström et al. 2018) yielding for all force-controlled load cases $SF_J = 10$, and for the displacement-controlled rock shearing $SF_J = 2$.

The basis for defect tolerance analyses in the following sections is described in Bolinder et al. (2025).

8.3.4 FE modelling

The numerical analyses covered in this section were performed with the finite element method (FEM) using the two commercial software tools Ansys and Abaqus. The choice of software for each load case was determined by the software features in relation to the problem at hand as well as historical reasons connected to the cast iron insert.

Ansys was used for global plastic collapse analyses of load cases 1a, 2a, 4a and 4b. The analyses of these load cases are not dependent on the presence of the buffer, contrary to the rock shearing load case, and the buffer is therefore excluded from the modelling. The swelling, hydrostatic and isostatic pressures were hence applied directly on the copper shell.

Abaqus was used for global plastic collapse analyses of load cases 5a and 5b and defect tolerance analyses of load case 4a and 5a. Abaqus models used for the previous analyses of the canister design with a cast iron insert were reused by replacing the cast iron inserts by the Rebus inserts while keeping the copper shell and buffer regions. Swelling and hydrostatic pressures were introduced as an initial pressure condition within the buffer while isostatic pressure was applied directly on the copper shell. The buffer was removed from the defect tolerance analysis of load case 4a and 4b by applying the swelling, hydrostatic and isostatic pressures directly on the copper shell. This approach is the same as the modelling for the plastic collapse analyses of load case 4a using Ansys.

Frictional contact was generally used to allow interaction between detached regions, e.g. the steel tube and the inner steel plate framework. The Rebus insert contains a much greater extent of detached regions compared to the cast iron insert. To reduce the numerical complexity, contact interaction was replaced by constraint equations or other approximations in regions where significant relative displacements between parts were not expected.

The effect of manufacturing tolerances was investigated in the plastic collapse analyses of load case 4a and 4b, while nominal dimensions were used in load cases 1a, 2a, 5a and 5b. In the damage tolerance analyses of load case 4a, the tolerances which were deemed to cause the weakest lid were used.

To reduce the computational demands, symmetry planes were employed when possible. After loading, the inner steel plate framework does not necessarily remain quarter-symmetric and the appropriateness of these idealisations was supported by analyses of complete models without taking advantage of symmetry planes, see Section 8.5.1. It was not possible to take advantage of symmetry planes for the analysis of asymmetric swelling or shear loads, due to the inner steel plate framework.

Details regarding modelling is covered in the respective analysis reports.

8.3.5 Materials data

Mechanical properties used in the numerical analyses of the Rebus insert are described in detail in Appendix A of each analysis report referenced in the following sections. Fracture toughness is covered in Bolinder et al. (2025).

The bentonite with a density of 2022 kg/m^3 at water saturation is defined with strain-rate-dependent data, isotropic hardening and elastic-plastic properties.

The modelled mechanical properties for the copper differ depending on the load case. In load case 1a, 2a, 4a and 4b, a copper model with low strain rate, isotropic hardening and elastic-plastic properties was used. In load case 5a and 5b, a copper model with strain rate of 0.005/s, isotropic hardening and elastic-plastic properties was used. The strain rate dependence for this load case is explained by the short duration of rock shear.

The mechanical properties for the tube material P355N are based on standard minimum yield strength and plastic hardening attained from mechanical testing. The hardening curve has been shifted to fit the standard minimum yield strength of P355N specified by the standard for seamless steel tubes for pressure purposes EN 10216-3:2013.

The mechanical properties for the lid and base material P355GH+N are based on standard minimum yield strength and the plastic hardening behaviour established for P355N which has been shifted to fit the standard minimal yield strength of P355GH+N specified by the standard for flat products made of steels for pressure purposes EN 10028-2:2017.

The mechanical properties for material S355J2+N used in the internal framework depend on the thickness of the plates. The plastic hardening behaviour established for P355N has been used by shifting it to fit the standard minimal yield strength of S355J2+N for each plate thickness specified by the standard for hot rolled products of structural steels EN 10025-2:2019.

Fracture mechanics tests at room temperature have been conducted for several samples from several steel tubes of the P355N material and for several samples from one lid/base of the P355GH+N material (Bolinder et al. 2025). The results show that all specimens experienced ductile fracture initiation and displayed high fracture toughness values overall. The conclusion in Bolinder et al. (2025) is that an upper limit of J_{mat} = 1000 kN/m and a lower limit of J_{mat} = 200 kN/m may be

chosen for P355N and P355GH+N for the defect tolerance analyses based on the available data. The reasoning behind defining J_{mat} with a range instead of a fixed value is to take into account possible impact of degradation mechanisms and uncertainties in variations of fracture toughness between different heats of material. A further benefit with defining a range of J_{mat} is that with a range, the analyses will also produce a range of acceptable crack sizes dependent on J_{mat}. This will facilitate the establishment of requirements that are robust both with respect to material fracture toughness and inspection capabilities.

Thermal development of the Rebus canister in the repository environment is discussed in Section 5.2.1. Figure 5-1 and Figure 5-2 suggest peak temperatures of about 95 °C for the copper shell, about 100 °C for the steel tube and about 130 °C for the internal framework. The peak temperatures are reached after about 10 years and the entire canister will attain a temperature of about 20 °C after 10 000 years.

The duration of the water saturation period depends on the conditions in the final repository. SKB 2022c mentions saturation times ranging from 20 to several thousand years. This means that full saturation may be reached before the canister temperature has decreased to the background temperature of the buffer and host rock. Temperate climate conditions are thereafter expected to last for tens of thousands of years, followed by permafrost and glacial conditions during which the canister temperature may drop to 0 °C.

This means that the canister temperature during the different evolution phases will vary between 0 °C to 100 °C for the copper shell, 0 °C to 100 °C for the steel tube, and 0 °C to 130 °C for the internal framework.

- The canister temperature is higher than 20 °C during the water saturation and temperate phases which involve load cases 1 and 2 (swelling pressure and hydrostatic pressure).
- The temperature is lower than 20 °C during the glaciation and deglaciation phases which involve load cases 4 and 5 (glacial isostatic pressure and shear loads).

The numerical analyses presented in this section have been performed with material data at 20 °C without regard to which evolution phase the respective load case belongs. It is therefore necessary to account for the effect that the repository relevant temperatures may have on fracture toughness and yield stress.

Fracture toughness is relevant for the defect tolerance assessments which have been performed for glacial isostatic pressure and shear loads. These load cases are most likely to occur during glaciation and deglaciation during which the canister temperature will range between 0 °C and 20 °C. It is expected that the material is ductile in this temperature range if it behaves similarly to other steels and is not degraded. Fracture toughness is expected to decrease in the upper-shelf region with increased temperature (Yu-De 1992, EricksonKirk and EricsonKirk 2006) and it is pessimistic to use fracture toughness values for 20 °C at a temperature of 0 °C (this does not consider potential degradation, which may affect whether the upper-shelf region has been reached at this temperature).

Yield stress is relevant primarily to assess the margin against plastic collapse. It is expected to decrease with increasing temperature and vice versa. This means that it is pessimistic to use room temperature data in the assessment of glacial isostatic pressure and shear loads during which the canister temperature will range between 0 °C to 20 °C. The opposite is true for swelling pressure and hydrostatic pressure loads during which the temperature is higher than 20 °C. It should be remembered that the experimentally measured hardening behaviour has been adjusted to match the minimum required yield stress for the materials. This means that the potential reduction in yield stress due to elevated temperatures must be accounted for in the analyses, which is done in Section 8.4.1 for load cases 1a and 2a. The influence of a change in yield stress on the margin against global plastic collapse has been investigated by probabilistic analyses for load case 4.

8.4 Asymmetric swelling, load cases 1a and 2a (L02 and L03)

One of the technical design requirements states that the canister has to maintain its ability to resist loads from bending due to asymmetric pressure on the copper shell. The causes for the asymmetric loads are uneven wetting of the buffer from the rock and deviations in deposition hole geometry. Asymmetric pressure during the saturation phase of the bentonite is analysed as load case 1a, and asymmetric pressure after complete water saturation is analysed as load case 2a.

Assessment of the margin against global plastic collapse was performed for the PWR version of Rebus canister. Note that input from Åkesson (2023) was used for these load cases. This reference was subsequently corrected to Åkesson (2024), where the correction implied slightly reduced loads.

8.4.1 Global plastic collapse

The margin against global plastic collapse was evaluated by 3D FEM using Ansys and is reported in Hammer and Fredriksson (2025). The work was performed with a complete model of the canister, since there are no symmetry planes for this load case. The internal framework plates were oriented such that the bending was applied at 45° from the plane of the largest internal framework plate.

The design loads for cases 1a and 2a are defined by the swelling pressures given in Ljustell (2024a). Hydrostatic pressure and axial swelling pressure acting on the base and lid have been added to load case 2a.

The copper shell was divided into different sections where pressure was directly applied to achieve the desired asymmetric conditions, depending on the load case. The load cases were divided into a base case and a pessimistic case, the latter with a more pessimistic handling of buffer uncertainties and thus with higher pressure magnitudes. For load case 2a, only the pessimistic case was evaluated. The outer pressure was propagated through the structure by contact between the main components. The steel tube was the focus of this analysis and was evaluated using the twice elastic slope acceptance criterion.

The results shown in Table 8-3 demonstrate sufficient margins against global plastic collapse. For load case 1a, the calculated collapse load was 32.7 MPa, meaning a margin against the design load by a factor of 2.9 for the base case and 2.4 for the pessimistic case. For load case 2a, the calculated collapse load was 32.5, meaning a margin against the design load by a factor of 1.8 for the pessimistic case.

The analyses were carried out with material data for 20 °C, though the peak temperature during this load case is 100 °C for the steel tube. The reduction in yield stress and tensile strength are approximately 13 % when comparing the minimum required values at 20 °C and 100 °C for P355NH in EN 10216-3:2013. It may be assumed that the hardening behaviour remains unchanged. A decrease in the yield stress is hence expected to result in a corresponding reduction of the collapse load, which would still result in margins against global plastic collapse exceeding a factor of 1.5.

Table 8-3. Margin against the collapse load predicted by the 3D FEM-analyses.

Load case	Base case	Pessimistic case
1a	32.7 MPa / 11.3 MPa = 2.9	32.7 MPa / 13.4 MPa = 2.4
2a*	-	32.5 MPa / 18.4 MPa = 1.8

*Only the pessimistic case was evaluated

For the assessment of SCC (see Section 7.2), it is of relevance to determine whether through-thickness tensile stresses in the copper shell and the steel tube occur in early stages of the repository development. Appendix D in Hammer and Fredriksson (2025) provides normal stresses along the inner and outer circumference at canister mid-height. The maximum 1st principal stress in the steel tube and copper shell are summarised in Table 8-4. The through-thickness stress distribution changes significantly around the circumference. The most significant membrane tensile stress at canister mid-height is the axial stress at 225° in the steel tube and copper shell for both load case 1a and 2a. Axial and hoop stresses for load case 1a along the inner and outer circumference of the steel tube and the copper shell at mid-height are shown in Figure 8-2 and Figure 8-3, respectively. Also for load case 2a there are through-thickness tensile stresses in the axial direction (although lower in magnitude

than for case 1a), while the hoop stresses are compressive. For the canister design with a cast iron insert, through-thickness tensile stresses also cannot be excluded neither for the copper shell nor for the insert. Those reported for the cast iron insert are, however, lower than those of the Rebus insert, see Section 7.2.2.

Table 8-4. Maximum principal stress at canister mid-height for the PWR canister predicted by the 3D FEM-analyses at the pessimistic case load levels.

Load case	Copper shell	Steel tube
1a	65.2 MPa	195.7 MPa
2a	48.8 MPa	179.3 MPa

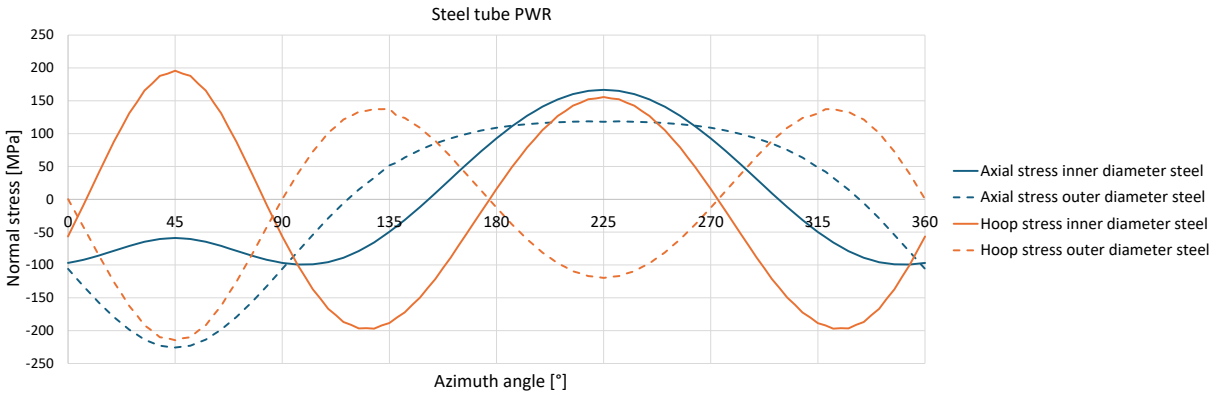

Figure 8-2. *Axial and hoop stress for the pessimistic version of load case 1a along the inner and outer circumference of the steel tube at mid-height, where 0° corresponds to a point where the internal framework meets the steel tube.*

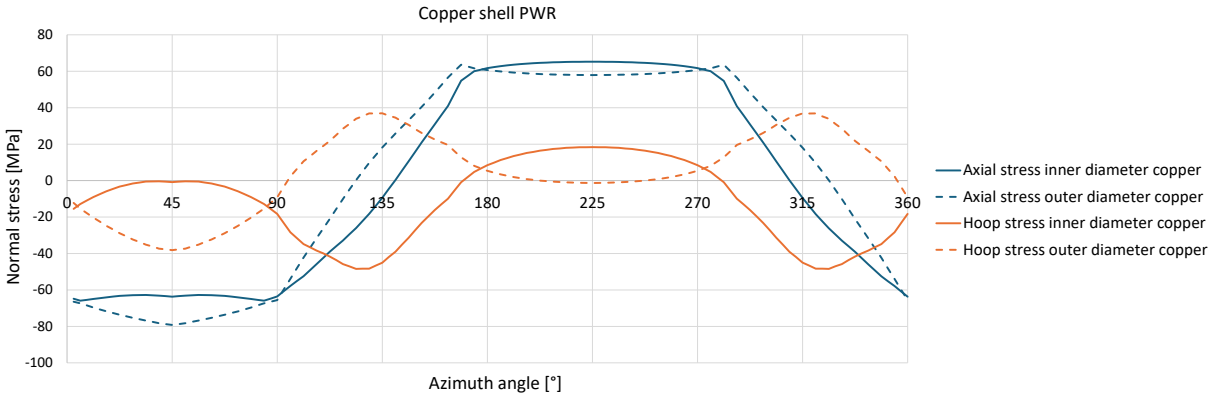

Figure 8-3. *Axial and hoop stress for the pessimistic version of load case 1a along the inner and outer circumference of the copper shell at mid-height, where 0° corresponds to a point where the internal framework meets the steel tube.*

8.5 Isostatic pressure with symmetric swelling, load case 4a (L05)

One of the technical design requirements states that the canister has to resist the normal load condition with isostatic swelling pressure, groundwater hydrostatic pressure and glacial isostatic pressure with a total value of 50 MPa. This corresponds to load case 4a and envelopes load case 3 in terms of the pressure magnitude.

Assessments of the margin against global plastic collapse and defect tolerance were performed for the BWR and PWR versions of the Rebus canister.

8.5.1 Global plastic collapse

The margin against global plastic collapse was evaluated by 3D FEM using Ansys and is reported in Hammer and von Unge (2024a, b). The work was performed using mainly quarter-symmetry models to reduce the computational demands and allow a higher resolution of critical areas. A complete model (without taking advantage of symmetry planes) was used to support the idealisations of the quarter-symmetry models. Results obtained with the two models are quite similar, see e.g. Table 8-5, and it was concluded that the quarter-symmetry idealisations were appropriate.

The outer pressure was propagated through the structure by contact between the main components. The steel tube, steel base and steel lid were evaluated using the twice elastic slope acceptance criterion. The influence of manufacturing tolerances was assessed by varying e.g. the gap between the steel lid and the internal framework ranging between 0.5 mm (minimum possible gap) and 3.8 mm (maximum possible gap). Two different combinations of manufacturing tolerances for the inner and outer diameters of the outer tube were also evaluated.

The results shown in Table 8-5 demonstrate a sufficient margin against global plastic collapse, with a collapse load exceeding 1.5 times the technical design requirement of 50 MPa, for all evaluated main components of the BWR and PWR versions. The outer tube was the limiting component for both versions. No conclusions could be drawn regarding the collapse load of the steel base and lid or the internal framework since the outer steel tube collapsed first.

Table 8-5. Collapse loads predicted by the quarter-symmetry FEM models. Collapse loads from the verification with the complete 3D model is shown in parentheses.

Axial gap	BWR	PWR
0.5 mm	75.1 MPa (75.3 MPa)	75.1 MPa (75.2 MPa)
3.8 mm	75.5 MPa	75.3 MPa

8.5.2 Defect tolerance

The defect tolerance for the isostatic load was evaluated by fracture mechanics 3D FEM using Abaqus and is reported in Öbrink et al. (2025d), and Öbrink and Bolinder (2025).

The steel tube of the insert was found to be in compression during the isostatic loading and was excluded from the assessment, which instead focused on the steel lid. As detailed in the methods document for defect tolerance analyses (Bolinder et al. 2025), the fracture mechanics analyses for the isostatic load case were performed by inserting regions containing a defect directly into the corresponding global plastic collapse models.

A fracture toughness of J_{mat}=200-1000 kN/m was used (Bolinder et al. 2025) for the defect tolerance analyses of the steel lid (P355GH+N). The isostatic loading is considered a normal operational state and requires a safety factor of SF_J=10 against fracture.

Results for the BWR and the PWR designs show that the most severe defect is a surface-breaking crack at the bottom of the steel lid, at roughly half the lid radius and oriented in the circumferential direction. Two positions (position 1 and position 2) were analysed for the BWR design, see Figure 8-4, while only position 1 was analysed for the PWR design, based on their respective stress and strain field results.

The results consist of acceptable crack dimensions for a range of fracture toughness values which are shown in Table 8-6, taking the safety factor SF_J=10 into account. This table includes a number of cracks, for both the BWR and PWR insert, with the same crack length. To obtain a more realistic length/depth ratio for defects with small depths, supplementary calculations were performed for the PWR insert, since the BWR insert had in initial analyses been shown to tolerate larger fractures. The results shown in Table 8-7 suggest that larger crack depths can be accepted for a given fracture toughness if a realistic length/depth ratio is assumed.

In the basis for the defect tolerance analyses (Bolinder et al. 2025), fracture toughness values for the steel lid and base material of at least 1000 kN/m are presented. In order to set requirements that are robust both with respect to possible variations in fracture toughness in the components and the inspection capability, a preliminary fracture toughness level of 375 kN/m is proposed. To give allowance for a 12 % decrease in fracture toughness (J_{Ic}) caused by possible hydrogen embrittlement (see Section 8.10.3), a fracture toughness level of 330 kN/m would apply, which in turn gives an acceptable crack depth of approximately 3 mm for a defect length of 18 mm, obtained by linear interpolation between the results for 200 and 400 kN/m fracture toughness in Table 8-7. The applied quality class in the inspection standard for penetrant testing (SIS 2016 SS-EN 10228-2:2016) state an acceptable defect length of 5 mm and that indications larger than 1 mm shall be recorded. This gives sufficient margins to the calculated acceptable defect size. Experience from the components manufactured by SKB and from general knowledge of manufacturing of steel plates suggest that surface-breaking cracks in the applied steel grade are unlikely. Based on this, on the margins between the acceptable defect sizes and on the inspection capability, it is assessed that unacceptable surface-breaking cracks in the steel lids can be readily avoided.

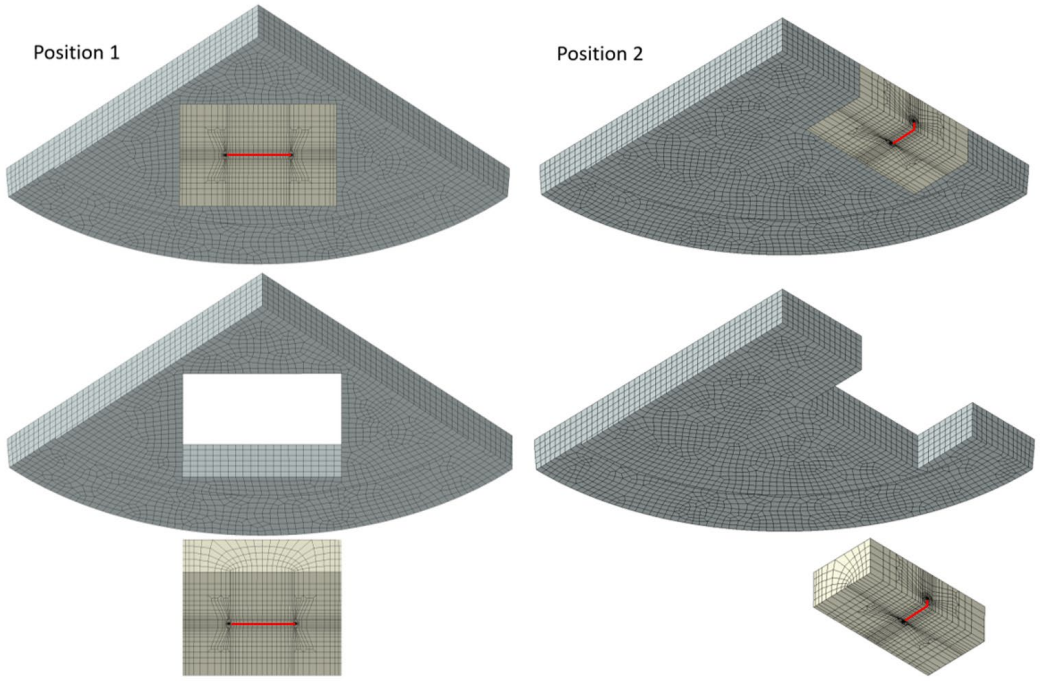

Figure 8-4. *Example defect regions containing a defect with length 84 mm and depth 14 mm in the canister models. The red lines show the location of the defect.*

Table 8-6. Acceptable crack dimensions (with fixed defect length) for the steel lid when the safety factor SF_J=10 has been taken into account.

Fracture toughness [kN/m]	BWR		PWR	
	Acceptable crack depth [mm]	Acceptable crack length [mm]	Acceptable crack depth [mm]	Acceptable crack length [mm]
200	1.6	84	1.1	84
400	3.7	84	2.3	84
600	10	84	4.3	84
800	21	84	10	84
1000	35	84	18	84

Table 8-7. Acceptable crack dimensions (with fixed defect length/depth ratio of 6) for the steel lid when the safety factor SF_J=10 has been taken into account.

Fracture toughness [kN/m]	PWR	
	Acceptable crack depth [mm]	Acceptable crack length [mm]
200	1.5	9.0
400	3.8	22.8
600	7.0	42.0
800	14	70.2

8.6 Isostatic pressure with asymmetric swelling, load case 4b (L06)

One of the technical design requirements states that the canister has to maintain its ability to resist loads from bending due to asymmetric pressure on the copper shell, as well as an isostatic pressure load consisting of a hydrostatic ground water pressure and a glacial pressure. The causes for the asymmetric loads are uneven wetting of the buffer from the rock and deviations in deposition hole geometry. Load case 4b (L06) combines the asymmetric pressure load from load case 2a (L03) with an isostatic load from load case 4a (L05).

Assessment of the margin against global plastic collapse was performed for the PWR version of Rebus canister. In the analysis, updated swelling pressures presented in Åkesson (2024) were considered.

The margin against plastic collapse was evaluated by 3D FEM using Ansys and is reported in Fredriksson (2025). The work was performed with a complete model of the canister, without the use of symmetry planes. The internal framework plates were oriented such that the bending was applied at 45° from the plane of the largest internal framework plate.

The copper shell was divided into different sections where pressure was directly applied to achieve the desired asymmetric conditions, depending on the swelling load case. The load case was divided into a base case and a pessimistic case with respect to magnitudes of the swelling pressure. The outer pressure was propagated through the structure by contact between the main components. The steel tube was the focus of this analysis and was evaluated using the twice elastic slope acceptance criterion.

The results shown in Table 8-8 demonstrate sufficient margins against global plastic collapse for the base case, but not for the pessimistic case. Note that the collapse pressure in Table 8-8 is presented for different surfaces relative to the respective design loads. This was done in the analysis due to different pressure magnitudes being applied on the sides where the evaluated nodes are located. The

lowest calculated collapse load for the base case was 73.38 MPa, with a margin against design load by a factor 1.57. For the pessimistic case, the lowest calculated collapse load was 73.89 MPa, with a margin against design load of a factor 1.46, which is less than the required 1.5. This is seen as acceptable since *i*) the deviation from 1.5 is small and *ii*) since a combination of the highest possible glacial ice sheet thickness, the highest possible buffer swelling pressure and the largest possible asymmetric swelling is assumed in the pessimistic case.

Table 8-8. Margin against the collapse load predicted by the 3D FEM-analyses.

Surface	Base case	Pessimistic case
σ_1	78.30 MPa / 49.0 MPa = 1.60	73.89 MPa / 50.7 MPa = 1.46
σ_2	73.38 MPa / 46.6 MPa = 1.57	78.31 MPa / 45.4 MPa = 1.72

8.7 Shear loads with symmetric swelling, load case 5a (L07)

One of the technical design requirements states that the canister has to resist the load condition with rock shear loading. This corresponds to load cases 5a and 5b. These load cases involve a horizontal rock shearing which is most probable when the glacial ice melts and least probable before full water saturation. This means that the state at onset of the shear displacement may be different depending on when the rock shear is activated, represented by two load sequences involving different combinations of swelling pressure, groundwater hydrostatic pressure and glacial isostatic pressure, see Table 8-2. The swelling pressure is symmetric in load case 5a and asymmetric in load case 5b. This section covers shear loads with symmetric swelling, i.e. load case 5a. Load case 5b is covered in Section 8.8.

Assessments of the margin against global plastic collapse and defect tolerance were performed for the BWR and PWR versions of the Rebus insert.

8.7.1 Global plastic collapse

The margin against global plastic collapse was evaluated by 3D FEM using Abaqus and is reported in (Feigin et al. 2024a, b). These analyses were performed with complete models (without symmetry planes) including modelling of the buffer.

The loads were applied in different sequences, see Table 8-2. A reference state corresponding to load state 2 of sequence A was used to determine the limiting configuration of shearing height and angle. Both sequence A and sequence B were considered for the assessment of global plastic collapse. The symmetric swelling pressure of the bentonite buffer (10 MPa) and the groundwater hydrostatic pressure (5 MPa) were introduced through an initial stress condition during load step 1. The rock shearing and glacial isostatic pressure loads (35 MPa) were introduced during load steps 2 and 3, depending on the sequence.

For increased understanding of the interaction between force-controlled pressure loads and displacement-controlled rock shear, a sensitivity analysis was performed where a load factor of 1.5 was applied to the design pressure 50 MPa.

The shearing results in bending of the canister, with one side of the outer tube in tension and the other in compression. Results show that the limiting horizontal shearing plane was found at 75 % of the insert height, and that the limiting shearing angle is 45° from the plane of the largest internal framework plate.

Results shown in Table 8-9 demonstrate a sufficient margin against plastic collapse, well below the strain-based limiting value of 5 %, for all evaluated main components of the BWR and PWR versions and for the event sequences defined in Table 8-2.

Table 8-9. Maximum absolute principal strains.

Load sequences	BWR	PWR
Reference sequence A2	0.96 %	1.06 %
Sequence A3 (50 MPa)	0.95 %	1.16 %
Sequence A3 (75 MPa)	1.08 %	1.46 %
Sequence B3 (50 MPa)	1.16 %	1.38 %
Sequence B3 (75 MPa)	1.85 %	2.74 %

8.7.2 Defect tolerance

The defect tolerance for the steel tube under the shear load was evaluated by fracture mechanics 3D FEM using Abaqus and is reported in (Öbrink et al. 2025a, b).

The steel tube and the internal framework were found to have high tensile stresses and were therefore studied in more detail. In Öbrink et al. (2025c), a consequence analysis of crack-like defects in the internal framework plates concluded that a damage tolerance analysis of these parts is not necessary as long as a crack-like defect grows by stable ductile tearing. Since the internal framework is made of a standardised ductile material, confirmed by the mechanical testing carried out (Bolinder et al. 2025), it is concluded that crack-like defects will indeed grow by stable ductile tearing. The damage tolerance analysis instead focused on the steel tube.

A fracture toughness of J_{mat}=200–1000 kN/m was used (Bolinder et al. 2025) for defect tolerance analyses of the steel tube (P355N). The shear loading is a displacement-controlled load case and requires the safety factor SF_J=2 against fracture.

A screening tool was created to help identify and target the most important regions of the insert, with respect to defect tolerance, based on principal stress and equivalent plastic strain. The analysed load sequence was the reference sequence A2, see Table 8-2, as the additional pressure loads present in the other sequences work to close cracks in the relevant regions. Large defects have been postulated to capture J-integral values of up to 1000 kN/m in the analyses.

The postulated defects are considered large enough to influence the global stiffness of the canister insert. As detailed in the methods document for defect tolerance analyses (Bolinder et al. 2025), the fracture mechanics analyses of the rock shear load case were therefore performed with a sub-modelling technique. The sub-model boundaries were subjected to displacements from global plastic collapse analyses modified with crack-like slits, at the locations determined by the screening tool, to account for the altered structural stiffness due to the presence of large cracks.

The most critical defect was a circumferential surface breaking crack on the outside of the steel tube. The results consist of acceptable crack dimensions for a range of fracture toughness values which are shown in Table 8-10, taking the safety factor SF_J=2 into account.

In the basis for the defect tolerance analyses (Bolinder et al. 2025), fracture toughness values for the steel tube material of at least 1000 kN/m are presented. In order to set requirements that are robust both with respect to possible variations in fracture toughness in the components and the inspection capability, a preliminary fracture toughness level of 500 kN/m is proposed. To give allowance for a 12 % decrease in fracture toughness caused by possible hydrogen embrittlement (see Section 8.10.3), a fracture toughness level of 440 kN/m would apply, which in turn gives an acceptable crack depth of approximately 12 mm for a 93 mm defect length, obtained by linear interpolation between the results for 400 and 600 kN/m fracture toughness. The applied acceptance level in the inspection standard for ultrasonic testing (SIS 2011 SS-EN 10893-10:2016) state an acceptable defect depth of 4.4 mm. This gives sufficient margins to the calculated acceptable defect size. Experience from the components manufactured by SKB and from general knowledge of manufacturing of steel tubes suggest that surface-breaking cracks in the applied steel grade are unlikely. Based on this, on the margins between the acceptable defect sizes and on the inspection capability, it is assessed that unacceptable surface-breaking cracks in the steel tubes can be readily avoided.

Table 8-10. Acceptable crack dimensions for the steel tube when the safety factor SF_J=2 has been taken into account.

Fracture toughness [kN/m]	BWR		PWR	
	Acceptable crack depth [mm]	Acceptable crack length [mm]	Acceptable crack depth [mm]	Acceptable crack length [mm]
200	5.7	42	5.8	43
400	11	84	11	86
600	17.0	126	17	129
800	20.0	147	20	149
1000	22.0	167	23	169

8.8 Shear loads with asymmetric swelling, load case 5b (L08)

Load case 5b covers shear loads with asymmetric swelling pressure due to imperfections in the deposition hole geometry and inhomogeneities in the initial buffer density. The analyses for load case 5b have been limited to global plastic collapse for the limiting configuration identified for load case 5a. Since load case 5b is a combination of two events, each with a low probability of occurrence, and since it is seen as unlikely that a critical defect would occur in the insert, no damage tolerance analysis has been performed for this case.

Assessment of the margin against global plastic collapse was performed for the PWR version of the Rebus insert with the horizontal shearing plane at 75 % of the insert height and the limiting shearing angle 45° from the plane of the largest framework plate since this shearing plane angle and location had been found to have the most severe impact on the canister in load case 5a.

8.8.1 Global plastic collapse

The margin against global plastic collapse was evaluated by 3D FEM using Abaqus and is reported in Feigin et al. (2024c). These analyses were performed with complete models (without taking advantage of symmetry planes) including modelling of the buffer.

As in load case 5a, both sequence A and sequence B were considered for the assessment of global plastic collapse. The asymmetric swelling pressure of the bentonite buffer (defined by σ_1 and σ_2 in Figure 2-1.) and the groundwater hydrostatic pressure (5 MPa) were introduced through an initial stress condition during load step 1. The maximum and minimum swelling pressures are given by the base case values in Åkesson (2024). The initial stress condition within the buffer was found by an iterative procedure to achieve the specified asymmetric swelling pressure plus groundwater hydrostatic pressure. The rock shearing and glacial isostatic pressure loads (35 MPa) were introduced during load steps 2 and 3, depending on the sequence.

For increased understanding of the interaction between force-controlled pressure loads and displacement-controlled rock shear, a sensitivity analysis was performed where a load factor of 1.5 was applied to the design pressure 50 MPa.

Results shown in Table 8-11 demonstrate a sufficient margin against plastic collapse, well below the strain-based limiting value of 5 %, for all evaluated main components of the PWR version.

Table 8-11. Maximum absolute principal strains.

Load sequences	PWR
Reference sequence A2	1.18 %
Sequence A3 (50 MPa)	1.27 %
Sequence A3 (75 MPa)	1.46 %
Sequence B3 (50 MPa)	1.42 %
Sequence B3 (75 MPa)	2.78 %

8.9 Creep

8.9.1 Insert material

Creep of canister inserts has been investigated in Storesund and von Unge (2022) and Storesund and Feigin (2025). Creep deformation and the creep rate are strongly dependent on both temperature and stress. Creep is traditionally considered above a certain limit temperature where the creep strength for a certain design lifetime starts to be lower than the yield stress. Typical design lifetimes are 100 000 or 200 000 hours. For C-Mn steels including fine-grained steels such as P355 the limit temperature for creep design is around 400 °C. Nevertheless, creep cracks and failures due to creep is relatively common also at temperatures below the limit temperature. Failures at 360 °C have been reported for this category of steels. This is due to the fact that significant creep can occur at local stress concentrations where the stress is above the yield stress.

The assessed peak temperature of the insert in the repository environment is around 130 °C (Section 5.2.1) and thus much lower than the temperature range for creep design as well as for observed creep cracks. On the other hand, the repository time frames are far longer than the creep design lifetimes and also for the high temperature pressure vessel components with the longest service times, and therefore significant creep cannot a priori be readily ruled out during the canister's service time in a repository. The insert temperature is higher than 20 °C during the water saturation and temperate phases which involve load cases 1 and 2 (swelling pressure and hydrostatic pressure). Creep is discussed because of this temperature enhancement.

The temperature is lower than 20 °C during the glaciation and deglaciation phases which involve load cases 4 and 5 (glacial isostatic pressure and shear loads). It is necessary to discuss possible creep for these phases as well if stresses above the yield stress of P355 appear.

Creep testing at repository temperatures has been reported for a nodular cast iron at 125 °C (Martinsson et. al. 2010) and for low alloy powder metallurgy (PM) steels at 120 °C (Sundaram 2013). The results showed logarithmic and negligible creep in both cases. Although P355 steels differ from the tested nodular cast iron and the low alloy PM steel, they are all ferritic and therefore P355 would most likely show logarithmic and negligible creep during repository conditions as well. In addition, extrapolation of creep data for P355 by Storesund and von Unge (2022) showed negligible creep at repository temperatures.

Analyses of load cases 4 and 5 by Storesund and Feigin (2025) showed stresses above the yield stress and tensile plastic strain around 1 % in PWR and BWR insert tubes whereas the compression strain is up to 2.7 %. In the creep testing of all the studies mentioned above the highest stresses were close to but below the yield stress. Creep data in standards is also below the yield stress. Therefore, the creep behaviour in the plastic region cannot be directly demonstrated by available creep data and creep testing.

Another approach is to consider that P355 steel is a very tough material. It was discussed by Storesund and von Unge (2022) that tough materials will be strengthened by creep in areas with enhanced stresses. This is in contrast to brittle materials with less than 5 % creep ductility. In light of this, approximately 1 % plastic tensile deformation and 2.7 % plastic compression deformation is a small fraction of the ductility of P355 and the remaining ductility can be considered as far from critical as the elongation value for P355GH (ambient temperature) is at least 20 % and the creep ductility can be expected to be significantly higher at stresses above 0.6 times the yield stress (Wen et al 2016).

In addition, it can be expected that the plastic deformations in the insert will appear during load cases 4 and 5 after 10 000 years. At that time the temperature has decreased to 20 °C, see section 8.3.2, and the creep activity, if any, would be even lower than at 130 °C.

The concepts of creep activity were further discussed by Storesund and Feigin (2025). Creep is by definition activated by diffusion processes. It was demonstrated that the diffusivity decreases by 15 magnitudes between the temperature for negligible creep, TNC, and 120 °C, i.e. the insert peak temperature during the first 10 000 years and 28 magnitudes between TNC and 20 °C, i.e. the insert temperature after 10 000 years (section 8.3.2). Those high magnitudes demonstrate how very far the insert repository conditions are from the creep regime.

Storesund and Feigin (2025) also looked at the effect of plastic deformation on diffusivity. Such investigations could only be found for aluminium in studies where an increase in diffusivity of 6 magnitudes was modelled at 100 °C by Robson (2020). It is unlikely that similar effects would be present in C-Mn steel at 20 °C and 110 °C since the diffusivity is related to the homologous temperature (the temperature as a fraction of the melting temperature expressed in Kelvin) which is significantly lower for C-Mn steel than for aluminium at 100 °C.

The overall conclusion of the approaches describes above is that creep is assessed to be negligible (< 0.2 %) at repository conditions for P355 steel.

8.9.2 Copper shell

No creep analyses for the copper shell with the Rebus insert design have been performed. Instead, a comparison was made in Öbrink and Mångård (2025) of how the choice of insert design affects the equivalent plastic strain and the principal stresses in the copper shell. This was done so that an evaluation could be made regarding whether the creep analyses of the copper shell with the cast iron insert discussed in Sections 12.7.5 and 12.8.2 of SKB (2022c) could be considered applicable to also the Rebus insert.

Isostatic load

A comparison was made for the isostatic load case 4a, with a total pressure load of 50 MPa, and for the reference sequence A2 of the rock shear load case 5a, see Table 8-2. The evaluation was made by 3D FEM using Abaqus. Existing models from earlier analyses were used, but with some moderate modifications to obtain reliable results in the copper shell. For the rock shear load case, a 5 cm horizontal shearing was applied at 90 % of the insert height at an angle of both 0 and 45° from the largest framework plate.

The highest equivalent plastic strain value was 15.5 % for the canister with a cast iron insert and 14.3 % for the Rebus canister. In both cases, the highest values appeared locally on the inner copper surface, at a small edge near the base where the copper wall thickness changes. Generally, both equivalent plastic strain and principal stress results from the isostatic load case were very similar between the two insert designs, with slightly higher maximum values for the cast iron insert.

Shear load

The results from the rock shear load case were also generally similar. They did, however, show that high equivalent plastic strains occur where the top of the insert comes in contact with the side of the copper shell, where there is also a change in the copper wall thickness. In this region, the highest plastic strains on the surface reached 91 % with the design with a cast iron insert and 144 % with the Rebus design, both exceeding the limiting value of 80 % used in Jonsson et al. (2018). The high strains are, however, very local, occurring at the point where the insert comes in contact with the copper shell and then quickly diminish deeper into the copper material, see Table 8-12. The maximum principal stress results at the same points are shown in Table 8-13. Details of the differences and their causes are discussed in Öbrink and Mångård (2025).

Table 8-12. Equivalent plastic strains through the thickness of the copper shell where the maximum value on the surface occurs for the shear load case.

Distance from inner surface [mm]		0	1	3	5	10
Equivalent plastic strain [%]	Cast iron	91	38	19	15	11
	Rebus 0°	144	45	22	16	11
	Rebus 45°	135	45	22	16	11

Table 8-13. Maximum principal stress through the thickness of the copper shell in the region where the maximum equivalent plastic strain on the surface occurs for the shear load case.

Distance from inner surface [mm]		0	1	3	5	10
Maximum principal stress [MPa]	Cast iron	−87.8	−120	−59.1	−27.8	28.6
	Rebus 0°	−355	−137	−80.9	−23.8	12.3
	Rebus 45°	−249	−125	−72.4	−18.9	15.6

Based on the above results, the following is concluded.

- For the isostatic load case, the elasto-plastic strain simulations by Öbrink and Mångård (2025) show that the copper shell deformation localises on the inner copper surface close to the insert top and base. The highest strain, caused by the gap between the shell and the insert, is limited to 15 %. This is higher compared to those on which the creep analyses for the canister with a cast iron insert in SKB (2022c) are based (but somewhat lower than the recalculated values for the cast iron insert above), but still lower than the requirement of creep elongation. That analysis led to the conclusion that copper creep will not jeopardise the post-closure integrity of the canisters with cast iron inserts, and the same conclusion is therefore drawn for the Rebus canisters.
- For the shear load case, elasto-plastic strain simulations show that the copper shell deformation localises on the inner copper surface. The strain is high, 140 percent (in compression), at the inner surface, but decreases down to 16 percent 5 millimetres from the inner surface. The shearing results in tensile stresses on the inner surfaces of the copper shell, but at a distance from the high strains. On the outside of the copper shell, limited areas of tensile stresses can result from the shearing, depending on the point of incidence of the shearing, but the strains are low in such areas. The stress-strain fields in the copper shell in response to a shear load in a Rebus canister resembles closely that in the canister with a cast iron insert, for which copper creep was analysed in Section 12.8.2 of SKB (2022c) leading to the conclusion that copper creep will not jeopardise the post-closure integrity of the canisters with cast iron inserts. The same conclusion is therefore drawn for the Rebus canisters.

8.10 Additional studies and issues

A number of additional post-closure safety related mechanical issues are discussed below. They concern a probabilistic analysis of the isostatic load case, a pressure test of the isostatic load and sensitivities to altered material properties.

8.10.1 Probabilistic analyses

As mentioned, a key element of the safety assessment of a KBS-3 repository is the evaluation of the canisters' ability to withstand expected mechanical loads in the repository. In particular, for the design with a cast iron insert, failure probabilities have therefore been assessed for isostatic pressures caused by severe glacial loads on the repository and shear loads in the case of the shearing of a fracture intersecting a deposition hole as a result of a major earthquake.

The main conclusions from the probabilistic analysis of the cast iron design in the case of an isostatic pressure load are as follows (Dillström and Manngård 2017):

- The probability of initiation of crack growth is negligible compared to the probability of a global plastic collapse.
- No insert is calculated to fail if the isostatic pressure load is below 79 MPa.
- All the inserts are calculated to fail if the isostatic pressure load is above 96 MPa.

The main conclusions from the probabilistic analysis of the cast iron design in the case of a rock shear load are as follows (Dillström 2014):

- The probability of global plastic collapse is much smaller than the probability of initiation of crack growth and the probability of 2 mm stable crack growth.
- The probability of failure of an insert, for a postulated rock shear displacement of 5 cm, is between 5.8×10^{-4} and 2.2×10^{-3}.

For the Rebus design, which utilizes high-toughness ductile steels, global plastic collapse was identified as the dominant and most probable failure mechanism under isostatic pressure loading, see Section 8.5. The probability of crack-induced fracture was considered very low based on the following reasoning. The Rebus design has different characteristics than the cast iron design. The Rebus insert design differs significantly from the cast iron insert design, both with respect to geometry, the used materials and the related manufacturing processes. This, together with the acceptable defect sizes presented in Section 8.7.2, yields a significantly higher robustness against the shear loads for the Rebus design. Manufacturing inspections are expected to identify any defects of concern, guided by the findings of damage tolerance analyses (Öbrink et al. 2025d), ensuring that the insert components in the Rebus design remain essentially free of potentially detrimental flaws.

The same reasoning is applicable for the damage tolerance analysis for the shear load case. Furthermore, since the margin against plastic collapse is considerable for this case, see Sections 8.7.1 and 8.8.1, no probabilistic analysis was undertaken for the shear load case.

The main conclusions from the probabilistic analysis of the Rebus design in the case of an isostatic pressure load are as follows (Shipsha, Dillström and Hammer 2025):

- Variability in yield strength for the steel tube has a significant influence on the calculated probability of global plastic collapse.
- Variability in the steel tube thickness, within the limits of manufacturing tolerances, has an insignificant impact on the probability of a global plastic collapse.
- Assuming that 6000 canisters are deposited in the final repository and that each canister is subjected to an isostatic pressure load, the following estimates regarding the number of failed inserts were calculated, see also Figure 8-5:
  - No insert is calculated to fail if the isostatic pressure load is below 73 MPa.
  - All 6000 inserts are calculated to fail if the isostatic pressure load is above 91 MPa.

The probabilistic results are consistent with the deterministic results reported in Section 8.5, where the resilience to an isostatic pressure of 75 MPa, applying a safety factor of 1.5 to the 50 MPa stipulated in the design requirements, is demonstrated. Additionally, it is important to note i) that the collapse criterion in these studies follow the pessimistic ASME twice elastic slope criterion as discussed in Section 8.3.3, and ii) that the maximum isostatic pressure anticipated in the final repository environment is 50 MPa. The probabilistic analyses show that the likelihood of a failure at this pressure is vanishingly small.

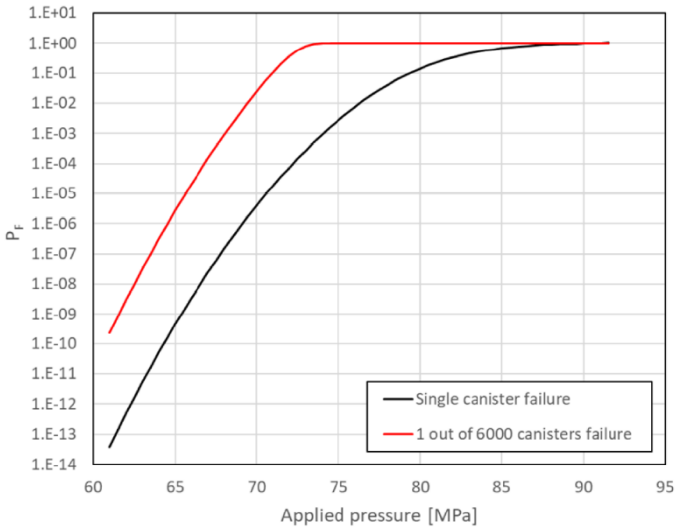

Figure 8-5. *Estimated probability of global plastic collapse for 6000 PWR canisters, based on analyses using a normal distribution of yield strength with a mean value of 340.38 MPa, based on mechanical data obtained from eight test manufactured Rebus tubes.*

8.10.2 Isostatic pressure test

Two isostatic pressure tests have been performed for the canister with a cast iron insert (Nilsson et al. 2005). The tests and the verification strength analyses by FE modelling for these are summarised in Dillström (2009) and Martin et al. (2009). The results indicate that the calculated collapse load for the canister with a cast iron insert is pessimistic, and form part of the basis for assessing the resilience of the that canister to expected isostatic loads in the final repository (SKB 2022c, Section 12.7).

Pressure tests and associated FE modelling of canisters with Rebus BWR and PWR inserts have also been performed (Ronneteg 2024). The tests are of particular significance since the margin of the calculated collapse load to the design criterion for the Rebus insert (Section 8.5) is smaller than the corresponding margin for the canister with a cast iron insert.

As for the canisters with cast iron inserts, the tests were made on Rebus canisters with a reduced height (1 m rather than 5 m), since the lifting capacity in the test facility was limited, see Figure 8-6.

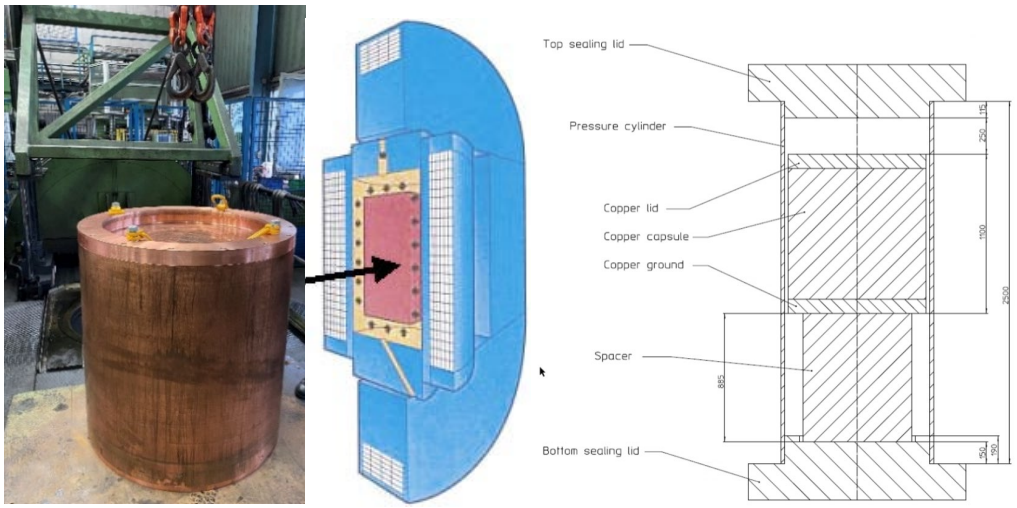

Figure 8-6. *Test canister in front of the press (left) and schematic illustration of the Quintus press (right).*

Prior to the tests, FE modelling of the reduced-height canisters was made (Hammer and Fredriksson 2024) to aid in the planning of the tests and as a basis for the evaluation of the test results. The calculations were done with both real, sampled materials data and with limiting data required by the specifications of the materials standard. The collapse pressures of the reduced-height canisters were calculated to be 91.1 MPa and 90.2 MPa with realistic data for the BWR and PWR canisters, respectively, which is about 10 % higher than those of the full-length canisters. It is recalled that the calculated collapse load is defined as one where the material starts to respond locally with large deformations to a limited increase in load and hence is not one where the canister is expected to structurally collapse in a global sense. The calculations were continued to 120 MPa. Figure 8-7 shows calculated deformations of the PWR insert as a function of the external pressure exerted on the copper shell. The corresponding results for the somewhat more resilient BWR insert are given in Ronneteg (2024).

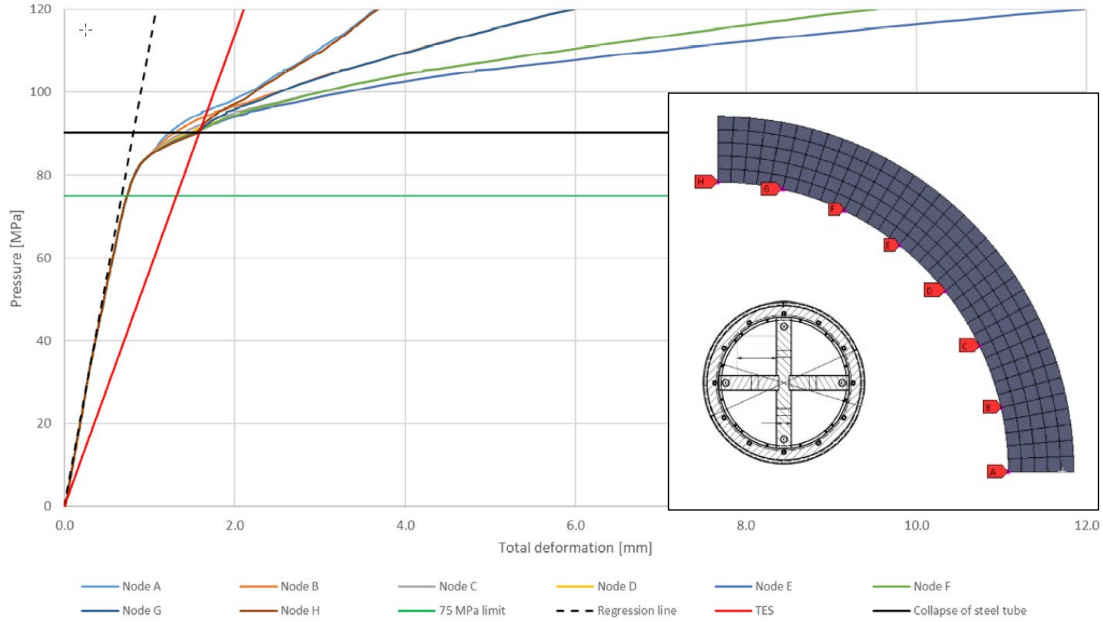

Figure 8-7. *Pressure-deformation curve for the short PWR canister insert with real material properties. The evaluation nodes A-H are shown with red markers in the insert. A is the lower right marker and H is the upper left. The figure also shows the design requirement of 75 MPa when the safety factor of 1.5 is applied (green horizontal line) and the calculated collapse load of 90.2 MPa (black horizontal line). The collapse load is obtained by applying the twice elastic slope approach (Section 8.3.3), that involves the dashed regression line marking the elastic region and the red line having half the slope of that of the regression line.*

In the test, the pressure was first increased to 80 MPa expected to be approximately the pressure required to reach the transition between elastic and plastic behaviour according to Figure 8-7. The pressure was then released and the deformation was measured using a calliper along the canister circumference at mid-height. The procedure was repeated in several steps with increasing pressures and larger resulting deformations, in particular in positions where the steel tube was not supported by the internal framework. Contrary to the tests of the canisters with cast iron inserts, the Rebus canister tests were discontinued before a global collapse occurred, to avoid damage to the test chamber. The maximum pressure in the test was 120 MPa and a global collapse had thus not occurred at this pressure. After the test, an additional measurement of the final deformations at 120 MPa were made by optical scanning.

A comparison between measured and calculated deformations of the PWR insert at 0°, 45° and 90° at 80 MPa, 100 MPa, 110 MPa and 120 MPa is shown in Figure 8-8. The corresponding results for the somewhat more resilient BWR insert are given in Ronneteg (2024). It is noted that for the data points reported as calculated, the initial approximately 1.5 mm gap between the copper shell and the insert has been added to the actual calculated values, in order to obtain an estimate of how much the copper shell has been deformed. As seen in the figure, the measured and calculated deformations are generally in good agreement, with the measured deformations being somewhat lower than those calculated.

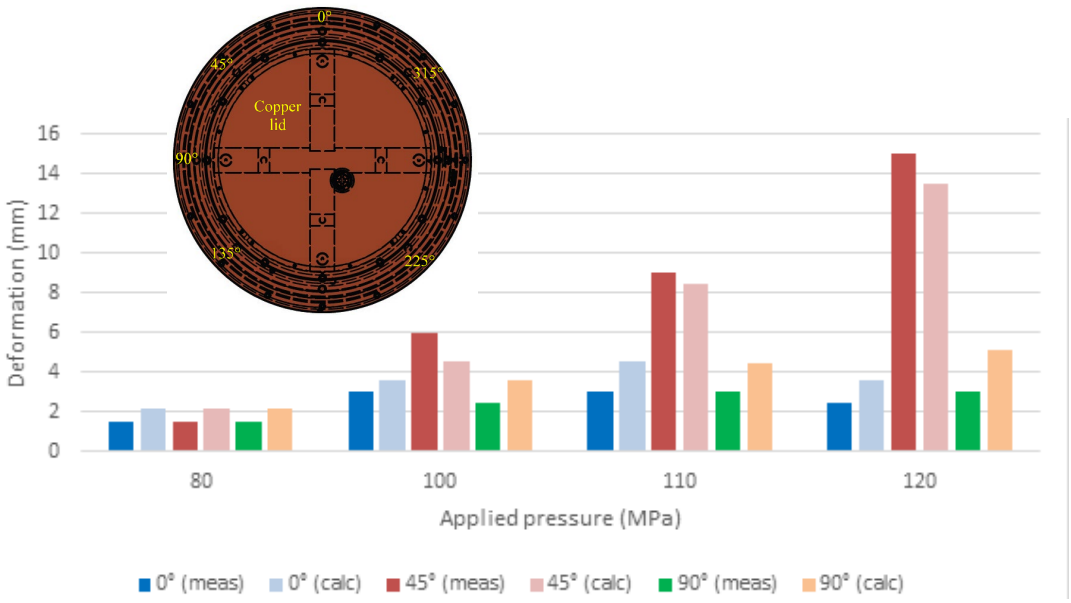

Figure 8-8. *Maximum total measured ("meas") and calculated ("calc") deformation as a function of circumferential position for the PWR canister. The measured values for the pressures 80, 100 and 110 MPa are from the calliper measurements in connection to the test, while the values for 120 MPa pressure are from the optical scanning. The calculated values are corrected with the estimated nominal gap between the insert and the copper shell of 1.5 mm.*

The following conclusions are drawn in Ronneteg (2024) regarding the isostatic pressure tests:

- *"The calculations of the collapse pressure for canisters with "real" material data show that the canisters have further margins to the governing isostatic load case.*
- *The calculated limited increases of collapse pressures (< 10 %) of the shorter canisters compared to full-length canisters show that they behave in a similar manner as regards response to isostatic pressures, thereby justifying the use of the shorter canisters in the test.*
- *The fact that inserts were intact at a pressure of 80 MPa shows that the canisters have margins to the 50 MPa pressure that is required with respect to the isostatic load. This is valid, also if the effect of canister length and material properties, is considered.*
- *The canisters remained tight at a level twice the design load when the test was discontinued at a pressure of 120 MPa.*
- *The measured deformation showed a good agreement with the values from the mechanical load calculations based on sampled data."*

In summary, the pressure test validates the mechanical load calculations and show that the designs have margins to the specified isostatic load of 50 MPa.

8.10.3 Sensitivity cases for altered material properties

The assessment of altered material properties in Chapter 7 led to the identification of two issues to which sensitivities need to be discussed for relevant load cases, namely potential embrittlement due to hydrogen absorption and due to radiation-induced copper cluster formation in the steel materials.

Potential embrittlement due to hydrogen absorption

Potential detrimental consequences on the fracture toughness of the insert materials due to hydrogen embrittlement in a sealed Rebus canister have been discussed in Section 7.3.3. Fracture toughness as a function of the H_2 pressure was studied from published data for two materials (X42 and A516) with a chemical composition similar to that of the insert materials (P355N and P355GH+N). Starting at a fracture toughness of K_{Ic} = 146.4 MPa√m for X42, the reduction in fracture toughness was estimated at 6 % for K_{Ic} (12 % on J_{Ic}) for a 0.1 MPa H_2 pressure and a strain rate of 0.0003 mm/s. The shearing displacement takes place on a time scale of typically one second, but the shear deformation remains after the shearing displacement is completed.

The performed fracture mechanical testing showed overall higher fracture toughness of as-received insert material (P355N and P355GH+N) than those of X42 ($J_{IC} \approx 92$ kN/m) and A516 ($J_{IC} \approx 118$ kN/m). This raises concerns whether these are similar materials regarding fracture toughness and hydrogen embrittlement. The insert materials possibly have less non-metallic inclusions, but it is not clear what this means for the influence on fracture toughness from hydrogen uptake. These concerns notwithstanding, and considering that the 12 % reduction of J_{IC} is an upper limit (pessimistically assumed hydrogen partial pressure) obtained for the most sensitive (X42) of the two materials, the 12 % reduction was adopted in the preliminary assessment of acceptable defect sizes in Sections 8.5.2 (steel lid) and 8.7.2 (steel tube). As seen in those sections, the derived defect sizes are expected to be rare and readily avoidable.

Potential embrittlement due to radiation-induced copper cluster formation

Precipitation of copper clusters is known to cause embrittlement of reactor pressure vessel steels after exposure to high radiation doses and these issues have been addressed for the quality of the P355N steel grade intended for use in the canister inserts, see Section 7.5.3. The copper cluster size distributions can be used to estimate an increase in ductile-to-brittle transition temperature. The results in Section 7.5.3 imply that the radiation exposure and temperature conditions in the repository lead to negligible impact on the transition temperature due to Cu cluster formation, also for a copper concentration of 0.35 weight %, which is considerably higher than the current (May 2025) requirement of 0.05 weight %. Nevertheless, it is of interest to discuss the sensitivity of the Rebus materials to a shift in transition temperature.

The ASTM E 1921-23 is a procedure for mechanical testing and statistical analysis of fracture toughness of ferritic steels in the ductile-to-brittle transition region. This procedure accounts for temperature dependence on the fracture toughness through an approach known as the Master Curve methodology. The Master Curve describes the temperature dependence and scatter of the fracture toughness within the ductile-to-brittle transition region for steels with one governing parameter, the reference temperature T_0. A shift in the reference temperature T_0 moves the fracture toughness curve accordingly. Hence, a possible embrittlement can be described as an upwards shift of the T_0 value.

For the canister insert it is vital to ensure that the temperature to which it will be subjected always corresponds to the ductile upper shelf region of the fracture toughness curve. Therefore, a possible shift of the ductile-to-brittle transition region due to embrittlement should be demonstrated not to violate this criterion.

Keeping the aforementioned in mind, it may be possible to obtain some preliminary guidance from the master curve. Impact toughness tests have established a reference temperature $T_0 = -90$ °C for P355N in its as-received condition (Öberg 2024). The size of the ductile-to-brittle transition region is not known for P355N. However, there exists guidance for reactor pressure vessel steels in Kirk et al. (2014) for determining the upper limit T_{US} of the ductile-to-brittle transition region. This guidance yields $T_{US} = -23$ °C. This would imply that also with an increase in T_0 by 20 °C there would be a sufficient margin against the ductile-to-brittle transition region. Mechanical testing of as-received Rebus materials (P355N and P355GH+N) indicates a ductility and fracture toughness higher than the reactor pressure vessel steels typically used to develop fracture toughness master curves. Mechanical

testing of as-received Rebus materials (P355N and P355GH+N) indicates a ductility and fracture toughness higher than reactor pressure vessel steels. Therefore, the determination of T_{US} for the as-received Rebus materials according to the guide given by Kirk et al. (2014) raises concerns. A series of impact toughness tests, alternatively fracture testing according to ASTM 1921, is recommended to study the entire transition region, thereby providing a better-founded basis for assessing a tolerable shift in T_0.

8.11 Conclusions of performed analyses

The main safety function of the canister insert in a KBS-3 repository is to withstand mechanical loads to which the canister may be subjected. Mechanical design analyses for the design with a cast iron insert are summarised in Jonsson et al. (2018). The Rebus canister with a steel insert is different than the canister with a cast iron insert in a way which warranted updated mechanical design analyses. A number of mechanical load cases have been formulated based on the design requirements for the KBS-3 canister and repository conditions. The analyses of these as accounted for in this chapter has yielded the following conclusions:

- Analyses of loads from asymmetric swelling due to uneven water saturation and deposition hole geometry, during temperate climate conditions expected to last for tens of thousands of years, show a sufficient margin against global plastic collapse. Tensile stresses all through the material are expected at certain locations in both the copper shell and the insert tube. This is of relevance for the assessment of SCC.
- The canister is required to withstand up to 50 MPa of isostatic load, caused by a combination of hydrostatic pressure at repository depth, swelling pressure from the water saturated buffer and an added load from a future glacial overburden. Deterministic analyses of the isostatic load have shown that the canister can withstand this load case. The margin against the failure mode global plastic collapse is larger than 1.5, as evaluated using a conservative ASME criterion. Probabilistic analyses of the isostatic load have shown that the risk of failure is insignificant when the load is 50 MPa. Furthermore, isostatic pressure tests confirm that the collapse of the insert will occur at a higher external pressure than the isostatic pressure in the repository. These tests showed a margin against global plastic collapse greater than 2.4. See bullet point further down concerning defect tolerances.
- The canister is also required to withstand a shear load. The governing case for the insert is a shear impact perpendicular to the canister main axis at approximately 75 % of its length. Deterministic analyses of global plastic collapse for the shear load have shown that the canister can withstand this load case with a considerable margin. See bullet point further down concerning defect tolerances.
- The combined load of isostatic pressure and rock shear is also analysed in different alternative sequences. Either the glacial load exists prior to and during the rock shear or it is applied after the rock shear. Deterministic analyses have shown that the canister can withstand these alternative load sequences.

The following additional conclusions have been reached:

- The analyses have been carried out with mechanical data obtained at room temperature. It has been shown that the margins against failure by plastic collapse are sufficient and the analysis results are valid for temperature ranges expected for the canister in the repository environment.
- Defect tolerance analyses have been performed for the steel tube (shear load case) and steel lid (isostatic load case) of both the BWR and PWR canisters. The resulting acceptable crack sizes are presented as ranges corresponding to fracture toughness values (J_{mat}) between 200 kN/m to 1000 kN/m. For the Rebus materials, fracture toughness values for the steel tube, lid and base material are measured to be above 1000 kN/m. In order to set requirements that are robust both with respect to possible variations in the fracture toughness in the components and the inspection capability, preliminary fracture toughness levels of 500 kN/m for the steel tube and 375 kN/m for the steel lid and base are proposed. These levels would give acceptable defect depths of approximately 3 mm for the steel lid and 12 mm for the steel tube, including allowance for pessimistically assessed potential fracture toughness reduction due to hydrogen embrittlement.

This gives sufficient margins to the sensitivity of the inspection methods applied. Experience from the components manufactured by SKB and the general knowledge of manufacturing of steel tubes and steel plates suggest that surface-breaking cracks are unlikely in the applied steel grades. Based on this and on the margins between the acceptable defect sizes and on the inspection capability, it is assessed that unacceptable surface-breaking cracks in the steel tubes and the steel plates can be readily avoided.

- Precipitation of copper clusters is known to cause embrittlement of reactor pressure vessel steels after exposure to high radiation doses. It could be of interest to relax the current requirement of a maximum Cu content of 0.05 wt%, for which it has been demonstrated that such effects are avoidable. Therefore, impact toughness tests have been performed to established a reference ductile-to-brittle transition temperature $T_0 = -90$ °C for P355N in its as-received condition (Öberg 2024). Considering knowledge available for reactor pressure vessel steels the upper limit of the transition region can be estimated to be $T_{US} = -23$ °C. This would imply that a shift in T_0 of 20 °C may provide a sufficient margin against the ductile-to-brittle transition region. It is however recommended that a series of impact toughness tests are performed to study the transition region, thereby providing a better-founded basis for assessing a tolerable shift in T_0.
- As is the case for the cast iron insert, the Rebus insert provides a sufficient support for the copper shell for all load cases considered. Creep of the insert material and copper shell have been assessed for the Rebus canister at repository conditions:
  - Creep is assessed to be negligible (< 0.2 %) for the insert material based on the numerically simulated stress-strain fields in combination with the temperatures at repository conditions.
  - A comparative study was performed for the copper shell based on differences in numerically simulated equivalent plastic strains and principal stresses for the cast iron insert and the Rebus insert. No major differences can be discerned for the isostatic or rock shear load cases in the present comparison. It is therefore concluded that the detailed creep analyses in SKB (2022c), for copper shells with cast iron inserts are valid also for Rebus inserts. Since that analysis lead to the conclusion that copper creep will not jeopardise the post-closure integrity of the canisters with cast iron inserts, the same conclusion is drawn for a Rebus canister. It is also noted that in a few small regions, the strains and stresses are higher in the current numerical simulations of the shear load case for both the cast iron and Rebus inserts compared to those of the assessment for the cast iron insert in SKB (2022c), ascribed to differences in the model mesh and possibly additional modelling details.

9 Criticality

9.1 Introduction

9.1.1 General

A key issue in the assessment of post-closure safety for a final repository for spent nuclear fuel is the reactivity of the fuel over time, with a focus on situations that would imply a risk of criticality. It needs to be demonstrated that criticality is avoided during the whole analysis period of one million years in the final repository. For criticality to be an issue of potential concern, the canister integrity must be breached so that water enters the canister interior and acts as a neutron moderator. In such scenarios, both an intact insert and one that has altered properties caused by corrosion of the insert after integrity failure are investigated.

This Chapter presents the effects on criticality safety in the canister with the Rebus PWR and BWR inserts based on studies of the long-term evolution (Johansson et al. (2024)) and a criticality analysis[16] for the most limiting scenarios. The analysis shows that it is necessary to use burnup credit both for PWR and BWR fuel to meet the requirements on subcriticality, and limits on burnup as a function of initial enrichment have been determined.

9.1.2 Requirement on criticality

To ensure that the canister in the final repository remains subcritical the design requirements (Section 2.1) state that the neutron multiplication factor (k_{eff}) must not exceed the following criteria:

- 0.95 for normal conditions, which is assumed to be a water-filled canister with intact geometry and
- 0.98 for unlikely scenarios, which are assumed to be a water-filled canister where the canister integrity is lost and corrosion processes have changed the material properties and the geometrical configuration.

In the criticality analyses, the bias of the model compared to real cases needs to be accounted for. This is done by lowering the above limits by values obtained from the validation of the model used. The so obtained lower values are called the upper safety limit, USL. For the scenarios in Section 9.3 and 9.4, USLs for fresh fuel[15] are used (0.93922 for normal conditions and 0.96922 for unlikely scenarios).

With burnup credit the USL is transformed into a limit on burnup, as elaborated in Section9.4. The USL is reduced to account for margins and uncertainties related to burnup and this value on reactivity transformed into burnup from calculated relations for the fuel and case in question. This gives values for the limit on burnup in combination with initial enrichment that ensure subcriticality.

9.1.3 Background

In the criticality analysis for the canister with a cast iron insert the above requirements have been demonstrated to be fulfilled for the most reactive fuel, see Johansson et. al (2019).

The criticality analysis of a failed canister with a cast iron insert and altered material and geometrical properties is studied in Agrenius and Spahiu (2016), forming a key reference to Johansson et al. (2019)[17]. The study by Agrenius and Spahiu forms the basis for a corresponding analysis of a Rebus canister in the following. The dominating process is the corrosion of cast iron which forms magnetite that could eventually fill the whole internal volume of the canister. In Johansson et al. (2024) the effects of corrosion on the Rebus insert have been further analysed.

[16] SKBdoc 2042952 ver 2.0, Kriticitetsanalys för slutförvarskapsel med Rebusinsats utformad enligt koncept 1 version 3. Svensk Kärnbränslehantering AB. (Internal document, in Swedish.)

[17] **Johansson F, Kirkegaard J, Zetterström P, 2019.** Kriticitetsanalys för slutförvaring av använt bränsle. SKBdoc 1605532, ver 1.0, Svensk Kärnbränslehantering AB. (Internal document, in Swedish.)

9.1.4 Method and assumptions

In the study for the Rebus canister, the same fuel types and enrichments as in Johansson et al (2019) have been used. For PWR it is the fuel type Westinghouse 15x15 Upgrade with an enrichment of 2.3 w/o U-235 and fresh (without burnup). For BWR it is the fuel type SVEA-96 Optima 3 with an enrichment of 3.4 w/o and fresh (without burnup). The assumptions on enrichment and burnup are chosen to be such that they bound conditions that do not require burnup credit or credit for burnable poison. These fuel types cover all different fuel types including MOX fuel and have thus been used as reference fuel types in this study. The reactivity of the spent nuclear fuel varies with time during the 1-million-year analysis period and as discussed in section 9.2.1, the reactivity during the analysed period for normal fuel types will reach its highest value after about one year of cooling time (i.e., after discharge from reactor).

The same computational tools have been used: Scale-6.2.2 for all reactivity calculations with the cross-section library ENDF/BVII.1 252 groups.

The main difference regarding criticality between the Rebus insert and the cast iron insert is the larger free volume in the fuel-filled Rebus canister. The presence of this larger volume and its asymmetrical distribution in the BWR insert makes it necessary to pessimistically assume that the magnetite produced through continuous water corrosion, after reaching the fuel channel (BWR Zircaloy box) wall in the central positions will be distributed in the free space of the peripheral positions instead of entering the space between fuel rods because this is the most penalising situation from a reactivity viewpoint.

The first study, Johansson et al. (2024), considers the long-term evolution of a failed canister in order to derive a set of cases after different extents of corrosion and other corrosion related assumptions for criticality calculations. These cases together constitute the scenarios that are considered in the criticality analyses. The water intrusion and corrosion sequences cover canister failures due to both corrosion and shear load. The relative positions of the framework plates and the fuel assemblies are not expected to change in the event of a shear movement of a few centimetres. Other geometrical changes, e.g. pitch reduction, are also analysed and result in a reactivity decrease. It is also noted that geometrical changes due to creep deformation of the inserts are expected to be insignificant, see Section 8.9.2.

Results for all the cases can be found in Johansson et al. (2024) and the cases with the highest reactivity are summarised in Section 9.5. The cases considered in Johansson et al. (2024) are:

- Main evolution scenario / Base case with waterfilled canister
- Other anoxic corrosion products (siderite and mackinawite)
- Magnetite falls down into the channels of the canister
- Magnetite layer grows resulting in reduced fuel rod pitch
- Magnetite extrudes into the fuel assembly
- Zirconium in the cladding and BWR fuel channel converted to zirconium oxide
- Radial movement of fuel rods
- Fuel pellets fall down to the bottom of the canister
- Corrosion of spent fuel (UO_2)

The second study[16] is a criticality analysis that investigates and estimates the effects on the fuel in final disposal in more detail. Johansson et al. (2024) was based on data for fresh fuel and it was concluded that burnup-credit is necessary in order to show subcriticality. This criticality analysis[16] includes descriptions of the fuel after burnup, i.e. considering suitable actinides and fission products and the uncertainties regarding burnup.

9.2 Long-term evolution

9.2.1 Long-term evolution of a failed canister

Immediately after water contact, simultaneous corrosion of several materials is expected to start and will cause changes in the geometry over time (metals will be consumed and corrosion products with higher molar volume will be produced) and in the material composition of all canister components. This is a complex process which depends on a multitude of parameters, and different geometrical configurations are obtained e.g., if the Zircaloy cladding is completely corroded before or after the filling of the internal free space in the canister with corrosion products.

As a first step, a base case describing a reasonable evolution of the system is evaluated, striving to use realistic corrosion rates for all components under the given conditions and not e.g. conservative upper values to cover for uncertainties. In subsequent steps, other configurations that can be derived from the range of possible corrosion rates and other corrosion-related assumptions for all materials are then analysed systematically by judging the consequences of different corrosion assumptions for a given component.

The approach followed is to evaluate all conceivable configurations in the canister, while the time at which they are achieved is less important from the reactivity point of view if all calculations are made with the fuel having the highest reactivity over time. The reactivity of the spent nuclear fuel varies with time during the 1-million-year period analysed, as shown in Johansson et al. (2019)[17]. The reactivity during the analysed period for normal fuel types will reach its highest value after about one year of cooling time (i.e. after discharge from reactor), see Figure 9-1. This reactivity value is used for the entire analysis period in the criticality assessments.

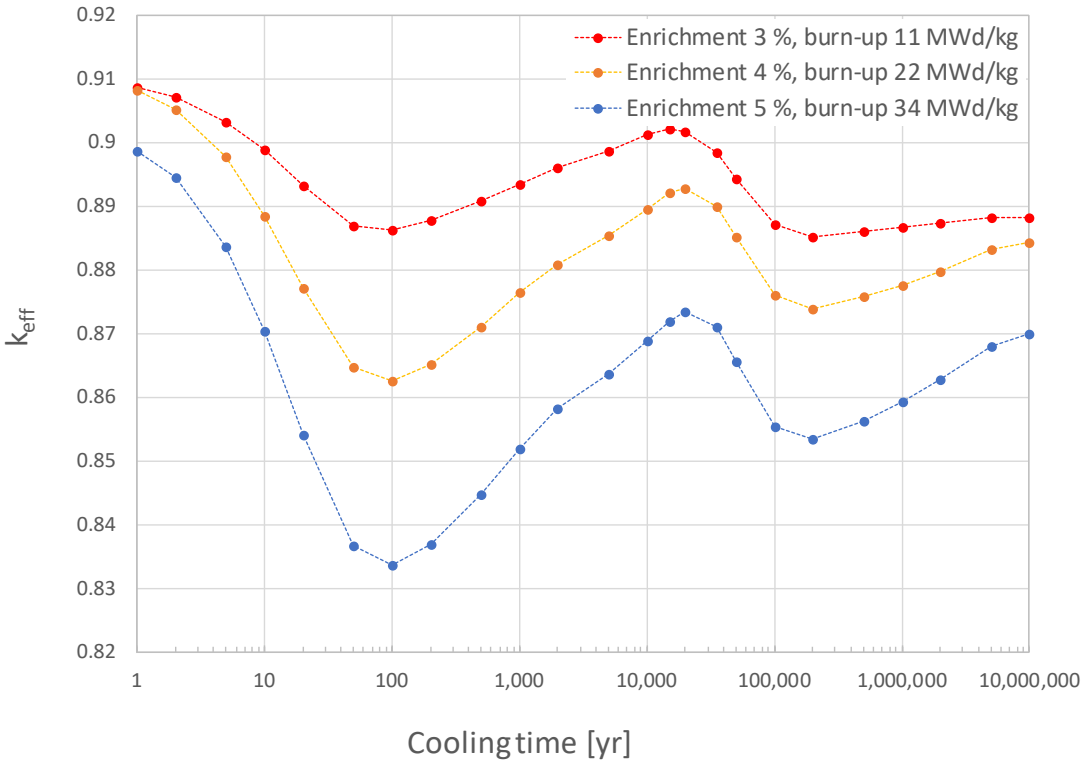

Figure 9-1. *Reactivity as function of cooling time for a PWR assembly with different burn-ups and enrichments. From Johansson et al. (2019)[17].*

9.2.2 Long term corrosion of carbon steel

The corrosion of carbon steel under the anoxic conditions prevailing in the canister interior occurs according to the following reaction:

$$Fe(s) + 2H_2O(l) \rightleftharpoons Fe(OH)_2(s) + H_2(g) \quad (1)$$

The ferrous hydroxide produced by this reaction transforms to the thermodynamically more stable product magnetite via the Schikorr reaction:

$$3Fe(OH)_2(s) \rightleftharpoons Fe_3O_4(s) + 2\ H_2O + H_2 \quad (2)$$

giving the overall reaction:

$$3Fe(s) + 4H_2O(l) \rightleftharpoons Fe_3O_4(s) + 4H_2(g) \quad (3)$$

The long-term corrosion rate under anoxic conditions is independent of whether or not water is present as liquid or as vapour at high relative humidity (Smart et el. 2002); thus here it is assumed that the whole surface of the carbon steel at the outer tube and the inner framework, corrodes at a constant rate. Several experimental studies have shown the absence of localized corrosion in these materials under repository conditions (SKB 2022a, Section 3.5.1); hence uniform corrosion is assumed to take place during the entire time interval analysed. This means that the thickness of the corroded layer is assumed equal for all surfaces of carbon steel in contact with water.

The corrosion product magnetite is reported to consist of two layers: a thin, strongly adherent layer and an outer layer of poor adhesion (Smart et al. 2002). According to these authors, the adherent layer is formed directly on the surface of the metal by reaction (1), while the looser layer is probably formed by the precipitation of dissolved Fe(II) ions. The adherent layer forms very quickly and then does not increase further in thickness, while continuing corrosion leads to the thickening of the non-protective layer. The corrosion rate is controlled by ion transport through the adherent layer and is expected to continue at constant rate over long periods of time.

The molar volume of the oxide is higher than that of the metal, meaning that the corrosion of the carbon steel insert will be accompanied by a volume increase. The magnetite formed at low temperature is also a softer material than the original metal which implies that the magnetite will not deform the insert framework or the fuel. The mechanical properties of the magnetite corrosion product formed at low temperature (Smart et al. 2001a) are due to its high proportion of water (Smart et al. 2006). This is in contrast to the situation in concrete, where the supply of water is limited, or the oxide films formed at high temperature, which have a much higher hardness and lower water content.

In the analysis of the evolution of a failed canister it is assumed, based on the results of Smart et al. (2006), that the magnetite formed in the region between the copper and cast iron will extrude into the free space in the canister, instead of causing a deformation of the copper shell. Even in other cases, when magnetite is formed in confined spaces as for example in the space between the framework and the fuel channel (BWR Zircaloy box), it has been assumed as more probable that the magnetite will extrude and fill the available free space, causing no or only a limited deformation of the fuel channel.

The corrosion rate of carbon steel in a failed canister under repository conditions is one of the most important parameters in evaluating the future evolution of the canister interior. An analysis of this issue was made in Agrenius and Spahiu (2016). Several more recent studies on corrosion of carbon steel under near neutral conditions are summarised and discussed in Johansson et al. (2024). The corrosion of carbon steel under anoxic conditions has been investigated mainly by waste management organisations due to its use as a canister material. In SKB´s program, the corrosion rate of carbon steel has been based on the experimental studies by Smart et al. (2001a, b, 2002) in synthetic groundwater. The conclusions in Johansson et al. (2024) on carbon steel corrosion under repository conditions is that a corrosion rate of 1 μm/year seems the most reasonable choice for discussing the main evolution case of a damaged canister. This rate is the same as in Agrenius and Spahiu (2016), and now with support from recent studies. As shown in Agrenius and Spahiu (2016), higher corrosion rates would just shorten the time to realise the cases analysed and would not add new cases. A lower corrosion rate of 0.1 μm/year is used in Johansson et al. (2024) to investigate the effects on reactivity from fissile material deposited on magnetite as a consequence of corrosion of spent fuel.

9.2.3 Potential formation of other anoxic corrosion products

Siderite, $FeCO_3(s)$ is usually formed in groundwaters with relatively high carbonate concentrations through the reaction:

$$Fe(s)+ HCO_3^- + H^+ \rightleftharpoons FeCO_3(s) + H2 \quad (4)$$

The formation of siderite with the predicted carbonate concentrations in Forsmark groundwater evolution seems relatively improbable. A potential pathway may be through Electrical Microbial Influenced Corrosion (EMIC) or through concretions formed by interaction of magnetite with groundwater (Smart and Adams, 2006). Further, the maximum amount of siderite that can be formed during the corrosion of the carbon steel insert of a KBS-3 container may be estimated from the average carbonate/bicarbonate concentration in the groundwater and an assumed high flow through the container. The amount of siderite in the siderite-magnetite mixtures is estimated in Johansson et al. (2024) and the criticality calculations have been made with a couple of mixtures of magnetite with siderite.

9.3 Effect on criticality in limiting scenarios

9.3.1 Canister with cast iron insert

In the criticality analysis for the canister with a cast iron insert in the final repository (Johansson et al. 2019), a water-filled canister with otherwise unaltered geometry and material properties and assumptions for the fuel as in section 9.1.4 resulted in k_{eff} = 0.93235[18] for PWR and k_{eff} = 0.93243 for BWR. It was also shown that the evolution of a failed canister would not increase the reactivity by more than 3 %. Thus the maximum reactivity requirement mentioned in section 9.1.2 of 0.95 for an intact, water-filled geometry and 0.98 for altered properties, were met. The maximum reactivity for the canister with a cast iron insert occurred when the cast iron and steel surfaces had corroded 9 mm, whereas further corrosion yielded a decreasing reactivity, since magnetite enters the space between the fuel rods when corrosion progresses further.

9.3.2 Rebus canister

To evaluate the maximum effect on reactivity from the long-term evolution during final disposal a conservative base case is identified and the reactivity calculated. This base case is complemented with reactivities calculated for less probable system evolutions and the effect of possible coexisting cases are also estimated. The base case is a water-filled canister for which the reactivity is calculated to be k_{eff} = 0.90772 for PWR and k_{eff} = 0.94695 for BWR, thus it is shown that for both fuel loadings the criterion for normal conditions have potential to be met in the following criticality analysis, where also uncertainties and USL are considered.

For PWR the maximum reactivity occurs when the layer of magnetite has grown and the gap between the magnetite and the fuel rod surface is around 3 mm. This corresponds to the corrosion of a carbon steel layer of about 6 mm. See Figure 9-2 for an illustration of the geometry of the case. This case results in k_{eff} = 0.91364.

For BWR the maximum reactivity occurs when the magnetite layer has grown against the wall of the fuel channel and fills the free space in the peripheral positions of the insert. This configuration is achieved after the corrosion of 6.33 mm carbon steel to crystalline magnetite. See Figure 9-2 for an illustration of the geometry of the case. This case results in k_{eff} = 0.98178.

[18] It is customary to give reactivity results with a high precision, even when the underlying data and assumptions suggest a lower precision.

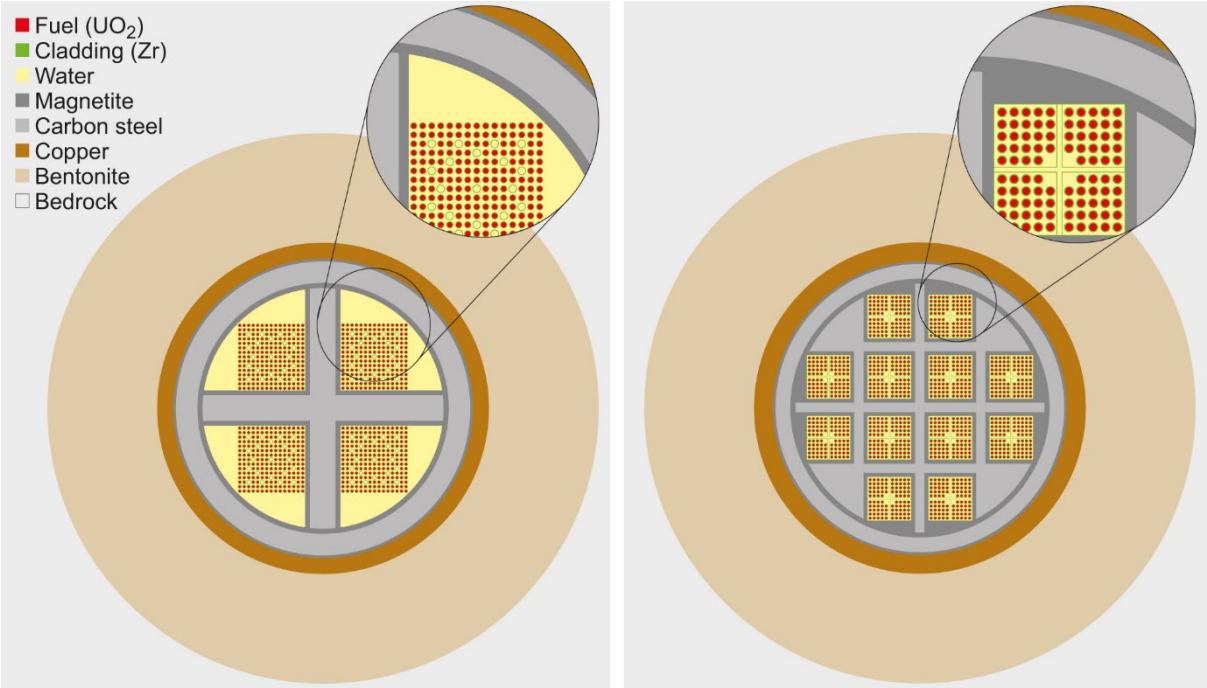

Figure 9-2. *Representation of cross sections of BWR and PWR inserts for the configurations yielding the highest reactivities. The area converted to magnetite in the framework plates and in the copper-carbon steel interface is also represented, see magnification.*

A summary of the results on k_{eff} for the canister with a cast iron insert from Johansson et al. (2019)[17] and the Rebus canister from Johansson et al. (2024), is given in Table 9-1 (PWR) and Table 9-2 (BWR). The last columns show the reactivities for the Rebus canister, including uncertainties as reported for fuel, model and nuclear data in Johansson et al. (2019)[17] (PWR $\Delta k_{eff} = 0.00260$[19] and BWR $\Delta k_{eff} = 0.00273$[20]).

Table 9-1. Summary of calculated k_{eff} for the Rebus inserts for PWR.

Case no	Description	k_{eff} canister with cast iron insert	k_{eff} Rebus canister	k_{eff} Rebus canister, incl uncertainties
2	Base case, water-filled canister, no corrosion	0.93235	0.90772	0.91032
3	Crystalline magnetite in gap	0.93434	0.91289	0.91549
9	$FeCO_3$ + Fe_3O_4 in gap	0.93495	0.91364	**0.91624**
	Summary of possible coexisting cases		0.91377	**0.91637**

[19] Uncertainties for fuel data and nuclear data from Table 13-2 in Johansson et al. (2019)[17].
[20] Uncertainties for fuel data, model and nuclear data from Table 14-1 in Johansson et al. (2019)[17].

Table 9-2. Summary of calculated k_{eff} for the Rebus inserts for BWR.

Case no	Description	k_{eff} canister with cast iron insert	k_{eff} Rebus canister	k_{eff} Rebus canister, incl uncertainties
2	Base case, water-filled canister, no corrosion	0.93243	0.94695	0.94968
3	Crystalline magnetite in all space outside fuel channels	0.95227	0.98178	**0.98451**
9	$FeCO_3$ + Fe_3O_4 in all space outside fuel channels	0.93613	0.98155	0.98428
	Summary of possible coexisting cases		0.98182	**0.98455**

As mentioned above, the criterion for normal conditions, case no 2, have potential to be met for both BWR and PWR. These calculation cases apply (as done also for the canister with a cast iron insert) burnup credit for PWR and credit for burnable poison for BWR. The results show an improvement for the PWR Rebus canister for unlikely scenarios (cases 3 and 9 in Table 9-1) compared to the canister with a cast iron insert. For the BWR cases, there is an increase in reactivity with the Rebus canister compared to the canister with a cast iron insert, and the values exceed the USL for both normal conditions and unlikely scenarios. It can also be deduced that the criterion for unlikely scenarios is exceeded by a larger margin and this is hence the limiting scenario for the BWR insert. For the PWR insert, the most limiting scenario is for normal conditions.

The amount with which the criterion is exceeded for the BWR cases is limited and can be handled with analytical measures. One way to solve this problem is to use burnup-credit for the Rebus canister also for BWR. Approximately 20 MWd/kgU will be needed for fuel with 4 % enrichment when degradation is accounted for. For PWR the required burnup will be less than that for the canister with a cast iron insert. The requirement on burnup is further analysed and results are presented in the next section.

Calculations of the case when the whole insert has corroded and magnetite has entered into the fuel assemblies and is present between the fuel rods, have also been made. The reactivity of the canister decreases considerably when corrosion products replace the moderating water between the fuel rods and results in $k_{eff} = 0.37385$ for PWR and $k_{eff} = 0.38953$ for BWR.

Studies have also been made with varying water content in the magnetite in both the scenario when magnetite has filled the space outside the fuel assemblies and when magnetite has intruded into the fuel assemblies. For the latter case with increasing water content in the magnetite inside the fuel assembly, it is shown that the reactivity increases due to better moderation. However, this improved moderation is not enough for the reactivity to reach as high values as for the case without magnetite inside the fuel assemblies. Increasing water content in the magnetite, when the magnetite is outside the fuel assembly will lead to a decrease in reactivity due to a decrease in the reflective properties of pure magnetite.

Other studies have been made and reported in Johansson et al. (2024), for example:

- Magnetite falls down into the channels of the canister
- Magnetite layer grows resulting in reduced fuel rod pitch
- Zirconium in the cladding and BWR fuel channel converted to zirconium oxide and production of hydrogen
- Corrosion of UO_2

These studies show limited impacts and mainly result in lower reactivity than the base case. The scenarios that can contribute to an increase in reactivity have been identified and included in the summary of possible coexisting cases. These cases are: H_2 dissolved in water and UO_2 on magnetite surface (PWR). All results can be found in Johansson et al. (2024).

9.4 Criticality analysis

9.4.1 Effects of burnup and uncertainties

As shown in the previous section, it is necessary to use burnup credit to demonstrate subcriticality and fulfilment of requirements in the Rebus canister. This has been done in a criticality analysis[16] for the most severe combinations of scenarios and fuel types and gives a limit on the burnup that is needed in the fuel as a function of initial enrichment. In summary the following has been made in the criticality analysis for the Rebus insert:

- Determination of reactivity in a canister as a function of burnup of the fuel. Assumptions that pessimistically minimizes the reduction in reactivity were made in these determinations.
- Estimation of uncertainties associated with conditions in the fuel, the Rebus canister and the analysis model.
- Extraction of values for the required burnup as a function of enrichment that ensures subcriticality in the Rebus insert in the final repository.

The most challenging cases in the long-term evolution of the canister is a water-filled canister for PWR (without the effects of corrosion since those increase reactivity by less than 3 % and hence the criteria for normal conditions will be the most limiting). For BWR the most challenging case is when the canister is water-filled and where corrosion of the insert has caused magnetite to form and fill all the free space up to the fuel channel.

9.4.2 Reactivity as a function of burnup

The calculated reactivity as a function of burnup and initial enrichment is shown in Figure 9-3 for single PWR and the BWR fuel elements immediately after operation. These curves describe the reactivity in the fuel after operation (regardless of application) in a realistic but conservative way. Operating conditions such as temperature, power distributions, void and control rod presence have effects and variations in these conditions are included.

These relations/curves are used to determine the corresponding burnup at the subcriticality limit including uncertainties.

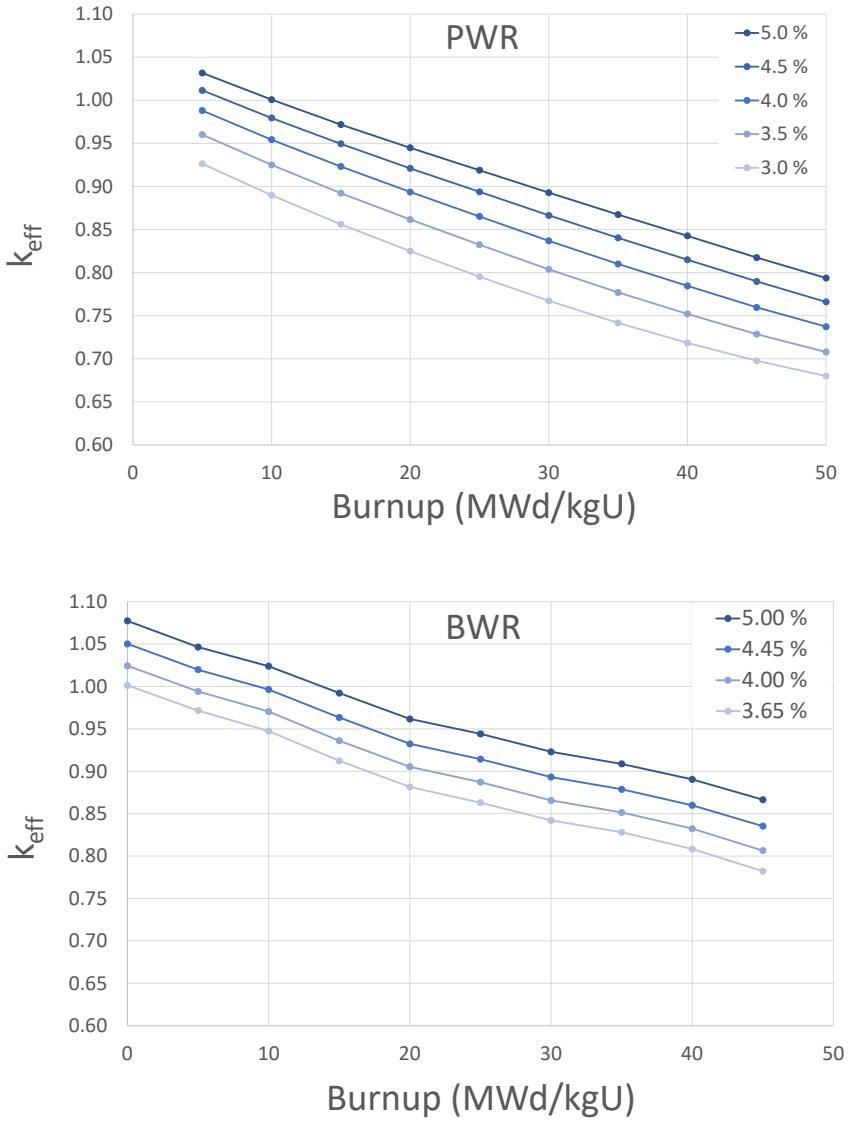

Figure 9-3. *Reactivity as a function of burnup and initial enrichment for single PWR (upper) and BWR (lower) fuel elements immediately after operation.*

9.4.3 Uncertainties

As mentioned in Section 9.1.2, the basic criteria for subcriticality for a water-filled canister ($k_{eff} < 0.95$ for intact geometry and < 0.98 for altered geometry) are lowered to account for uncertainties related to the criticality model and to neutron data, yielding a so called Upper Safety Limit (USL) for the criticality analysis. Additional uncertainties concern parameters related to e.g. burnup, manufacturing data, operational data and various model assumptions. The impact of each of these latter parameters on reactivity is estimated and the impacts are summed, yielding a total impact in terms of a reactivity value that is subtracted from the USL. This yields a subcriticality limit in terms of a k_{eff} -value that takes all identified uncertainties into account. The USL and the additional uncertainties for a selection of burnups are given in Table 9-3 and Table 9-4 for PWR and BWR fuel, respectively. For example, the USL for a PWR fuel with an enrichment of 5 % in a water filled, intact canister is 0.93688 and the additional uncertainties yield an impact on criticality of 0.02041. This yields a subcriticality limit of a $k_{eff} = 0.93688 – 0.02041 = 0.91647$. The additional uncertainties are the same for the Rebus and the cast iron analyses, since these types of uncertainties are related to the fuel and the operation of them, and not to the canister design.

9.4.4 Loading curves

For both PWR and BWR, loading curves are determined from the acceptance criteria and with consideration of all significant uncertainties. The loading curve shows the combination of initial enrichment and burnup that ensures subcriticality. The values of burnup are extracted from the relations of reactivity as a function of burnup and initial enrichment as shown in Figure 9-3. The required burnup is the value that corresponds to the reactivity at the subcritical level for the corresponding initial enrichment. The values on uncertainties, USL and corresponding burnup is shown in Table 9-3 and Table 9-4. Independent uncertainties are summarised statistically.

Conservatisms are included in the analysis through:

- conditions that minimize the reduction of reactivity in the calculations of reactivity as a function of burnup
- uncertainties are set with 2σ accuracy
- all uncertainties are included in the analysis.

Illustrations of the burnup limit together with representations of the fuel currently at Clab can be seen in Figure 9-4 and Figure 9-5.

Table 9-3. Requirement on burnup for PWR fuel extracted from the upper safety limit and uncertainties.

	5 % U-235 initial enrichment	4 % U-235 initial enrichment	3 % U-235 initial enrichment
Upper Safety Limit for the case with a water-filled canister	0.93688	0.93688	0.93688
Summed effect of additional uncertainties	0.02041	0.01967	0.01849
k_{eff} at the subcriticality limit including uncertainties	0.91647	0.91721	0.91839
Limit translated into burnup, MWd/kgU	**25.4**	**16.0**	**6.2**

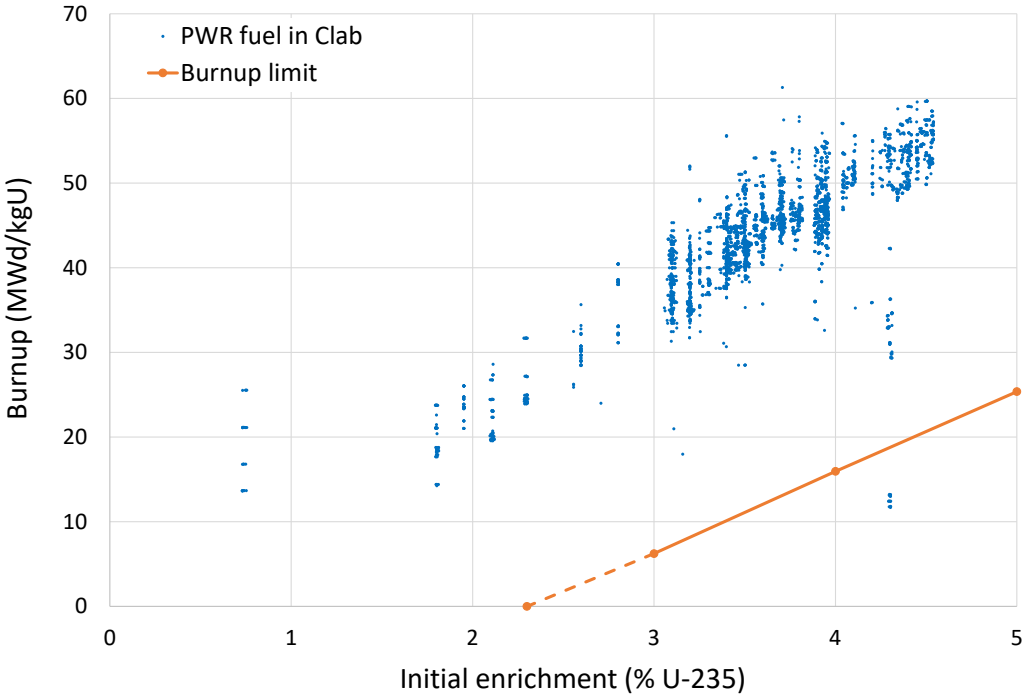

Figure 9-4. *Loading curve for PWR fuel together with representations of the conditions for PWR fuel in Clab.*

Table 9-4. Requirement on burnup for BWR fuel extracted from the upper safety limit and uncertainties.

	5.0 % U-235 initial enrichment	4.45 % U-235 initial enrichment	4.0 % U-235 initial enrichment	3.65 % U-235 initial enrichment
Upper Safety Limit, for the case with a water-filled and corroded insert	0.95832	0.95832	0.95832	0.96737
Summed effect of additional uncertainties	0.05745	0.05694	0.05676	0.05699
k_{eff} at the subcriticality limit including uncertainties	0.90087	0.90138	0.90156	0.91038
Limit translated into burnup, MWd/kgU	**36.5**	**28.4**	**21.2**	**15.4**

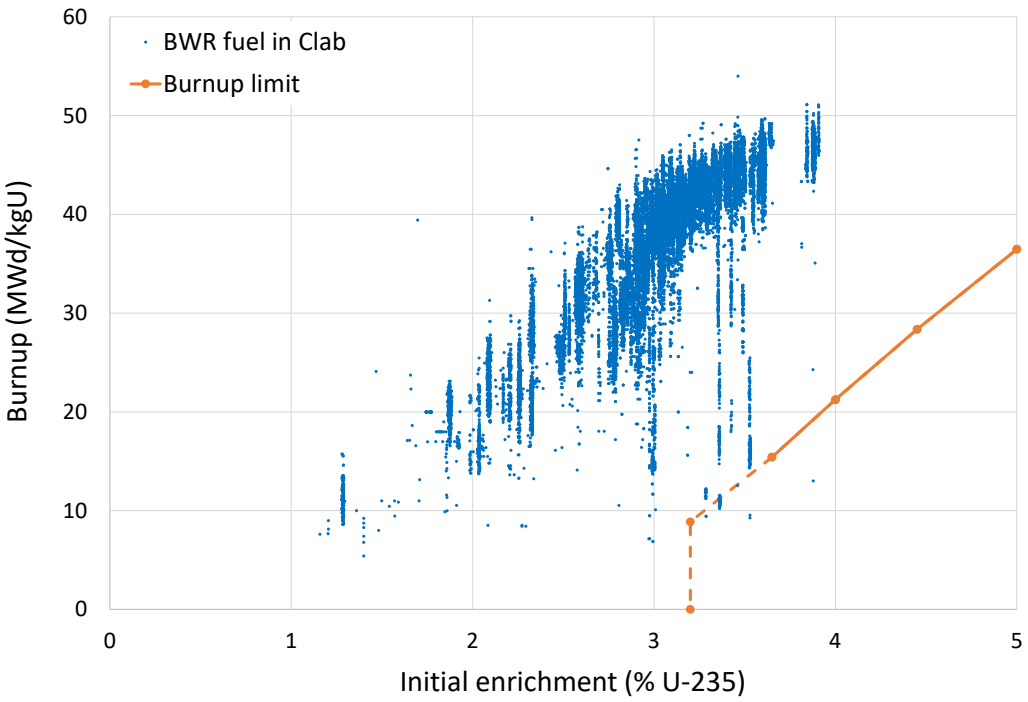

Figure 9-5. *Loading curve for BWR fuel together with representations of the conditions for BWR fuel in Clab.*

9.4.5 Empty positions in the canister

For various reasons it might be necessary to leave a position empty in a canister. From a criticality perspective the above described analysis assumes completely filled canisters. The need to leave an assembly space empty could arise from a thermal perspective with fuel with exceptionally high residual power or if unforeseen issues arise during loading.

An assessment has been made of whether empty positions pose a risk regarding criticality safety.[16] Generally, the reactivity of a *fixed* configuration with a fully loaded canister will decrease if one of the assemblies is replaced by air, water or corrosion products. The assessment of empty positions discusses the rate and volume of corrosion in the canister and the possible movement of the fuel. It is shown that almost all of the insert will be corroded for both the PWR and the BWR inserts, when the empty position has filled up with corrosion products. When all the empty space in the canister is filled with corrosion products there are very small possibilities of movement of the fuel within the canister. When the insert corrodes and the empty space is filling up, it is more likely that the fuel assemblies will be pushed further apart by the developing corrosion layers rather than closer to each other. Other than this, the evolution with an empty position is not expected to be significantly different from the cases included in the criticality analysis. This suggests that a failed, corroding canister with an empty position would have a reduced reactivity compared to the corresponding case with a fully loaded canister.

9.5 Discussion and conclusion

The difference in design between the Rebus PWR and BWR inserts and the cast iron inserts have a considerable impact on the propensity for criticality. This warranted a detailed evaluation of criticality for the Rebus inserts, in line with what has been done for the cast iron inserts. The long-term evolution in a failed canister can be either of several scenarios and in Johansson et al. (2024) these scenarios are identified and estimates of reactivity were made in order to find the most limiting case and its associated reactivity level for the Rebus inserts. For the Rebus PWR canister the effects on reactivity are less demanding and the limiting case is a water-filled canister, otherwise unaffected canister for which the requirement on reactivity is $k_{eff} < 0.95$. For BWR the limiting case is when the canister is water-filled and where corrosion of the insert has caused magnetite to form and fill all the free space up to the fuel channel, a case for which the requirement on reactivity is $k_{eff} < 0.98$.

According to the complementing criticality analysis, the vast majority of the fuel currently in Clab can be deposited safely with regards to criticality in canisters with the Rebus insert. It is necessary to utilize fuel properties that reduces reactivity to show compliance with criteria and burnup credit has been used to this end. Subcriticality will be ensured by showing that the fuel loaded in the canisters will meet requirements on burnup that includes margins for uncertainties.

Margins regarding criticality are required but an overly conservative system will be both expensive and possibly use materials for the canister in a less sustainable way. This demonstrates the importance of the criticality evaluation being an integral part of the design process when developing a final disposal insert and canister. It is also apparent that burnup credit is an important tool in the criticality safety evaluation that is based on passive features and enables a realistic analysis with conservative assumptions.

Criticality safety in the final repository in canisters with the Rebus insert is upheld for fuel that meet the following:

- For PWR fuel, burnup credit is necessary from initial enrichments of 2.3 % U-235. At 5 % it is necessary that the fuel has a burnup of at least 25 MWd/kgU.
- For BWR fuel, burnup credit is necessary from initial enrichments of 3.2 % U-235. At 5 % it is necessary that the fuel has a burnup of at least 38 MWd/kgU.

A minor part of the fuel assemblies does not comply with the requirement on burnup and those assemblies need to be handled in a case-specific manner, for example by loading these assemblies in canisters together with less-reactive fuel and showing subcriticality with case-specific calculations. Finally, it is assessed that criticality safety in the final repository will not be adversely affected by leaving a position empty in a canister with a Rebus insert.

10 Additional issues

10.1 Introduction

A number of issues that do not obviously belong to the topics of the previous chapters are addressed in this chapter, in order to obtain a complete coverage of all the issues related to post-closure safety identified in Chapter 3.

10.2 Hydrogen evolution in a failed canister and its impact on fuel matrix dissolution/conversion

In a failed canister, hydrogen evolving from corrosion of the insert is expected to suppress the dissolution of the fuel matrix. For the cast iron BWR and PWR canister inserts, the volumes and areas of corroding iron have been assessed as sufficient to uphold this effect for as long as required. Canister failures are assessed as being very rare and occurring after tens of thousands of years in the most pessimistic cases that have to be considered on scientific grounds (SKB 2022c). In the case of a hypothetical, initial canister breach, when the fuel radiation field is still high, the hydrogen pressures are expected to rapidly reach values exceeding 1 bar H_2, shown to counteract the oxidative dissolution of relatively fresh fuel (Ekeroth et al. 2020). For fuel older than 1000 years, very low hydrogen concentrations are expected to completely inhibit the oxidative dissolution of spent fuel (Jonsson et al. 2007, Trummer and Jonsson 2010). Even the background concentration of dissolved H_2 in the groundwater at the Forsmark site of around 10^{-6} M is expected to achieve this effect with a margin, whereas iron corrosion in the cast iron insert is expected to provide several orders of magnitude higher concentrations for tens of thousands of years (Sellin and Hedin 2013).

Since the Rebus concept has a similar amount of iron-based construction material as the cast iron insert and since the corrosion properties of the low-alloy carbon steel in the Rebus concept are similar to those of cast iron in the same environment, the hydrogen evolution is assessed as being fully sufficient to also suppress fuel matrix dissolution for the Rebus concept.

In more detail, the surface area of carbon steel in the BWR and PWR inserts are around 57 and 28 m^2, respectively, Table 2-2, while in the cast iron insert it is 35 m^2 for the BWR insert and 17 m^2 for the PWR insert (SKB 2010). This means that the initial rate of hydrogen production will be higher in the Rebus inserts than in the cast iron insert. The hydrogen production will continue during a time period after canister breach which depends on the long-term corrosion rate of carbon steel; at least 40 000 years for a corrosion for rate of 1 μm/year and proportionally longer if the corrosion rate becomes lower as the thickness of the corrosion layer increases.

10.3 Internal pressure build-up

Internal pressure build-up due to e.g. hydrogen gas generation from iron corrosion by residual water in the sealed canister and helium generation due to alpha decays in the fuel needs to be considered. This pressure build-up has been demonstrated to be of no concern for the canister with a cast iron insert (SKB 2022a, Section 2.5.8). Since the contents of gas-generating agents (water and alpha emitters) are the same in a Rebus canister and since the void volumes are larger (PWR) or similar (BWR), the issue of internal pressure build-up is also assessed as being of no concern for the Rebus concept.

10.4 Evolution of a failed canister

The evolution of a failed Rebus canister is largely expected to be similar to that of a failed canister with a cast iron insert. Criticality is a key aspect in this evolution and this is addressed in Chapter 9.

The evolution is determined by the failure mode, the canister properties at the time of failure and the external conditions. Since the canister is assumed to be failed, its mechanical properties are of secondary importance for the continued evolution, simplifying a comparison between the Rebus and cast iron inserts. Failure modes considered in the post-closure safety assessment of the canister with a cast iron insert (SKB 2022c) are failure due to shear loads and due to corrosion of the copper shell. The former is assessed to be a rare event in the million-year perspective of the post-closure safety

assessment, and the latter is assessed as possibly affecting a few canisters if the protective clay buffer has been lost due to erosion caused by low salinity groundwaters. A hypothetical initial failure mode with a pinhole-shaped penetrating defect in the lid or base weld of the copper shell is also considered for the canister with a cast iron insert.

Besides preventing criticality, a failed canister has no formal safety functions in the repository. It does, however, play a role in the release of radionuclides through i) providing hydrogen that suppresses dissolution of the fuel matrix as addressed in Section 10.2 and ii) may possibly limit the outward transport of radionuclides by providing a physical hindrance if the dimensions of the transport path through the canister are limited. The latter role is neglected in the assessment of the corrosion and shear load failure modes, since these are assessed to cause large damages in the copper shell. For the hypothetical pinhole failure mode, it is concluded in Section 13.7.2 of SKB (2022c) that an initial pinhole may provide a transport resistance in a 1000-year perspective depending essentially on the corrosion behaviour of the insert in conjunction with the pinhole and on the mechanical properties of the copper shell. The corrosion of the insert in this case includes galvanic effects caused by the presence of the copper shell. These effects would be essentially equal for the Rebus insert.

Since the nature of the failure modes and the properties of the copper shell are identical for canisters with a Rebus and a cast iron insert, and since the corrosion behaviour is similar for the two inserts, the impact on the release of radionuclides of the Rebus canister may be assessed as negligible (as for the canister with a cast iron insert) for the corrosion and shear load failure modes. Also, a limited impact for the hypothetical pinhole failure mode may be assumed for the Rebus canister, again similar to that of a canister with a cast iron insert.

10.5 Copper corrosion caused by radiolytic oxidants

Copper corrosion caused by oxidants produced by radiolysis outside the copper shell has been thoroughly evaluated in post-closure safety assessments of the canister with a cast iron insert. It has been found that there are considerable margins to any significant impacts on post-closure safety if the dose rate on the copper shell surface is below the design requirement of 1 Gy/h. Since this is the case for the Rebus canister concept (Section 0), this form of copper corrosion is assessed as negligible also for the Rebus concept.

11 Conclusions and outlook

11.1 Summary of conclusions from the analyses presented in this report

The following is a brief summary of the results and conclusions presented in the preceding Chapters.

Radiation intensity

The neutron and gamma radiation intensity in and around a Rebus canister is similar to that of the canister with a cast iron insert, see Chapter 4. This is expected since the two are to be loaded with the same fuel and since the dimensions and the radiation attenuation properties of the insert materials are similar. The rate of radiation induced damage (the rate of creation of pairs of vacancies and interstitial atoms) in the metal materials is also similar, Section 4.4. The peak dose rate outside a Rebus canister is well below the requirement of <1 Gy/h, and somewhat lower than that of a canister with a cast iron insert.

Thermal evolution

The fuel temperature in a Rebus insert would be somewhat higher than that in the cast iron insert, primarily due to the gaps between the Rebus insert outer tube and inner framework, Section 5.2. The peak fuel temperatures are, however, far lower than any temperature of concern for post-closure safety. The framework of the Rebus insert is expected to experience peak temperature in the repository (around 130 °C and 125 °C for 1700 W BWR and PWR canisters, respectively) that are somewhat higher than those of the cast iron insert, and the temperature will have decreased to much lower values when the highest mechanical loads are expected. The Rebus tubes are expected to experience repository temperatures (peak around 100 °C) that are very similar to those of the outer surface of the cast iron insert. The temperature development of the copper shell and the system parts external to the canister are identical for the Rebus and cast iron inserts since these temperatures are determined by the residual power of the fuel and the thermal properties of the system external to the canister. A requirement on a maximum residual power of 1700 W per canister together with a site-specific layout is used to ensure that detrimental temperatures do not occur in the repository, see e.g. Section 10.3.4 of SKB (2022c).

Hydrological evolution

The hydrological evolution inside a sealed Rebus canister is largely determined by the temperature development, the amount of residual water in the sealed insert and the progress of aqueous corrosion of the insert material, in particular its dependence on relative humidity (RH), Section 5.3. The development is generally quite similar to that of the canister with a cast iron insert, with some differences caused by differences in geometry and thermal development. Few, if any, of the around 6000 sealed canister inserts are expected to contain amounts of residual water even close to the allowed maximum of 600 g, Section 2.3. For the majority of canisters containing no leaking fuel pins, the amount of water is expected to be negligible from the point-of-view of post-closure safety. For some tens of canisters up to 240 g of water is pessimistically assessed to remain. If the corrosion is assumed to proceed independent of RH, then all water is expected to be consumed within a few years after closure, whereas if there is an RH limit below which corrosion does not occur, a small amount of water vapour, but no liquid water, could remain in the insert for a very long time. The limited amount of water assessed to be present in the majority of canisters is an important finding for subsequent evaluations of radiolysis and hydrogen embrittlement.

Radiolysis

Radiolysis could lead to the formation of agents active in stress corrosion cracking (SCC) of the canister materials. The extent of radiolysis reactions in the gas phase of the insert interior are, in addition to the radiation intensity, largely determined by the amounts of argon, residual water and air in the sealed insert. With a requirement of > 97 % Ar and with the limited amounts of residual water expected in the canister insert, limited amounts of SCC active agents are generated according to the radiolysis calculations performed, Section 6.3. These are used in the assessment of SCC.

Stress corrosion cracking, SCC

Stress corrosion cracking of the Rebus insert materials and/or of the copper shell requires a simultaneous occurrence of tensile stresses and a chemical environment conducive to SCC, see Section 7.2. The SCC promoting factors related to the chemical environment in a sealed canister concern the occurrence of oxidising conditions and the radiation induced SCC active agents ammonium (NH_4^+), nitrate (NO_3^-) and nitrite (NO_2^-). Comparing the times of occurrence of tensile stresses (as an effect of saturation of the clay buffer surrounding the canister) and the persistence of the SCC active agents and of oxidising species, it is concluded that the likelihood of SCC in the Rebus insert is negligible. The same is concluded for the copper shell regarding SCC from the interior atmosphere.

Hydrogen embrittlement

Hydrogen embrittlement is not expected to affect the Rebus materials with their as-manufactured properties because of the low initial hydrogen content. Hydrogen gas generated due to anaerobic steel corrosion by residual water is the only identified significant additional hydrogen source in a sealed canister insert. It has been demonstrated that this hydrogen would have only a limited impact on the mechanical properties (the fracture toughness) of the Rebus materials if the maximum allowed 600 g of residual water in the canister is pessimistically assumed. Hydrogen embrittlement is therefore not expected to deteriorate the Rebus insert materials in a sealed canister, Section 7.3. This was further corroborated by demonstrating that the pessimistically assessed limited reduction in fracture toughness causes a reduction of acceptable defect sizes that is of no concern.

Static and dynamic strain ageing

Static and dynamic strain ageing could lead to deteriorated mechanical properties over time. The phenomena have been investigated experimentally with the conclusion that both are expected to have a negligible impact on post-closure safety, Section 7.4, in agreement with earlier findings for the canister with a cast iron insert.

Radiation-induced embrittlement

The direct effects of damage caused by the radiation doses are assessed as negligible, Section 7.5.2, even when annealing effects that greatly reduce the damage are neglected. Radiation-induced embrittlement could be caused by radiation-enhanced i) precipitation of Cu clusters, ii) precipitation of more complex intermetallic phases or iii) phosphorous segregation to grain boundaries.

Updated calculations of Cu cluster formation, with a dislocation density measured for the Rebus material and with repository-relevant temperatures and damage rates, confirm earlier findings that a Cu content of at most 0.05 at.% is sufficient to avoid detrimental Cu cluster formation in the Rebus material, Section 7.5.3. Results of calculations with higher Cu concentrations indicate that a relaxation to the standard requirement of 0.35 at.% Cu for the quality of the P355N steel grade intended for use in the canister inserts would not yield an unacceptable extent of Cu clustering. This indication would be strengthened if verified experimentally.

Precipitation of more complex intermetallic phases consisting of in particular Ni, Mn and Si has been observed in irradiated reactor steels. Based on available literature data, it is concluded for the Rebus steel that irradiation induced precipitation of such intermetallic phases will give negligible, if any, degradation of the insert under repository conditions, Section 7.5.4. The conclusion is primarily based on the fact that total radiation doses many orders of magnitude higher than those in a final repository are required for such effects to be observed.

Radiation enhanced phosphorus segregation to grain boundaries may embrittle steel, as has been observed in studies of reactor steels that resemble the steel suggested as the Rebus insert material. However, effects have only been seen in conditions where dose rates and total doses are several orders of magnitude higher than in the repository environment, and at temperatures exceeding what is expected for the canister insert in the repository. It is therefore concluded that irradiation induced phosphorus segregation will give negligible, if any, degradation of the insert, see Section 7.5.5.

Resilience to mechanical loads

The assessment of the Rebus canisters' resilience to mechanical loads in a repository environment reported in Chapter 8 lead in summary to the following key conclusions.

- Analyses of loads from asymmetric swelling due to uneven water saturation of the bentonite buffer and deposition hole geometry, during temperate climate conditions expected to last for tens of thousands of years, show a sufficient margin against global plastic collapse for load cases stipulated in the design requirements.
- Deterministic and probabilistic analyses show that the Rebus canisters will withstand a 50 MPa isostatic load, as stipulated in the design requirements. The modelling is verified by isostatic pressure tests.
- The Rebus canisters are also demonstrated to withstand a 5 cm shear load occurring at a rate of up to 1 m/s and for the buffer properties as stipulated in the design requirements. The canisters are also demonstrated to withstand possible sequences of shear and isostatic loads.
- Defect tolerance analyses for the load cases yield, together with measured fracture toughness data for the Rebus materials, acceptable defect sizes that are expected to be rare and readily avoidable with available detection methods. The derived acceptable defect sizes include allowance for a pessimistically assessed extent of hydrogen embrittlement.
- Creep in insert materials is assessed to be negligible. Creep in the copper shell has not been explicitly modelled. Rather, it has been demonstrated that stresses and strains in the copper shell with a Rebus insert for the shear and isostatic load cases will be similar to those with a cast iron insert. Since copper creep is assessed not to jeopardise the post-closure integrity of canisters with cast iron inserts, the same conclusion is drawn for the Rebus canisters.

Criticality

In order to rule out criticality in the final repository it needs to be demonstrated that the neutron multiplication factor (k_{eff}) does not exceed 0.95 for normal conditions, which is assumed to be a water-filled canister with intact geometry and 0.98 for unlikely scenarios, which are assumed to be a water-filled canister where the canister integrity is lost and corrosion processes have changed the material properties and the geometrical configuration.

The criticality assessment in Chapter 9 demonstrates that the vast majority of the fuel currently in Clab can be deposited safely with regards to criticality in canisters with Rebus inserts. It is necessary to utilize fuel properties that reduces reactivity to show compliance with criteria and burnup credit has been used to this end.

Criticality safety in the final repository in canisters with the Rebus insert is upheld for fuel that meet the following:

- For PWR fuel, burnup credit is necessary from initial enrichments of 2.3 % U-235. At 5 % it is necessary that the fuel has a burnup of at least 25 MWd/kgU.
- For BWR fuel, burnup credit is necessary from initial enrichments of 3.2 % U-235. At 5 % it is necessary that the fuel has a burnup of at least 38 MWd/kgU.

A minor part of the fuel assemblies does not comply with the requirement on burnup and those assemblies need to be handled in a case specific manner, for example by loading these assemblies in canisters together with less-reactive fuel and showing subcriticality with case-specific calculations. It is also assessed that criticality safety in the final repository will not be adversely affected by leaving a position empty in a canister with a Rebus insert.

The Rebus PWR canisters have a somewhat larger margin to the criticality requirements than the canisters with cast iron inserts. The opposite is true for the BWR canisters, where burn-up credit is not required to demonstrate non-criticality in the final repository for the cast iron design.

Additional issues

Some minor additional issues are assessed in Chapter 10 and shown to be either beneficial or of no concern for post-closure safety, similar to what has been found for the canister with a cast iron insert.

11.2 Fulfilment of report purposes

In Section 1.1, the purposes of the present report are stated as *i*) to evaluate issues related to post-closure safety for the Rebus canisters to the level achieved for canisters with a cast iron insert and *ii*) to assess the ability of the Rebus canisters to fulfil stipulated design requirements in a KBS-3 repository.

The first purpose is assessed as having been achieved based on the results presented in preceding chapters. For many of the issues addressed, e.g. the thermal and hydrological evolution, radiolysis, SCC, and embrittlement due to radiation induced copper clusters, the work has resulted in an advanced level of knowledge also for the cast iron design.

Regarding the second purpose, based on the conclusions summarised above, with details provided in the preceding chapters, the canister design requirements according to Section 2.1.2 and applicable requirements on the handling of the spent nuclear fuel according to Section 2.1.3, are assessed to be fulfilled for a Rebus canister with a design according to Section 2.2. The focus has been on insert-related aspects of the requirements, whereas aspects related to the copper shell have been treated only if they are affected by the design of the insert. The only insert-related requirement that has not been addressed is the one stating that organic materials are not allowed in the insert components. There is no reason to believe that the fulfilment of this requirement would be more demanding for the Rebus inserts than for the cast iron inserts.

A canister with a cast iron insert has also been assessed to fulfil design requirements according to Section 2.1.2 (Jonsson et al. 2018). The margins are in some respects different, such as that against plastic collapse for an isostatic pressure of 50 MPa where the cast iron insert has a somewhat higher margin, or the resilience against shear load where larger defects are acceptable in the Rebus inserts.

As noted in Section 1.1, an assessment of the prospects of producing canister inserts according to specifications on an industrial scale such that the design requirements are achieved is beyond the scope of the present report.

11.3 Further work

As with many aspects of post-closure safety for the KBS-3 repository concept, continued research could further strengthen the conclusions and be used as a basis for further optimisations. Some issues that could be considered for further research are listed below. Many of these are also relevant for the cast iron insert.

- A more complete numerical treatment of thermal expansion and contraction effects in the copper shell (Section 5.2.2) could yield a more definite assessment of this issue, for both canisters with cast iron and Rebus inserts.
- A better understanding of the RH dependence of anoxic corrosion of the insert materials by water (Section 5.3.3) This is of relevance for the analyses of radiolysis in Chapter 6 and of the evaluation of species formed through radiolysis in Chapter 7.
- Issues mentioned as potential future work related to radiolysis in Section 6.4.
- It could be of interest to carry out e.g. a J-integral test of the type mentioned in Section 7.3.5 for the Rebus materials at repository relevant temperatures and internal H_2 pressures in order to further verify that the material is not susceptible to hydrogen embrittlement under such conditions.
- As mentioned above, model calculation results indicate that the requirement of a maximum Cu concentration in the Rebus materials of 0.05 at.% to avoid radiation-induced detrimental Cu cluster formation in the Rebus material can be relaxed to the standard requirement of 0.35 at.% Cu (Section 7.5.3). The basis for such a change could to some extent be further substantiated by determining the full range of the ductile-to-brittle transition region (Section 8.10.3), hereby

establishing a tolerable increase in ductile-to-brittle transition temperature. It could also be strengthened by experimentally verifying that non-detrimental amounts of Cu clusters are formed when Rebus-like materials with a higher Cu content are exposed to radiation doses similar to those expected in a final repository, and that the exposed material has intact mechanical properties.

- An analysis of the resilience of the canister to a 10 cm shear load could be of interest in the overall optimisation of the KBS 3 system. Here, requirements on the canister interplay with requirements on limited shear movements in the host rock in the evaluation of the likelihood of this failure mode of the canister.

References

SKB's (Svensk Kärnbränslehantering AB) publications can be found at www.skb.com/publications. SKBdoc documents and unpublished SKB reports will be submitted upon request to document@skb.se.

Agrenius L, Spahiu K, 2016. Criticality effects of long-term changes in the material compositions and geometry in disposal canisters. SKB TR-16-06, Svensk Kärnbränslehantering AB.

Alvarez Holston A-M, 2021. Delayed Hydride Cracking in KBS-3. Studsvik report N-21/062, Studsvik Nuclear AB. SKBdoc 1948837 ver 3.0, Svensk Kärnbränslehantering AB.

Andgren K, 2023. Analysis of radiation damage in canister steel – project REBUS. R-23-17, Svensk Kärnbränslehantering AB.

Bergendal E, 2024. Graphite as a sealing material for a KBS-3 canister insert. SKBdoc 1987421 ver 1.0, Svensk Kärnbränslehantering AB.

Björkbacka Å, Johnson C M, Leygraf C, Jonsson M, 2017. Radiation induced corrosion of copper in humid air and argon atmospheres. Journal of The Electrochemical Society 164, C201–C206.

Blackwood D J, Henshaw J, Platts N, Hilditch J P, 1996. Stress corrosion cracking of the advanced cold process canister: Carbon steel in nitric acid. SKB Inkapsling Projektrapport 96-05, Svensk Kärnbränslehantering AB.

Boellinghaus T, Hoffmeister H, Dangeleit A, 1995. A scatterband for hydrogen diffusion coefficients in micro-alloyed and low carbon structural steels, Welding in the World 35, 83-96.

Bolinder T, Dillström P, Gunnars J, 2025. KBP3021 Project REBUS – SKB Main Study – Basis for defect tolerance analyses of insert design concept-1. Report No. 5002622-100-1 rev 8.0, Kiwa Technical Consulting AB. SKBdoc 2032620 ver 4.0, Svensk Kärnbränslehantering AB.

Brissonneau L, Barbu A, Bocquer J-L, 2004. Radiation effects on the long-term ageing of spent fuel storage containers. Packaging, Transport, Storage & Security of Radioactive Material 15, 121-130.

Carslaw H S, Jaeger J C, 1959. Conduction of heat in solids. 2nd ed. Oxford: Oxford University Press.

Chaouadi R, Gèrard R, Sterger E, van Renterghem W, 2019. Neutron irradiation hardening of chemically-tailored RPV steels with respect to Cu/P and Ni/Mn elements, Journal of Nuclear Materials, vol 519, pp. 188-204.

Ciaraldi S W, 1992. Stress-corrosion cracking of carbon and low-alloy steels (yield strengths less than 1241 MPa), in Stress-Corrosion Cracking Materials Performance and Evaluation, R.H. Jones (ed.). ASM International (Metals Park, OH), chap. 2.

Dawson T J, 1956. Behavior of welded pressure vessels in agricultural ammonia service. Weld J 35 p. 568.

Dillström P, 2009. Updated probabilistic analysis of canister inserts for spent nuclear fuel. 50006980-2, Rev. 1, Inspecta Technology AB. SKBdoc 1207426 ver 1.0, Svensk Kärnbränslehantering AB.

Dillström P, 2014. Probabilistic analysis of BWR canister inserts for spent nuclear fuel in the case of an earthquake induced rock shear load. Report No. 50014130-1, Inspecta Technology AB. SKBdoc 1412158 ver 1.0, Svensk Kärnbränslehantering AB.

Dillström P, Manngård T, 2017. Probabilistic analysis of BWR canister inserts for spent nuclear fuel in the case of an isostatic pressure load. Report No. 5001090-1, Inspecta Technology AB. SKBdoc 1585534 ver 1.0, Svensk Kärnbränslehantering AB.

Dillström P, Gunnars J, von Unge P, Mångård D, 2018. Procedure for Safety Assessment of Components with Defects, SSM2018:18, Swedish Radiation Safety Authority.

Domain C, Becquart C S, 2005. Diffusion of phosphorus in alpha-Fe: An ab initio study. Phys. Rev. B 71.

Ekeroth E, Granfors M, Schild D, Spahiu K, 2020. The effect of temperature and fuel surface area on spent nuclear fuel dissolution kinetics under H_2 atmosphere, J. Nucl. Mater. 531, paper 151081.

EricksonKirk M, 2006. An upper-shelf fracture toughness master curve for ferritic steels. International Journal of Pressure Vessels and Piping, 83, 571-583. http://dx.doi.org/10.1016/j.ijpvp.2006.05.001

Faulkner R G, Song S H, Flewitt P E J, 1996. A model describing neutron irradiation-induced segregation to grain boundaries in dilute alloys. Met Mater Trans A 27 pp. 3381-3390.

Faulkner R G, Jones R B, Lu Z, Flewitt P E J, 2005. Grain boundary impurity segregation and neutron irradiation effects in ferritic alloys. Philosophical Magazine, Vol. 85, No. 19, 2065–2099.

Feigin E, Öbrink E, Bolinder T, Mångård D, 2024a. KBP3021 Project REBUS – SKB Main Study – PWR Canister Insert – Load Case L07 (5a) – Assessment of global plastic collapse. Report No. 5002622-102-2 rev 2.0, Kiwa Technical Consulting AB. SKBdoc 2039029 ver 1.0, Svensk Kärnbränslehantering AB.

Feigin E, Öbrink E, Bolinder T, Mångård D, 2024b. KBP3021 Project REBUS – SKB Main Study – BWR Canister Insert – Load Case L07 (5a) – Assessment of global plastic collapse. Report No. 5002622-102-3 rev 2.0, Kiwa Technical Consulting AB. SKBdoc 2039910 ver 1.0, Svensk Kärnbränslehantering AB.

Feigin E, Öbrink E, Bolinder T, Mångård D, 2024c. KBP3021 Project REBUS – SKB Main Study – PWR Canister Insert – Load Case L08 (5b) – Assessment of global plastic collapse. Report No. 5002622-105-1 rev 2.0, Kiwa Technical Consulting AB. SKBdoc 2047929 ver 1.0, Svensk Kärnbränslehantering AB.

Fredriksson L, 2025. KBP3021 Project REBUS – SKB Main Study – PWR Canister Insert – Load Case L06 (4b) – Assessment of global plastic collapse. Report No. 5003088-111-1 rev 1.0, Kiwa Technical Consulting AB. SKBdoc 2085341 ver 1.0, Svensk Kärnbränslehantering AB.

Guinan M W, 2001. Radiation effects in spent nuclear fuel canisters. SKB TR-01-32, Svensk Kärnbränslehantering AB.

Gutierrez-Solana F, Elices M, 1986. High-Pressure Hydrogen Behavior of a Pipe-Line Steel, in Current Solutions to Hydrogen Problems in Steel, CG Interrante and GM Pressouyre Eds., American Society for Metals, Metal Park, OH, 181-185.

Hagström J, 2024. Microstructure and dislocation density analysis of P355N pressure vessel steel grade. SKB R-24-02, Svensk Kärnbränslehantering AB.

Hammer T, Fredriksson L, 2024. KBP3021 Project REBUS – SKB Main Study – A sensitivity analysis (FEA) of a short canister as a verification of an isostatic pressure test. Report No. 5003075-100-1 rev 1.0, Kiwa Technical Consulting AB. SKBdoc 2064634 ver 1.0, Svensk Kärnbränslehantering AB.

Hammer T, Fredriksson L, 2025. KBP3021 Project REBUS – SKB Main Study – PWR Canister Insert – Load Case L02 (1a) & L03 (2a) – Assessment of global plastic collapse. Report No. 5002622-104-1 rev 3.0, Kiwa Technical Consulting AB. SKBdoc 2049802 ver 2.0, Svensk Kärnbränslehantering AB.

Hammer T, von Unge P, 2024a. KBP3021 Project REBUS – SKB Main Study – PWR Canister Insert – Load Case L05 (4a) – Assessment of global plastic collapse. Report No. 5002622-101-1 rev 2.0, Kiwa Technical Consulting AB. SKBdoc 2040003 ver 1.0, Svensk Kärnbränslehantering AB.

Hammer T, von Unge P, 2024b. KBP3021 Project REBUS – SKB Main Study – BWR Canister Insert – Load Case L05 (4a) – Assessment of global plastic collapse. Report No. 5002622-101-2 rev 2.0, Kiwa Technical Consulting AB. SKBdoc 2043766 ver 1.0, Svensk Kärnbränslehantering AB.

Hedin A, 2004. Integrated near-field evolution model for a KBS-3 repository. SKB R-04-36, Svensk Kärnbränslehantering AB.

Hedin A, 2024. Modelling of radiation enhanced Cu cluster formation in Fe. SKBdoc 2037360, ver 1.0, Svensk Kärnbränslehantering AB.

Hedin A, 2025. Thermal and hydrological conditions in a sealed KBS-3 canister. SKBdoc 1999391 ver 2.0, Svensk Kärnbränslehantering AB.

Hedin A, Högberg J, 2024. Hydrogen absorption by insert materials in a sealed KBS-3 canister. SKBdoc 2041188, ver 1.0, Svensk Kärnbränslehantering AB.

Henshaw J, 1994. Modelling of nitric acid production in the Advanced Cold Process Canister due to irradiation of moist air. AEA-D&W 0706/RS3429, AEA Technology, UK (also published as SKB TR 94-15, Svensk Kärnbränslehantering AB).

Henshaw J, Evins L Z, 2023. Radiolysis calculations of gases in a KBS-3 canister. SKB TR-22-15, Svensk Kärnbränslehantering AB.

Henshaw J, Spahiu K, 2021. Radiolysis calculations of air, argon and water mixtures in a KBS-3 canister. SKB TR-21-11, Svensk Kärnbränslehantering AB.

Hjerpe T, 2022. Avstämning mot NEA IFEP 3.0. SKBdoc 1860518 ver 1.0, Svensk Kärnbränslehantering AB (In Swedish).

Hökmark H, Lönnqvist M, Kristensson O, Sundberg J, Hellström G, 2009. Strategy for thermal dimensioning of the final repository for spent nuclear fuel. SKB R-09-04, Svensk Kärnbränslehantering AB.

Hökmark H, Lönnqvist M, Fälth B, 2010. THM-issues in repository rock. Thermal, mechanical, thermo-mechanical and hydro-mechanical evolution of the rock at the Forsmark and Laxemar sites. SKB TR-10-23, Svensk Kärnbränslehantering AB.

IAEA, 2005. Effects of nickel on irradiation embrittlement of light water reactor pressure vessel steels, IAEA TECDOC-1441, Vienna.

Ibrahim B, Zagidulin D, Behazin M, Ramamurthy S, Wren J C, Shoesmith D W, 2018. The corrosion of copper in irradiated and unirradiated humid air. Corrosion Science 141, 53–62.

Ikonen K, 2020. Temperatures inside SKB and Posiva type canisters for spent fuel. Posiva SKB report 12, Posiva Oy, Svensk Kärnbränslehantering AB.

Johansson F, Zetterström P, Spahiu K, 2024. Criticality effects of long-term changes in material compositions and geometry in disposal canisters with insert Rebus Concept 1 P355N and P460N. SKB TR-23-26, Svensk Kärnbränslehantering AB.

Johansson J, 2023. Inspection report chemical analysis ST-ST3 D-lab 75125. SKBdoc 2000788 ver 1.0, Svensk Kärnbränslehantering AB.

Jones A R, 1959. Radiation–induced reactions in the N_2–O_2–H_2O system. Radiation Research 10, 655–663.

Jonsson M, Nielsen F, Roth O, Ekeroth E, Nilsson S, Hossain M M, 2007. Radiation induced spent nuclear fuel dissolution under deep repository conditions. Envir. Sci. Technol. 41, pp.7087-7093.

Jonsson M, Emilsson G, Emilsson L, 2018. Mechanical design analysis for the canister. Posiva SKB Report 04, Posiva Oy, Svensk Kärnbränslehantering AB.

Karlsson M, 2009. Strålskärmsberäkningar för kopparkapslar innehållande BWR, MOX och PWR bränsleelement, ALARA 07-0014R Rev1-Final-091119. SKBdoc 1077122 ver 2.0, Svensk Kärnbränslehantering AB. (In Swedish.)

King F, 2009. Hydrogen Effects on Carbon Steel Used Fuel Containers, NWMO-TR-2009-29, Nuclear Waste Management Organization, Canada.

King F, 2010. Stress corrosion cracking of carbon steel used fuel containers in a Canadian deep geological repository in sedimentary rock. NWMO TR-2010-21, Nuclear Waste Management Organization, Canada.

Kirk M, Erickson M, Server W, Stevens G, Cipolla R, 2014. PVP2014-28540 - Assessment of Fracture Toughness Models for Ferritic Steels Used in Section Xi of the ASME Code Relative to Current Data-Based Models, Proceedings of PVP2014, 2014 ASME Pressure Vessels and Piping Division Conference, July 20-24, 2014, Anaheim, CA, USA.

Kiuchi K, McLellan R B, 1983. The solubility and diffusivity of hydrogen in well-annealed and deformed iron, Acta Metall. 31, 961-984.

Korzhavyi P, Gorbatov O, Selleby, M, 2018. Precipitation of late blooming phases in iron-based Alloys. Theoretical modelling. SKB R-16-07, Svensk Kärnbränslehantering AB.

Laitinen H, 2025. Kravuppfyllnad vid rymning av deponeringshål. SKBdoc 2006465 ver 3.0, Svensk Kärnbränslehantering AB. (Internal document, in Swedish.)

Ljustell P, 2024a. Prerequisites loadings for structural verification of an alternative insert design Concept 1. Report No. 5002622-100-2 rev 1.0, Kiwa Technical Consulting AB. SKBdoc 2043628 ver 1.0, Svensk Kärnbränslehantering AB.

Ljustell P, 2024b. KBP3021 Project REBUS – SKB Main Study – Prerequisites loadings for structural verification of an alternative insert design Concept 1 – Excel Appendix. Report No. 5002622-100-2 rev 1.0, Kiwa Technical Consulting AB. SKBdoc 2043629 ver 1.0, Svensk Kärnbränslehantering AB.

Ljustell P, Lorentzon M, Shipsha A, 2024a. KBP3021 Project REBUS – SKB Main Study – Design basis (KFM) for Mechanical Equipment in the Canister. SKBdoc 2032618 ver 1.0, Svensk Kärnbränslehantering AB.

Ljustell P, Lorentzon M, Shipsha A, 2024b. KBP3021 Project REBUS – SKB Main Study – Complementary Design basis (KKFM) for Mechanical Equipment in the Canister. SKBdoc 2032619 ver 1.0, Svensk Kärnbränslehantering AB.

Loberg J, 2023. Dose rate calculations – project REBUS. SKB R-22-08, Svensk Kärnbränslehantering AB.

Lundin P, Holmberg J, 2024. Residual stress measurements of steel tubes, Ø 950 mm, ST7. Rapport: 2024-01-23-23027, Lundin Stress Service AB. SKBdoc 2035847 ver 1.0, Svensk Kärnbränslehantering AB.

Lundin P, Holmberg J, 2025. Residual stress measurements of steel tubes, Ø 950 mm, ST13 and ST17. Lundin Stress Service AB. Report: 25011-2025-03-11, Lundin Stress Service AB. SKBdoc 2080379 ver 1.0, Svensk Kärnbränslehantering AB.

Malmström D, 2023. Hydrogen analysis with TD-MS. Swerim. SKBdoc 2012443 ver 1.0, Svensk Kärnbränslehantering AB.

Martin O, Nilsson K-F, Jakšić N, 2009. Numerical simulation of plastic collapse of copper-cast iron canister for spent nuclear fuel. Engineering Failure Analysis 16, 225–241.

Martinsson Å, Wu R, Sandström R, 2009. Influence of hydrogen on mechanical properties of nodular cast iron. KIMAB-2009-118, Swerea KIMAB AB, Sweden.

Martinsson Å, Andersson-Östling H, Seitislam F, Wu R, Sandström R, 2010. Creep testing of nodular iron at ambient and elevated temperatures. SKB R-10-64, Svensk Kärnbränslehantering AB.

Morco R P, Joseph J M, Hall D S, Medri C, Shoesmith D W, Wren J C, 2017. Modelling of radiolytic production of HNO_3 relevant to corrosion of a used fuel container in deep geologic repository environments. Corrosion Engineering, Science and Technology, 52:sup1, 141-147. https://doi.org/10.1080/1478422X.2017.1340227

Mångård D, von Unge P, Dillström P, 2023. Feasibility study regarding verifying calculations of an alternative insert design concept 1 – Review and evaluation of the load cases reported in Posiva SKB Report 04. Report No. 5002502-100-1 rev 1.0, Kiwa Technical Consulting AB. SKBdoc 2012508 ver 1.0, Svensk Kärnbränslehantering AB.

NEA, 2006. Electronic version 2.1 of the NEA FEP Database developed on behalf of the Nuclear Energy Agency by Safety Assessment Management Ltd.

NEA, 2019. International Features, Events and Processes (IFEP) List for the Deep Geological Disposal of Radioactive Waste. Version 3.0. NEA/RWM/R(2019)1. Nuclear Energy Agency/Organisation for Economic Cooperation and Development (NEA/OECD), Paris.

Nilsson K-F, Lofaj F, Burström M, Andersson C-G, 2005. Pressure tests of two KBS-3 canister mock-ups. SKB TR-05-18, Svensk Kärnbränslehantering AB.

Ogawa Y, Hino M, Nakamura M, Matsunaga H, 2021. Pearlite-driven surface-cracking and associated loss of tensile ductility in plain-carbon steels under exposure to high-pressure gaseous hydrogen. International Journal of Hydrogen Energy, 46, 6945–6959.

Otterberg R, Karlsson C, 1979. Åldring i svetsgods i reaktortryckkärl. IM-1358. Stockholm: Institutet för metallforskning.

Padovani C, Pletser D, Jurkschat K, Armstrong D, Dugdale S, Brunt D, Faulkner R, Was G, Johansson A J, 2019. Assessment of microstructural changes in copper due to gamma radiation damage. SKB TR-19-12, Svensk Kärnbränslehantering AB.

Posiva SKB, 2017. Safety functions, performance targets and technical design requirements for a KBS-3V repository. Conclusions and recommendations from a joint SKB and Posiva working group. Posiva SKB Report 01, Posiva Oy, Svensk Kärnbränslehantering AB.

Renström P, 2020. Numerical study of the influence from deposited gamma radiation energy on canister temperature in the Spent Fuel Repository. SKB R-19-26, Svensk Kärnbränslehantering AB.

Robson J D, 2020. Deformation Enhanced Diffusion in Aluminium Alloys. Metall Mater Trans A 51, 5401–5413. https://doi.org/10.1007/s11661-020-05960-5

Ronneteg U, 2022. KBP3021 REBUS - Input parameters post-closure safety - Concept 1. SKBdoc 1939700 ver 4.0, Svensk Kärnbränslehantering AB.

Ronneteg U, 2024. KBP3021 - Isostatic pressure test of the Rebus BWR and PWR inserts. SKBdoc 2067727 ver 1.0, Svensk Kärnbränslehantering AB.

Ronneteg U, 2025. KBP3021 REBUS - Input parameters post-closure safety - Concept 1. SKBdoc 1939700 ver 9.0, Svensk Kärnbränslehantering AB.

Roudén J, Blomström J, Efsing P, Berglund M, 2023. Thermal Aging of LAS Weld Metal from Decommissioned Nuclear Components in Swedish PWRs in Radiation Embrittlement Trend Curves and Equations and Their Use for RPV Integrity Evaluations, ed. W. L. Server, M. Brumovsky´, and M. Kirk (West Conshohocken, PA: ASTM International), 204–216, http://doi.org/10.1520/STP164720220064

Russel K, Brown L M, 1972. A dispersion strengthening model based on differing elastic moduli applied to the iron-copper system. Acta Metall, 969.

Sahiluoma P, Yagodzinskyy Y, Forsström A, Hänninen H, Bossuyt S, 2021. Hydrogen embrittlement of nodular cast iron. Materials and Corrosion 72, 245–254.

Sandberg N, Korzhavyi P, 2009. Theoretical study of irradiation induced hardening and embrittlement in spent nuclear fuel holders, relevant for the Swedish long-term storage. SKB R-09-15, Svensk Kärnbränslehantering AB.

Sander R, 2023. Compilation of Henry's law constants (version 5.0.0) for water as solvent. Atmospheric Chemistry and Physics 23, 10901–12440. https://doi.org/10.5194/acp-23-10901-2023

San Marchi C, Somerday B P, 2012. Technical reference on hydrogen compatibility of materials. SAND2012-7321. Livermore, CA: Sandia National Laboratories.

Sarnet J, 2022. Några mätningar av segjärns åldring. SKB R-22-04, Svensk Kärnbränslehantering AB. (In Swedish.)

Sarnet J, 2024a. Hydrogen embrittlement of low carbon steels. SKBdoc 2000114 ver 1.0, Svensk Kärnbränslehantering AB.

Sarnet J, 2024b. Some measurements of the ageing of a carbon steel. SKB R-24-04, Svensk Kärnbränslehantering AB.

Sarrasin L, Tisyadi M F, Abdelouas A, Šachlová Š, Kašpar V, Dobrev D, Gõtz D, Kolomá K, Večerník P, Zuna M, Alonso U, Diéguez M, Soto C, Fernández A M, Gutiérrez M G, Valdivieso P, Missana T, 2024. Synthesis of irradiation results under repository conditions. Final version as of 13.05.2024 of deliverable D.15.8 of the HORIZON 2020 project EURAD. EC Grant agreement no: 847593.

Sefer B, 2025. Hydrogen analysis before and after gaseous hydrogen exposure and influence of hydrogen on mechanical properties of P355N steel. Report No. 2025-174, Swerim AB. SKBdoc 2080758 ver 1.0, Svensk Kärnbränslehantering AB.

Seifert H P, Ritter S, 2005. Research and service experience with environmentally-assisted cracking in carbon and low-alloy steels in high-temperature water". SKI Report 2005:60, Swedish Nuclear Power Inspectorate.

Sellin P, Hedin A, 2013. Svar till SSM på begäran om komplettering rörande vätgastransport i slutförvaret. SKBdoc 1385070 ver1.0, Svensk Kärnbränslehantering. (In Swedish.)

Shipsha A, Dillström P, Hammer T, 2025. KBP3021 Project REBUS – SKB Main Study – PWR Canister Insert – Load Case L05 (4a) – Probabilistic analysis. Report No. 5003088-104-1 rev 2.0, Kiwa Technical Consulting AB. SKBdoc 2076525 ver 1.0, Svensk Kärnbränslehantering AB.

SKB, 2009. Underground design Forsmark Layout D2. SKB R-08-116, Svensk Kärnbränslehantering AB.

SKB, 2010. Design, production and initial state of the canister. SKB TR-10-14, Svensk Kärnbränslehantering AB.

SKB, 2012. Komplettering ang. Kapselredovisning. SKBdoc 1333256 ver 2.0, Svensk Kärnbränslehantering AB. (In Swedish.)

SKB, 2017. Svar till SSM på begäran om komplettering kring försprödningsmekanismer för kapseln. SKBdoc 1602500 ver 1.0, Svensk Kärnbränslehantering AB. (In Swedish.)

SKB, 2019. Supplementary information on canister integrity issues. SKB TR-19-15, Svensk Kärnbränslehantering AB.

SKB, 2022a. Post-closure safety for the final repository for spent nuclear fuel at Forsmark. Fuel and canister process report, PSAR version. SKB TR-21-02, Svensk Kärnbränslehantering AB.

SKB, 2022b. Post-closure safety for the final repository for spent nuclear fuel at Forsmark. Data report, PSAR version. SKB TR-21-06, Svensk Kärnbränslehantering AB.

SKB 2022c. Post-closure safety for the final repository for spent nuclear fuel at Forsmark. Main report, PSAR version. SKB TR-21-01, Svensk Kärnbränslehantering AB.

Smart N R, Adams R, 2006. Natural analogues for expansion due to the anaerobic corrosion of ferrous materials. SKB TR-06-44, Svensk Kärnbränslehantering AB.

Smart N R, Rance A P, 2005. Effect of radiation on anaerobic corrosion of iron. SKB TR-05-05, Svensk Kärnbränslehantering AB.

Smart N R, Bond A E, Crossley J A, Lovegrove P C and Werme L, 2001a. Mechanical properties of oxides formed by anaerobic corrosion of steel, MRS Symp. Proc. 663, pp. 477-485.

Smart N R, Blackwood D J, Werme L O, 2001b. The anaerobic corrosion of carbon steel and cast iron in artificial groundwaters. SKB TR-01-22, Svensk Kärnbränslehantering AB.

Smart N R, Blackwood D J, Werme L, 2002. Anaerobic corrosion of carbon steel and cast iron in artificial groundwaters: Part 2-Gas generation. Corrosion 58, pp 627-637.

Smart N R, Rance A P, Fennell P A H, 2006. Expansion due to the anaerobic corrosion of iron. SKB TR-06-41, Svensk Kärnbränslehantering AB.

Spahiu K, 2021. Residual water and gases in a KBS-3 canister and their effect on post-closure safety. SKB TR-21-12, Svensk Kärnbränslehantering AB.

Storesund J, Feigin E, 2025. Evaluation of possible cracking damage mechanisms in KBS-3 alternative insert designs. Technical Document No 5003088-103-1 rev 2.0, Kiwa Technical Consulting AB. SKBdoc 2071979 ver 1.0, Svensk Kärnbränslehantering AB.

Storesund J, von Unge P, 2022. Creep of inserts in copper canisters for final repository for spent nuclear fuel. Report No. 5002274-100-1 rev 2.0, Kiwa Technical Consulting AB. SKBdoc 1997414 ver 1.0, Svensk Kärnbränslehantering AB.

Sundaram M, 2013. Low Temperature Creep/Relaxation Behaviour of PM Steels under Static Loading, Diploma work No. 121/2013 at Department of Materials and Manufacturing Technology Chalmers University of Technology, Gothenburg, Sweden.

Trummer M, Jonsson M, 2010. Resolving the H_2 effect on radiation induced dissolution of UO_2-based spent nuclear fuel. J. Nucl. Mater. 396, 163–169.

Turnbull A, 2009. A Review of the Possible Effects of Hydrogen on Lifetime of Carbon Steel Nuclear Waste Canisters, Nagra Technical Report 09-04, Nagra, Switzerland.

Turnbull A, Hutchings R B, Ferriss D H, 1997. Modelling of thermal desorption of hydrogen from metals, Mater Sci Eng A238, 317–328.

Turnbull J, Szukalo R, Zagidulin D, Shoesmith D, 2021. Nitrite effects on copper corrosion in nitric acid solutions. Corrosion Science 179, 109147.

Valmalle M, Widell K, Iiola R, Bossuyt S, 2024. DIC analyses and parameter calibration of a strain aging sensistive ductile cast iron. Comptes Rendus Méchanique 352, 1–17.

Wang O, Adolfsson S, Siwecki T, 2004. Critical hydrogen level for mechanical property degradation of high strength steels. IM-2004-538, Stockholm: Institutet för metallforskning.

Wen J, Tu S, Xuan F, Zhan X, Gan X, 2016. Effects of Stress Level and Stress State on Creep Ductility: Evaluation of Different Models, Journal of Materials Science & Technology, 32 695-704.

Wu R, Ahlström J, Magnusson H, Frisk K, Martinsson Å, 2015. Charging, degassing and distribution of hydrogen in cast iron. SKB R-13-45, Svensk Kärnbränslehantering AB.

Yang Q, Toijer E, Olsson P, 2019. Analysis of radiation damage in the KBS-3 canister materials. SKB TR-19-14, Svensk Kärnbränslehantering AB.

Yang Q, Chang Z, Messina L, Sandberg N, Castin N, Yousfi A, Toijer E, Thuvander M, Boizot B, Metayer V, Gorse-Pomonit D, Olsson P, 2022. Cu precipitation in electron-irradiated iron alloys for spent-fuel canisters, Journal of Nuclear Materials 572. https://doi.org/10.1016/j.jnucmat.2022.154038

Yu S-H, Lee S-M, Lee S, Nam J-H, Lee J-S, Bae C-M, Lee Y-K, 2019. Effects of lamellar structure on tensile properties and resistance to hydrogen embrittlement of pearlitic steel. Acta Materialia, 172, 92–101.

Yu-De L, 1992. An explanation of the relationship of fracture toughness to temperature in the range from upper shelf to first phase transformation. Engineering Fracture Mechanics 43, 305-311. https://doi.org/10.1016/0013-7944(92)90129-3

Åkesson M, 2023. Uppdaterade lastfall till designanalys inom Rebus. SKBdoc 2008518 ver 1.0, Svensk Kärnbränslehantering AB. (In Swedish).

Åkesson M, 2024. Uppdaterade lastfall till designanalys inom Rebus. SKBdoc 2008518 ver 2.0, Svensk Kärnbränslehantering AB. (In Swedish).

Öberg M, 2024. Fracture toughness testing to find the reference temperature, T_0, of steel from ST1 and ST4, order 4501776154. SKBdoc 2067923 ver 1.0, Svensk Kärnbränslehantering AB.

Öbrink E, Bolinder T, 2025. KBP3021 Project REBUS – SKB Main Study – BWR Canister Insert – Load Case L05 (4a) – Damage Tolerance Analysis. Report No. 5002622-101-4 rev 6.0, Kiwa Technical Consulting AB. SKBdoc 2044764 ver 3.0, Svensk Kärnbränslehantering AB.

Öbrink E, Mångård D, 2025. KBP3021 Project REBUS – SKB Main Study – An assessment of equivalent plastic strains and principal stresses in the copper shell under the isostatic and the rock shear load case – A comparison to the reference design. Report No. 5003088-102-1, Rev 1.0, Kiwa Technical Consulting AB. SKBdoc 2072002 ver 1.0, Svensk Kärnbränslehantering AB.

Öbrink E, Feigin E, Bolinder T, 2025a. KBP3021 Project REBUS – SKB Main Study – PWR Canister Insert – Load Case L07 (5a) – Damage tolerance analyses. Report No. 5002622-102-4 rev 6.0, Kiwa Technical Consulting AB. SKBdoc 2039030 ver 3.0, Svensk Kärnbränslehantering AB.

Öbrink E, Feigin E, Bolinder T, 2025b. KBP3021 Project REBUS – SKB Main Study – BWR Canister Insert – Load Case L07 (5a) – Damage tolerance analyses. Report No. 5002622-102-5 rev 6.0, Kiwa Technical Consulting AB. SKBdoc 2039911 ver 3.0, Svensk Kärnbränslehantering AB.

Öbrink E, Feigin E, Bolinder T, 2025c. KBP3021 Project REBUS – SKB Main Study – Consequence analysis of crack-like defects in the internal structure framework. Report No. 5003088-107-1, Rev 0.0, Kiwa Technical Consulting AB. SKBdoc 2079058 ver 1.0, Svensk Kärnbränslehantering AB.

Öbrink E, Bolinder T, Mångård D, 2025d. KBP3021 Project REBUS – SKB Main Study – PWR Canister Insert – Load Case L05 (4a) – Damage Tolerance Analysis. Report No. 5002622-101-3 rev 6.0, Kiwa Technical Consulting AB. SKBdoc 2043408 ver 3.0, Svensk Kärnbränslehantering AB.

Appendix A – Revisiting the Features, Events and Processes (FEPs) of relevance for the insert design alternative considered in the Rebus project

Background

Available databases of features, events and processes (FEPs), relevant to post-closure safety, are an important and formal tool used to ensure that all relevant factors have been considered in the safety assessment. SKB's work with FEPs in earlier safety assessments for the KBS-3 repository (e.g. SR-Site) has mainly been concerned with cast iron as an insert material, as this has been the material used in the design for the KBS-3 canister.

In the safety assessment, the FEP processing consists of identifying all the factors that need to be included in the analysis. The FEPs are classified as being one of the following types: *i)* initial state FEPs, *ii)* internal processes, or *iii)* external FEPs. Remaining FEPs are either related to assessment methodology in general or determined to be irrelevant for the KBS-3 concept.

The design alternative suggested in the Rebus project is an insert made of carbon steel, instead of cast iron. During the project, a number of issues related to the change of insert material from cast iron to carbon steel have been identified and analysed in the context of post-closure safety. In addition, as a formality and since SKB's earlier FEP processing does not contain information for carbon steel, it was decided to make a check of international FEP lists compiled by the Nuclear Energy Agency (NEA). Since carbon steel is used as a construction material of waste packages in other repository concepts, information of relevance could be expected to be found in these lists. The lists considered are *i)* a compilation of NEA Project-specific FEP (PFEP) Lists version 2.1 (NEA 2006) made within the SR-Site project, and *ii)* a review of NEA International FEP (IFEP) List version 3.0 (NEA 2019) performed within the PSAR-PSU project (Hjerpe 2022).

Method

The check of NEA PFEP lists was done by searching with the following exact keywords: *carbon steel, steel, embrittle, ageing, aging, degrad, radiation, and radioly*. The resulting subsets of FEPs were then checked manually by reading the FEP descriptions and for each FEP making a judgement of its relevance for the Rebus project due to the change of cast iron for carbon steel or due to dimensional changes compared with the cast iron design.

The IFEP list is structured around a classification scheme based on external factors and disposal components (waste package, repository, geosphere and biosphere). Each FEP contains a description, category, and commentary on its relevance to performance and post-closure safety. The IFEP list (Hjerpe 2022) was checked by searching for the same keywords as for the PFEP list.

Results and discussion

NEA PFEPs

In general, the results of checking the NEA PFEP list can be summarised by the following points:

- Several of the FEPs matching the keywords *steel*, *carbon steel* and *degrad* are related to long-term corrosion due to contact with groundwater, which in most cases is not of direct relevance for the Rebus project since the insert is not assigned any corrosion-related containment function in the safety assessment; this function is provided by the copper shell. A failure of the copper shell is regarded as a complete loss of containment and the time for corrosion to penetrate the insert material is (pessimistically) not accounted for.

- Several FEPs, e.g. A 1.64 *Radiation damage*, A 2.52 *Radiation effects*, E SFL-36 *Radiation effect on the canister*, I 238 *Radiation effects*, and M 3.4.02 *Material property changes*, concern radiation effects on materials, specifically radiation damage. This has been assessed in earlier safety assessments for the cast iron insert and is re-evaluated for Rebus, since the altered design of the insert leads to changes in the attenuation of radiation and in the doses and dose rates to the canister materials.
- The FEP E SFL-39 *Reduced mechanical strength of the canister* and to some of the FEPs referred to in the former bullet point (e.g. E SFL-36), concern long-term effects due to e.g. radiation exposure, which may affect the material properties and the mechanical integrity of the insert. This issue is studied further for the Rebus insert as well as for the cast iron insert. In addition to revised radiation shielding calculations, long-term chemical alterations of the materials (both for cast iron and carbon steel), such as precipitation of phosphide-phases at grain boundaries, precipitation of Cu-particles, and so-called late blooming phases, have also been further investigated.
- The FEPs S014 (E SFL-10) *Corrosion prior to wetting*, S045 (E SFL-25) *Gas generation in the canister,* and S072 (E SFL-37) *Radiolysis inside the canister prior to wetting*, are all of relevance for the Rebus insert as well as for the cast iron insert. These FEPs concern the production of radiolytic species and corrosive agents, e.g. nitric acid and ammonia, which are of importance in the assessment of the long-term properties and degradation of the canister materials. The changes in geometry and material composition suggested by Rebus impose altered dose/dose rate to the materials, and the effect on carbon steel may differ from the effect on cast iron. Therefore, the effects of radiolysis on the chemical environment inside the canister are addressed in the Rebus project.
- The FEP S022 *Differential thermal expansion of near-field barriers* concern differences in thermal expansion of the near field barrier materials (buffer, canister, insert) which may affect the stresses in the materials and potentially their physical properties. This is of relevance for Rebus since the dimensional and compositional changes could give a different stress field than for the cast iron design. This is handled through revised modelling of the thermal evolution of the near field and an evaluation of the mechanical stresses in the barrier components.

NEA IFEPs

The FEPs compiled in the NEA IFEP list are of more general nature compared with the NEA PFEP list. The following FEPs were identified as relevant for the Rebus project using the same search keywords as for the NEA PFEP list:

FEP 2.3.3.1: Deformation

FEP 2.3.3.4: Stress corrosion cracking

FEP 2.3.6.6: Criticality

FEP 3.2.6.2: Radiolysis

FEP 3.2.6.4: Radiation damage

Within these, the FEPs 2.3.3.1: Deformation and 2.3.6.6: Criticality were not identified searching the NEA PFEP list. The issues of mechanical strength and criticality were, however, both identified within Rebus before the FEP search and the issues have been addressed for the Rebus insert.

Conclusions

The NEA PFEP and IFEP lists have been searched using the keywords *carbon steel, steel, embrittle, ageing, aging, degrad, radiation, and radioly* in order to identify FEPs which may be relevant due to the dimensional and/or compositional changes on the canister insert imposed by Rebus. It was concluded that all the FEPs found as relevant for the Rebus project are already identified and have been addressed in the project.

Appendix B – Analysis of temperature evolution for a Rebus canister

Introduction

Thermal analysis of KBS 3 canisters with cast iron inserts is reported in e.g. Ikonen, (2020). The Rebus designs of the canister inserts warrants an updated thermal analysis of the canister interior. In particular, temperature differences across argon filled gaps between insert components need to be taken into account, as does the generally more complex geometry of the Rebus inserts.

In this Appendix the temperature distribution in Rebus BWR and PWR inserts are analysed and compared with those of the cast iron inserts. A canister thermal model is set up and steady external temperature and fuel heat flux conditions are analysed in a first step. Results for the canisters with cast iron inserts are benchmarked against those reported by Ikonen (2020).

Then the thermal evolution under repository conditions over time is analysed, applying thermal data for the host rock at the Forsmark site to a thermal model for the canister copper shell, the buffer and the host rock. Results from that model are applied to the canister thermal model to obtain the temporal evolution of the canister internal temperature distribution.

Canister thermal 2D steady-state model

Software and mathematical model

A 2D model of the thermal conditions at canister mid-height, where the highest temperatures occur, has been developed in COMSOL Multiphysics version 6.0. The heat transfer in the canister is calculated with the heat equation, Equ 1.

$$-\nabla \cdot (\lambda \nabla T) = Q \qquad \text{Equ. 1}$$

where T is temperature and λ is thermal conductivity. The heat generation in the fuel is modelled with the source term, Q.

In the argon-filled gaps thermal radiation is modelled as a gray body with Stefan-Boltzmann law, Equ 2.

$$j = \varepsilon \sigma T^4 \qquad \text{Equ. 2}$$

where j is the heat flux, ε is the emissivity and σ is the Stefan-Boltzmann constant.

Geometry

The geometry of the modelled cross-section for the cast iron case is taken from (Ikonen, 2020) while the geometry for the Rebus insert is described in Section 2.2.1. The copper shell and the gap between the copper shell and the insert are the same for both cases. In a first analysis, a 1 mm gap is considered between the inner framework and the steel tube for the Rebus insert. In a more detailed and realistic version, flat surfaces on the internal framework where it contacts the outer tube are evaluated. The differences between the two models are shown in Figure B-1 and Figure B-2.

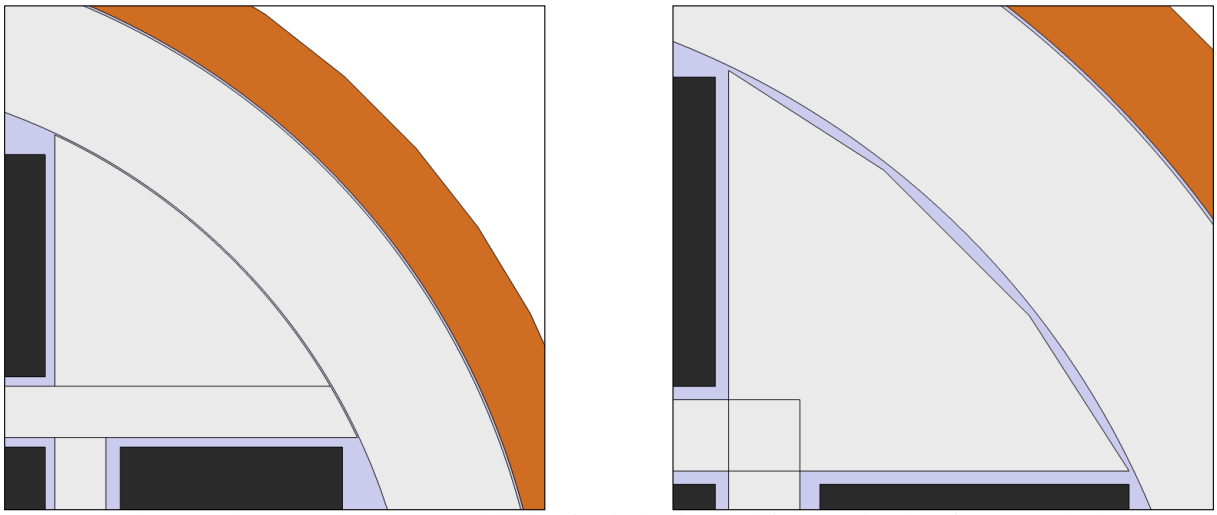

Figure B-1 *The two Rebus BWR alternatives modelled. Left: Idealised, curved framework end surfaces towards the outer tube and a gap width of 1mm. Right: Flat (polygon-shaped) framework end surfaces towards the outer tube. This shape is in agreement with the detailed BWR design. Here, the minimum distance between the tube and the framework plates is 1.5 mm.*

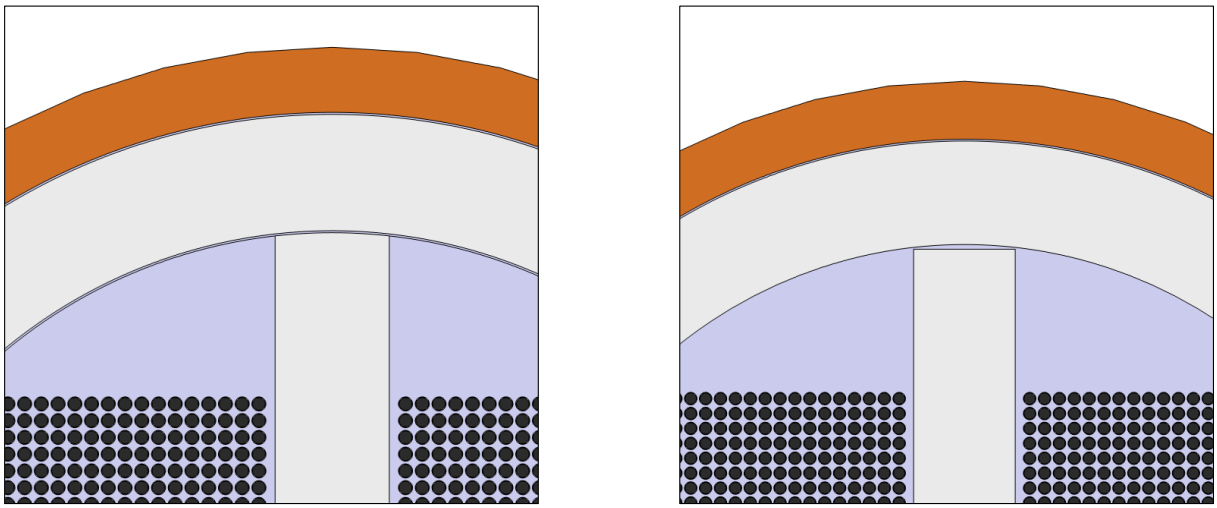

Figure B-2 *The two Rebus PWR alternatives modelled. Left: Idealised, curved framework end surfaces towards the outer tube and a gap width of 1 mm. Right: Flat framework end surfaces towards the outer tube. This shape is in agreement with the detailed PWR design. Here, the minimum distance between the tube and the framework is 1.5 mm.*

Material and boundary conditions

Material properties

The material properties are taken from (Ikonen, 2020) and shown in Table B-1 and Table B-2. Since steady-state conditions are modelled, the specific heat capacities are of no importance and are not shown here.

Table B-1. Thermal conductivities used. From Ikonen (2020).

Material	Thermal conductivity (W/mK)
Copper	390
Cast iron	35.5
Steel	57.5
Zirconium	$7.51+0.0209\ T-1.45\ 10^{-5}\ T^2+7.67\ 10^{-9}\ T^3$
Argon	$4.0921\ 10^{-4}\ T^{0.6748}$
Uranium oxide	$3.21-1.93\ 10^{-3}\ (T-273.15)$

Table B-2. Emissivities used. From Ikonen (2020).

Material	Emissivity
Copper	0.1
Steel	0.6
Zirconium	0.6
Cast iron	0.6

BWR boundary conditions and materials

The materials in the BWR canisters are shown Figure B-3. The fuel elements have been approximated with a homogeneous model where the individual fuel rods are replaced with a material that approximates how the fuel element behaves globally, following the approach by Ikonen (2020). The homogeneous model for the 8x8 fuel rod setup is used. The approximated thermal conductivity for the homogeneous model is shown in Equ 3. For details about the simplification, see Ikonen (2020).

$$\lambda_{fuel} = 0.1304 + 8.13\times10^{-4}\,(T-273.15) + 2.91\times10^{-6}\,(T-273.15)^2 \text{ W/mK} \qquad \text{Equ. 3}$$

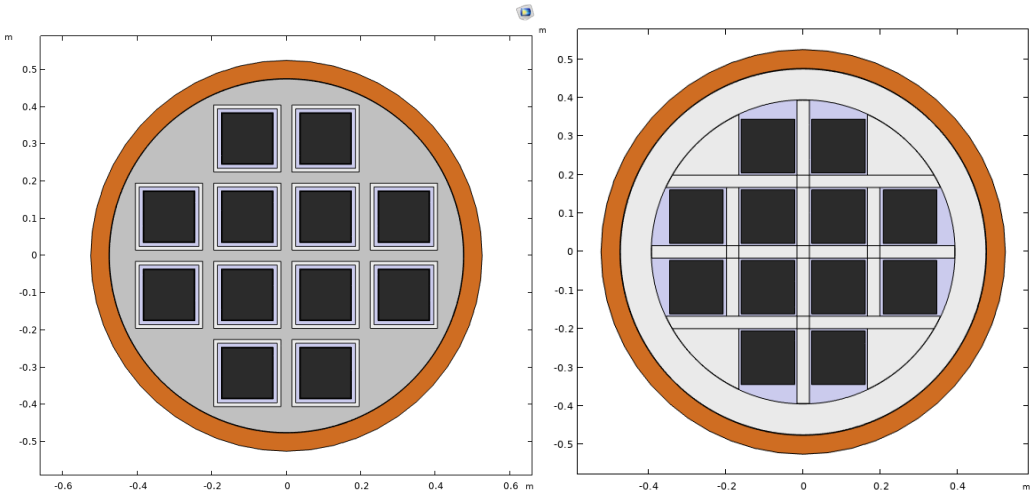

Figure B-3. *The materials used in the BWR models. Blue is argon, black is fuel, orange is copper, light grey is steel, grey is cast iron. Left: Cast iron BWR, Right: Rebus BWR.*

In the argon-filled gaps between the copper and the insert, between the insert and the fuel elements and between the Rebus framework and the Rebus steel tube, heat is transferred by both heat conduction by the Ar gas and thermal radiation.

The outer boundary of the copper shell is kept at 100 °C and a total residual thermal power of 1700 W is assumed for the fuel. The residual thermal power density is highest at the mid part of the fuel rods. To capture this peak power, the thermal power is multiplied by a factor of 1.16 for the BWR canister in accordance with Ikonen (2020).

PWR boundary conditions and materials

The materials in the PWR canisters with cast iron and carbon steel inserts are shown in Figure B-4 and Figure B-5, respectively. For the PWR assemblies all the fuel rods are represented in the model, contrary to the treatment by Ikonen (2020) where a homogeneous model was used for PWR. For details about the fuel geometry, see Ikonen (2020).

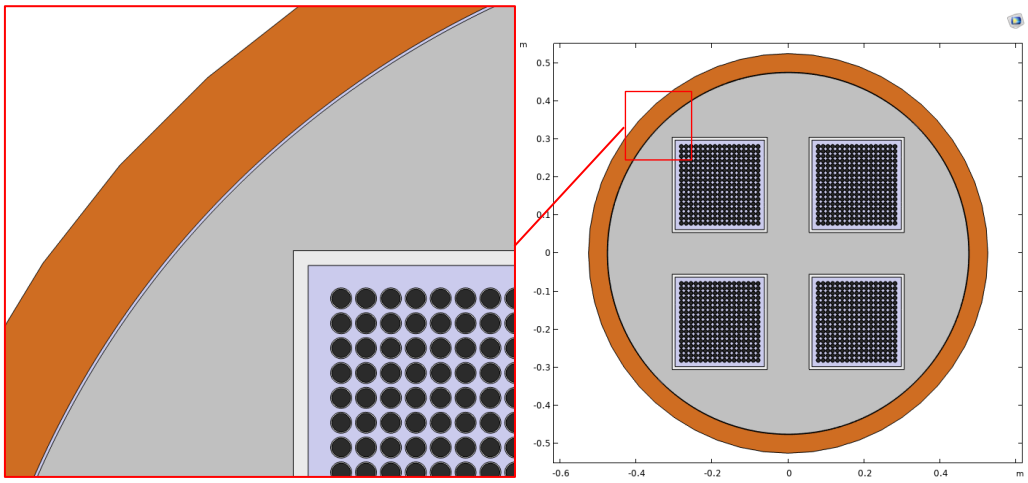

Figure B-4. *The materials used in the model for the cast iron insert. Blue is argon, black is uranium dioxide, orange is copper, light grey is steel, grey is cast iron and there is a thin layer of zirconium around the fuel rods, not shown in this figure.*

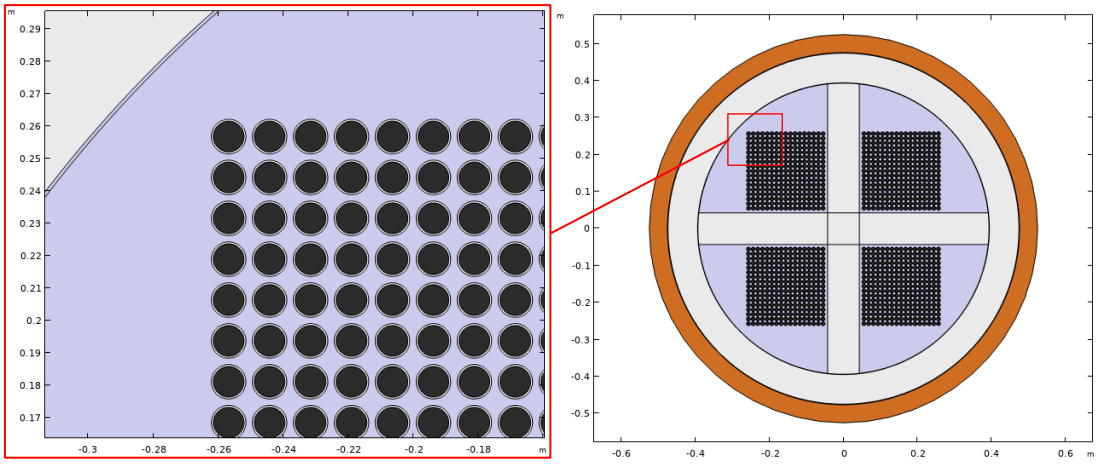

Figure B-5. *The materials used in the model for the Rebus canister. Blue is argon, black is uranium dioxide, orange is copper, grey is steel, and there is a thin layer of zirconium around the fuel rods (barely visible in this figure).*

In the argon-filled gaps between the copper and the insert, between the insert and the fuel elements and between the Rebus framework and the Rebus steel tube, heat is transferred by both heat conduction by the Ar gas and thermal radiation.

The outer boundary of the copper shell is kept at 100 °C and a total residual thermal power of 1700 W is assumed for the fuel. The residual thermal power density is highest at the mid part of the fuel rods. To capture this peak power, the thermal power is multiplied by a factor of 1.06 for the PWR canister in accordance with Ikonen (2020).

Canister steady state results

BWR

The modelled temperatures are shown in Figure B-6 and relevant temperatures are also shown in Table B-3. These are, for the cast iron case: maximum temperature in the fuel and minimum and maximum temperatures in the insert. For the Rebus case the following are given: maximum temperature for the fuel, maximum temperature for the insert, minimum temperature for the framework and the temperature on each side of the gaps in points B1-B3. The maximum temperature in the insert tube is also given. It is noted that the modelled maximum fuel temperature for the cast iron insert (138.8 °C) exceeds that obtained by Ikonen (2020) by 3.8 °C. The reason for this has not been possible to clarify based on the information in Ikonen (2020). It is, however, also noted *i*) that the temperature obtained here is higher than that in Ikonen (2020) but still far from any temperature that would be of concern for the any of the evaluations in the present report and *ii*) that it would be fully possible to model also the BWR fuel as individual fuel rods, thereby avoiding any issue relating to the homogenised fuel model, but this has not been carried out in the present work.

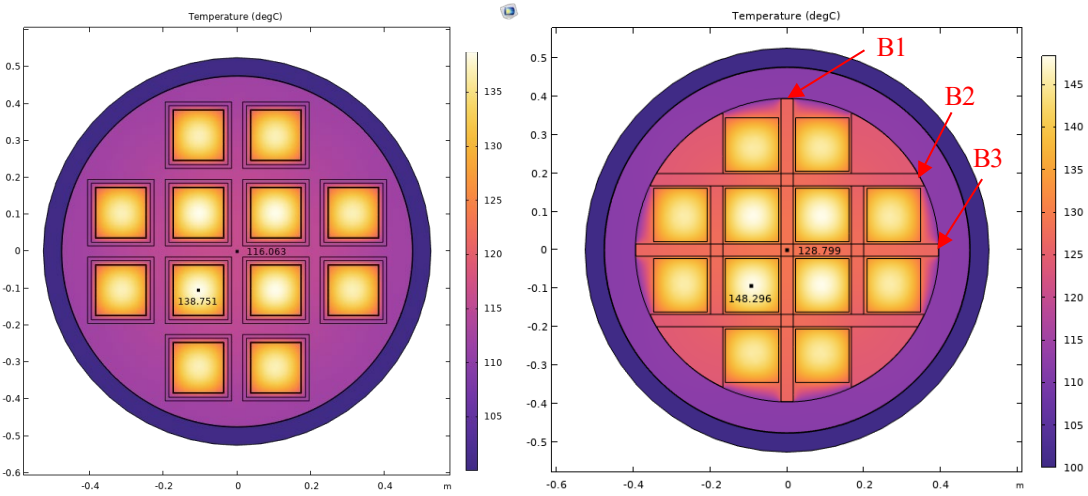

Figure B-6. *Modelled temperatures for the BWR canister. Cast iron insert (left), Rebus insert (right).*

Table B-3. Maximum and minimum temperatures (°C) in the BWR insert.

	Reference	Reference (Ikonen, 2020)	Rebus 1 mm gap	Rebus Flat contact surfaces
Maximum temperature fuel	138.8	135.0	148.3	158.6
Maximum temperature insert	116.1	115.0	128.8	140.1
Minimum temperature insert (reference case)/framework (Rebus case)	111.8	111.2	123.8	135.8
B1 inner			126.5	136.8
B1 outer			112.1	112.4
B2 inner			129.9	136.0
B2 outer			112.4	112.4
B3 inner			126.5	136.9
B3 outer			112.2	112.4
Maximum temperature insert tube			112.6	112.4

PWR

The modelled temperatures are shown in Figure B-7 and relevant temperatures are also shown in Table B-4. These are, for the cast iron case: maximum temperature on the fuel and minimum and maximum temperatures in the insert. For the Rebus case the following are given: maximum temperature for the fuel, maximum temperature for the insert, minimum temperature for framework. The maximum temperature in the insert tube is also given.

It is noted that the difference in peak temperature between the fuel and the insert is higher for the cast iron insert than for the Rebus insert. The cause for this has not been investigated in detail, but is likely the overall higher temperatures in the Rebus insert, making the radiant heat flux a more efficient mode of heat transfer between fuel and insert in the Rebus case.

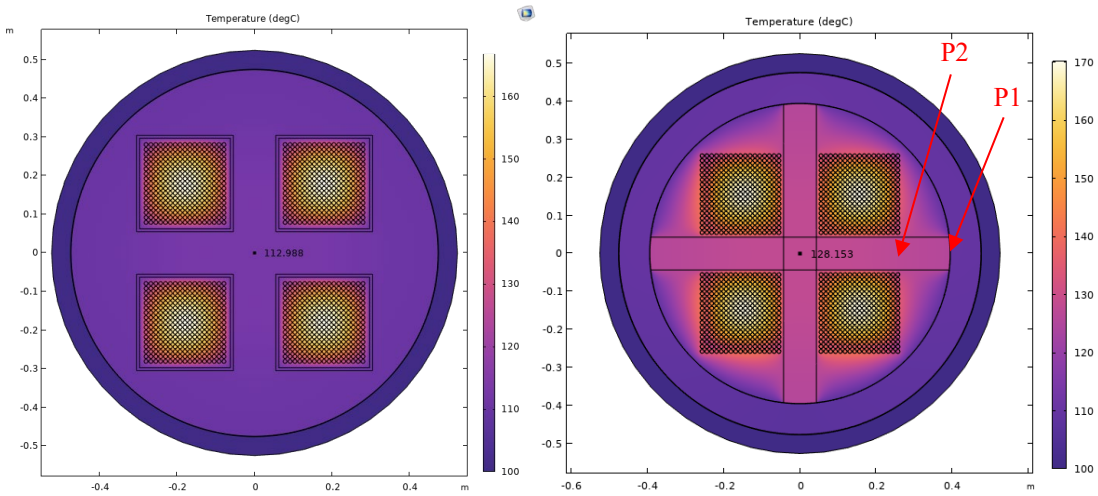

Figure B-7. *Modelled temperatures for the PWR canister. Cast iron insert (left), Rebus insert (right).*

Table B-4. Maximum and minimum temperatures (°C) in the PWR insert.

	Cast iron	Cast iron (Ikonen 2020)	Rebus 1 mm gap	Rebus Flat contact surfaces
Maximum temperature fuel	166.8	165.4	170.1	175.1
Maximum temperature insert	113	112.7	128.2	134.5
Minimum temperature insert (cast iron case) / framework (Rebus case)	110.1	110.2	125.7	132.5
P1 inner			125.8	132.4
P1 outer			109.8	110.3
P2			126.9	133.3
Maximum temperature insert tube			110.2	110.3

Thermal development in the repository

To obtain the thermal development of the Rebus canisters in a repository environment, an analytical model (Hedin 2004) implemented in Microsoft Excel and used in earlier assessments of the repository thermal evolution is utilised. This model simulates the thermal development of the fuel, the copper shell, the buffer and the host rock and has been shown to give results in good agreement with more complex models, see benchmark examples in Hedin (2004). The model is capable of approximately accounting for the canister interior development for the BWR canister with a cast iron insert, but not the more complex internal structures of the Rebus inserts. Therefore, the copper shell temperature and associated fuel heat fluxes over time calculated with the repository model are subsequently applied to the canister thermal model described above, yielding the thermal development of the canister interior.

Dimensions and thermal data for the buffer surrounding the canister and for the rock at the Forsmark site are taken from SKB's SR-Site assessment of the KBS 3 system, for which the thermal analysis is reported in Hökmark et al. (2010). The repository contains 6916 canisters distributed according to the so-called Layout D2 described in SKB (2009). The deposition hole coordinates are the same as those used in the hydrogeological modelling of the repository. The thermal conductivity of the host rock is pessimistically selected as the dimensioning case reported in Hökmark et al. (2010), This and other data used in the model are given in Table B-5. The temperatures were calculated for the most central deposition hole position in the repository.

The buffer is assumed to be dry, i.e. in the same hydraulic condition as when deposited as this yields higher canister temperatures than a water-saturated buffer. The following conceptual alterations to the model described in Hedin (2004) have been made:

- An effective buffer thermal conductivity of 1 W/(m·K) that covers both the buffer block and the pellet-filled gap between the buffer and the rock wall is adopted from Section 3.2.2, p. 32 of Hökmark et al. (2009). There is thus no explicit modelling of the pellet-filled gap between the rock wall and the buffer and both the pellets and the buffer blocks are assumed to be in their as-deposited unsaturated state.
- The temperature difference over the 1 cm gap between the buffer and the copper shell is modelled according to Section 3.3.2 of Hökmark et al. (2009) where the temperature difference over the buffer/canister gap, ΔT (°C), for a canister with time dependent heat power $Q(t)$ (W) is modelled as

  $$\Delta T = 16\frac{Q(t)}{1700} = 0.00941 \cdot Q(t)$$

  This expression is based on empirical observations in SKB's prototype repository and deemed more reliable than expressions based on uncertain data of emissivities of the buffer inner and the copper outer surfaces applied in Hedin (2004). The expression yields the temperature difference between the inner buffer wall at canister mid-height and the canister top for a dry buffer. The canister temperature at canister mid-height is expected to be up to 2 °C higher than at the top, see Figure 3-9 of Hökmark et al. (2009), and this difference is ignored here.

$Q(t)$, where t is the time after deposition, is modelled as a sum of exponentially decaying terms according to Eq. 5-1 and Table 5-1 in Hökmark et al. (2010). The initial canister power, Q_0, is set to 1700 W (SKB 2009, Section 3.6.3).

Table B-5 Geometric and thermal data used in the modelling of the thermal development of the repository.

Factor	Value	Reference
Repository depth	460 m	Hökmark et al. (2010), Section 5.8.1
Canister spacing	6 m	SKB (2009), Section 3.6.3
Tunnel spacing	40 m	SKB (2009), Section 3.6.3
Gap copper/buffer, air-filled	0.01 m	Hökmark et al. (2010), Section 5.3
Initial canister power, Q_0	1700 W	SKB (2009), Section 3.6.3
Rock thermal conductivity	2.9 W/(m·K)	Hökmark et al. (2010), Table 5-2, dimensioning case for RFM 029
Rock heat capacity	2.06 MJ/(m^3·K)	Hökmark et al. (2010), Table 5-2
Temperature at repository depth	11.2 °C	Hökmark et al. (2010), Section 5.8.1
Buffer thermal conductivity	1 W/(m·K)	Hökmark et al. (2009), Section 3.2.2 p 32

With these data, the model yields results according to Figure B-8. The peak temperature of the rock wall, reached after 30 years, is 67 °C. This result, and the entire rock wall curve, is in quite good agreement with the black, dashed curve in the left part of Figure 5-15 in Hökmark et al. (2010), where the same fuel heat flux and rock thermal data were used. (Results for the dry buffer temperature in the figure mentioned in Hökmark et al. cannot be compared to those obtained here, since Hökmark's results for a dry buffer refer to the top block of the buffer that is in direct contact with the canister. This is the point where the peak buffer temperature occurs for dry holes, whereas the peak canister temperature, that is of interest in the present study, occurs at canister mid-height for both dry and wet holes (Hökmark et al. 2010). However, applying the repository model to wet holes with a buffer thermal conductivity of 1.3 W/(m·K) as in Hökmark et al. (2010) and no gap between the buffer and the canister, yields a peak buffer temperature of 78.9 °C and a curve in good agreement with the blue dashed curve in the mentioned figure in Hökmark et al., representing the wet buffer temperature at canister mid-height.) It is also noted that the peak canister temperature for dry holes is under-estimated by up to 2 °C due to the treatment of the gap according to the above, meaning that the calculation of the peak canister temperature is not strictly pessimistic for a dry deposition hole.

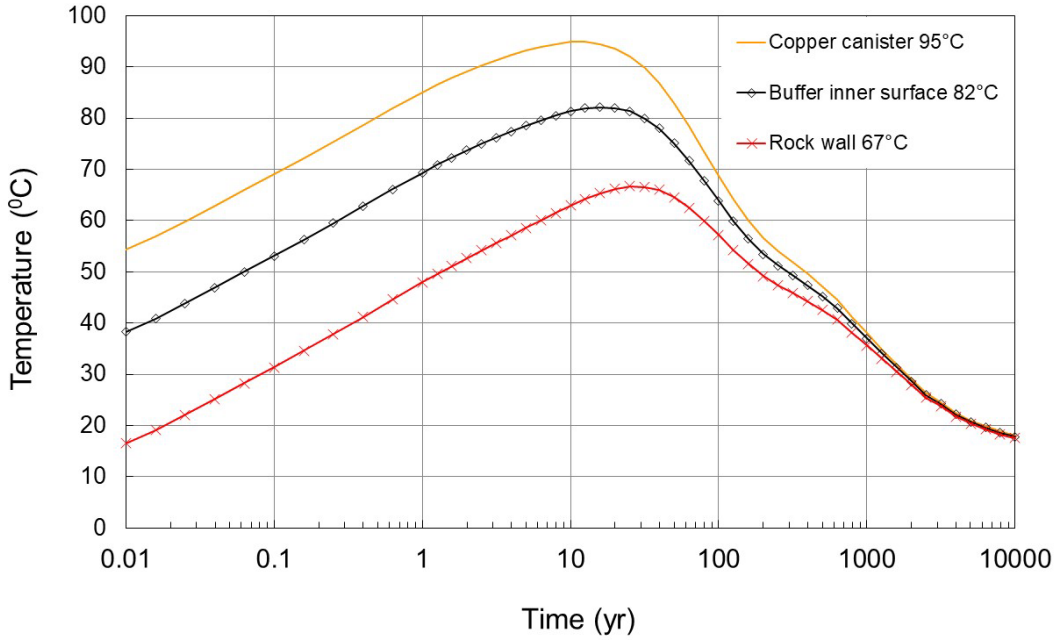

***Figure B-8**. Temperature evolution of the rock wall, the buffer inner surface and the canister outer surface for a centrally located canister at the Forsmark site. All canisters are assumed to have an initial residual power of 1700 W. The rock thermal conductivity is pessimistically set to the dimensioning, low value selected for the Forsmark site.*

In order to obtain the canister interior temperatures under repository conditions, time-dependent fuel powers and copper shell temperatures calculated with the repository model are applied to the canister steady-state thermal model described in the preceding section. This approach is justified since the canister interior adjusts to varying external temperatures and heat fluxes in a matter of a few weeks whereas the external temperature and fuel heat fluxes change much more slowly (disregarding the weeks immediately after deposition as regards the external temperature). This yielded the canister internal temperatures shown in Table B-6. These data are used in the accounts of the thermal development of the canisters with cast iron and Rebus inserts in Figure 5-1 and Figure 5-2.

Table B-6 Internal temperatures in canisters with cast iron inserts and Rebus canisters for repository relevant fuel residual powers and copper shell temperature in the time interval 0.01-1995 years. All temperatures in °C.

Time after deposition (yr)	0.01	0.1	1	3.16	10	20	50	158	631	1995
Power (W)	1700	1697	1671	1611	1439	1233	827	382	173	50.0
Copper temperature	54.2	69.1	85.0	91.4	94.9	93.6	82.9	60.0	44.5	29.2
Cast iron BWR										
Max. temp. fuel	100.8	112.8	125.5	129.6	128.9	123.2	104.2	71.3	50.1	31.0
Max. temp. insert	71.6	86.0	101.2	106.9	108.6	105.4	91.0	63.9	46.3	29.7
Cast iron PWR										
Max. temp. fuel	166.8	134.7	144.7	154.9	157.4	153.9	143.4	121.0	80.7	55.0
Max. temp. insert	113.0	68.3	82.8	98.1	103.9	106.0	102.8	89.5	63.2	46.0
Rebus BWR										
Max. temp. fuel	124.1	135.0	146.1	149.2	146.5	138.8	115.7	77.6	53.3	32.0
Max. temp. framework	101.4	113.7	126.6	130.7	129.8	124.0	104.5	71.2	50	30.9
Min. temp. framework	97.0	109.5	122.4	126.7	126.4	120.9	102.4	70.2	49.5	30.8
Max. temp. tube	67.9	82.3	97.6	103.4	105.5	102.7	89.2	63.1	45.9	29.6
Rebus PWR										
Max. temp. fuel	148.2	157.3	164.1	166.1	164.0	154.5	127.93	84.7	57.2	33.4
Max. temp. framework	97.8	109.8	121.3	125.5	126.2	120.8	102.5	70.4	49.7	30.8
Min. temp. framework	95.4	107.5	119.1	123.4	124.2	119.2	101.4	69.8	49.5	30.8
Max. temp. tube	66.0	80.5	95.5	101.4	104.0	101.5	88.3	62.6	45.7	29.6

Appendix C – Hydrogen absorption by insert materials in a sealed KBS-3 canister

This Appendix is a copy of Hedin and Högberg (2024), except that the term "memo" has been changed to "Appendix".

Introduction

This Appendix contains a discussion of the possible absorption of atomic hydrogen by the iron-based metal of the KBS-3 canister insert, once a canister has been loaded with spent fuel and sealed. Various sources of hydrogen are considered and the maximum diffusible hydrogen concentration (the sum of the lattice hydrogen and that located in reversible traps) is estimated. The potential consequences of this diffusible hydrogen on the mechanical properties of the insert are also considered. Whereas the contents are primarily focussed on the low-alloyed carbon steels P355N, P355J2+N and P355GH+N intended to be used in an alternative design of the insert, much of the discussion is also relevant for the nodular cast iron insert design. The alternative so-called Rebus design consists of an outer 8 cm hollow cylinder and an inner framework, designed to house either 12 BWR fuel elements or 4 PWR elements (Ronneteg 2025). It is noted that both the extent and the effects of H absorption by cast iron are deemed to be negligible in SKB (2022a, Section 3.4.2).

Generally, hydrogen in a metal may occur as atomic H dissolved in the metal lattice and as more or less firmly bound to traps. It may also occur as molecular hydrogen in microscopic voids in the metal. Traps may be found for example at grain boundaries, phase boundaries, dislocations, interfaces between the lattice and inclusions and particles, vacancies and solute atoms. If the binding energy of a trap site is sufficiently high, a trapped hydrogen atom will not be released below temperatures close to the melting temperature of the metal. Such traps tend to be filled during the metallurgical processing and essentially remain filled unless the material is melted. The lattice hydrogen and the hydrogen in shallower traps is termed the diffusible hydrogen. See, e.g., Section 3.1 in Turnbull (2009) for more details.

As regards detrimental effects on mechanical properties, it is primarily the concentration of hydrogen in the metal lattice, c_L, that is of concern, even if other forms of hydrogen may also play a role in particular failure mechanisms, see, e.g., Section 3.2 in Turnbull (2009) and chapter 4 in King (2009). The treatment in the following is, therefore, focussed on how hydrogen sources in the void in a canister insert could influence the lattice concentration c_L. The main reasoning is based on an equilibrium between gas phase hydrogen in the void and lattice hydrogen.

Hydrogen sources

Initial hydrogen content

The initial total hydrogen concentration in the P355N carbon steel intended for the manufacture of tubes for the Rebus inserts has been determined to be typically around 0.5 wt.ppm (average of log-normal distribution fitted to data), see section 3.2 in Sarnet (2024a). As in any steel material, most of the hydrogen is expected to be bound in traps, with only a small fraction occurring as dissolved hydrogen in the lattice. The distribution between reversible and irreversible traps is not known, as the total concentration has been measured by melt analysis that does not provide a distinction between trap types.

For the discussion to follow, it is of interest to have an order-of-magnitude estimate of the initial lattice concentration. Data in Table 1 in Turnbull et al. (1997) suggests a trap density for low-alloy carbon steel at 23 °C of 2×10^{18} sites/cm^3, a trap energy of −48 kJ/mol, an initial trap occupancy of 0.5 and a resulting lattice concentration of about 2×10^{15} atoms/cm^3 (3.7×10^{-4} wt.ppm). With these data, virtually all hydrogen is bound in traps, and the example trap density and occupation corresponds to a concentration of diffusible hydrogen of 0.2 wt.ppm. This value is compatible with the total hydrogen content of P355N steel of 0.5 wt.ppm mentioned above.

The total Fe mass in the Rebus BWR and PWR inserts are 13.9 and 13.0 tonnes, respectively (Ronneteg 2025). The amount of diffusible hydrogen in a Rebus insert would thus be around 2.6 g.

Additional hydrogen sources

Two additional hydrogen sources in the sealed canister have been identified:

- Up to 600 g of water is allowed in a canister after drying and sealing according to current design requirements. With current drying methods and rules for loading canisters with leaking fuel pins, it is, however, not plausible that any of the around 6000 canisters will contain this amount of water and the majority of canisters are essentially expected to be dry. Nevertheless, 600 g of water in a canister void will pessimistically be considered in the following.
- Hydrogen is also to some extent expected to be present as zirconium hydrides in the fuel cladding. The possible amount is uncertain, and was assessed to range between 22 and 480 g per canister in SKB (2022a, Section 3.4.2). This hydrogen is, however, strongly bound in the fuel cladding and not expected to be liberated at the peak temperature of up to around 150 °C experienced by the fuel cladding in the sealed canisters. In SKB (2022a, Section 3.4.2) it is estimated that "*…only a very small fraction, if any, of this hydrogen should be considered as a source of hydrogen for embrittlement of the cast iron*". If some portion is liberated, it would be expected to be in the form of molecular hydrogen in the gas phase.

Water in the canister void is expected to be consumed during oxic corrosion and, once the available oxygen in the void has been consumed, by anoxic corrosion of the iron based insert material. In a matter of a few years, it is likely that a considerable fraction of the hydrogen initially bound in water molecules will be present as hydrogen gas in the insert void, see e.g. Henshaw and Spahiu (2021) and Henshaw and Evins (2023). 600 g of water corresponds to about 33 mol of H_2.

Hydrogen absorption equilibrium

The void volume of a loaded Rebus insert is 0.97 m^3 for the BWR version and 1.25 m^3 for the PWR version. The temperature of the outer steel tube reaches a maximum of around 100 °C some ten years after deposition in the final repository and then slowly decreases but stays above 50 °C for several hundred years. The hottest part of the inner framework may reach temperatures of around 125 °C and then cools somewhat faster than the tube so that the difference between the two is evened out with time. Similar volumes and temperatures apply for the nodular cast iron inserts.

The initial maximum of 33 mol of H_2 in a void volume of 1 m^3 corresponds to a hydrogen partial pressure of 1.0 atm at 100 °C, and 0.80 atm at 20 °C. Kiuchi and McLellan (1983) give an expression for the hydrogen solubility in pure iron in equilibrium with 1 atm H_2, applicable up to 100 °C:

$$\ln\left(\theta T^{7/4}\right) = -\frac{3120 \pm 90}{T} + (3.21 \pm 0.32) \qquad (2)$$

Here, θ is the lattice solubility in units of H/Fe atoms and T is the absolute temperature. This expression yields a lattice H concentration in Fe at 1 atm and 100 °C of 1.8×10^{-7} at/at or 3.3×10^{-3} wt.ppm. At 20 °C and 50 °C, the corresponding values are (for 1 atm) 5.1×10^{-4} wt.ppm and 1.1×10^{-3} wt.ppm, respectively. These lattice concentrations are thus an order of magnitude higher than that estimated for the Rebus materials in the as-delivered condition above.

A lattice concentration of 1×10^{-3} wt.ppm in 13 tonnes of Fe corresponds to around 0.013 g H, i.e. a negligible fraction of the 66 g assumed in the gas phase after anoxic corrosion of 600 g of water. If, as assumed above, the density of shallow traps is 2×10^{18} sites/cm^3, with a trap energy of −48 kJ/mol and an initial occupancy of 0.5, the occupancy would be expected to be close to 1 after a tenfold increase in lattice concentration. Accordingly, the concentration of diffusible hydrogen would also increase by a factor of two, assuming that the trapping situation is unchanged. This would mean an increase in diffusible hydrogen by 0.2 wt.ppm, i.e. by about 2.6 g. Essentially all the 66 g of H would thus still remain in the gas phase as H_2.

Turnbull (2009) mentions threshold concentrations as low as 4×10^{-4} wt.ppm for the development of microscopic voids in steel, meaning that also this H sink in the metal would have to be considered for a full treatment. At equilibrium, the H_2 pressure in the micro voids in the metal would be expected to be the same as that in the roughly 1 m^3 void of the insert interior.

Dynamics of hydrogen absorption

In an environment free from hydrogen gas, the hydrogen concentration in the lattice and in the shallow traps is expected to decrease asymptotically to zero by outgassing, with a time constant $\tau = L^2/(4D_a)$ (Carslaw and Jaeger 1959). Here, D_a is an apparent diffusivity that approximately accounts for the diffusivity in the lattice and the retarding effect of shallow traps. At room temperature and at 100 °C, lower bounds of D_a can be estimated to be 10^{-7} cm^2/s and 2×10^{-6} cm^2/s, respectively (Boellinghaus et al., 1995). With L = 8 cm this yields time constants τ of around 5 and 0.25 years, respectively. The same time constants govern the equilibration of the lattice concentration with a hydrogen pressure in the canister interior. (In more detail, hydrogen absorbed at the inner surface of the steel tube would diffuse through the tube and be released at the outside void between the insert and the copper shell. The void volume outside the insert is, however, much smaller than that of the inside, meaning that the outside volume will have a secondary effect on the dynamics of the establishment of an equilibrium. Furthermore, the diffusivity of copper is much lower than that of the insert; the 5 cm copper shell is regarded as impermeable to hydrogen in this treatment.)

The insert lid, having a thickness of 5 cm, is expected to be outgassed/equilibrated in less than half the time required for the tube, and the 3.2 cm thick steel plates of the inner framework in the BWR design in even shorter time.

The above is based on the assumption that any H being absorbed in the anoxic corrosion of iron by water will not cause irreversible mechanical effects like blister formation close to the metal surface, but will eventually be distributed between the lattice, traps and the exterior as part of the equilibrium described above. It is well-known that aggressive charging of metals with hydrogen can cause such effects, see e.g. Martinsson et al. (2009) and Wu et al. (2015). This requires electrochemical conditions conducive to hydrogen charging and where recombination inhibitors are usually also added to the electrolyte to prevent atomic hydrogen liberated in the charging process from forming H_2 and thereby promoting the absorption of atomic H by the metal. Also, as evidenced in e.g. Wu et al. (2015), charged H will to a large extent leave the metal by outgassing shortly after the charging process.

The conditions during corrosion in the canister insert are much less aggressive compared to electrochemical charging experiments. For example, in the experiments reported by Martinsson et al. (2009) and Wu et al. (2015), the H generation rates (as determined from the charging currents) are of the order of 10^{-7} mol/(cm^2·s) whereas the anoxic corrosion rate in the canister insert is assessed to be typically around 3 μm/yr (Smart and Rance 2005), corresponding to an H generation rate of the order of 3.5×10^{-12} mol/(cm^2·s). The efficiency of hydrogen pick-up by the metal may be higher for the slower corrosion process, since an H atom on the metal surface will encounter other H atoms to form H_2 less frequently than in the charging experiments. However, considering the many orders of magnitude difference in generation rates and the fact that hydrogen pick-up is enhanced by the use of recombination inhibitors in the charging experiments, it should be possible to rule out irreversible mechanical effects close to the metal surface in the sealed canister insert. Furthermore, such effects appear to be tacitly assumed to be irrelevant in both Turnbull (2009) and King (2009). It is also noted that the efficiency of H absorption will decrease in the presence of corrosion product films on the insert.

Impact on mechanical properties

Mechanical effects of hydrogen in low-alloyed carbon steels under geological repository conditions are discussed by Turnbull (2009) and King (2009). Those reports concern hydrogen impact on waste containers of carbon steel being exposed to external hydrogen pressures of up to 10 MPa at 90 °C (Turnbull 2009) and 8 MPa at a maximum of 100 °C (King 2009). The pressures are thus two orders of magnitude higher than that in the Rebus canister insert according to the above, while the temperatures are similar. Since the equilibrium between an external H_2 pressure and the lattice concentration of H, c_L, is governed by Sieverts' law, which states that c_L varies in proportion to the square root of the pressure, the c_L values discussed in the reports by Turnbull and by King are one order of magnitude higher than that of about 0.1 MPa caused by 33 mol of H_2 in a Rebus insert.

For the external pressure of 8 MPa, King (2009) concludes the following:

"*The probability of H-related failure is deemed to be minimal, primarily because of:*

1. *the benign nature of the environment and the consequent low absorbed H concentration,*
2. *the moderate levels of applied [40 MPa, p. 48] and residual [500-600 MPa, p. 48] stress, and*
3. *the use of low-strength C-steel as the container material."*

Tables 4 a, b and c in King (2009) give critical lattice concentrations for a range of hydrogen related failure mechanisms for various temperatures and steel qualities, based on a number of studies for each failure mechanism. Compared to the lattice concentrations determined above for the Rebus canister insert at different temperatures, the critical concentrations given in King (2009) are:

- more than an order of magnitude higher for blister formation; Table 4a in King (2009),
- more than two orders of magnitude higher for hydrogen-induced cracking (HIC); Table 4b in King (2009), and
- two orders of magnitude higher for hydrogen embrittlement (HE); Table 4c in King (2009). (Table 4c also addresses sulphide stress cracking that is not of relevance for the Rebus insert.)

There is a general caveat in King (2009) that in some of the cited studies, it is not clear if the authors are reporting lattice concentrations or total diffusible hydrogen.

The following conclusions from Turnbull (2009) are relevant for the Rebus insert, noting again that they are made for a tenfold higher lattice H concentrations than the maximum expected in the insert (conclusions relating to welds and surface pits and exposures to sulphur have been excluded since they are not relevant for the insert):

- *"Low strength carbon steel of the type projected for the nuclear waste canister can be envisaged to fail by a hydrogen assisted cracking mechanism only if the following conditions prevail: the hydrogen content exceeds the threshold for HIC or SOHIC [Stress Oriented Hydrogen-Induced Cracking]".*
- *"Assuming that hydrogen gas pockets with a pressure of 10 MPa exist as predicted then the lattice hydrogen solubility at 90 °C in equilibrium would be about 0.03 ppm. This is likely to be a maximum value, a progressive lowering of temperature reducing this over time to 0.01 ppm".*
- *"In relation to HIC or SOHIC, there are insufficient data to define a lower bound lattice concentration below which cracking could not develop irrespective of the steel composition and impurity level, and stress in the case of SOHIC. Thus, we cannot conclude a priori that these mechanisms are not feasible for the waste canister with a lattice concentration of 0.03 ppm. Nevertheless, their occurrence can be prevented by appropriate materials selection and welding practice, noting that for a modern steel the threshold lattice hydrogen concentration is projected to be about 60 times the lattice hydrogen concentration estimated for these waste containment conditions."*

Turnbull (2009) also discusses mitigation strategies to minimise the likelihood of cracking associated with hydrogen, but these are mainly aimed at preventing situations that are not relevant for the Rebus insert.

To further corroborate their conclusions, both King (2009) and Turnbull (2009) recommend that some issues are further studied. It is though noted that the conditions to which the canisters in those references are exposed are more severe in terms of hydrogen pressures and corroding environments and that they also contain welded parts, that can be more susceptible to hydrogen related failure.

The steel grade selected for the tube in the Rebus canister insert belongs to the P355-family, where 355 indicates the yield strength in MPa. (The inner framework plates may be of even lower strength). This is a ductile, low-strength carbon steel, or mild steel. The microstructure allows for considerable strain from the yield point to the ultimate strength and further on to the point of fracture. (In a high strength carbon steel, on the other hand, the yield strength approaches that of the ultimate strength. This allows for a more slender design within the elastic range and hence more efficient use of material. The drawback is a reduced ductility, and the susceptibility to hydrogen effects is increased.)

The design of the Rebus inserts is optimised such that the thickness of the tube is maximised while leaving just enough space to house the spent fuel elements. For this thickness, the selected steel P355 is optimised such that the yield strength is kept low to provide a high ductility, while the material is still able to carry the specified loads. This is consistent with the advice on material selection from the point-of -view of minimising the susceptibility to hydrogen related failure given in King (2009) and Turnbull (2009).

Conclusion and potential further work

Most of the Rebus canisters are expected to contain much less than the allowed 600 g of water according to the design premises. Even for the equivalent of 600 g of water, the lattice concentration of H is about one order of magnitude lower than that for which King (2009) and Turnbull (2009) argue that hydrogen damage should be a limited problem. Apart from the higher pressure in those evaluations, there are also other negative aspects of the environment that need to be considered for the application in question (steel containers for geological disposal) that are not relevant for the Rebus inserts, like the presence of sulphide. Also, the Rebus design is free of welds in contrast to the designs considered in the cited evaluations.

Aside from the presence of hydrogen and a susceptible material, a mechanical load is required to drive the propagation of most forms of damage (where blister formation is an exception). The load on the canister in the repository is expected to be low; the highest stresses and strains are generally expected to be significantly lower than the yield strength, the ultimate tensile strength and the elongation at failure of the material. There are no welds in the design, and measurements have confirmed very low residual stresses from manufacture of the components (Lundin and Holmberg 2024). There are no cyclic loads that can cause fatigue or crack growth.

A fracture mechanics assessment based on the expected hydrogen pressure and the presence of an assumed initial defect could be considered to verify the structural integrity for a selection of representative load cases. This may be done by comparing calculated values of the stress intensity factor K_I with literature data of critical values of this parameter for relevant H_2 pressures. The literature data for the particular steel qualities of interest are somewhat scarce and available data are for H_2 pressures much higher than 0.1 MPa, whereas there appears to be no measurable reduction in toughness at 0.1 MPa, see Figure C-1, copied from San Marchi and Somerday (2012). The figure shows the impact on fracture toughness for the steel qualities X42 and A516 that resemble the qualities intended for the Rebus inserts. The figure indicates that the impact of an H_2 partial pressure of 0.1 MPa would be negligible.

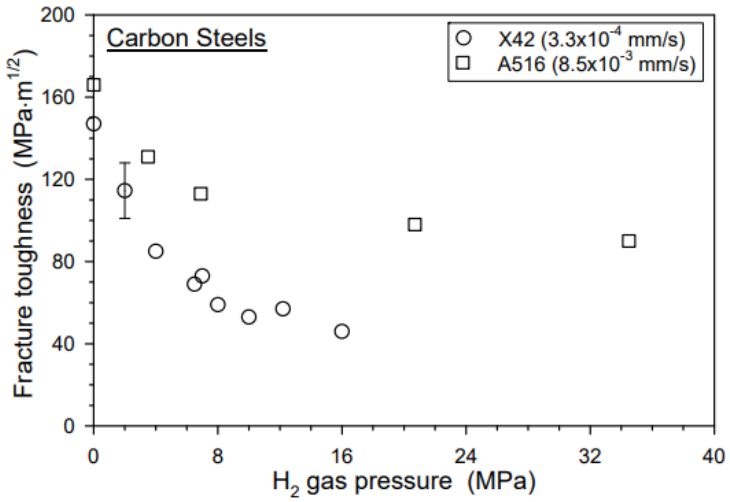

***Figure C-1**. Effect of hydrogen gas pressure on fracture toughness for two carbon steels tested at different strain rates (San Marchi and Somerday 2012).*

To better understand the nature of the hydrogen content in the canister insert materials, it would be of interest to determine not only the total content, but also the fraction of diffusible hydrogen, and how that fraction is bound in the material. This could be achieved with thermal desorption spectrometry (TDS) of samples from the insert. In planning such a measurement, it is to be noted that a small sample could be degassed already at room temperature in a limited time, meaning that care must be taken to preserve the *in situ* conditions prior to the measurement. The total hydrogen content should be determined through melt analysis of a parallel sample to that on which the TDS measurement is carried out. Also the TDS sample could be subjected to melt analysis after the TDS measurement, a procedure followed in Malmström (2023).

To substantiate the conclusions in this Appendix even further, fracture mechanics testing of hydrogen charged specimens (or directly on specimens in an autoclave with a hydrogen atmosphere) could be considered.

Appendix D – Updated estimate of phosphorus segregation to grain boundaries

Sandberg and Korzhavyi (2009) discuss radiation-enhanced P segregation to grain boundaries in Fe. For a constant vacancy supersaturation, i.e. the ratio of vacancy concentrations with and without radiation, of $S = 5\times10^{13}$ at 100 °C during 300 years they estimate that detrimental radiation enhanced P segregation to grain boundaries is unlikely for a P concentration of 0.01 % unless the P diffusivity, D_P, at 100 °C is of the order of 10^{-37} m^2/s or larger. Evaluating experimental and theoretically calculated data they conclude that P diffusivities of up to the order of 10^{-37} m^2/s cannot be ruled out. Here, it is noted that the diffusivity of $4.48\times\exp(-2.30\ \text{eV}/k_BT)$ m^2/s theoretically calculated by Domain and Becquart (2005) yields a diffusivity of 3.9×10^{-38} m^2/s at 100 °C. Sandberg and Korzhavyi (2009) cite this value and claim that it is too high and that this is a well-known deficiency in this type of calculation. Therefore, it seems that calculated values are expected to yield values below 10^{-37} m^2/s, in contrast to the evaluation in Sandberg and Korzhavyi (2009).

The vacancy supersaturation of 5×10^{13} assumed in the estimate by Sandberg and Korzhavyi (2009) is based on the input data and calculations made by Brissonneau et al. (2004), i.e. on parameter set A in Yang et al. (2022), a dpa rate for G4 UOX fuel according to Eq. 3 in Brissonneau et al. (2004) and a dislocation density of 10^{12}/m^2. Applying instead the updated parameter set B in Yang et al. (2022), the dpa rate according to Eq (1) in Section 4.4 and the experimentally determined dislocation density of 10^{14}/m^2 for the Rebus materials (Hagström 2024) yields an average S ≈ 10^{12} during the 300 year period considered by Sandberg and Korzhavyi (2009).

In more detail, Sandberg and Korzhavyi (2009) determined the depth near a grain surface that would have to be depleted in P through outward diffusion in order for a monolayer of P to form on the grain boundary, assuming that the boundary is a perfect sink for P. For a P concentration of 0.01 at.% Sandberg and Korzhavyi (2009) estimate this depth as $d_{diff,P} \approx 2.3\times10^{-6}$ m.

Assuming constant diffusivity as was done by Sandberg and Korzhavyi (2009), the depletion depth, d, as a function of time can be approximated by

$$d \approx \sqrt{tD_P} \tag{3}$$

With a varying diffusivity, d is approximated by

$$d \approx \sqrt{\int D_P(t)dt} \tag{4}$$

The depletion depth d has been calculated with Eq (4) for 300 years and for 10^6 years assuming a thermal diffusivity of $4.48\times\exp(-2.30\ \text{eV}/k_BT)$ m^2/s (Domain and Becquart 2005) and for various assumptions regarding temperature and parameters related to vacancy concentration. Results are presented in Table D-1. The dpa rate is according to Andgren (2023). Using instead the dpa rate from Brissonneau (2004) yields differences of about 10 % for the 300 year results which is negligible in this type of estimate. For the 10^6 year calculations it is unrealistic to use the rate given by Brissonneau et al. (2004) since it underestimates the contribution from neutrons to the dpa rate beyond the first thousand years.

As seen in Table D-1, the 300 year results are well below the guideline value of 2.3×10^{-6} m, whereas many of the 10^6 year results are near this value. It is, however, difficult to draw any firm conclusions from this type of crude estimate of whether P segregation at grain boundaries could be problematic. There are large uncertainties regarding the P diffusivity, and extrapolating down to repository temperatures may be associated with particular uncertainties. It is unclear if a monolayer of P on the boundary is a relevant criterion for detrimental effects. The boundary is likely not a perfect sink for P as there will be competition with e.g. C atoms, etc. Furthermore, the diffusion of P in Fe with significant amounts of other impurities is more complex than pure Fickian diffusion that is the basis for Eqs (3) and (4), see e.g. Faulkner et al. (2005). As mentioned in Section 7.5.5, experimental results suggest limited effects for total doses below around 7×10^{-3} dpa, which is many orders of magnitude higher than the 3.7×10^{-6} obtained by integrating the dpa rate for the Rebus materials over 10^6 years according to Section 4.4.

It would be advantageous if the thermal diffusivity of phosphorus in iron could be more reliably estimated at the temperatures of concern.

Table D-1. Depletion depths for various assumptions regarding temperature, model parameter sets and dislocation density. Thermal P diffusivity $4.48\times\exp(-2.30\ \text{eV}/k_BT)$ m^2/s. For a P concentration of 0.01 at.%, depletion to a depth of around 2.3×10^{-6} m is required to form a monolayer of P on a grain boundary. Repository temperature from Section 5.2.1.

Temperature	Parameter Set	Dislocation density (m^{-2})	*d* at 300 years (m)	*d* at 10^6 years (m)
100 °C	A	10^{12}	1.4×10^{-7}	1.3×10^{-6}
100 °C	A	10^{14}	4.8×10^{-8}	1.6×10^{-7}
100 °C	B	10^{12}	2.9×10^{-8}	2.9×10^{-7}
100 °C	B	10^{14}	8.9×10^{-9}	2.9×10^{-8}
Repository temp	A	10^{12}	4.3×10^{-8}	1.6×10^{-6}
Repository temp	A	10^{14}	2.8×10^{-8}	1.4×10^{-6}
Repository temp	B	10^{12}	4.5×10^{-8}	2.3×10^{-6}
Repository temp	B	10^{14}	4.5×10^{-9}	2.3×10^{-7}